Usability of phase synchrony neuromarkers in neurofeedback protocols for epileptic seizures reduction

Côme Le Breton

UNIVERSITÉ CÔTE D'AZUR

ÉCOLE DOCTORALE
SCIENCES ET TECHNOLOGIES DE L'INFORMATION ET DE LA COMMUNICATION

THÈSE DE DOCTORAT

Utilisabilité des marqueurs de synchronie de phase dans les protocoles de neurofeedback EEG pour la réduction des crises épileptiques

Côme LE BRETON

Centre Inria d'Université Côte d'Azur, Équipe-Projet Athena

Présentée en vue de l'obtention du grade de Docteur en Automatique, Traitement du Signal et des Images de l'**Université Côte d'Azur**

Dirigée par : Maureen CLERC
Co-dirigée par : Théodore PAPADOPOULO

Date de soutenance : 18 octobre 2022

Devant le jury composé de :
Mme Maureen CLERC, Directrice de Recherche, Centre Inria d'Université Côte d'Azur, Directrice de thèse
M. Théodore PAPADOPOULO, Directeur de Recherche, Centre Inria d'Université Côte d'Azur, Co-directeur de thèse
M. Fabien LOTTE, Directeur de Recherche, Centre Inria de l'Université de Bordeaux, Rapporteur
M. Sylvain CHEVALLIER, Maître de Conférences, Université Versailles - Saint Quentin, Rapporteur
M. Mathieu DESROCHES, Directeur de Recherche, Centre Inria d'Université Côte d'Azur, Examinateur
M. Christian BÉNAR, Directeur de Recherche, INSERM, Examinateur

Utilisabilité des marqueurs de synchronie de phase dans les protocoles de neurofeedback EEG pour la réduction des crises épileptiques

Résumé

Le cerveau est un organe qui supervise de nombreuses fonctions vitales. Malgré sa fascinante complexité associée à une incroyable fiabilité, des disfonctionnements peuvent survenir et avoir des conséquences graves comme dans les troubles épileptiques. Certaines fonctions du cerveau sont permises par l'activité oscillatoire de populations de neurones. En fonction de la tâche mentale, ces oscillations se produisent à des rythmes et dans des régions corticales différents. Elles peuvent être décrites par deux grandeurs : l'amplitude et la phase. En particulier, la phase caractérise dans le temps les cycles d'activation d'une population neuronale. La synchronie de phase mesure la similitude entre deux oscillations en capturant la stabilité d'une relation de phase. Elle peut donc informer sur une relation fonctionnelle entre ces ensembles. Alors que la synchronie entre activités oscillatoires de régions cérébrales est présentée comme un coordinateur nécessaire entre ces dernières, son excès, comme dans les épilepsies, a des conséquences dramatiques, indiquant qu'un équilibre est nécessaire. Ce travail se concentre donc sur la modulation en temps réel de la synchronisation de phase entre des zones cérébrales distinctes dont l'activité est mesurée au moyen de l'électroencéphalographie (EEG). Cela dans le but d'offrir de nouvelles opportunités de traitement pour certains troubles épileptiques.

Dans une première contribution, focalisée sur l'extraction de la phase dans les signaux EEG, les transformées en ondelettes de Morlet de sinusoïdes, de sommes pondérées de sinusoïdes, de bouffées oscillantes et de bouffées oscillantes superposées sont dévelopées formellement. Des simplifications sont proposées pour permettre des expressions compactes de ces phases. Ces développements montrent notamment que pour des composantes fréquentielles proches et d'énergie similaire ou pour des salves trop rapprochées, la phase ne peut pas être récupérée de manière fiable. Néanmoins, dans des conditions raisonnables (et réalistes), les paramètres des bouffées du rhytme alpha (amplitude et phase) peuvent être récupérés par le biais de la transformée en ondelettes de Morlet. Des résultats préliminaires satisfaisants sur des données réelles sélectionnées sont proposés.

Une deuxième contribution consiste en une tentative de reproduction d'une étude montrant le potentiel de la synchronie de phase par la différenciation entre cerveaux épileptiques et sains avec des améliorations statistiques pour prendre en compte des données hautement corrélées, inhérentes aux mesures EEG et de synchronie de phase. Des stratégies originales pour corriger les biais sont proposées et détaillées. Contrairement à ce qui a été publié, la synchronie de phase s'avère généralement plus élevée chez les patients atteints d'épilepsie temporale que chez les témoins. Si l'adaptation de l'analyse statistique a modéré les résultats, elle n'en a pas changé les conclusions.

Dans une troisième contribution, un ensemble de données EEG de repos et de tâches simples a été acquis sur des sujets sains pour identifier des neuromarqueurs de synchronie de phase entraînables. L'étude des différences de phase brutes le long de l'axe antéropostérieur a montré qu'il existe des différences de phase prédominantes dans la bande de fréquence alpha, notamment lors de l'état de repos avec les yeux fermés. Ces déphasages, différents d'un sujet à l'autre, sont stables d'un enregistrement à l'autre sur de longues périodes de temps. Un modèle simple de deux sources est proposé pour rendre compte de ce résultat et conduire à reconsidérer certaines propriétés des mesures de synchronie de phase.

Au final, alors que l'objectif de modulation en temps réel d'un marqueur de synchronie de phase n'a pas été atteint, notamment parce que l'identification d'un tel marqueur a été démontrée non triviale, les différentes contributions ajoutent aux fondations nécessaires à la recherche de tels marqueurs neuronaux basés sur la phase.

Mots clés: EEG, neurofeedback, neuromarqueur, épilepsie, phase, synchronie

Usability of phase synchrony neuromarkers in neurofeedback protocols for epileptic seizures reduction

Summary

The brain is an organ that oversees many vital functions. Despite its fascinating complexity associated to its incredible consistency, failures can occur and have severe consequences such as in epilepsy disorders. Major functions in the brain are enabled through the oscillatory activity of neuronal assemblies. These oscillations occur at different rhythms, over different regions, depending on the mental task. They can be described by two quantities: their amplitude and their phase. In particular, the phase characterizes over time the oscillatory pattern of a neuronal assembly. Phase synchrony measures the similarity between two oscillations by capturing the stability of a phase relationship between neuronal assembly activities and informs on a functional relationship between these assemblies. While synchronization between the oscillatory activities of brain regions is presented as a necessary coordinator between brain areas, its excess, such as in epilepsy, causes dramatic outcomes, indicating that a balance is necessary. For these reasons and others detailed in this manuscript, this work focuses on the real-time modulation of phase synchrony between distinct brain areas by means of electroencephalography (EEG) to offer new treatment opportunities for certain epileptic disorders.

In a first contribution, focusing on the retrieval of the phase from EEG signals, the Morlet wavelet transforms of sinusoids, weighted sums of sinusoids, oscillating bursts and overlapping oscillating bursts are formally derived.Simplifications are proposed to allow for compact expressions of the phase.Their properties and parameters are discussed.These derivations notably show that for close frequency components with similar energy the phase is not trustworthy.They also show that for too close bursts, the phase cannot be reliably recovered. Nonetheless, in reasonable and practical conditions, the recovery based on the Morlet Wavelet transform of the properties of alpha bursts (amplitude and phase) is attempted and provides satisfactory preliminary results on selected real data.

The second contribution is an attempt to reproduce a study showing the potential of phase synchrony in differentiating between epileptic and healthy brains with statistical improvements to handle highly correlated data, inherent to EEG and phase synchrony measures. Original strategies to correct for the biases are proposed and detailed. Contrarily to what was published, the mean phase coherence is shown to be generally higher in temporal lobe epilepsy patients than in controls. While adapting the statistical analysis moderated the results, it did not overturn the conclusions.

In a third contribution, an EEG dataset of resting states and simple tasks was acquired on healthy subjects to search for trainable phase synchrony neuromarkers. The study of bare phase differences along the anteroposterior axis showed that there exists predominant phase differences in the alpha frequency band, notably during eyes closed resting state. These phase differences, which are different from one subject to the other, are stable across recordings over long periods. A simple model of two sources is proposed to account for this finding and lead to reconsider some properties of phase synchrony measures.

Ultimately, while the real-time modulation of a phase synchrony marker was not achieved, especially because the identification of such a marker was demonstrated non-trivial, the various contributions lay more foundations to the search for phase-based neural markers. Primarily through the development of theoretical but also software contributions. These software contributions are part of an ongoing research protocol with hospital La Timone in Marseille.

Keywords: EEG, neurofeedback, neuromarker, epilepsy, phase, synchrony

Acknowlegments

I express my sincere gratitude to my advisers Maureen Clerc and Théodore Papadopoulo for the continuous support throughout my Ph.D study and related research, for thoughtful advice and multiple corrections despite their heavy agenda. This is probably the place to congratulate director of research Rachid Deriche, head of the Athena team, for being rewarded an ERC (European Research Council) grant. Indeed, the European Research Council under the European Union's Horizon 2020 research and innovation program (ERC Advanced Grantagreement No 694665: CoBCoM - Computational Brain Connectivity Mapping) funded this work.

Besides my advisers, I thank my thesis committee: director of research Fabien Lotte and assistant professor Sylvain Chevallier for accepting to review this manuscript.

It is also a pleasure to acknowledge directors of research Patricia Reynaud-Bouret and Fabien Lotte participation to the CSI (Individual Follow-up Committee for Ph.D students) who provided priceless advice and encouragements to publish results, thank you. I wish to send my sincere gratitude to statisticians Jean-Marc Freyermuth and Christophe Pouet for taking the time to comment on the delicate subject of statistical testing.

I shall not forget the team at hospital La Timone in Marseille: Christian Bénard, Fabrice Bartolomei, Jean-Michel Badier and others...

I thank my fellow lab-mates for the stimulating discussions, the Athena team: Rachid (again), Théo (again), Maureen (again), Sara, Sarah, Ivana, Isa, Mauro, Joan, Sam, Igor, Petru, Agathe, Abib, Matteo, Kostia, Pierre, Johann, Patryk for the entertainment, but also for listening to my presentations and complaints. Mathieu Desroches won't be forgotten for willingly discussing dynamical model theory. Additionally, some special thanks should go to the team member: Joan Belo (again), for the numerous scientific coffee breaks which challenged various original (loony ?) ideas...

A great thank you goes to you, Jeanne Benoit, neurologist at the CHU in Nice, who showed relentless motivation on this bold project and never showed reluctance in listening to my sometimes absurd and hollow stance on results that had just showed up. She provided help up to the very final deadline, although working full time (and more) at the hospital.

The team at the SED (Service Expérimentation et Développement) in Sophia Antipolis deserves their share of thanks as well, for they were always present when needed, be it for software architecture (Julien), conda packacing (Nicolas) or general talks on politics (Thibaud) and silly jokes (Jean-Luc).

I realize that a PhD thesis involves a lot of people, despite the single name figuring on the front page.

The final note on this page goes to my family, to my grandmas who left this journey before the finish line, and my parents who have always been encouraging despite not fully understanding the practical reasons leading to starting this in the first place, and my brother who didn't dare confront it (he is the youngest one after all). I wish to say all my dearest thoughts to Claudia and Alice for being part of this, and for what lies ahead for us.

Contents

General introduction

Context

The brain is the organ, in vertebrate and most invertebrate animals, that oversees vital functions, such as heart beating and breathing and allows for the extensive adaptation of the animal behavior to its surroundings. Although it has not always been considered the processing unit of the animal, it dictates its behavior (its reactions), from the short time scale of the reflex, to the longer time scale of the thinking and beyond. Despite its fascinating complexity (in the variety of tasks an animal can achieve) associated to an incredible consistency (most animals achieve roughly the same as their peers), failure can occur and have severe consequences such as in epilepsy disorders. An attempt to develop a methodology on the control of one's brain activity to reduce the symptoms of epilepsy disorders, requires first to grasp (as much as possible) the workings of such a unit, as well as the possible disruptions in these workings. Fortunately, the field is now rich of three centuries of ex-vivo / in-vitro / in-vivo experiments at all possible scales, on human and non-human animals.

Major brain functions are mediated through the timely and repetitive activations of neuronal assemblies, i.e. their oscillations. These oscillations occur at different rhythms, over different regions, depending on the mental task. Their phase describes over time the pace at which the neuronal assembly goes from inactivated to activated (recruited by Excitatory Post Synaptic Potentials) back to inactivated. Phase synchrony defines the consistency in the phase relationships (linear or non-linear) of two (or more) neuronal assemblies. In its simplest form, it amounts to a constant phase difference across time, which may provide information on the functional relationship between these assemblies. Phase synchrony between oscillatory activities of brain regions is hailed as one of the main coordinators of brain functional integration.

For these reasons (and others described in the introduction), this thesis work engages with the online modulation of synchronous activity between separate brain areas by means of ElectroEncephaloGraphy (EEG) to provide new opportunities to treat some epilepsy disorders.

As mentioned by Egner and Sterman [63], long date practitioners of EEG neurofeedback, "skilled practice of neurofeedback requires a good understanding of the neurophysiology underlying EEG oscillations, of operant learning mechanisms, and an in-depth appreciation of the various hardware/software equipment options open to the practitioner."

Overview of the thesis

Chapter 1: Neurophysiology and neuropathophysiology in the light of brain oscillations Chapter 1 is a state of the art introduction dedicated to the emergence of oscillations in the brain electrical activity. A special care is dedicated to the links that have been made with epilepsy syndromes. It reviews state of the art experiments investigating the role of oscillations and their relationship to function. In a second overview, it emphasizes on the role of long range synchronization, much less described with regard to oscillations. It should prove useful for the further analysis of results observed in different frequency bands. A specific point is made regarding traveling waves, which at the level of the scalp may be the manifestation of long range synchrony, and

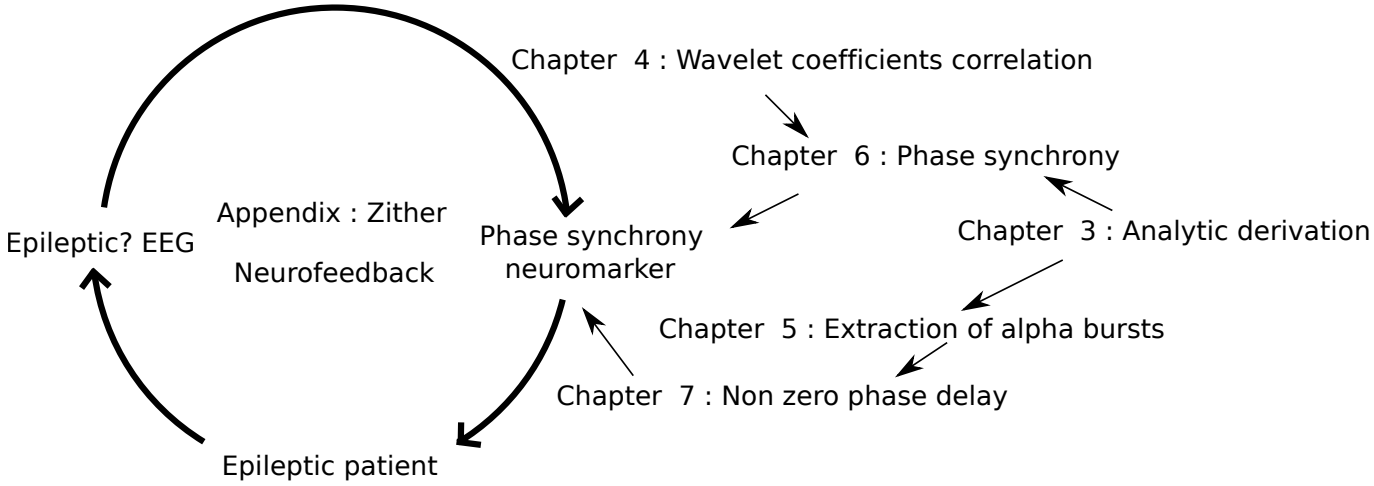

Figure 1

is the physiological basis of chapter 7.

Chapter 2: Measuring and modeling oscillations and oscillating systems, EEG experimation and mathematical modeling Chapter 2 provides a range of measures that help quantify the level of synchronization between brain areas based on their oscillatory activity. This oscillatory activity is well measured with ElectroEncephaloGraphy (EEG), therefore it brings details on how one can set up properly such experiments. These setups are employed in chapter 7 and chapter 6. This chapter also describes Neurofeedback setups, and more precisely those that have been hailed as reducing the frequency and / or severity of epileptic seizures.

Chapter 3: Analytic derivation of Morlet Wavelet Transform applied to sum of sinusoids Chapter 3 derives mathematically the convolution of sinusoids, weighted sums of sinusoids and oscillating bursts by the Morlet Wavelet Transform. Simplifications are proposed that allow a compact expression of the phase. Its properties and parameters are discussed. It notably shows the frequency over spatial trade-off, and that for close frequency components with similar energy, the phase is not trustworthy.

Chapter 4: Correlation between close wavelet coefficients Chapter 4 deals with the issue of dependence between samples in statistical testing of phase synchrony measures. The correlation coefficient is calculated for δ distant complex coefficients computed through the Morlet Wavelet Transform, first by considering that the autocorrelation of the signal is null, then by releasing this constraint. When the autocorrelation of the signal is assumed to be 0, the autocorrelation function of the wavelet coefficients is a Gaussian function centered at 0.

Chapter 5: Extraction of alpha bursts parameters based on Morlet Wavelet Transforms Chapter 5 provides a simple tool to extract the bursts parameters of the EEG signal in the alpha band based on the complex coefficients obtained by the Morlet Wavelet transform. The parameters of greatest interest are the temporal localization and the phase shift. The ambition of this procedure is to obtain a new way to compute delays between brain areas. The limits of this approach are linked to chapter 3.

Chapter 6: Phase synchrony in epileptic patients ElectroEncephaloGraphic recordings Chapter 6 compares two groups of healthy and epileptic (temporal lobe epilepsy during the interictal stage) subjects, with regard to common phase synchrony measures. It notably shows the bias in using Mann-Whitney U tests in such a configuration, and provides ways to circumvent this bias. The end-goal of this contribution is to ascertain the

feasibility of using these measures as neuromarkers in neurofeedback protocols, by making sure that they allow to differentiate the two populations.

Chapter 7: Non-zero phase delays in the alpha band along the antero-posterior axis Chapter 7 shows that there not only exists stable phase differences along the anteroposterior axis in the alpha frequency band, notably during eyes closed condition, but that this stable phase difference, which is different from one subject to the other, is stable across recordings over long periods up to 2 years. These observations arose by chance while searching for patterns in phase synchrony measures.

General conclusion This chapter gives a wrap-up of the contributions of the thesis. It discusses the main limitations of the methods and studies and proposes perspectives for future work.

Part I

Background

Chapter 1

Neurophysiology and neuropathophysiology in the light of brain oscillations

This chapter presents a state of the art introduction dedicated to the emergence of oscillations in the brain electrical activity. A special care is dedicated to the links that have been made with epilepsy syndromes. It reviews state of the art experiments investigating the role of oscillations and their relationship to function. In a second overview, it emphasizes on the role of long range synchronization, much less described with regard to oscillations. It should prove useful for the further analysis of results observed in different frequency bands. A specific point is made regarding traveling waves, which at the level of the scalp may be the manifestation of long range synchrony, and is the physiological basis of chapter 7.

1.1 The source of electrical activity in the brain

While the spark of consciousness will remain a mystery by the end of this biochemical introduction, the basic concepts for the generation of electric fields in the brain should be laid out.

1.1.1 All cells manage a potential difference between the intra and extracellular spaces

Any animal cell exhibits a double layer of lipids and proteins surrounding and protecting its organelles. This layer, called the membrane, has the chemical and bio-mechanical properties of selectively favoring certain molecules to enter and exit the cell. Whereas oxygen and water molecules freely pass, charged or larger molecules passage is regulated by dedicated carrier proteins in that membrane.

Two main forces drive molecules around the aqueous extracellular and intracellular media. Firstly, the diffusion, enforced by a chemical gradient (i.e a difference in concentration of a given molecule across space). This force will drive molecules from where they are the denser to areas of lower concentration. Secondly, the electrical motion, forcing any charged molecule to move along current lines joining areas of different electrical potentials. This force will drive positively charged particles from higher potential area to the lower potential area, and negatively charged particles reversely.

If the membrane was permeable to any molecules, the potential difference and the concentration difference between the intra and extracellular media would cancel. The ion permeability selectivity of the membrane allows for a

potential difference at the membrane, called resting membrane potential. This potential difference can be altered by the activation (voltage or signaling dependent) of protein channels that let ions follow their electrochemical gradient, or protein ion pumps consuming chemical energy to force given ions to pass though the membrane against their electrochemical gradient.

For any cell, this energy is stored in the form of an electric potential energy (voltage) and can be used by any protein in the membrane to achieve a given operation. A radically different usage of this energy is possible, such as in the case of muscle cells and neurons, where this variable potential difference (polarization / depolarization of the membrane), is turned into information to transmit from one cell to another.

The membrane voltage is always measured as the difference of potential between the intra and extracellular media ($V_m = V_{intra} - V_{extra}$). At rest, the resting membrane voltage (V_m) of human neurons is measured at about $-70mV$, and is said polarized. A depolarization [1] of the membrane implies inverting the polarization of the membrane towards a more positive voltage. The re-polarization, implies the return of the voltage to resting membrane voltage. A hyper-polarization, implies increasing the polarization, i.e. increasing the measured voltage towards values more negative than the resting membrane voltage.

1.1.2 Neurons convert membrane potential differences into trains of action potentials

An action potential is a strong and brief (about one-thousandth of a second) reversal of electric polarization of the membrane [2]. It is followed by a refractory period during which the neuron cannot repeat an action potential. While a depolarization may trigger an action potential in most neuronal membranes, an hyperpolarization will not.

These action potentials are usually elicited by the activation of Na^+ / Ca^{2+} (and other) voltage gated channels, opening below a certain membrane voltage threshold. Na^+ ions flow inside the cell with their electrochemical gradient mostly influenced by the concentration gradient. This depolarization (the action potential) propagates along the axon of the neuron, down to the synapses.

The modalities of the conversion from membrane potential difference to action potential are diverse. While some neurons integrate the input: an increase in activation will increase the action potential firing rate of the neuron (up to a rate fixed by the refractory period), other will filter the input: a timely activation (at the rate of the subthreshold membrane oscillation (1.2.1)) of these neurons will optimize their firing.

1.1.3 An action potential either triggers an excitatory or an inhibitory post-synaptic potential

Depending on the neurotransmitter discharged by the synapses, it may either have an inhibitory (contributing negatively to the elicitation of an action potential) or excitatory (contributing positively to the elicitation of an action potential) influence on the neurons they are bound to.

A large number of channels must be opened so that a neuronal cell triggers an action potential: it involves possibly hundreds of synchronous neuronal cells and excitatory neurons must release their neurotransmitters approximately together. Because a neuron from the central nervous system can be innervated by up to thousands of synapses, each of these inputs acting as either excitatory or inhibitory, it makes the complexity of the brain as a system even greater.

While this complexity is overwhelming, correlates / condensates of this machinery emerge at larger scales offering meager although useful perspectives on the system, such as event related potentials and brain oscillations.

[1] the prefix "de" is to be understood as inverting, and not removing

[2] depolarization, followed by repolarization, then by hyperpolarization and return to initial resting membrane voltage

1.2 Oscillations in the brain

Oscillatory systems are observed all over the brain, at different scales: from the membrane of a neuron [71], to the interacting regions within a neuron [222], or even within networks of neurons [231]. A system is said oscillatory if some of its inner variables / properties (e.g., membrane potentials, currents, calcium concentrations...) are periodic with a well defined period [71]. A period is defined as the time required by the property to return to the same state (one oscillation). For periodic signals, it is the time between two successive maxima. Initially, oscillations were termed waves [5] (and still are), for their oscillating shape, the fact that they propagate, and that they can be measured far from where they originate.

Devising models for the generation of oscillations that are macroscopically observable requires investigating the possible links between oscillations at different spatial and frequential scales.

1.2.1 Sub-threshold membrane potential oscillations

At the (arguably) smallest scale stand subthreshold membrane potential oscillations, which are difficult to measure in-vivo (let alone with scalp EEG setups). They are a good starter for obtaining hints on what make neurons sensible to oscillating behaviors, how oscillations emerge and how they can be put to use. They occur in such a wide range of cells, and provide a determinant means of influencing the oscillations of a large number of cells, such that they could determine the frequency of network oscillations [311].

These oscillations share a common dynamic. They either develop after an excitatory input, or are emitted constantly in some neuronal cells. The peak amplitude of such oscillations is small (of the order of 5mV [101]) with respect to spike amplitudes.

A large diversity of neurons, after electrical or chemical stimulation, display dampened oscillations at various frequencies in the subthreshold range of their membrane potentials. In vitro studies revealed these oscillations in :

- the inferior olivary neurons (located in the medulla oblongata) of guinea pigs: their oscillations occur in the 3-10Hz band and depend on external voltage and calcium concentration [20], [155];
- the magnocellular neurons of the rat supra-optic nucleus (located in the hypothalamus) (10-70Hz, spontaneous, Na+ voltage dependent) [33];
- the stellate cells of layer II of the entorhinal cortex ($\approx$ 10Hz, voltage and Na+ dependent)
- as well as neurons of the deep layers of the entorhinal cortex (10Hz or 20Hz, voltage and Na+ dependent) [266],
- or half the neurons of the frontal cortex of guinea-pigs ($>$ 6s of depolarizing pulses, voltage dependent, 4-20Hz) [101].

Not only are there a common dynamic, they are also powerful. They offer a mechanism for timing control in which action potentials are more likely to occur during peaks than throughs. The cerebellar Purkinje neurons are spontaneously active, and thought to encode timing signals in the rate and pattern of their activity [334]. Minimal changes in the membrane potential at the proper frequency can trigger an action potential. This selectivity is called resonance [119].

1.2.2 Local Field Potential (LFP) oscillations

It is not possible to track the activity of an individual neuron in the inter-cellular space, for they are too many and their activities mix up. In vivo neurophysiological studies and applications most often measure the mass activity

of neuronal microcircuits: the Local Field Potential (LFP). The LFP is the electric potential of the extra-cellular space (in between neurons and inter-neurons). To fill the gap between individual neurons firing and LFP, a large body of neuroscience research focuses on the relationship between LFP and neural discharges as it is central to understanding the type of information carried by oscillations [58].

The LFP integrates all the transient electrical events occurring in the neighborhood of a measuring electrode. It is usually distinguished from multiunit activity (reflecting axonal firing rates) as the lower part of the frequency spectrum (< 300 / 400 Hz). Hence, it represents slower events, reflecting cooperative and independent activity of close-by neurons in the form of synaptic potentials, after-potentials of somatodendritic spikes [100], and voltage-gated membrane oscillations [232].

These synchronous discharges can occur as single events (i.e.: ponto-geniculo-occipital waves generated in the brain stem), or repetitive events. In the latter case, they give rise to oscillatory field potentials [277].

Could these LFP pathlines, driving the ions in the extra-cellular medium, play a role in neural communication ? According to Tiganj et al. [306], computational models of the CA1 and CA3 pyramidal cells, suggest that the contribution of these oscillations are too weak to be responsible for a dedicated communication mechanism, by opposition to the effect of transcranial magnetic stimulation or perhaps epileptic seizures. Which does not rule out that they can stochastically perturb communication.

1.2.3 Large amplitude oscillations at the scalp

The cooperative activity of neuronal cells is not sufficient to elicit a strong LFP standing out at the surface of the scalp. Spatial factors enter the equation: the distribution of co-activated synapses, the neuronal morphology, and the architectonic configuration of the cell population [77]. Despite a given topology for a neuron, it may operate as many different sources of current with varying geometry, depending on which of the connected synapses are co-activated [111]. The variety of electrical geometries impact the orientation and the range of the source as it depends on which multi-pole type it behaves like (varying attenuation with distance) [240] 2.1.

Pyramidal cells are radially oriented in the neocortex. They are present in its most external layers and the closest to the scalp. Oscillations measured at the scalp level are therefore mostly generated by pyramidal cells, whether they are the drive or not.

These oscillations at the scalp appear to follow the rule that the amplitude of the fluctuations decreases with increasing frequency of the oscillation. Oostendorp et al. [203] challenges the idea that the skull can act as a low pass filter for frequency comprised in the 100 - 10 kHz range. According to Singer [277] the explanation could come from the fact that it is the small cell assemblies that oscillate rapidly, while bigger cell assemblies oscillate slower. For this reason and the small solid angle at which they would appear to the electrode or the coil, the activity of a small synchronously active population of neurons is unlikely to be observed from the scalp.

1.2.4 Brain rhythms are oscillations at dedicated frequencies and locations

The denomination of the brain rhythms follows the historical course of their discovery, starting with the α rhythm identified by Berger [21] in 1929. They are currently mostly used to describe the frequency at which they oscillate, so that α rhythm means from 8-12Hz, regardless of the location. This denomination is rather coarse: it is not always spatially relevant, and lacks frequency accuracy. The reason for the frequency inaccuracy is likely the frequency variability of cognition related rhythms across subjects. Spatial inaccuracy is due to the difficulty in localizing brain oscillating sources with scalp recording. Ensues a classification of brain rhythms based on frequency alone (or as first discriminant) that is sometimes difficult to follow.

The origins (drives) of these oscillations have been a long lasting topic [165], and still have a lot of unknowns. As a rule of thumb, the slower rhythms (sleep spindles [184], α rhythms...) are attributed to functional relationship between the thalamus and the neocortex [287]. Faster rhythms have been linked to the behavior of GABAergic

interneurons [95], due to the response of these oscillations to GABA_A [3] blockers and / or the consequence of local interactions.

δ rhythms (1.5 - 4 Hz)

δ rhythms are also termed cortical slow waves. They have mostly been associated with the deep stage 3 of NREM (Non-Rapid Eye Movement) sleep and anesthesia. Variations of the δ rhythm have been observed, notably during concentration tasks, where the rhythm increases in frontal areas. For more details, [140] provides an extensive review on the δ rhythms.

Origin The motor of the δ waves has not been consensual, while some works [288] favor the interactions between thalamic and cortical circuits, other studies using localization techniques from electroencephalographic recordings suggest these rhythms may originate from the frontal ventro-medial-prefrontal areas. While it is possible that delta oscillations are generated in the cortex alone (Capone et al. [44] show slow waves oscillation in cortical slices), it remains plausible that the control of the rhythm is achieved through ascending cholinergic (acetylcholine mediates both excitatory and inhibitory effects) subcortical–cortical projections from the thalamus [289].

θ rhythms (4 - 8 Hz)

θ rhythms are present in the hippocampus: the Type 1 θ ($\approx$ 3.5 Hz) is associated to wakefulness and voluntary movements (such as walking) [90], while the Type 2 θ ($\approx$ 6.5 Hz)is associated to desynchronized sleep. The θ rhythms also appear in the frontal midline electrodes of EEG setups, in non pathological subjects θ waves appear in short bursts, high frequency, low voltage and regular waveform, with amplitude peaks at electrode Fz. As a side note, Maulsby [178] remarks that affective emotional stimuli in infants trigger rhythmic θ activity.

Origin Gemma et al. [90] study shows a positive correlation between the type 1 θ (atropine resistant) activity and the levels of serotonin. This suggests that part of the hippocampal rhythmical slow activity is generated by a serotonergic mechanism.

α rhythms (8 - 13 Hz)

At coarse grain, α rhythms are inhibition rhythms. As example: in the sensorimotor cortex, α rhythms are thought to strongly inhibit spike timing (relative timing of a neuron's output and input action potentials) and firing rate. Firing rates of neurons increase with a decrease in α-power during a vibrotactile discrimination task in monkeys [103]. α magnitude decreases with attention [230], it predicts better discrimination tasks performance [103], or correlates with enhanced sensory processing [13]. There exists a positive relationship between event-related α desynchronization [4] and cognitive performance in tasks that specifically require semantic memory or long-term memory (LTM) performance [139]. Finally, α rhythms can be top-down [5] inhibitory control markers [139].

Origin Da Silva et al. [53] supposed early that a thalamic drive for α waves was unlikely because of the variety of α rhythms. Halgren et al. [104] prove that unlike sleep spindles, α bursts during quiet wakefulness are driven by the cortex (in line with previous work and the α thalamocortical loop).

[3] GABA_A receptors are ligand-gated ion channels while GABA_B receptors are G protein-coupled receptors.
[4] reduction of signal power in the α band
[5] Top-down attention refers to "internal guidance of attention based on prior knowledge, willful plans, and current goals" [132].

μ rhythm (8 - 12 Hz)

Often considered part of the α rhythms, because of its oscillating frequency of about 10Hz, the μ rhythm is located over the sensorimotor cortex. It traduces the synchronization of neurons in the motor cortex regions. It is distinct from the occipital and parietal α rhythms [148] and identical to the SensoriMotor Rhythms (SMR) observed in felines. It is disrupted by input to the somatosensory system [148]. In humans, the μ rhythm can also be called SMR [188].

Origin The neural mechanisms regulating the μ rhythms were not elucidated at all until 2009 [130], since a lot remains to be understood (their implication in movement preparation for instance). Interestingly, it would seem that the μ rhythm is related to the sympathetic activity (of the autonomic nervous system) regulating heart rate, due to the negative correlation between μ cortical sources of low-frequency β rhythms and the low-frequency band power of tachogram spectrum [309].

σ rhythm (12 - 14 Hz or 14 - 16 Hz)

The σ rhythm is mostly associated to sleep. Sleep spindles bursts last between 0.5 and 2 seconds [227].

Origin By opposition to the parieto-occipital α, σ bursts are driven by the thalamus Halgren et al. [104].

β rhythms (13 - 30 Hz)

β oscillations occur as brief and variable bursts [168] [76], they are thought of as a default state, interrupted by encoding and decoding of sensory information.

β oscillation's power increases over the sensorimotor area during stable postures, after movement or even imaginary movements, while they are reduced during the movement itself [137]. Similarly to the α rhythm, the β power typically reflects changes in the probability of beta bursts [19] [264]. They occur immediately after evoked gamma oscillations in sensory evoked potentials [142]. For these reasons, β rhythms appear as inhibiting rhythms.

They were proposed as a medium to protect from sensory information interference during a working memory task, as well as a "clear out" afterwards [264]. A decrease in β event related synchronization in neural networks could serve working memory maintenance [82].

According to [280], β-synchronization is a "mechanism for the formation of functional neuronal ensembles during endogenous (re)activation of cortical representations", in accordance with [319]. This mechanism is involved in top-down attention, visual working-memory attention and working memory maintenance.

Palacios-García et al. [208] also observe an increase in β activity during top-down modulation. Top-down attention is impaired during a β TMS experiment targeting superior-precentral and intraparietal sulci [239]. This implies that β oscillations in these sulci participate to the voluntary allocation of attention in goal driven tasks.

Origin The supposed mechanisms for the generation of β occur in the basal ganglia and the cortex [264]. They are mostly studied in relation to the Parkinson's disease [29]. β rhythms can be artificially produced by lowering gamma activity with barbiturates. This is only visible in isolated interneuron networks [332]. β rhythms in excitatory neurons can be coherently sustained by gamma rhythms in interneuron networks [331].

γ rhythms ($>$ 30 Hz)

The γ rhythm was first observed in the hedgehog and the cat olfactory bulb [4], and only later, on multiple occasions in the primary visual cortex (for a review on γ oscillations in the visual cortex see: [106]).

In rodents, CA1 (entorhinal cortex) γ oscillations are involved in providing information about object and place recognition [43]. Studies on rat vibrissae led Ahissar and Kleinfeld [6] to consider at least in part that cortical oscillatory activity is generated independently to measure the input periodicity. The thalamic relay neurons would serve as phase detectors.

The role of γ rhythms is not restricted to these faculties. In humans, the neocortical 35–45 Hz γ rhythms increase in early age and stabilize around the age of five, especially in the frontal areas. It is associated to long-term memory and cognitive task performance, both relatively modest in the first years of life.

Other studies link γ oscillations to sound perception and linguistic stimuli [238], REM dream states [162], attention, movement and perception [9], face recognition [243].

But overall, γ oscillations play a role in the integration of various sensory stimuli and possibly internal representations. γ rhythms are often related to bottom-up attention [6]. They could support the binding of different functional areas of the brain to create coherent representation of objects [226, 294, 295].

Origin Their generation involves a complex system. In the primary visual cortex only, γ rhythms of different origin coexist [106]. It is known that interneuron networks alone can generate gamma oscillations [308] [332]. Nonetheless, Ribary et al. [238] suggest, with magnetic field tomography that auditory related 40Hz oscillations would be generated within a thalamocortical network.

1.3 Synchronization / Synchrony / Desynchronization of neuronal assemblies

Neurons and neuronal assemblies are physically interconnected: locally (within a cortical column), and at range between columns. This implies that the simultaneous activation of a certain population of neurons at a given time may lead to the activation of another certain population of neurons at some later time. In case of loops in this circuitry, such as the thalamocortical loop [28], or even within a cortical column, oscillations can arise. The oscillation within a cortical column can also be transmitted to other regions. The small-world topology [327] of axonal connections within the brain allows at the same time the segregation and integration of functional relationships of cortical units.

1.3.1 Definition

Disambiguation

Synchronization and synchrony are two terms that are easily used in place of the other. Their disambiguation provides a richer description of the events at hand by proposing a larger panel of terms, each with a distinct meaning. Synchrony should be a state, which lasts after a process of synchronization, and before a process of desynchronization. Synchronization not only defines the passage from desynchronized (not in synchrony) to synchronized (in synchrony), but also the process (the means involved, the speed at which it synchronizes...). In that sense it may corresponds to the adjustment of rhythms of dynamic oscillators [246] due to their interaction.

[6] "Attentional guidance purely by externally driven factors to stimuli that are salient because of their inherent properties relative to the background" [132])

Etymology

Initially used in the french language by Raymond in 1827 as the "art of comparing, reconciling the dates of history", and by Ferdinand de Saussure in 1916, as "synchronie" to describe the study of language at a specific point in time (as opposed to diachrony). The term adopted a more general usage, in alignment with the Greek construction of the word : *syn-* with, together, in accompany of; -*chronos* time, duration. An even more general sense is given when establishing synchrony in sciences, where it does not strictly mean "at the same time", but "linked to the same task".

Definition

The concept of synchrony was already a subject of interest in ancient times, maybe as far as the Egyptian history goes. Pythagoras of Samos (ca. 570–495 BC) studied the structure of the cosmos, later theorized as the Music / Harmony of spheres [261]. Tidal locking of low orbiting spherical objects, is an example of synchrony: because the rotation of the moon around the earth is synchronized with its own self-rotation, one face of the moon is always hidden from us.

In the field of neurosciences, synchronization was initially used to describe high-amplitude events reflecting large neural populations firing within the same cortical areas such as in seizures or mid-line anterior theta bursts for "hedonic hypersynchrony" in children [178]. Brain activity can be partially modeled with help of dynamical oscillating systems. Hence, the study of synchrony between brain areas in that perspective is possible and relevant [164]. In dynamical system theory terms, two dynamical systems X and Y are said to be synchronized if there exists a continuous function (two close points in X on the attractor of X, are also close in Y) that can predict the state of the system Y given X [283]. The theorization and development of synchronization and synchrony in the frame of chaotic oscillators led to the mathematical definition of generalized synchrony [253], which encompasses possible linear or non linear relationships. The relationship between the many variables of possibly many systems being of many possible kinds makes the space search for relevant synchrony measures extremely large. Preferred relationships have been put forward as good descriptors of synchrony describing functional relationships. As an example, Rosenblum et al. [245] define the phase synchronization of a chaotic system as the occurrence of a certain relationship (a function F) between the phases of interacting systems, neglecting any possible relationship concerning the amplitudes. It is worth noting that the notions of phase and amplitude of chaotic systems are non-trivial [245], and partly detailed in chapter 3. An extended definition of synchrony, in the frame of neurosciences, is that the similarity of a property between a given set of systems implies a possible functional relationship between them.

Brown and Kocarev [37] propose a generalized work-flow to identify "synchronization" (synchrony) that goes beyond the scope of chaotic systems, which is composed of four tasks : 1) Separating the dynamics of a large dynamical system into the dynamics of subsystems 2) Measuring properties of the subsystems 3) Comparing properties of the subsystems 4) Determining whether the properties agree in time.

Despite the highly stochastic and far from predictable spiking discharges of individual neurons in the cortex, collective network dynamics manage to emerge from synaptic circuits. One can learn from *in vitro* or *in silico* experiments on few neurons, before attempting to interpret synchrony at the high end level of the scalp measurements.

1.3.2 Synchrony at the level of neuronal cells

Two groups of neurons, firing each at different but similar rhythms, can synchronize within a few cycles at a zero phase delay [277]. Wang and Rinzel [322]'s model of mutually inhibiting neurons with post-inhibitory rebound responses (such as most neurons in the thalamic relay nuclei and of the thalamic reticular nucleus) shows that oscillations can arise with as few as two neurons, and that this synchronization does not depend on a conduction delay. This specific properties of the membrane only occur in some neurons, and is possibly the result of a specific genetic expression. It may play a role in compartmentalizing certain functions, such as centralizing cortical

inhibition drive in the thalamus.

In the primary visual cortex of the cat, distinct neuronal populations oscillate at 40Hz, but asynchronously from one another. Only for certain stimuli, these populations synchronize at a zero phase delay [74]. This synchronization can be observed within a cortical column, but also between columns with on average no phase delay [96]. Ultimately, homologous left and right visual cortical areas can also synchronize their discharges at zero phase delay. According to these findings, it appears that the participation of a neuron to a given task may be dictated by the synchrony at zero phase lag with other neurons of the assembly. It is a complementary or adversary theory to population coding [278], in which the participation of a given neuron to a particular mental task is dictated by the context set by other neurons of the assembly.

In Traub et al. [308] *in silico* experiment, a model of network of neurons that would account for the generation and synchronization of the 40Hz rhythms is developed. The model produces "gamma oscillations that are synchronized on a millisecond timescale from one end of the chain to the other", and predicts that pyramidal cells and at least some interneuron spikes should occur with near-zero phase delay. While it appears reasonable for medium distances (conduction delays of up to 20ms), it has been debated that this model could synchronize brain areas over long distances. The coherence of fast rhythms is spatially limited [290].

Wang et al. [325] suggests that the electrotonic coupling of pyramidal cells plays a unique role in the generation of neuronal synchronization in the neocortex : they measure a high junctional conductance, which permits the direct transmission of action potentials and even tonic firing between coupled neurons.

The coherent oscillation of a large population of neurons implies its synchronization at about zero phase delay. There is for this reason a terminology overlap (oscillation / synchronization) in the literature. An Event Related Potential is categorized either as an Event Related Synchronization, or as an Event Related Desynchronization, but is seen, on the electroencephalogram as an oscillation at possibly only one electrode site. A variation in EEG power within a given frequency range translates into the synchronization of neuronal cells, not necessarily into the synchronization between distant brain areas. The synchronization between distant brain areas, observable with scalp EEG, is usually termed "long-range" synchronization.

While synchronization seems to play a major role in communication, it is not the only mechanism: spike timing, rate coding, rank order coding, phase coding... are also to be considered when appropriate (motor control for instance) [315].

1.3.3 Occurrence and interest of synchrony in cognition

The versatile cognitive capacities of the human brain require the neural activity across this (these) widespread small-world brain network(s) to coordinate efficiently. Notably, temporal binding theory (appropriate binding of event related multisensory inputs and segregation of the others) assumes that synchrony between distributed neurons is required for object representation, response selection, attention and sensorimotor integration [66].

Koralek et al. [143] show that temporally precise coherence appears during learning in output-relevant neuronal populations and thus suggest that correlations in oscillatory activity serve to synchronize widespread brain networks to produce behavior.

The interest in oscillations and their synchronization takes root in the possibility that these precise spatio-temporal relations are a fantastic proxy over the complexity inherent to the activity of billions of neurons relayed by their trillions of synaptic connections, considerably reducing the dimensionality of the problems.

θ long range synchrony

θ synchrony (measured as across-trials coherence in [258], which is described in 2.3.2) between prefrontal and posterior electrodes is found during retention (between perception and reproduction) intervals. A transcranial magnetic stimulation experiment [182] stimulating either the frontal or the sensory area shows that only the

stimulation of sensory area disrupted the working memory task and therefore that this network in unidirectional (from sensory to frontal area) and likely bottom-up (rather than top-down).

Decision based behaviors require the integration of distinct cortical area. In a maze-based experiment, [129] measures correlation in firing rates between CA1 in the hippocampus and medial prefrontal cortex. These two structures notably synchronize during the choice phase of a task.

α long range synchrony

While long range synchrony in the α frequency band is generally attributed to inhibition processes, few studies were identified to specifically study synchrony between distant areas in that band of frequencies.

Outside the scope of inhibition, Von Stein and Sarnthein [319] notice long range fronto-parietal interactions during working memory retention and mental imagery in the α band. In the same fashion, Sadaghiani et al. [255] identify a "well defined intrinsic functional connectivity network" related to the upper α band involving the frontal and parietal lobe regions.

β long range synchrony

Low β (12-18Hz) synchronization between temporal and parietal could be involved in multi-modal semantic binding [319]. Schmiedt et al. [265] suggests that the generation of cortical β is driven by thalamic and/or top-down cortical inputs. Roelfsema et al. [244] correlate β activity with the long-range synchronous activity of neocortical regions during visuomotor reflex activation. Palva et al. [211] suppose the inter-area (long-range) phase synchrony in the β (, α and γ) frequency bands among frontoparietal and visual regions could be a system level mechanism for coordinating and regulating the maintenance of neuronal object representations in visual working-memory.

γ long range synchrony

Although γ oscillations were mostly attributed to local synchronization [142], some studies relate possible long range coordination.

Bhattacharya et al. [26] observe in EEG recordings a γ-band phase synchronization between posterior and frontal cortex during mental rotation in humans. In Bhattacharya et al. [27] long-range synchrony is found to be higher in musicians while listening to music. Ribary et al. [238] observe during audio stimuli, with magnetic field tomography, a 40Hz coherence between cortical and subcortical sites "with a time shift that is consistent with thalamocortical conduction times. Rodriguez et al. [243] measure γ (40Hz) long range synchrony related to face perception (by opposition to meaningless shapes).

Traveling and Standing waves

The discovery of traveling waves may be accredited to Nunez [196] who described a wavelike shape of the alpha component along midline scalp EEG electrodes.

The role of traveling waves in cognition Traveling waves have been observed intracortically on many occasions. Probably firstly observed by Adrian and Matthews [5] in the cortex of cats and rabbits, it has since been revealed in the hippocampus [167], as well as in the visual cortex [313]. More recently, Zhang et al. [344] observed traveling waves all over the cortex with intra-cranial EEG analysis in θ and α band for epilepstic patients. These traveling waves are organized into oscillation clusters, and are behaviorally relevant.

According to Patten et al. [215], these waves travel mostly either from occipital region to frontal regions, or reversely. As waves traveling in multiple directions cross each other, their either damp out or interfere, it is thus expected that the patterns might be more complex. Visser et al. [318] theorizes that the cortex being homeomorph (topologically identical) to the sphere and thus closed on itself, it could be assumed that traveling waves, as they interfere, form standing waves, a concept shared in [112]. However, no strong experimental evidence for "standing waves" was reported [312].

Nunez [196] correlated the speed of the wave to the frequency of oscillation : "high alpha frequency components (alpha + 1.5 Hz) have shorter midline wavelengths than low alpha components(alpha - 1.5 Hz)", i.e. fast oscillations propagates faster. This property was extended by Patten et al. in a study where propagation speeds of θ and α rhythms are compared during a Go-NoGo experimental paradigm.

Although they have been observed in the ongoing brain activity, traveling waves also can be evoked ([112] : semantic judgment task).

Due to their ubiquity, these traveling waves have been proposed as coordinators, transferring or communicating information between different parts of the brain [215].

The motor and means of traveling waves As an introduction to [312], a short review classifies the different biophysical models that could account for the traveling waves : pacemakers (thalamic), local (cortical) and local-global (thalamo-cortical). They aim at describing what generates the rhythms, and how they propagate. The role of subcortial units on the general control and tuning of the activation of the brain was already suggested in [65]. Nunez [196] challenged the fact that it would be specific thalamocortical fibers that would account for the high spatial variability of the alpha field. Valdés-Hernández et al. [312] shows that white matter architecture rather than cortical surface area correlates with the EEG alpha rhythm. It opposes to a view proposed in [198] where the size of the head correlated to the position of the α peak.

Halgren et al. [104] proposed, based on ECoG and EEG depth recordings, that α bursts during quiet wakefulness originate from the cortex and reach the thalamus (pulvinar) afterwards, by opposition to sleep spindles.

Ito et al. [123] analyses the phase differences between electrodes positioned on the anterio-posterior axis. They observe two distinct cases of phase differences: an abrupt shift from 0 to π phase lag, or a positive phase shift from electrode to electrode from frontal to posterior areas. These correspond to the traveling and standing waves postulated by Nunez [196]. Halgren et al. [104] show with ECoG and EEG depth recordings, during quiet wakefulness, that the median speed of the α waves are of about 1 m/s (median speed across patients: 0.9134 ± 0.1563 m/s), while their propagation is prevalent along the anteroposterior axis [215].

Alamia and VanRullen [10] show that for predictive coding (a model in which the brain learns to make better predictions) to occur, given the biological temporal constraints, α traveling waves have to exist. They notably notice forward waves in humans attending visual stimulation and backward waves for participants with eyes closed, effect they say corroborate their model of predictive coding. Lastly, Patten et al. [215] correlate prestimulus alpha waves to reaction speed.

Alteration of traveling waves Traveling waves have been shown to be subject to alterations, episodically, and following long periods of meditation. As evidence, van Lutterveld et al. [314] shows statistical differences between a meditation group and a healthy group in centrality of minimum spanning tree (minimum number of edges connecting all the vertices of a graph). Also, Hebert et al. [109] shows that the speed of propagation of the α traveling wave is statistically different between TM (Transcendental Meditation) [7] practitioners and control group.

[7] Transcendental meditation is a meditation technique attempting to lower the brain activity. It is based on apprehending a word by its sound at different pitches rather than its sense. As the word is discovered through different pitches, until it is completely "understood", the brain enters a state of transcendence.

1.4 Epilepsy

Not only is epilepsy a handicapping disease widely spread among animal species, it is also difficult to treat in some human cases. It concerns an often underestimated number of people, more than fifty million: roughly one in a hundred worldwide [205] and affects people of all ages.

Epilepsy is not "one" condition but a "syndrome": it manifests itself over a wide range of symptoms, with different etiologies. The symptoms vary in frequency and severity, from less than one per year to several per day, and from the briefest lapses of attention or muscle jerks to severe and prolonged convulsions. They are categorized as either partial or generalized depending on the origin of the seizure. Partial seizures originate from a single location in the brain, the onset is said focal [214] whereas generalized seizures involve both hemispheres of the brain.

Epilepsies are also biased towards low income and / or tropical countries, especially those suffering from malaria and / or neurocysticercosis. In other countries with strong religious beliefs, people with epilepsy and their families suffer from stigma and discrimination. In developed countries, over half the incidence cases are partial [205] and about 60% of people with focal epilepsy have temporal lobe epilepsy (TLE).

Another overlooked, although important, aspect are the SUDEPs (Sudden Unexpected Deaths in Epilepsy). They are not caused by injury, drowning, or other known causes, but caused by either breathing, heart rythm failure, or unknown causes. They happen to about one in a thousand epileptic patient [305]. It is a concern of life and death for any patient and his/her family.

This altogether has lead to extensive extra and intra-cranial research on the syndrome, increasing in addition knowledge of the human brain. Epileptic brains are now decisively characterized by the presence of interictal epileptic discharges (IEDs) in the EEG and by epileptic seizures. The condition is characterized by cortical and/or thalamocortical hyper-excitability ([63]). Clinically, a subject is diagnosed epileptic after "two unprovoked seizures occurring more than 24 hours apart; or one unprovoked (or reflex) seizure and a probability of further seizures similar to the general recurrence risk (at least 60%) after two unprovoked seizures, occurring over the next 10 years or diagnosis of an epilepsy syndrome" [81] [80].

1.4.1 Temporal Lobe Epilepsy

Temporal lobe epilepsy (TLE) seizures involve the temporal lobe of the brain. They usually implicate small areas of the lobe, but highly connected such as the hippocampus and amygdalae. The hippocampus is a sea-horse shaped brain structure located in the temporal lobe [128]. It is strongly involved in learning and memory (especially long-term memory formation). The amygdalae are two almond shaped structures located near the base of the brain that participate to the management of emotional information [202], to memory and fight-or-flight response.

Mesial temporal lobe epilepsy

Mesial Temporal Lobe Epilepsy (MTLE) is the most common form of focal epilepsy (80% of all TLE) [298]. It involves the hippocampus, the parahippocampus, or the amygdala.

Hippocampal Sclerosis Hippocampal Sclerosis (HS) is a MTLE and the most common histopathological abnormality found in patients with drug-resistant TLE. In Blumcke et al. [31], of about 10 000 patients undergoing surgery: 36.4% had hippocampal sclerosis, 23.6% had long-term epilepsy-associated tumors and 19.8% focal cortical dysplasia. HS is present in 56% of cases of Medial Temporal Lobe Epilepsy (MTLE).

HS is characterized by a loss of neuronal cells, a granule cell dispersion, or a gliosis of the hippocampus, often localized in CA-1 or the subiculum. The subiculum is the hippocampal hub and gate to interegional communication [177] [282]. It consists in a large population of endogenously bursting excitatory neurons [16]. Therefore,

deregulation of this complex can greatly impact the activity of the whole brain.

Causes for hippocampal sclerosis epileptogenicity For LTLE, the impaired GABAergic signaling in the subiculum (hippocampus) could be the gate to secondary generalized seizures. In rodent models, the activation of subicular GABAergic neurons retards the generalization of the seizure by inhibiting the firing of pyramidal neurons, and degradation of GABAergic inhibition contributes to secondary generalized seizure expression [323]. It suggests that the malfunctioning GABAergic neurons of the subiculum are a possible bridge to secondary generalized seizures in temporal lobe epilepsy.

Alteration of ion channels / transporters in the neurons of the subiculum can result in the aforementioned impaired inhibition [8]. A study on Potassium / Chloride transporters [209] and a study on sodium channels [16], show respectively a default in inhibition of GABAergic neurons and a facilitation to hyper-excitability of the pyramidal neurons. Both conditions lead to hypersynchronous events.

Causes for hippocampal sclerosis The possible identified cause for HS are febrile seizures, genetic susceptibility, inflammatory and neurodevelopmental disorders [303]. The febrile seizures in childhood could damage the hippocampus and prime it for HS development later on. Notably, the prevalence of epilepsy in Alzheimer patients is higher than in healthy subjects.

Amygdala Enlargement Amygdala Enlargement (AE-TLE) differs from HS-TLE morphologycally and functionally. As in HS, the AE can be the epileptic focus. The enlargement consists in an augmentation of gray matter volume [297]. Patients presenting an enlargement of the amygdala sometimes suffer autoimmune encephalitis. On rare occasions, AE is linked to post psychological trauma epilepsies.

Lateral temporal lobe epilepsy

While TLE is often associated with hippocampal sclerosis [22] or to a lesser extent amygdala enlargement, the seizures do not necessarily originate from these regions [49]. Lateral Temporal Lobe Epilepsy (LTLE) corresponds to this specific case, where lesions in the temporal neocortex generate epileptiform discharges that preferentially propagate to mesiotemporal structures. Auras are often described in relations to these epilepsies: premonitory and epigastric sensations, olfactory hallucinations and automatic behaviors [118].

1.4.2 Alteration of brain structure

Kindling is a process by which a seizure or other brain event is both initiated and its recurrence made more likely, notably by lowering the threshold at which stimuli elicit electrographic seizures [94].

In Morgan et al. [183], the duration of seizure is associated with ipsilateral temporal lobe to a diminished connectivity between the contralateral temporal lobe, the precuneus, and the mid cingulate cortex in MTLE patients. This suggests a gradual functional isolation of the ipsilateral temporal lobe over the years [183]. Similarly, in an fMRI protocol, Haneef et al. [107] show a progressive reduction in connectivity diversity (variance of correlation between regions) over time.

Using Lévesque and Avoli [158] rodent kainate epilepsy model, Sheybani et al. [273] give more evidence that induced focal epilepsy is an evolving disease. The location of the sites from which generalized spikes and fast ripples are generated evolves with the disease. Also, the suppression of epileptic activity with TTX (Tetrodotoxin) at the stimulation site is not necessarily enough to suppress epileptic activity. This shows that a single epileptic focus can become a widespread disease [41]. These evidences are possibly in line with seizures still occurring after the resection of the presumed epileptic focus (up to 40% attributable to either incomplete resection of seizure focus, incorrect identification of seizure focus and recurrence of tumor [233], or distributed epileptic loci).

Notably, seizures can trigger in the developed brain the phenomenon of axonal sprouting [170], a common process in the developing brain.

In animals, Holmes et al. [114] observed that treating the flurothyl-induced limbic epilepsy with bumetanide not only freed the rats from epileptic behaviors but also restored the impaired functional connectivity (increased functional connectivity between the dorsal and ventral hippocampus and prefrontal cortex compared to control animals). This indicates that in certain cases, the damage is not structural but functional.

The alteration of brain structures is not necessarily observable with imaging techniques. The study of the changes in oscillatory activity can shed more light onto the effects of the disease, and relate them to cognitive alteration. Synchronous oscillatory activity between distant regions appears as an interesting lead to unveil some specificities of epilepsies, mostly because of the network dis-regulation property of some epilepsies.

1.4.3 Oscillations in epilepsy

Oscillations are one, if not "the", hallmark of brain activity. They offer a prism through which pathology is analyzed, and epilepsy does not escape the rule. This classification could allow to make parallels with healthy cognitive functions associated to the frequency bands of these oscillations.

δ rhythms (1.5 - 4 Hz)

δ rhythms occur in the epilepsy literature: post-ictal delta unveils the lateralization of the epileptogenic focus of TLE patients in 60% of cases [145]. Also, temporal intermittent rhythmic delta activity is highly specific for the diagnosis of complex partial epilepsy [195] (the most common type of epilepsy in adults, with seizures that can last up to 2 minutes).

θ rhythms (4 - 8 Hz)

Fu et al. [85] (in humans) and Ge et al. [88] (in rats) found that interictal spikes had a significant inhibitory effect on theta rhythm. Moreover, inhibition of the θ rhythm was greater when epileptogenic areas involved the anterior hippocampus and the entorhinal cortex [85]. The reduction of seizures during wakefulness and REM sleep could be explained by the increase of θ rhythm during these conditions [51].

α rhythms (8 - 13 Hz)

Links between the α component and epilepsy are scarce. In Abela et al. [1], slower α rhythm associates with poorer seizure control in epilepsy. It is specially in focal epilepsies, where the α power shift is even greater than for idiopathic generalized epilepsies.

μ rhythm (8 - 12 Hz)

Altered μ rhythms are rarely described or associated to epilepsy. Nonetheless, Saradzhishvili et al. [257] observe that the μ rhythm seems more disorganized when the epileptic focus is located in the temporal lobe.

σ rhythm (12 - 14 Hz or 14 - 16 Hz)

Sleep spindles are associated with an increase of interictal epileptic discharges [275]. In Tezer et al. [301], it is reported that sleep spindle density and power decrease before the first seizure. This decrease before secondarily

generalized seizures is less pronounced than before focal seizures.

β rhythms (13 - 30 Hz)

Focal beta activity on scalp EEG is a rare seizure pattern [34].

γ rhythms ($>$ 30 Hz)

γ rhythms are strongly linked to epilepsy, possibly because of the role of the hippocampus in temporal lobe epilepsy, and its implication in γ rhythms generation. These high-frequency bursts are an alternative marker for epileptic spikes [333]. In vitro, γ oscillations increase in frequency from the pre-ictal to ictal state [136].

1.4.4 Long range synchrony in epilepsy

The reorganization of the large-scale structural network in epilepsy in not clear [343], especially given the range of possible causes for epilepsy. A similar observation regarding the large-scale functional network can be made.

Nonetheless, intracranial electrode recordings allowed Warren et al. [326] to show a disconnection of the epileptic zone from the rest of the brain network. A similar finding arose in Lagarde et al. [152], who compared the connectivity inside and between epileptogenic / propagation / non involved zones, and found that there was a preferential coupling between epileptogenic and propagation zone than with the non-involved zone. In parallel, Englot et al. [68] observed a decreased resting-state functional connectivity in widespread regions, including perisylvian, posterior temporo-parietal, and orbitofrontal cortices. The degree of connectivity decrease correlates with longer duration and higher frequency seizures. Similarly, Luo et al. [169] observed, in a resting-state fMRI protocol, a reduced connectivity between the epileptogenic locus and distal regions (while augmented in the neighborhood).

1.4.5 Treatments

LTLE seizures are usually easily controlled with medication [67], while MTLE seizures are not.

AED (Anti-epileptic drugs)

A review concerning AEDs can be found in Sankaraneni and Lachhwani [256]. Interestingly, AEDs can at best only abolish the symptoms of seizures while under medication. They do not reverse nor stop epileptogenesis.

As an AED example, one may consider Diazepam. Diazepam is "effective in calming people who experience mild to moderate levels of anxiety, which could trigger epileptic seizures", and is mostly used as an emergency anticonvulsant. Its mechanism involves the interaction with GABAergic neurons. Diazepam alters hipocampal interneurons networks activity that produces gamma oscillations. It halves the frequency while doubling the amplitudes of the gamma rhythms [332]. Gamma EEG stands as a potential marker of underlying ion channel or neurotransmitter receptor dysfunction in primary generalized epilepsies [333].

Surgery

Although deemed safe, epilepsy surgery is associated with cognitive changes [272], mostly because pre-surgical screening of brain functions can only be partial. In a meta-analysis on surgical outcomes, Sherman et al. [272] note an increased risk of verbal memory and naming impairment with left-sided temporal surgery.

Neurofeedback

Brain cells and brain networks are malleable to some extent, which is the basis to learning. Training subjects to regulate specific brain patterns can diminish the frequency and severity of seizures. This topic is discussed at length in a further section 2.4.

Chapter 2

Measuring oscillations and oscillating systems in scalp EEG experimentations

This chapter provides a range of measures that help quantify the level of synchronization between brain areas based on their oscillatory activity. This oscillatory activity is well measured with ElectroEncephaloGraphy (EEG), therefore it brings details on how one can set up properly such experiments. These setups are employed in chapter 7 and chapter 6. This chapter also describes neurofeedback setups, and more precisely those that have been hailed as reducing the frequency and / or severity of epileptic seizures.

2.1 ElectroEncephaloGraphy (EEG)

Electroencephalography amounts to measuring potential differences between electrodes [87] resulting from neuronal activations and inhibitions.

2.1.1 EEG, one among many media for exploration: low cost, high time / weak spatial resolution

Instruments to measure the inner workings of the human brain are various, mostly providing indirect measurements. Some measure the electrical field generated by brain cells at different levels: electrocorticography (ECoG: grid of electrodes laid directly on the cortex), iEEG (needles with contact electrodes inside the cortex), EEG (electrodes at the surface of the scalp). Other instruments measure the magnetic field (MEG (coils at the surface of the scalp)). fMRI measures the blood deoxygenation (BOLD signal). New devices are still emerging, such as functional near-infrared spectroscopy (fNIRS) which captures the concentration of oxygen in hemoglobin.

All these instruments provide a wide range of information, either complementary or redundant, but mostly complementary. Of the non invasive tools at hand: EEG and MEG provide sub-millisecond accuracy, but low spatial accuracy (several centimeters), and only in superficial layers of the cortex (MEG to a lesser extent). MEG is mildly sensitive to radial sources, whereas EEG is much less sensitive to tangential orientations [7]. MEG will capture more of the activity of neurons located in folds (sulci), whereas EEG will capture more of the activity of the closest gyrus [281]. MEG provides a better SNR than EEG. Both can improve the spatialization of the electromagnetic sources by densifying the sensors, at the cost of increasing the preparation time of the experiment, and only to a certain extent (volume conduction in the case of EEG). fMRI on the other hand gives a coverage of the whole brain, at a millimeter accuracy, but the time sampling is usually of the order of the second. Invasive recordings provide information with a high SNR because of a smaller distance to the sources and reduced mixing [146]. But in the case of ECoG, only a fraction of the brain is usually covered. As with iEEG, the contacts

are usually sparse, and do not match from one subject to the other, as they are implanted with respect to the upcoming surgery needs. Moreover, in humans, they only are laid / implanted in impaired subjects.

Any measurement is valuable, any combination of measurements is even more valuable. But linking (making sense of) synchronous recordings of different kind is often a challenge. Eventually, the cost of experiment / treatment have to be considered. This cost concerns either the risks of the measurements (in the case of ECOG or iEEG), or the dependence on costly hardware (fMRI), or the dependence on costly consumables (MEG), or the scarcity of installations (MEG again). Because of the will of pushing neurofeedback in large scale usages, and despite all the aforementioned benefits of multi-modal analysis, this thesis work abides by medium resolution scalp EEG (21-32 channels) analysis alone.

2.1.2 Large amplitude potentials at the scalp have cortical sources: the pyramidal cells

The electrostatic sources generating the electrostatic potential are in the order of the number of neurons regarding their occurrence in space, and in the order of the number of connections between neurons / synapses regarding their occurrence in time.

Large amplitude potentials do not reflect action potentials (briefly introduced in section 1.1.2). Action potentials are brief events, moving along the axon at approximately 3m.s^{-1}, or the dendrites at approximately 0.5m.s^{-1} [156], and hardly sum up in a cortical area. They contribute mostly to noise in the EEG and cannot be modeled with simple electric dipoles. On the other hand, the post-synaptic potentials, i.e. the longer-lasting depolarizations / polarizations at the dendrites and soma are more likely to sum up and thus to be observed at the scalp in a macroscopically comprehensive manner [61].

Because the current generated by a single cell is too small to be discriminated from the ambient noise at the surface of the scalp, the synchronous activation of a large assembly of similarly oriented cells (open field [335]) in some mm^3 (10^4 neurons) of cortex is required [87]. The pyramidal cells of the neocortex qualify for this office. Not only the distance from the dipole to the electrode lowers the amplitude of the potential at the electrode, but also the angle between the direction of the dipole and the direction from the dipole to the electrode [259] [87]. Dipoles whose direction are radial with regard to the surface of the scalp are most likely produced in gyri of the cortex, whether dipoles with tangential direction are most likely produced in sulci [87]. This activation can be approximated by a dipole representation, whose activity is of the order of 10 nA [87].

Nonetheless, not every electrical field generated by a summation of post-synaptic potentials can be observed at the surface of the scalp. The application of the Maxwell equations by Elbert [64] to a spherical onion with homogeneous layers (a simplistic model of the head) provides insights into what can and what can't be measured from scalp electrodes. Sub-cortical structures activity can rarely be measured from the scalp because they are too small and too distant from the scalp, and it is not possible to distinguish an extended superficial cortical source from a more focal one in deeper structures [64]. Event Related Potentials (ERPs, such as the P3 (P300) or the Contingent Negative Variation (CNV)) are strong ($> 10\mu V$) positive or negative shifts in polarization observed at one or more scalp electrodes. They occur when a large number of neuronal cells, oriented in a similar direction, have ions flowing in a specific direction. The larger ERPs have electrical sources distributed in extended cortical regions ("an active, but small, planar area, with a diameter of 1 cm contributes about 1/25 of the activity shown by an extended layer 10 cm in diameter" [64]). Depending on the nature of the stimulation (excitatory or inhibitory), and the location of the stimulation on the cells, the direction of the flow of ions can be reversed. In other words, excitatory or inhibitory activity cannot be assessed from polarity at the scalp [124]. Lastly, the depth of the activation / inhibition cannot be assessed from scalp EEG either, because the distance to the electrode and the number of synchronous post-synaptic potentials can hardly be disentangled. Therefore, the EEG alone cannot help assess much of the diverse possible characteristics of the underlying process. To nuance such claims, approaches of source localization based on EEG exist. They provide meaningful results, especially on dense EEG setups (LORETA [213] or beamformers [330]), and to some extent to sparser EEG setups [171].

2.1.3 EEG amplifiers

To limit the influence of the noise that is introduced by induction in the wire from the electrode to the amplifier device, the active electrodes will increase the amplitude of the signal at the electrodes. To remove the problem of induction noise from the amplifier to the processing device, the signal is digitized and stored on the amplifier (which has a small digital memory (RAM)). It is sent by packets to the processing device when requested, through the use of a dedicated application programming interface.

2.1.4 EEG electrodes

The first electroencephalograph on humans was recorded and published by Hans Berger in 1929 [21]. Although the technical means have evolved (to some relatively reasonable extent), the principle has remained the same over the years.

By Ohm's Law:

$$U = Z * I$$

where:

U is the voltage
Z is the impedance
I is the current

, high electrode impedance cause voltage measurement errors when electrical current flows through the electrodes. Reducing the electrode's impedance mitigates this source of noise. EEG electrodes can be divided in active or passive and wet or dry types.

Passive electrodes With passive electrodes, the impedance can only be reduced by optimizing the contact between the scalp and the electrode. In the case of passive dry electrodes, the impedance is high, and currents unrelated to neuronal activity flowing through the electrode strongly impact the voltage between electrodes. In the case of wet electrodes, the application of conductive gel at the surface of the skin decreases the impedance, and thus reduces the voltage due to the noisy currents. The most common way of wetting the electrodes is either with saline solution (short duration experiments), or conductive gel (longer to very long experiments). The quality of the conductive gel conditions the duration of the experiment (hours or days). The choice of electrodes depends on the experiment: active dry electrodes can be sufficient to measure ERP albeit with increased level of noise [176]. These electrodes are already used in ecological situations, despite muscular artifacts generating a lot of noise (figure 2.1.6); such as in mobile brain/body imaging (MoBI).

Active electrodes Active electrodes add an active amplification stage right at the electrode transforming its impedance [180]. They consist is an amplifier circuit, controlling its input and output impedance. To limit the current flowing through the electrode a high input impedance is required as well as an extremely low output impedance. Active electrodes therefore eliminates interference currents flowing through the electrode. The amplification stage minimizes the noise to signal ratio to disregard the noise captured by the wire running to the amplifier. Active shielding, on the other hand, is also called "guarding", and is a technique used to minimize current leakage from a high impedance source.

Ground electrode The ground electrode is an extra consideration for the security of the subject as it controls the potential leakage that could occur in case the insulation of the amplifier from the Alternative Current (outlet) was to fail. It triggers a security system which may differ from amplifier to amplifier. Nonetheless, optical coupling within the amplifier makes the experiment 100% safe.

2.1.5 Referencing

Isolated populations of neurons act as a source (multipole) (described in section 1.1). The electrical correlate of this activity is a potential field. Because an absolute electrical potential cannot be measured, one must introduce a reference electrode in the setup. This reference electrode is used to measure the potential difference with all the other electrodes [87]. Choosing properly the reference electrode(s) and referencing is a matter of first importance, and one of EEG's main limitations [91].

If the common reference is any electrode on the scalp, the raw values provided by the amplifier are hardly intelligible, since they vary from one arbitrary choice or the other, unless they are chosen carefully and documented.

Common reference montage The EEG signal can be measured between one electrode located in the electric field of a cortical region of interest, and another reference electrode, as silent as possible, with respect to the brain properties under analysis. Since silent electrodes do only exist in theory, there will always be some noise. What matters is that the properties of this noise are not mistaken for brain properties involved in the process of analysis.

Bipolar montage A short distance bipolar montage allows to measure the difference of potential between pairs of electrodes located in the same electric field of neural area of interest. Their instantaneous difference is due to the different geometries with the activated/deactivated population of neurons, the variation of this difference is a good indicator of the dynamics of the neural area of interest. In other words, "if the paired electrodes are close together, then the data can be interpreted as an estimate of the first spatial derivative in the direction along the line from one electrode to the other"[75]. Bipolar longitudinal referencing is a common practice in neurology. It amounts to computing local potential differences. By opposition, long distances potential differences on the scalp are used when attempting to prove a flat EEG to ascertain death before, for instance, the removal of organs.

Average reference montage This montage amounts to re-referencing all the channels to the average.

Bertrand et al. [23] theorizes with the head modeled by a sphere and sources as dipoles inside this sphere, that the average of potentials differences measured on the scalp (sphere surface), is zero, for a sufficient sampling. For obvious reasons EEG caps cannot cover the whole head and this theory is not observed in practice.

2.1.6 Filtering external noise

Filtering Artifacts

Artifacts are the manifestation in electroencephalographic signals of the environment (line noise...) or events (blinks, heart beats, muscular contractions...) that are not relevant to the study. Any computation or analysis of the brain electrical activity may be impaired by such unsettling perturbations.

Some artifacts can be detected and filtered out. Because they differ in nature, there is not a single method to handle each artifact. Sometimes they can be detected but hardly removed or large portions of the signal would have to be ignored (such as ample muscular artifacts).

In figure 2.1, different frequency spectra are computed over periods of 20s for: eye blinks, jaw clench, head movements and swallowing. They are compared to a baseline signal (averaged over 6 periods of 20 seconds), in the eyes open fixation condition. The baseline displays a 1/f trend with a moderate bump between 11 and 12 Hz. Eyes blinks are greatly energetic compared to the baseline, especially at low frequencies; the 1/f rule is not valid for low frequencies. Jaw clench is slightly more energetic than the baseline, but for all frequencies. Head movements and swallowing mostly impact the lower end of the frequency spectrum.

From these observations, all frequencies are subject to energy increase during the artifacts period, regardless of the artifact. Therefore the analysis of the signal during the occurrence of one of these artifacts must be done with great care.

Digital Filtering

In the case of artifacts that have a constant frequency across time, such as AC current noise, frequency based filters can be used. There exists a range of filters for this purpose, with varying properties. When selecting a filter for a specific application, one has to take heed of the trade-off between time domain accuracy (less ringing) and a sharp frequency cutoff. Ideally, one is looking for a "brick wall" (Heaviside) filter, that would filter out all the frequencies above a given threshold, and keep the rest.

For EEG applications, linear time-invariant filters are applied. Time invariance is expected so that the filter constantly behaves the same; Linearity: $f(\alpha_1 s_1 + \alpha_2 s_2) = \alpha_1 f(s_1) + \alpha_2 f(s_2)$ is also expected (f being the filter, α_1, α_2 two scaling constants, and s_1, s_2 two signals or signal components).

Phase delay

Considering an harmonic (signal):

$$e^{i\omega t}$$

where:

ω is the pulsation
t is the time

, the response of a digital filter, can be expressed as $|H(i\omega)|\, e^{i(\omega t + \phi(\omega))}$, where H is the transfer function. By identification of $\omega(t - \delta t)$ to $\omega t + \phi(\omega)$, the phase delay (δt) of the filter is $-\frac{\phi(\omega)}{\omega}$, and thus depends on ω.

One must be careful in analyzing delays between signals and especially across frequencies, given that the use of a given non linear phase (response) filter will add phase delays depending on the frequency of oscillation. It is of first matter in cross-frequency coupling problems, and not necessarily addressed in the literature [210][173]. A zero-phase digital filtering must be applied, consisting of filtering the signal from start to end, then end to start. The second pass cancels the delay introduced by the first one. Its effect is presented in 2.2.

Unfortunately, this strategy is not possible for online neuromarkers computation. A compromise must be made on the cut-off slope. For the special cases of linear phase filters: the phase delay does not depend on the frequency, is constant and known. The Bessel filter, for instance, is a Finite Impulse Response filter that approximates a linear phase filter, and may be used as an alternative for online frequency coupling measurement.

2.2 Phase and amplitude of oscillations

The course of neuronal activity within one period (from deactivated to activated back to deactivated) can be represented on the trigonometric circle. It lasts 2π, and is called the phase. The unwrapped phase is the quantity $\Phi(t) = \omega t + \Phi_0$ (ω being the pulsation, t the time and Φ_0 the phase for $t = 0$). It tracks over time the evolution of the phase. It extends beyond 2π, and may be brought back to $[0 : 2\pi]$ by taking the 2π modulo. The cosine of the phase, gives the time course of a mono-frequency ($f = \omega/2 * \pi$) signal.

For multi-frequency signals (or approximated as such) i.e. $\sum \alpha_i cos(\omega_i t + \phi_i)$, the phase is not easily defined. One way to define it more generally requires the introduction of analytic signals, and is detailed further down and in chapter 3.

2.2.1 Phase extraction

An analytic signal is a signal that has no energy in the negative part of its frequency spectrum. A real signal can be made analytic by finding a complex part counterbalancing the energy in the negative part of the frequency spectrum. This problem can be solved using the Hilbert transform, through a windowed Fourier Transform or by convolution with a Morlet wavelet kernel. These methods holding fundamentally equivalent results under the right set of parameters [157][229][39].

A Morlet wavelet transform (WT) is the convolution of the signal with a wavelet kernel. In the case of Morlet wavelet:

$$e^{i2\pi\nu_w t} e^{-\frac{2t^2\pi^2\nu_w^2}{\Omega_w^2}}$$

where:

t is the time variable
ν_w is the frequency of oscillation of the wavelet
Ω_w is the number of oscillations of the wavelet before it zeroes out (usually fixed at 7)

the convolution is expressed as:

$$WT_f(t,\nu_w) = \int_{-\infty}^{\infty} f(t-k)\left(\cos(2\pi\nu_w k) + \mathrm{i}\sin(2\pi\nu_w k)\right) e^{-\frac{2k^2\pi^2\nu_w^2}{\Omega_w^2}}\, dk$$

where:

f is the signal / function under analysis

Therefore, at each chosen time point and frequency step, a complex coefficient can be obtained:

$$WT_f(t,\nu_w) = A(t,\nu_w)e^{i\Phi(t,\nu_w)}$$

where:

A represents the amplitude
Φ represents the phase

It is usually assumed [3] [157] that the phase $\Phi(t,\nu)$ and the amplitude $A(t,\nu)$ can be retrieved from the angle of complex coefficients calculated with an analytic wavelet transform. Unfortunately the physical significance of this phase may become doubtful, or hardly interpretable if the signal is not oscillating enough, i.e. if the phase varies slowly compared to the amplitude, or when the signal is the sum of two (or more) sine functions [54] [32]. This idea is analyzed in depth as one of the contributions chapter 3.

atan2 Retrieving the phase information from a complex coefficient involves retrieving the angle of the coefficient in the complex plane $\Phi(t,\nu)$, it is obtained as the arc-tangent of the imaginary part over the real part of the complex coefficient in its Euler form. The tangent function is mathematically defined as the quotient of the sine function over the cosine function.

$$tan(\theta) = \frac{sin(\theta)}{cos(\theta)} \tag{2.1}$$

$atan2$ uses the numerator and the denominator to guess the angle in $]-\pi;\pi[$, by opposition to $atan$, that uses the quotient to provide an angle between $]-\frac{\pi}{2};\frac{\pi}{2}[$. The "2" corresponds to the number of argument the function retrieves. It was first implemented in IBM's implementation FORTRAN-IV (1961). It is therefore necessary to use $atan2$ with wavelet coefficients.

Large band Hilbert transform The literature seems partly mistaken on the usage of large band Hilbert Transform. Frei et al. [84] explains, supposedly based on Boashash [32] and Osterhage et al. [207], that a "phase variable generally reflects the dominant frequency in the spectral composition of a signal". While Osterhage et al. [207] writes "the instantaneous phase/frequency based on this technique always relates to the predominant frequency in the spectrum", it does not provide any explanation as to why but cites Boashash [32] as a justification. On the other hand Boashash [32] explains that "the more closely a signal approaches a narrow-band condition, the better the Hilbert Transformed (HT) signal approximates the quadrature signal, and the more likely the HT-based analytic signal is to provide an accurate model of a real system with a particular IF; also the better in general will be the estimate of instantaneous frequency.", and insists on "the phase has resulted from a nonlinear combination of the two phase factors and may possess erratic behavior". Therefore, we would discourage using the Hilbert Transform on large frequency bands, in chapter 3 lies an attempt to provide some more hints as to why. Frei et al. [84] interestingly points out that phase extracted from narrow-band filtering will reflect a constant frequency, whether there is energy at that frequency or not, as discussed in chapter 3. Nonetheless, considering the time-frequency plane of amplitudes circumvents this issue, an application is presented in chapter 7. There is much to believe that achieving broad-band analyses by a bank of narrow-band analysis can hold more accurate result, and provide more tractability.

2.3 Measuring synchrony

2.3.1 Linearity

Measures of synchronization can be categorized either as linear or non-linear, in the sense that they capture the linear or non linear relationships of a property between different neuronal systems in the brain. At the level of the scalp, potential fluctuations and phase information are such properties.

Linear synchrony A perfect linear relationship of the same property between two systems i and j, seen as a function of time holds if :

$$f_j(t) = af_i(t) + b, \forall t \in \mathbb{R}, (a, b) \in \mathbb{R}$$

A perfect linear relationship of the same property between two systems i and j, seen as a random variable holds if :

$$X_j = aX_i + b, (a, b) \in \mathbb{R}$$

for all synchronous realizations between X_i and X_j. The k^{th} synchronous realization can be noted $(X_i, X_j)_k$. It may seem unsettling, since random variables are usually of different nature when compared (i.e. number of petals and length of petals), and their (linear) relationship compared over different items (i.e. flowers). Here the random variables are a same property on two distinct systems, and their linear relationship compared over different timings. A perfect linear relationship is rarely reached, possibly because of noise in the measurements, non-linearities in the relationship or no relationship at all, and is best approximated with a least-square (Gauss-Markov theorem) linear regression. It consists in finding a and b minimizing the error of the prediction of X_j knowing X_i. The analytic solution of this minimization problem gives

$$a = \frac{\mathbb{V}(X_i, X_j)}{\mathbb{V}(X_j)}$$

where:

$\mathbb{V}(X_i)$ is the variance of X_i
$\mathbb{V}(X_i, X_j)$ is the covariance between X_i and X_j

The deviation from this linear regression provides the degree of non-linearity of the relationship. It is commonly measured in a cross-plot as the sum of the vertical or orthogonal distances between the n $(X_i, X_j)_p$ points and

the line with slope a and intercept b. This sum can be written as

$$S = n * \mathbb{V}(X_j) * \left(1 - \left(\frac{\mathbb{V}(X_i, X_j)}{\sqrt{\mathbb{V}(X_i)\,\mathbb{V}(X_j)}}\right)^2\right)$$

for vertical projection, and involves the Pearson coefficient.

The Pearson coefficient

$$\frac{\mathbb{V}(X_i, X_j)}{\sqrt{\mathbb{V}(X_i)\mathbb{V}(X_j)}}$$

is a value contained in $[-1, 1]$, which is extreme when X_i and X_j are linearly correlated / anti-correlated ($S = 0$) and equal to zero when linearly uncorrelated (S is maximal).

While these measures are good estimates of the linear relationships between two variables defined on $\mathbb{R}$, they are not especially adequate for variables defined on the circle, such as the phase. The relationship between two phase functions would be more naturally investigated on the torus (the Cartesian product of two circular spaces). While this work did not follow this lead, it could provide some interesting means to develop more adapted synchrony measures.

For the purpose of illustration of this obstacle, figures 2.3 show that while estimating phase differences for phases expressed in the Euclidean space presents no difficulty, assessing phase differences with phase defined on the circle is not straightforward. When phases are expressed on the circle (figure 2.3 II), estimating phase differences (figure 2.3 VI) become more delicate as several (2) states of phase differences appear. It is particularly troublesome as the instantaneous phase recovered from the Morlet Wavelet transform is concerned. The transform returns the phase information in the $[-\pi; \pi]$ interval. Attempting to unwrap this phase information that is especially noisy in real case scenarios can induce strong artifacts at a given time that will impact measures for all remaining samples. In order to counterbalance this, without having to resort to dedicated measures on the toroidal space, hypothesis on transmission delays are made. They are notably supposed short enough, such as in chapter 7, so that:

$$\Phi(t) = \begin{cases} \Phi(t) + 2\pi & \text{if } \Phi(t) < \pi \\ \Phi(t) - 2\pi & \text{if } \Phi(t) > \pi \end{cases} \tag{2.2}$$

This basically turns a too large advance in a short delay, and reversely, a too large delay in a short advance. With this hypothesis, the bias introduced by folding the phase information on the $[-\pi; \pi]$ interval is partially corrected (figure 2.3 VII).

Non linear synchrony The brain is a highly non linear system [146], in which information is passed around the cortex following non linear mechanisms [2], primarily because of the integration property of the neuronal membranes, but also because of feedback loops. This non-linearity does not imply a chaotic spatial distribution on the scalp [146]. The mapping from electrical activity of sources in the cortex to potential field measured at the sensors on the scalp is linear (the result of a product of source activities with the gain matrix, a function of the properties of the different tissues of the head). Thus, any non-linear synchrony observed at the level of the sensors, cannot be due to volume conduction. And the non-linear synchrony observed at the level of the sensors is a linear function of the non-linear synchrony that exists at the level of the sources. It is therefore plausible that there exists, at the scalp level, a measurable non linear relationship between properties of the activity of distinct populations of neurons, unveiling functional dependencies between brain areas. While numerous metrics have been devised to capture such synchronization between neural assemblies, it is not clear which stands out [127].

2.3.2 Coherence

Coherence is especially well suited for time-locked analysis [1] but can also be applied to single trial analysis such as in Nunez et al. [199].

$$Coh^2_{AB} = \frac{|\mathbb{E}[\Gamma_{AB}]|^2}{\mathbb{E}[\Gamma_A]\,\mathbb{E}[\Gamma_B]} \tag{2.3}$$

where:

Γ_{AB} is the cross-spectrum between X_A and X_B
Γ_A is the auto-spectrum of X_A
Γ_B is the auto-spectrum of X_B
$\mathbb{E}$ is the expectation over trials

The cross-spectrum is defined as follows :

$$\Gamma_{AB} = \widetilde{X_A}\overline{\widetilde{X_B}} \tag{2.4}$$

where:

$\widetilde{X_A}$ is the Fourier transform of X_A
$\overline{\widetilde{X_B}}$ is the conjugate of the Fourier transform of X_B

The normalization by the auto-spectra isolates the influence of coupling between X_A and X_B from large values of the cross-spectrum occurring only because of high amplitude.

Coherence decrease may happen for several reasons: the increase of noise in any of the two signals, the appearance of a non-linear relationship, an inadequation between the size of window and the frequency of the signal, an interaction delay greater than that of analysis [149].

2.3.3 Imaginary Coherence

Nolte et al. [194] provide imaginary coherence as an interesting alternative to the coherence measure, especially for EEG which is very sensitive to volume conduction.

$$ImCoh_{AB} = Im\left(\frac{\mathbb{E}[\Gamma_{AB}]}{\sqrt{\mathbb{E}[\Gamma_A]\,\mathbb{E}[\Gamma_B]}}\right) \tag{2.5}$$

The construction of the measure is a *reductio ad absurdum*, based on the supposition that sources in the brain are independent, which is not the case. Under this assumption, since all signals measured at the scalp are, by volume conduction, linear combination of source activities :

$$X_i = \sum_{k=1}^{M} \alpha_{i,k} S_k$$

where:

[1] Time-locked analysis refers to the study of a given neural response after repeated identical stimuli, or event of interest (peak of the heart beat for instance).

X_i is the signal at the electrode i
S_k is the activity at source k, among M sources
$\alpha_{i,k}$ is the (scalar) contribution of the source k to the electrode i

and since the Fourier transform of a sum is a sum of Fourier transforms:

$$\widetilde{X_i} = \sum_{k=1}^{M} \alpha_{i,k} \widetilde{S_k}$$

the cross-spectrum gives:

$$\widetilde{X_i}\overline{\widetilde{X_j}} = \left(\sum_{k=1}^{M} \alpha_{i,k} \widetilde{S_k} \right) \left(\sum_{k=1}^{M} \alpha_{j,k} \overline{\widetilde{S_k}} \right)$$

and since the sources are supposed independent:

$$\widetilde{S_l}\overline{\widetilde{S_m}} = 0, \forall l \neq m$$

the cross-spectrum equals :

$$\widetilde{X_i}\overline{\widetilde{X_j}} = \sum_{k=1}^{M} \alpha_{i,k}\alpha_{j,k} \widetilde{S_k}\overline{\widetilde{S_k}} = \sum_{k=1}^{M} \alpha_{i,k}\alpha_{j,k} \left| \widetilde{S_k} \right|^2$$

This cross spectrum is thus necessarily real valued, the product of a complex number $\widetilde{S_k}$ by its conjugate $\overline{\widetilde{S_k}}$ removes the imaginary part. In practice, the imaginary part of the cross spectrum is rarely null, therefore it contains information about the dependence between sources.

2.3.4 Phase synchrony

Phase synchrony commonly consists in assessing or quantifying the linear relationship between two phase variables (or more). Yet, nonlinear operations are required to extract the phase from the EEG correlates of neuronal population activities, and were presented in 2.2. In the following, $\Phi(t, \nu)$ is simplified to $\Phi(t)$, supposing that the phase is computed for a given frequency (ν).

Phase locking

$$|\Phi_{n,m}(t)| < \delta, \text{ where } \Phi_{n,m}(t) = n\Phi_1(t) - m\Phi_2(t), \text{ and } n, m \in \mathbb{Z} \tag{2.6}$$

Phase locking can be assessed through the consistency of phase difference across time. Rosenblum et al. [245] describes the phase locking period as a period during which the phases of two oscillating variables stay close (within δ) to one another. Commonly, in equation 2.6, it is the relationship with $n = m = 1$ that is assessed.

Phase Locking Value / Mean Phase Coherence The Phase Locking Value (PLV, equation 2.7) and the Mean Phase Coherence (MPC) track the consistency of phase difference, respectively over trials [151] or over time [185]. It is based on the circular variance of the angular distribution of phase differences.

$$PLV(t) = \left| \frac{1}{N} \sum_{j=1}^{N} e^{i(\Phi_A j(t) - \Phi_B j(t))} \right| \tag{2.7}$$

where:

j is the index of the trial among N repeated trials
$\Phi_X(t)$ is the phase angle of signal X at locked time t

$$MPC(w) = \left| \sum_{k=wc-L/2}^{wc+L/2} e^{i(\Phi_A(k)-\Phi_B(k))} \right| \tag{2.8}$$

where:

L is the duration of a time window
wc is the window center
w is the window $[wc - L/2; wc + L/2]$
$\Phi_X(k)$ is the phase angle of signal X at time k

In EEG, PLV is maximal for two channels measuring the activity of the same source, in which case the synchrony is purely introduced by volume conduction, therefore spurious.

Aydore et al. [12] show that the PLV is a biased estimator which depends on the distribution of phase differences while the PLV^2 is unbiased (it only depends on the number of samples), and identical to Vinck et al. [316] Pairwise Phase Consistency metric. Interestingly, for phase differences following a Von Mises distribution, the PLV_{VM} can be estimated from the concentration parameter κ, agnostically of the location (mean) [126]:

$$PLV_{VM} = \frac{I_0(\kappa)}{I_1(\kappa)} \tag{2.9}$$

where:

κ is the concentration parameter of the Von Mises distribution
$I_i(\kappa)$ is the modified Bessel function of i^{th} order

The inherent difficulty is to properly estimate the Von Mises distribution parameters, a difficulty faced in chapter 7.

Phase Lag Index The Phase Lag Index (PLI) [284] also tracks the consistency of phase difference over time, but only considers the sign of the phase difference. Volume conduction in EEG experiments occurs at zero time delays, which corresponds in the phase space to either zero phase angle delay or π phase angle delay. For any symmetric distribution of phase differences about zero or π angle, the PLI is minimal (half of the signs are plus, half are minus), making the PLI insensitive to volume conduction effects.

$$PLI(w) = \left| \frac{1}{N} \sum_{k=wc-L/2}^{wc+L/2} \text{sign}(\Phi_A(k) - \Phi_B(k)) \right| \tag{2.10}$$

where:

L is the duration of a time window
wc is the window center
w is the window $[wc - L/2; wc + L/2]$
$\Phi_X(k)$ is the phase angle of signal X at time k

A hardware implementation of PLI have been realized to minimize the latency of the system [200].

Both methods (PLI and MPC) are rough estimates of the actual distributions of phase differences and completely fail at describing some usual cases (Von Mises bimodal distribution with high concentration parameter for instance). Nonetheless, they are complementary: a high MPC associated to a high PLI indicates a stable phase

difference that is not due to volume conduction. These measures are valid only under the assumption that the signals are stationary, somewhat encouraging to consider short windows [12]. Taking short complex coefficient windows in offline analysis is possible since the coefficients at the border of the window have been computed with the knowledge of what lies beyond. It becomes a problem in online analysis as it introduce a non-negligible delay.

Weighted Phase Lag Index Although based on the PLI, the Weighted Phase Lag Index (WPLI) was designed for repeated trials [317]. The phase differences are weighted by the amplitude of the imaginary component.

$$WPLI(w) = \frac{\left|\sum_{k=wc-L/2}^{wc+L/2} |Im(X)| \operatorname{sign}(\Delta(\Phi_A(k) - \Phi_B(k)))\right|}{\sum_{k=wc-L/2}^{wc+L/2} |Im(X)|} \tag{2.11}$$

where:

X is the cross-spectrum of A and B

Phase Synchrony Referencing

The studies considering phase synchrony computed from EEG data are legion, table 2.1 collects only a fraction of the studies involving phase synchrony EEG, all later than 2000. This recollection shows that referencing strategies are so diverse that there does not seem to be a consensus as to which is to be used.

Referencing in EEG is one of the most difficult point to address, notably with regard to phase synchrony. Some even strongly discouraged conducting phase synchrony analysis on EEG data [263] [75] [99] and [310] to a lesser extent. The issue lies in the activity of the common reference, whose frequency content might overlap with the frequency content at locations of interest, or with the average reference removing most of the genuine synchrony [224]. A first proposal is to consider bipolar montages of pairs of the closest electrodes without repetition of electrodes, which unfortunately considerably reduces the dimensionality of the data, especially for setups with a reduced number of electrodes. A second proposal lies in computing the source current densities at the scalp, a solution that definitely should be put forward when the study benefits from a dense electrode coverage of the scalp. As a third option, artificial montages (combination of electrodes) can be considered as a good reference electrode. As a last proposal, Pockett et al. [224] suggest considering at the same time the common and average reference, as "there is no reason to suppose that episodes of genuine, average-referenced synchrony should occur at the same time as artifactual episodes of common-referenced synchrony".

2.3.5 Ensuring the statistical robustness of the synchrony

Synchrony can occur by chance, even for signals that are completely uncorrelated. Therefore, it is paramount to assess the likelihood that a given synchrony value is obtained.

One option is to compute a p-value, as the probability that a synchrony measure as extreme as the observed value might occur [38]. It can be done by permutations, shuffling one of the two random variables, so that the pairs $(X_i, X_j)_p$ are no longer synchronous, computing a synchrony measure on this surrogate data and repeating this operation a great number of times. The p-value is the number of times the observed synchrony is bigger / lower than the surrogate over all the repetitions. Finally, how to assess the threshold for p-value stating that the synchrony is significant? If it was computed on a stationary signal with accurate measurements, only a high threshold should reveal a relationship. On the opposite, on highly perturbed signals with an assumed high level of noise, a lower threshold can be tolerated, but with a lower level of confidence. A second option to estimate the p-value is to test it against a probabilistic distribution model of the synchrony measure derived from the probabilistic distribution models of random variables X_i and X_j.

Paper	Reference	Measure	W.L.	S.R.	A./S.T.	Kind	Electrodes	Surrogates
van Lutterveld et al. [314]	AR	Centrality of MST with PLI	x	2048	x	Scalp	19 (≈ 10-20)	x
Lachaux et al. [151]	AR	PLS	x	?	S.T.	Cortico	4 Plots * 8	x
Nuno and Maharatna [200]	?	PLI	0.5s	256	x	Scalp	16	?
Bhattacharya and Petsche [25]	2EL	Shanon	x	128	S.T.	Scalp	19 (10-20)	G.C.
Pockett et al. [224]	Fp1-LH, Fp2-RH	SAPD	x	512	S.T.	Scalp	64 (10-10)	x
Bhattacharya [24]	2EL	Shanon/MPC	8s	128	S.T.	Scalp	19 (10-20)	G.C.
Tokariev et al. [307]	? → Laplacian	PLV/PLV of BAF	“6 cycles”	256	S.T.	Scalp	28 (10-10)	Permutations
Gruber and Müller [97]	Cz	PLV	≈ 100ms	500	A.	Scalp	128 (10-20)	Permutations
Kawano et al. [134]	2EL	PLV / PLI	1s	500	S.T.	Scalp	19 (10-20)	None
Cavanagh et al. [46]	Cz → CSD	ITPC/PLV	200 / 400ms	500	A. /S.T.	Scalp	62	None
Trujillo et al. [310]	Nose → Laplacian	PLV	N.A.	512	A.	Scalp	30 (10-20)	Permutations
Reiterer et al. [235]	2EL	PLI/CGMC/MPC	?	128	S.T.	Scalp	19 (10-20)	G.C.
Wang et al. [324]	POz	PLV	2-8s	256	S.T.	Scalp	32 (10-20)	Multiple trials
Gysels and Celka [102]	≈ Vertex	PLV/Coh	1s	512	S.T.	Scalp	32 (10-20)	None
Kawano et al. [135]	2EL	PLV/PLI	“8 cycles”	500	S.T.	Scalp	19 (10-20)	G.C.

Table 2.1: ?: Not disclosed by the authors, N.A.: Not Applicable, W.L.: Window Length, S. R.: Sampling Rate, A. / S.T.: Average / Single Trial, AR: Average Reference, 2EL: mean of EarLobes, G.C.: 2 Groups Comparison, PLS: Phase Locking Statistics [151], Shanon: Shannon's entropy of the distribution function of phase difference [24], MPC: Mean Phase Coherence, SAPD: spatial analytic phase difference, ITPC: InterTrial Phase Coherence, CGMC: Coarse-Graining of Markov Chains, BAF: Band Amplitude Fluctuation, Fp1-LH: Fp1 for Left Hemisphere [224], →: re-referencing

Statistical significance also has to be checked when comparing two groups. To check whether long range synchrony is significantly different in healthy and epileptic patients, [24] apply a Wilcoxon Rank Sum test. It is studied in much detail as a contribution in chapter 6.

Once a measure has been identified to capture a property of interest, it can be introduced in protocols where the objective is to control it at will: neurofeedback protocols.

2.4 Neurofeedback

Neurofeedback is a protocol involving a Brain Computer Interface (BCI) to provide a feedback to the participant of features of his own brain activity. It aims at regulating putative neural substrates serving specific behavior or pathology [279]. Not only can control of some features be achieved, but these skills can be conserved over time (from hours to months after training) and match changes in brain topology [279]. Neurofeedback is either defined as a specialization of biofeedback protocols when they encompass all possible bio-signal measures, or as a complement to biofeedback protocols when the latter involve only physiological signals (heart-beating, breathing, Galvanic Skin Response (GSR), pupillometry)...

2.4.1 Neural substrates for self-regulation

Operant conditioning successfully train the output behavior of a single cell Fetz [78] showed that monkeys could be trained by neurofeedback to increase the discharge rate of a single neuron of the motor cortex by 50 to 500 percent, hence brain cell networks can be trained to modulate the activity of a single brain cell. Sitaram et al. [279] suggest that neurofeedback involves a reward processing network (comprising the anterior cingulate cortex (ACC), anterior insular cortex (AIC) and ventral striatum (VS)), a control network (comprising the lateral occipital cortex (LOC), dorsolateral prefrontal cortex (dlPFC), posterior parietal cortex (PPC) and thalamus) and a learning network (the dorsal striatum (DS)).

Learning to control the activity of one specific brain regions modifies functional connectivity Ruiz et al. [252] show with real-time Functional Magnetic Resonance Imaging that acquired self-control of bilateral anterior insula cortex modulates brain network connectivity in schizophrenia patients. Rota et al. [247] show that subjects who learned to deliberately increase activation in the right Inferior Frontal Gyrus (rIFG), saw the connectivity of the rIFG to a widespread network of frontal and temporal areas decrease and lateralize to the right hemisphere.

2.4.2 BCIs are diverse and Neurofeedback is an Active BCI

BCIs are the hardware and software means to transfer information of the brain activity and its environment to the computer and analyze it.

The common part of all BCIs is that they monitor brain activity correlates: they recover data informing on the brain workings, either as fMRI data (contrasts in blood oxygenation) [328], EEG / iEEG / sEEG data (electric potential differences between locations on/in the head), MEG data (magnetic fields), fNIRS data (cortical hemodynamic activity) or several at once [216]. It comes down to measuring the activation (excitation or inhibition) of neurons by other neurons.

Additionally, some BCI systems integrate information from the body, such as galvanic skin response, body temperature, heart rate... Furthermore, they can also add information from the surroundings, such as light exposure, background noise, room temperature...

Do BCIs differ not only in the data they process, but also in their purpose. A now widely shared formal categorization of BCIs [340], [342] was proposed. It splits the BCI between passive, active, reactive and hybrids.

Passive Brain Computer Interfaces (PBCI) use implicit (and are sometimes named as such [92]) information recovered from the brain and analyzed without the active participation of the user. A number of PBCI protocols have been developed: to adapt the music to a predicted user's task [93], to detect if the user perceived a system's error (consciously or unconsciously) [341], and to many other goals. One can imagine an infinitely number of practical use for PBCI aiming at increasing quality of life such as controlling light intensity in a room to reduce stress markers.

Active Brain Computer Interfaces (ABCI) let the user voluntarily modulate brain activity to generate a specific command, or control a given neuromarker. They offer new means of control over either a physical or digital environment.

Neurofeedback is a form of ABCI, where information not only goes from the brain to the computer, but also back from the computer to the senses of the user (visual, auditory, haptic or electrical). This feedback loop extends the control of the machine to the control of ones' own brain states.

Neurofeedback has been used as a therapeutic tool [242] to help ease Attention Deficit Hyperactivity Disorder (ADHD) [70], motor (re-)learning after stroke [237], epilepsy symptoms... but also as a performance training tool in healthy subjects [98] to enhance various skills (spatial rotation, perceptual binding, mood and well-being among many other), although in some cases the neurofeedback was detrimental [45].

Neurofeedback is made possible by the processing of brain signals into neuromarkers and their representation to the subject.

2.4.3 Modalities, type of feedback and presentation rate must be carefully chosen

Neurofeedback involves the presentation of one or several neuromarkers at once, which can be derived from either one or more simultaneous modalities of acquisition. Visual, auditory, haptic or electrical representations of these neuromarkers are created and submitted to the subject.

Multimodal brain activity acquisition ?

Because the different acquisition modalities have complementary specificities (temporal vs spatial resolution, and different proxys on neurons stimulation), it appears appealing to consider combining markers from different modalities of acquisition (such as EEG and fMRI [216]). The inherent complexity and cost of setting up and running a (neuro)multimodal experiment, the design of the neuromarkers, and the multiple feedback (or combination) it imposes, suggest more theoretical research should be dedicated before clinical research can build on this basis for possible clinical applications.

Some constraints (setup complexity) can be alleviated by combining neuro and bio feedbacks such as the galvanic response, heart rate or breathing. Moreover, they are often integrated on some devices as supplementary channels with sampling rate identical to the EEG channels.

Means of neuromarker presentation

Of the five senses, olfaction and gustation are difficult to artificially stimulate in real time. Leaving vision, audition and tactile perception as the main modalities of feeding back the neuromarker(s).

How to choose the feedback delivery modality ? The best feedback modality (or combination) is constrained by the experiment. First, not all feedbacks can be implemented depending on the constraints of the experiment (for example, an eyes closed experiment rules out using visual feedback). Then it should minimize the possible interactions between the brain activity tracked by the neuromarker and the brain activity related to processing the feedback. Some brain regions have been identified to activate during visual neurofeedback (anterior insular cortex (AIC), dorsolateral prefrontal cortex (dlPFC), anterior cingulate cortex (ACC) and posterior parietal cortex (PPC) for visual feedback [279]), their activation should not influence the neuromarker. The investigator must ensure that while the subject is told not to attempt to control the neuromarker, the neuromarker is statistically identical when a sham feedback is presented and when no feedback is presented.

Should one choose more that one feedback modality ? Multimodal feedback presentation is possible, but definitely not encouraged in all situations, with any combination of feedbacks. Visual-haptic multimodal feedback is the most promising, especially in motor function recovery / enhancement [242]. Meanwhile, visual-auditory show much more reserved conclusions.

How to choose the feedback delivery features ? The content (its features) of the feedback must be informative, supportive [242] and motivating. While informative is objective, the supportive and motivating aspect are rather subjective. Supportive: it must encourage any effort first, then encourage efforts in the good direction, it may trigger emotional rewards systems (as in the presentation of a smiling face). Motivating: it's highly psychological, and beyond the scope of the feedback. Subjects must be convinced that there is this option of coming out of the experiment having made progress, especially subjects that struggle against a debilitating disease for years, with successive medication / surgery failures. It is nonetheless conspicuous that their expectations should not be raised unrealistically.

How to choose the number of features ? Multifeature feedback may be considered, but the more feedback features to integrate the harder it gets. Perronnet [216] reports that 1D feedback is easier to control on single-session. This result is in line with mental workload witnessed during Multi-Attribute Task Battery-II (MATB-II) developed by the NASA: as the number of gauges to control increases, not only does the mental workload increase, but also the level of errors.

How often should the feedback be presented ? According to Roc et al. [242], Mental Task BCI feedback comes at a high presentation rate, when it should be timely, i.e. when the learner "most needs it". The moment at which the learner "most needs it" could be measured with attention measures. Subjects cannot constantly learn, mind wandering may occur. Feedback should be given when the subject is the most receptive and can make the best of it.

How quickly should the feedback be ready for presentation ? In Jackson et al. [125]'s intracortical experiment, where the spiking recorded in one area of the motor cortex are stimulated in another area, long-term changes occurred only when the duration between recording and stimulation was less than 50 ms. Belinskaia et al. [19] establishes that EEG neurofeedback latency has a strong effect on learning some features. Neurofeedback latency having a strong impact on learning outcomes, hardware implementations of neuromarkers have been developed [200], allowing for considerable gains on processing time.

Any marker computed over a window is inherently delayed Any neuromarker computed over a window: statistical measures or measures involving convolution (Hilbert Transform, Wavelet Transform...) are delayed by half the duration of the window used for their computation. The reason is that the measure is centered over the time point at which it makes sense. This is a a fact not necessarily considered in all latency analyzes.

There is still a need to better understand how the characteristics of feedback impact the acquisition of skills (capacity to up-regulate a given neuromarker) [242].

2.4.4 Neuromarkers

Neuromarkers are proxys / filters on specific brain states / events

Brain activity is the result of the continuous stimulations of billions of neurons. Local integration (spatial and temporal) of these stimulations gives rise to what are commonly named "(di/multi-pole) sources". A neuromarker is a well designed proxy to some sources (or even some stimulations), and filter to specific electric events produced by these sources.

The goal of neuromarkers is to faithfully capture information linked to specific electric events and at the same time reduce wisely the dimensionality of the data so that it can be interpreted quickly and easily by the subject. Quickly because the marker may be updated on a regular basis (as quickly as the sampling rate of the recording device). Easily because it must not perturb the subject's ability to focus on a chosen mental strategy.

Neuromarkers may be ahead of biomarkers

The search for neural correlates to physiological changes, is of great interest with regard to any successful biofeedback experiment as it can provide significant performance increase. The first advantage of neuromarkers over biomarkers (such as GSR or pupillometry) is due to the shorter time scale of some brain activity recording modalities such as EEG or MEG. The second is the precedence of brain activity over physiological correlates. The first drawback regarding the study of brain activity is the difficulty in making sense of brain signals. The second drawback stems from the fact that the most obvious correlates may be located in deep structures, at distance from the extracranial sensors [120].

α power

The α power neuromarker may serve as a mean to improve cognitive performance in human subjects [108]. In Belinskaia et al. [19], the subjects were able to increase the power of their alpha activity during 30 minutes of neurofeedback training. α power can also be trained specifically to one hemisphere [13], in which case, a reduction in alpha was associated with enhanced sensory processing. Belinskaia et al. [19] show that alpha power training lasts beyond the duration of the session. Counter-intuitively, the increase in alpha power would not be due to an increase in instantaneous amplitude, but in an increase in incidence rate [19] [206].

α power is a neuromarker for which voluntary control can be quickly acquired and lasts in time. Nonetheless the effects on cognitive functions are diverse, and typically may depend on the target (location, spread...).

In a large experiment involving 50 subjects, over 3 neurofeedback sessions per week for 4 weeks, Hsueh et al. [116] show a progressive significant increase in the α amplitude and total α duration of the frontoparietal region. This increase is correlated with accuracies of both working and episodic memories.

Sensorimotor Rhythm

The control of the sensorimotor rhythms have been used widely in neurofeedback protocols for a variety of applications, such as :

- improving golf putting performance [50],
- improving memory functions [141],
- improving attention processing [50],
- reducing conscious control of the motor task [276],

- reducing severity of anxiety [160],
- reducing MPTP(1-methyl-4-phenyl-1,2,3,6-tetrahydropyridine)-induced parkinsonian symptoms and both ON and OFF scores during classical L-DOPA (l-3,4-dihydroxyphenylalanine) treatment in non-human primates [221],
- improving cognitive performance in elderly with mild cognitive impairment [174] (sensorimotor over theta),
- reducing the frequency and severity of epileptic seizures [292] [291] [267] [79] [166] [268]

The beginning of the sensorimotor rhythms Roth et al. [248]'s experiment paves the way to the introduction of SensoriMotor Rhythms (SMR) in reinforcement paradigms. A simplification of the original protocol gives: cats are initially taught to press a bar during a light signal to be delivered food; then the food is only delivered when the cats restrain from pressing the bar during the same light signal. They observed during that period a 12-20c/sec activity over the coronal gyrus and adjacent sensorimotor cortex. They named this activity the SMR. The development by Sterman et al. [293] of this initial study consisted in the usage of SMR as a positive reinforcement trigger based on neuronal rhythms: a neurofeedback protocol. This protocol would be simplified as: food-deprived cats with no training were delivered food only if they managed to spontaneously exhibit SMR. They observed after 50/60 reinforcements, that the animals began to adopt a fixed position (motionless with eyes fixed straight ahead) and to exhibit SMR.

Effect of SMR on somatosensory systems In the meantime, Chase and Harper [48] studied in cats the changes in central and peripheral processes co-occuring with the SMR. They observed that the tonic activity of the neck musculature decreased and eye movements ceased, that the amount of integrated activity decreased significantly, that the pattern of respiration was closely regulated and that heart rate was significantly decreased (by up to 30%). Howe and Sterman [115] looked into the synaptic transmission changes occuring during the different behaviourial states (described partly with SMR activity and oculogram). They noted that: "During SMR in the awake animal, almost no evoked response amplitude changes occurred in somatosensory cortex, a small decrease was present at the thalamus while a large increase was observed at the 1Sn, supporting the hypothesis that neural mechanisms associated with the suppression of CNS functions during quiet sleep are also operative in awake and active sleep states". In [115], it is supposed that "The marked decrease in the thalamic evoked response observed during the SMR supports the hypothesis that this rhythmic EEG activity is generated, at least in part, by recurrent inhibitory processes located at the thalamic level." In humans, Thompson et al. [304] obtained results supporting the hypothesis that SMR modulation had predictable effects on spinal reflex excitability: a property of inhibition, and Boulay et al. [35] that the bidirectional modulation of SMR was associated to reduction in reaction time, suggesting that not only the rhythm should be investigated, but also the mean of modulation. Thompson et al. [304] notes that the modulation of SMR has predictable effects on spinal reflex excitability. A bio-physiological model of the SMR is illustrated and summarized in [63].

Contingent Negative Variation, a Slow Cortical Potential

Slow cortical potentials are another neuromarker commonly used in neurofeedback experiments. They consist in very slow shifts (positive or negative) of brain activity lasting up to several seconds. It was suggested that negative shifts reflect activity of large cell assemblies that are responsible for planning and initiation of goal directed behavior.

The Contingent Negative Variation (CNV) is a SCP that is elicited in a Go/No Go S2 (second stimulus) paradigm. The protocol followed by the subjects in [105] is: (S1) A first low tone burst is heard (S2) 2 seconds after S1 either (at random) a medium (Go) or a high (No Go) tone burst is heard triggering in the medium case a finger extension.

The CNV was first discovered by Walter et al. [320] as a brief surface positive wave superimposed by a brief surface negative wave and a more prolonged surface negative component lasting several seconds, generally limited to the anterior regions. The temporal and spatial dynamics of the CNV are precised by Hamano et al. [105] in

subdural investigations: multiple cortical potentials with different origins and possibly different functions sum up at the scalp. Moreover they are not related to motor preparation alone, unlike the Bereitshaftpotential [30].

2.4.5 Neurofeedback and epilepsy

SensoriMotor Rhythms

In Cats The first study of SMR and epilepsy by Sterman et al. [292] was led on cats under convulsant (MMH). It showed that SMR trained animals were less sensitive to convulsants, i.e. escape behavior and convulsions were delayed substantially compared to a control group.

In Humans The first study of the impact of SMR training on epilepsy in humans was conducted by Sterman and Friar [291]. They observed a significant suppression of seizures after the neurofeedback training of the SMR. A number of trials followed, on a restricted number of epileptic patients, and under various prescription medicines [293][291][166][79][267], with overall many reported positive outcomes ([296] for a meta-analysis).

‘

2.4.6 Neuromarker as online measures

A neuromarker in neurofeedback is an online measure: a continuous calculation, on the fly, as the signal is being recorded. Online measures are relevant to BCI interfaces (e.g.: the continuous computation of power in the β band), or more specifically neurofeedback protocols (e.g.: the continuous computation of amplitude of the μ rhythm, or perhaps synchrony between brain areas). This constraint gives rise to several concerns that have to be addressed: the speed of the calculus and blindness to the future.

Speed While offline analysis can afford to be computationally expensive, online analysis, requiring a measure in real-time demands high-efficiency and/or light and/or parallelized (on Central Processing Unit/Graphical Processing Unit) algorithms. It poses a limit to how much data can be processed at once. While delay could be tolerated (with impact on learning [19]), it has to be constant (no accumulation and no variation from one measure to the next). Computationally efficient accumulators may in some cases be designed such as moving average and variance. Other signal processing algorithms have been developed with real-time usage in mind. From signal filtering, to amplitude extraction, where the ratio latency/accuracy can be controlled. Lastly, hardware improvement may reduce processing time.

Blindness to the future For various reasons, such as mitigating the high temporal variations of some brain activity correlates or phase extraction, some measures are computed as a weighted average. At a given time step t, it is not possible to compute a mean from $t - \delta_t$ to $t + \delta_t$, because the data from t to $t + \delta_t$ is unknown (as opposed to offline measures with the exception at the end). Either one accepts a delay of δ_t, and returns the measure of for time t at $t + \delta_t$, and a balance between a low δ_t and a high variation of the measure (a large δ_t implies many less overlapping values, and higher variation for close-by measures) must be set. Or the future samples can be guessed with a model (auto-regressive / neural network...). Again, a balance between a low δ_t (higher accuracy of guessed samples) and a high variation must be set.

No averaging over repeated trials The brain is constantly at work. Most often, if not always, multitasking, rearranging memories, planning for possible events... When recording EEG during a task, much of the signal can be the result of this undergoing and uncontrollable activity. Nonetheless, this undergoing activity varies on repeated tasks, while the activity strictly time locked to the task is repeated. Averaging across tasks the time

locked recordings zeroes out the signal that varies from task to task and amplifies the signal that is stable, i.e. amplifies the signal-to-noise ratio [277].

Averaging can be applied when a given stimulus elicits a neural response at a fixed delay from the stimulus. Otherwise, not only the undergoing activity is zeroed out, but also the activity elicited by the stimuli. Averaging may also be applied if specific EEG patterns are identified (epileptic spikes, sleep spindle, end of a characteristic state such as epiletic discharges...) and used as triggers.

It would not be accurate to assert that stimulus based averaging is to be excluded from online analysis. The P300 [241] is an example of such a paradigm (event related potential). Averaging is achieved across several calibrations (tasks), the result of averaging is then used during online classification. To further improve classification, several stimuli are presented, each new stimulus improving the classification outcome.

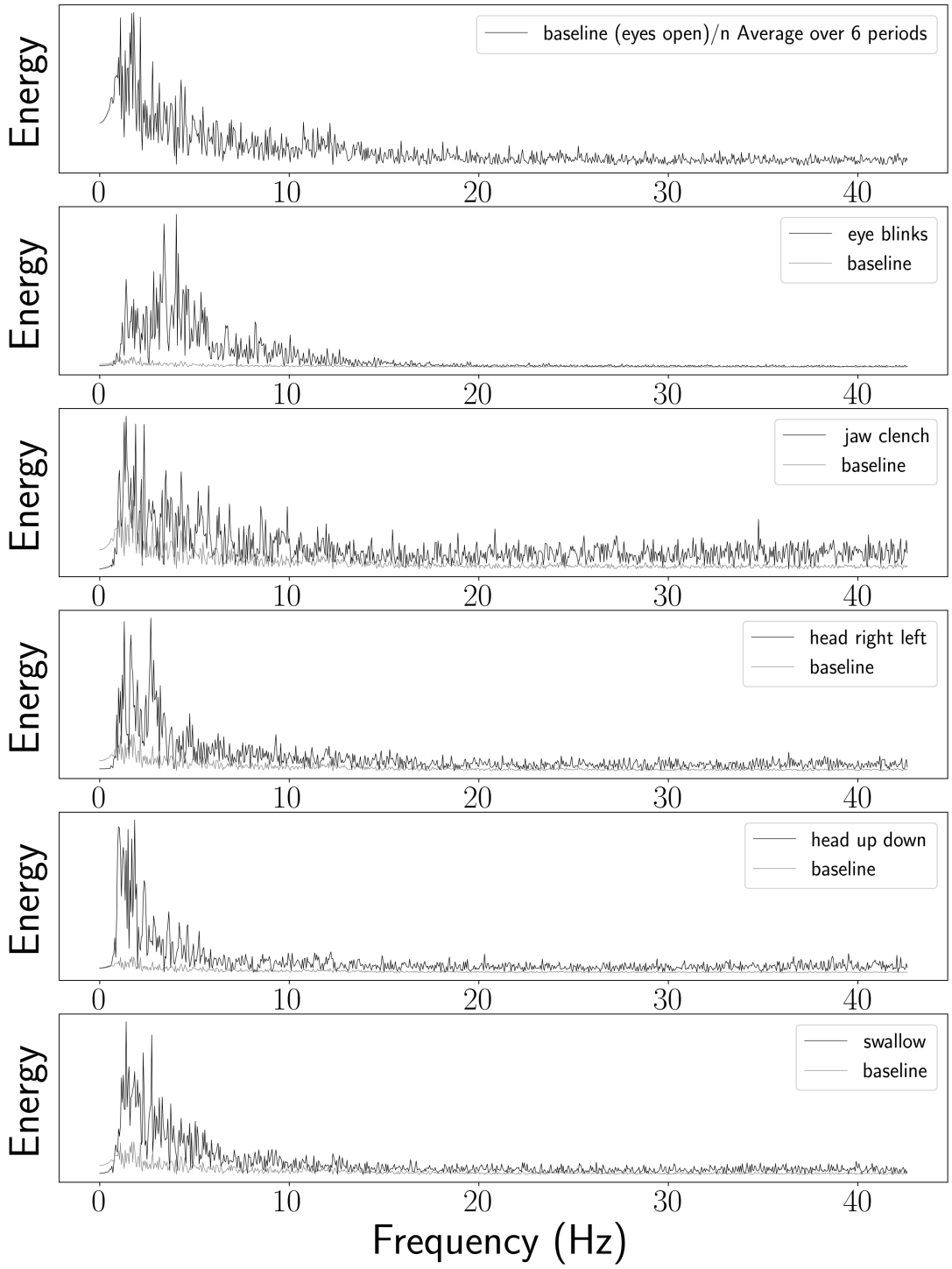

Figure 2.1: Fourier power spectrum are presented for under different artifact conditions, and compared to a baseline. The upper most plot corresponds to the baseline (eyes open fixation). The baseline is compared (in grey), in descending order to (in black): eye blinks, jaw clench, head moving right and left, head moving up and down, and swallowing.

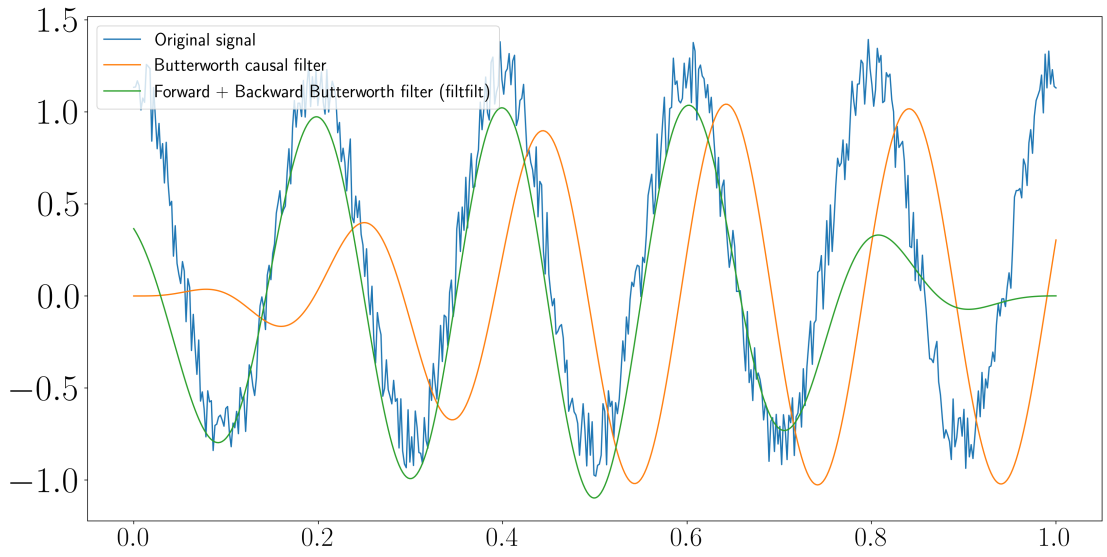

Figure 2.2: An original signal (in blue) oscillating at 10 Hz, to which is added some gaussian noise, is one pass filtered with a Butterworth causal filter (in orange), and two-pass filtered (filtfilt method) with the same Butterworth filter (in green). x-axis: time, y-axis: amplitude.

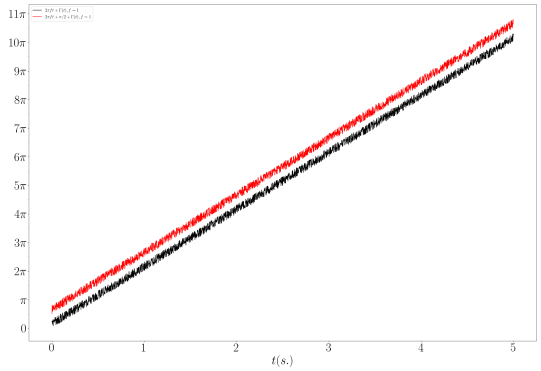
11π
10π
9π
8π
7π
6π
5π
4π
3π
2π
π
0
0
1
2
3
4
5
$t(s.)$

I

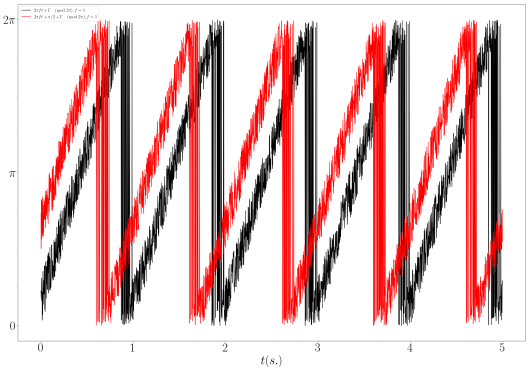
2π
π
0
0
1
2
3
4
5
$t(s.)$

II

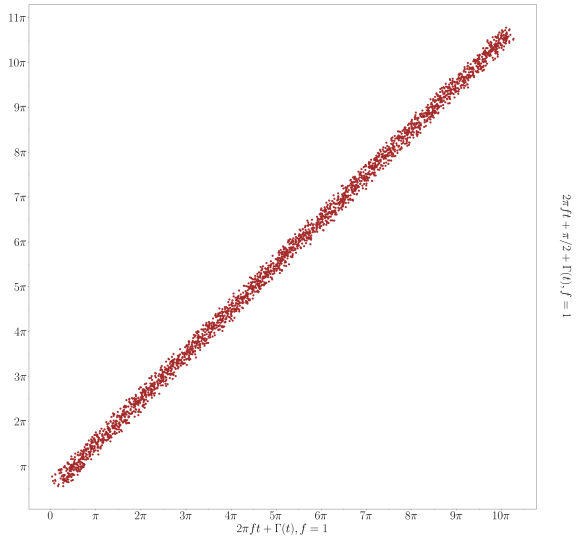
11π
10π
9π
8π
7π
6π
5π
4π
3π
2π
π
0
π
2π
3π
4π
5π
6π
7π
8π
9π
10π
$2\pi ft + \Gamma(t), f = 1$
$2\pi ft + \pi/2 + \Gamma(t), f = 1$

III

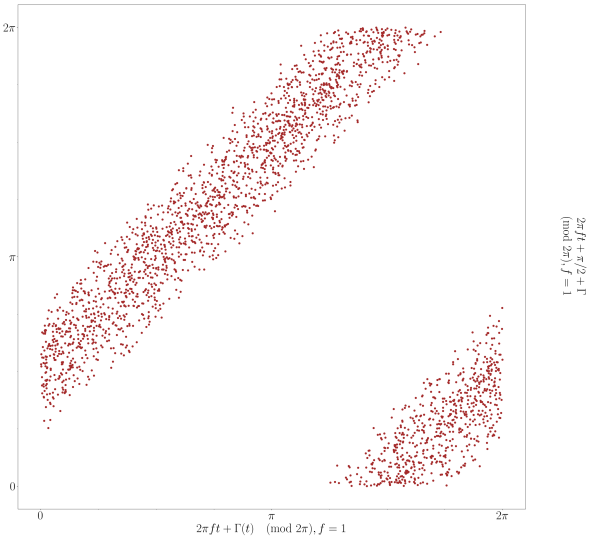
2π
π
0
0
π
2π
$2\pi ft + \Gamma(t) \pmod{2\pi}, f = 1$
$2\pi ft + \pi/2 + \Gamma \pmod{2\pi}, f = 1$

IV

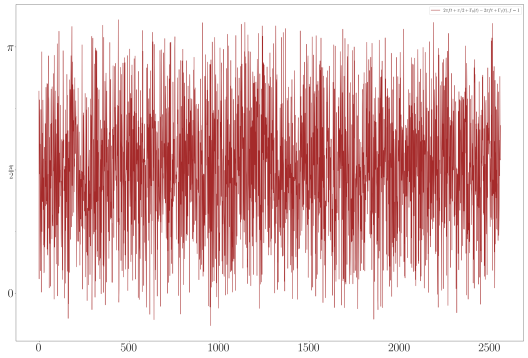

V

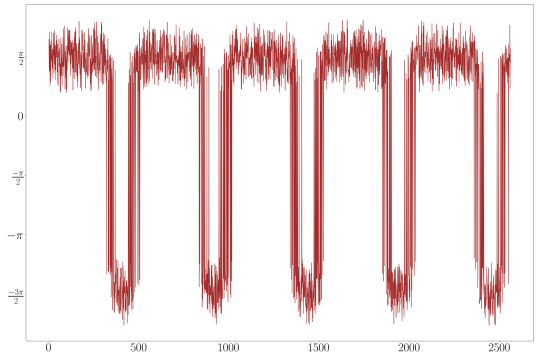

VI

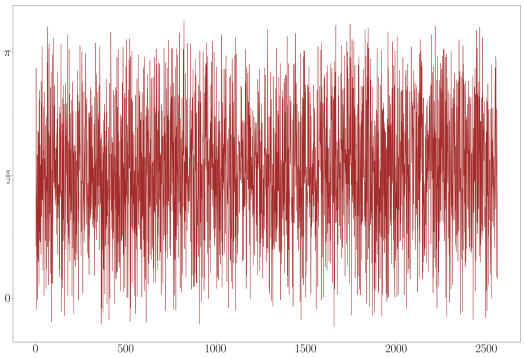

VII

Figure 2.3: In I is displayed the temporal evolution of phase functions in the Euclidean space. In II is a representation of the same temporal evolution of phase functions but restricted to $[-\pi;\pi]$, as it could be recovered with the Morlet wavelet transform. In III the phase functions of I are plotted against each other. In IV the phase functions of II are plotted against each other. In V is plotted the temporal evolution of the phase differences between the phase functions of I. In VI is plotted the temporal evolution of the phase differences between the phase functions of II. In VII is plotted the temporal evolution of the phase differences between the phase functions of II after a correction of phase differences based on the distances of the phase differences to 0.

Part II

Contributions

Chapter 3

Analytic derivation of Morlet Wavelet Transform applied to sum of sinusoids

Phase retrieval is an inevitable step to compute phase synchrony measures. The available tools prone to the task are implemented in mainstream libraries and used without much concern about their actual accuracy. It is most often used with fixed parameters that are almost never debated. Thanks to the very formulations of Morlet wavelet transforms applied to sinusoids or Gaussian modulated sinusoids, the derivations are possible. The analysis of these derivations provides insights on the accuracy of the method to retrieve the phase information.

3.1 Introduction

The usage of continuous (and most often Morlet) wavelet transforms is ubiquitous in fields where rhythmicity occurs. Not only because it is convenient (largely implemented in common libraries) but also because it is well adapted to problems where ephemeral oscillations arise at different frequencies. Its usage notably bloomed in the EEG field from the early 1990s, and served different purposes: interictal EEG spike detection [270, 269, 131], epileptic seizure prediction, reconstruction of evoked potentials [17], induced oscillatory activity [295]... Thirty years later, several thousand scientific papers yearly employ continuous wavelet transforms to analyze EEG signal. While its interest is unquestionable, the extent to which it can be used and interpreted is sometimes unclear. One aim of the following derivations is to provide a tighter grasp on what can, and what cannot be extracted from EEG signals with the Morlet wavelet transform (MWT), by offering another perspective on the trade-off between time and frequency accuracy. It is based on the hypothesis of local stationarity of the frequency and amplitude properties. The latter hypothesis is relaxed in the last section.

Two components are usually extracted from analytic wavelet transforms, namely the envelope and the phase angle. The envelope (instantaneous amplitude) at a given time point corresponds to the modulus of the complex wavelet coefficient. It is a good indicator of the signal's energy around a given time point and within a frequency band. The phase angle (instantaneous phase) is taken as the argument of this same complex coefficient. For mono-frequency signals, the phase angle informs on the angular location within the current oscillation. It can be represented on the trigonometric circle, hence takes values between $-\pi$ and π. For more complex signals, there is no simple interpretation of the phase. This is discussed in length hereafter.

This chapter is organized as follows. First, the phase angle of the MWT of a sine wave is analytically derived. Some properties of the formula are discussed to draw some connections with the width of the Morlet wavelet. Second, the phase angle of a sum of sine waves oscillating at arbitrary frequencies (a more realistic approximation of a biologically inspired signal) is calculated by the MWT. Hypotheses are proposed to provide a simplification of this expression. It provides a useful view on the mixing of frequency components that occur during the phase extraction. Third, the phase angle MWT of a sine wave modulated by a Gaussian window is derived to show the

influence of the Gaussian modulation on phase extraction. Lastly, the overlapping of two Gaussian modulated sine waves is considered.

3.1.1 Brief introduction of the Morlet Wavelet Transform

An analytic signal has no energy in the negative part of its frequency spectrum. It can be expressed as a complex exponential, which enables the retrieval of the envelope and the phase angle. A real signal can be made analytic by finding a complex part offsetting the energy in the negative part of the frequency spectrum. This problem can be solved using the Hilbert transform [36], the windowed Fourier Transform or by convolution with an analytic wavelet kernel. These strategies were shown to hold fundamentally equivalent results under the right set of parameters [157, 229, 39].

Several analytic wavelets have been designed, such as the complex Cauchy wavelet, the complex Mexican Hat wavelet or the complex Morlet Wavelet. They are analytic, meaning their real part is orthogonal to their imaginary part :

$$\int_{-\infty}^{\infty} \Im(w(t))\Re(w(t)) = 0 \tag{3.1}$$

where:

w is any analytic wavelet function

The convolution of a function $f : t \to f(t)$ with a kernel function $g : t \to g(t)$ is expressed as: $\int_{-\infty}^{\infty} f(u-t)g(t)dt$. A Wavelet Transform ($WT$) is a convolution of the signal with a wavelet kernel.

The principal aim of the Morlet wavelet transform is therefore to produce an analytic signal while constraining the information locally (in time and frequency). The Morlet wavelet w is a function of time t :

$$w(t) = \frac{\sqrt{2\pi}\nu_w e^{\frac{\Omega_w^2}{2}}}{\Omega_w} e^{i2\pi\nu_w t} e^{-\frac{2t^2\pi^2\nu_w^2}{\Omega_w^2}} \tag{3.2}$$

where:

ν_w is the frequency of oscillation of the wavelet (in Hz)
Ω_w is the number of oscillations (approximately) contained within the Gaussian window

The Morlet wavelet is the product of a complex exponential function (oscillating at ν_w Hz in the complex plane), and a Gaussian function centered at zero (whose width Ω_w depends on ν_w and a chosen number of oscillations in the time domain). It is is plotted in figure 3.1.

Its Fourier transformed counterpart is a function of the frequency ν :

$$F_w(\nu) = e^{\frac{\Omega_w^2}{2}} e^{-\frac{(-2\pi(\nu_w+\nu))^2\Omega_w^2}{8\pi^2\nu_w^2}} \tag{3.3}$$

Note: Although the Gaussian function is symmetric, the complex exponential is not, thus the Morlet wavelet is not symmetric. Increasing Ω_w enlarges the wavelet in the time domain and reduces its Fourier counterpart in the frequency domain. The larger the wavelet in the time domain, the more time samples are needed to compute its transform, reducing the time accuracy to the benefit of improving the frequency accuracy. Figuring the best compromise between time and frequency accuracies depends on the duration of events of interest in the signal.

The convolution of a function f with a Morlet wavelet is written :

$$WT_f(u) = \frac{\sqrt{2\pi}e^{\frac{\Omega_w^2}{2}}}{\Omega_w} \int_{-\infty}^{\infty} f(u-t) e^{i2\pi\nu_w t} e^{-\frac{2t^2\pi^2\nu_w^2}{\Omega_w^2}}\, dt \tag{3.4}$$

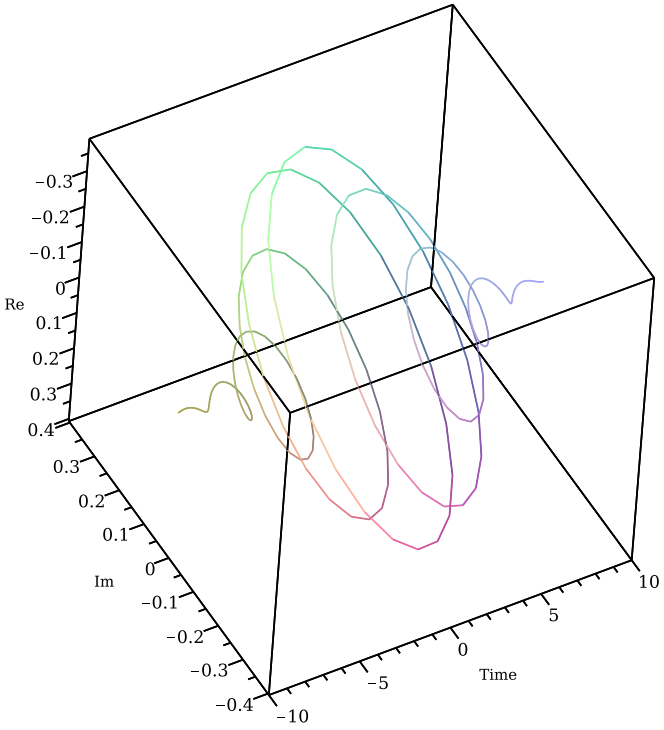

Figure 3.1: Morlet Wavelet $w(t) = \frac{\sqrt{2\pi}\nu_w e^{\frac{-\Omega_w^2}{2}}}{\Omega_w} e^{i2\pi\nu_w t} e^{-\frac{2t^2\pi^2\nu_w^2}{\Omega_w^2}}$. Time: t. $\Im(w(t))$ and $\Re(w(t))$ are represented as a function of time. It oscillates at 3 Hz in the complex plane ($\nu_w = 3$), with a width(Ω_w) of 10.

3.2 Phase angle of a sine wave

It is usually assumed [3, 157] that the phase angle can be retrieved from the argument of complex coefficients calculated with the analytic wavelet transform, i.e.: $\phi(u) = arctan\left(\frac{\Im(WT_f(u))}{\Re(WT_f(u))}\right)$. To challenge this stand, this quantity is calculated analytically for a sinusoid $f : t \to cos(2\pi\nu_c t + \phi_c)$. The derivation is simplified by rewriting f with the Euler formula, $f \to \frac{1}{2}(e^{i(2\pi\nu_c t+\phi_c)} + e^{-i(2\pi\nu_c t+\phi_c)})$ and supposing known the Fourier Transform (FT) of the Morlet wavelet :

$$
\begin{aligned}
&\frac{\Omega_w}{\sqrt{2\pi}\nu_w e^{\frac{\Omega_w^2}{2}}} WT_f(u) \\
&= \int_{-\infty}^{\infty} \cos(2\pi\nu_c(u-t)+\phi_c) e^{i2\pi\nu_w t} e^{-\frac{t^2(2\pi\nu_w)^2}{2\Omega_w^2}}\, dt \\
&= \int_{-\infty}^{\infty} \frac{1}{2}(e^{i(2\pi\nu_c(u-t)+\phi_c)} + e^{-i(2\pi\nu_c(u-t)+\phi_c)}) e^{i2\pi\nu_w t} e^{-\frac{t^2(2\pi\nu_w)^2}{2\Omega_w^2}}\, dt \\
&= \frac{1}{2}\left(\int_{-\infty}^{\infty} e^{i(2\pi\nu_c(u-t)+\phi_c)} e^{i2\pi\nu_w t} e^{-\frac{t^2(2\pi\nu_w)^2}{2\Omega_w^2}}\, dt + \int_{-\infty}^{\infty} e^{-i(2\pi\nu_c(u-t)+\phi_c)} e^{i2\pi\nu_w t} e^{-\frac{t^2(2\pi\nu_w)^2}{2\Omega_w^2}}\, dt \right) \\
&= \frac{1}{2}\left(e^{i(2\pi\nu_c u+\phi_c)} \int_{-\infty}^{\infty} e^{i2\pi\nu_w t} e^{-\frac{t^2(2\pi\nu_w)^2}{2\Omega_w^2}} e^{-i2\pi\nu_c t}\, dt + e^{-i(2\pi\nu_c u+\phi_c)} \int_{-\infty}^{\infty} e^{i2\pi\nu_w t} e^{-\frac{t^2(2\pi\nu_w)^2}{2\Omega_w^2}} e^{i2\pi\nu_c t}\, dt \right) \\
&= \frac{1}{2}\left(e^{i(2\pi\nu_c u+\phi_c)} FT(e^{i2\pi\nu_w t} e^{-\frac{t^2(2\pi\nu_w)^2}{2\Omega_w^2}})(2\pi\nu_c) + e^{-i(2\pi\nu_c u+\phi_c)} FT(e^{i2\pi\nu_w t} e^{-\frac{t^2(2\pi\nu_w)^2}{\Omega_w^2}})(-2\pi\nu_c) \right) \\
&= \frac{1}{2}\left(e^{i(2\pi\nu_c u+\phi_c)} \frac{\Omega_w}{\sqrt{2\pi}\nu_w} e^{-\frac{\Omega_w^2(2\pi\nu_c-2\pi\nu_w)^2}{2(2\pi\nu_w)^2}} + e^{-i(2\pi\nu_c u+\phi_c)} \frac{\Omega_w}{\sqrt{2\pi}\nu_w} e^{-\frac{\Omega_w^2(2\pi\nu_c+2\pi\nu_w)^2}{2(2\pi\nu_w)^2}} \right)
\end{aligned}
$$

For the numerator :

$$
\begin{aligned}
&\frac{e^{\frac{-\Omega_w^2}{2}}\Omega_w}{\sqrt{2\pi}} \Im\left(WT_f(u)\right) \\
&= \frac{\Omega_w}{\sqrt{2\pi}\nu_w} \frac{1}{2}\left(sin(2\pi\nu_c u+\phi_c) e^{-\frac{\Omega_w^2(\nu_c-\nu_w)^2}{2\nu_w^2}} - sin(2\pi\nu_c u+\phi_c) e^{-\frac{\Omega_w^2(\nu_c+\nu_w)^2}{2\nu_w^2}} \right) \\
&= \frac{\Omega_w}{\sqrt{2\pi}\nu_w} \frac{1}{2} sin(2\pi\nu_c u+\phi_c)\left(e^{-\frac{\Omega_w^2(\nu_c-\nu_w)^2}{2\nu_w^2}} - e^{-\frac{\Omega_w^2(\nu_c+\nu_w)^2}{2\nu_w^2}} \right) \\
&= \frac{\Omega_w}{\sqrt{2\pi}\nu_w} \mathrm{e}^{-\frac{\Omega_w^2}{2}} sin(2\pi\nu_c u+\phi_c) \mathrm{e}^{-\frac{\Omega_w^2\nu_c^2}{2\nu_w^2}} \sinh\left(\frac{\Omega_w^2\nu_c}{\nu_w}\right)
\end{aligned}
$$

and similarly for the denominator :

$$
\begin{aligned}
&\frac{e^{\frac{-\Omega_w^2}{2}}\Omega_w}{\sqrt{2\pi}} \Re\left(WT_f(u)\right) \\
&= \frac{\Omega_w}{\sqrt{2\pi}\nu_w} \mathrm{e}^{-\frac{\Omega_w^2}{2}} cos(2\pi\nu_c u+\phi_c) \mathrm{e}^{-\frac{\Omega_w^2\nu_c^2}{2\nu_w^2}} \cosh\left(\frac{\Omega_w^2\nu_c}{\nu_w}\right)
\end{aligned}
$$

The phase is therefore expressed as :

$$
\phi(u) = arctan\left(\frac{\Im(WT_f(u))}{\Re(WT_f(u))}\right) = arctan\left(tan\left(2\pi\nu_c u+\phi_c\right) tanh\left(\frac{\Omega_w^2\nu_c}{\nu_w}\right)\right) \tag{3.5}
$$

The assumption that: $\phi(u) = arctan\left(\frac{\Im(WT_f(u))}{\Re(WT_f(u))}\right)$ is the phase of the signal, holds true only for mono-frequency signals, if the frequency of the signal matches the frequency of the wavelet (i.e. $\nu_c = \nu_w$), and yet, in this specific case, it depends on the number of oscillations (Ω_w).

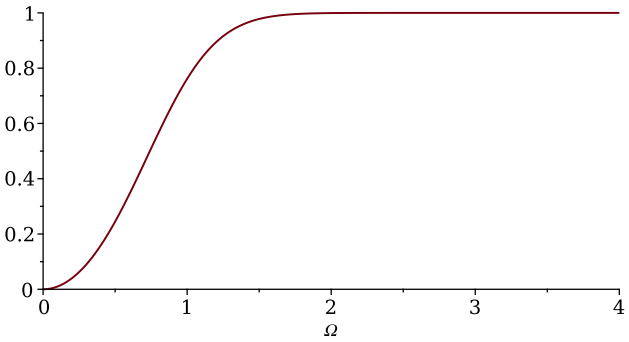

Figure 3.2: $\tanh(\Omega^2)$, Ω varying from 0 to 4. No units.

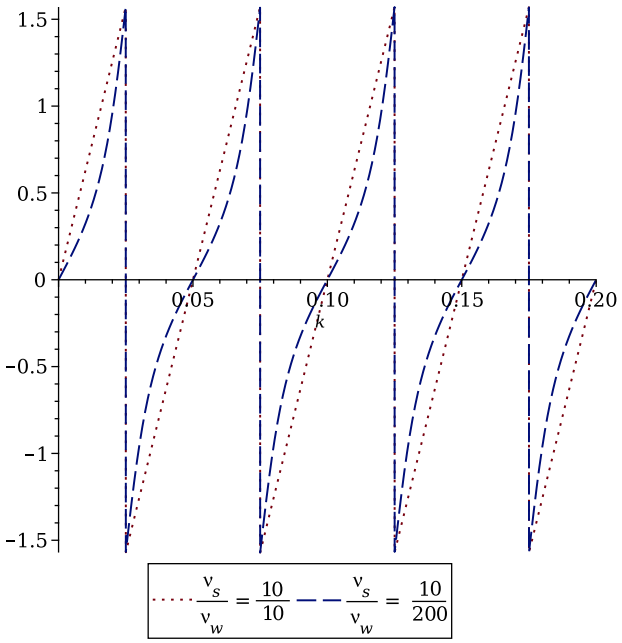

Figure 3.3: Evolution of the phase extracted by the WT of a sinus oscillating at 10Hz ($\nu_s = \nu_c + \pi/2$). x-axis: u varies from 0 to 0.2 seconds, equivalently two oscillations. y-axis: phase angle ranging from $-\pi/2$ to $\pi/2$. The dotted line corresponds to the case where the frequency of the wavelet matches the frequency of the signal. The dashed line corresponds to the case where the frequency of the wavelet is much higher than the frequency of the signal. $\Omega_w = 10$.

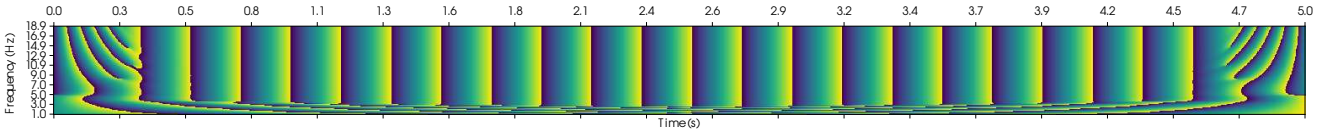

Figure 3.4: Time Frequency plane of the phase of $sin(10 * 2\pi t)$, t varying from 0 to 5. The signal is decomposed on frequencies varying from 1 to 19 with wavelets composed of 7 oscillations ($\Omega_w = 7$). The plot is obtained by numerical convolution (computed by multiplication in the Fourier domain of the Fourier Transform of the signal and the Fourier Transform of the wavelet followed by Fourier Inverse Transform of the product). Despite the absence of energy in the signal for frequencies different from 10Hz phase information is available but not meaningful. Behavior at the edges and for low frequencies is not discussed here.

When $\nu_c = \nu_w$ one can observe in figure 3.2 that $\tanh(\Omega_w^2)$ is close to 1 for values of Ω_w higher than 2.

When the frequency of the sinusoid differs from the frequency of the wavelet, the hyperbolic tangent is close to 1 when $\Omega_w^2 \nu_c >> \nu_w$. In cases where this is not observed, such as in figure 3.3, the phase angle trajectory gets curved, while the singularities (jumps) still occur at the same time points (due to the unaffected tangent).

Formula 3.5 also helps understand the numerical values of the phase in frequency bands with no energy observed in figure 3.4. The phase angle is dictated by the closest frequency components of the signal and not the frequency of the wavelet, as it will be unveiled in section 3.3. Hence, for a mono-frequency signal oscillating at 10 Hz, for Ω_w large enough and far enough from the edges, regardless of the frequency of the wavelet, the phase is always the phase of the signal.

3.3 Phase angle for combination of sine waves

The WT applied to a sum of sinusoids $f(t) = \sum \alpha_i cos(2\pi\nu_i t + \phi_i)$ is a sum of WT applied to single sinusoids. It leads to the expression of a "phase"[1] :

$$\phi(u) = arctan\left(\frac{\Im(WT_f(u))}{\Re(WT_f(u))}\right) = arctan\left(\frac{\sum \alpha_i \left(e^{-\frac{\Omega_w^2(\nu_i-\nu_w)^2}{2\nu_w^2}} - e^{-\frac{\Omega_w^2(\nu_i+\nu_w)^2}{2\nu_w^2}}\right) sin(2\pi\nu_i u + \phi_i)}{\sum \alpha_i \left(e^{-\frac{\Omega_w^2(\nu_i-\nu_w)^2}{2\nu_w^2}} + e^{-\frac{\Omega_w^2(\nu_i+\nu_w)^2}{2\nu_w^2}}\right) cos(2\pi\nu_i u + \phi_i)}\right) \tag{3.6}$$

For Ω_w values higher than a threshold γ, equation 3.6 simplifies to [2] :

$$\phi(u) \approx arctan\left(\frac{\sum \alpha_i e^{-\frac{\Omega_w^2(\nu_i-\nu_w)^2}{2\nu_w^2}} sin(2\pi\nu_i u + \phi_i)}{\sum \alpha_i e^{-\frac{\Omega_w^2(\nu_i-\nu_w)^2}{2\nu_w^2}} cos(2\pi\nu_i u + \phi_i)}\right) \tag{3.7}$$

The threshold γ is the value Ω_w solution of: $\frac{e^{-\frac{\Omega_w^2(\overline{\nu}+1)^2}{2}}}{e^{-\frac{\Omega_w^2(\overline{\nu}-1)^2}{2}}} = 10^{-\theta}$, where $\overline{\omega} = \frac{\nu_i}{\nu_w}$, θ being the requested precision. $\gamma = \frac{\sqrt{-2\overline{\nu}\ln(10^{-\theta})}}{2\overline{\nu}}$. For example, with $\theta = 2$ and $\nu_i = \nu_w$: $\gamma \approx 2.15$

[1] The exponential form is used instead of the hyperbolic sine / cosine for the simple reason that the hyperbolic tangent cannot appear due to the sums at the numerator and denominator.

[2] The coefficients $\alpha_i e^{-\frac{\Omega_w^2(2\pi\nu_i-2\pi\nu_w)^2}{22\pi\nu_w^2}}$ can be further simplified to $\alpha_i e^{-\frac{\Omega_w^2 2\pi\nu_i^2}{22\pi\nu_w^2}} e^{\frac{\Omega_w^2 2\pi\nu_i}{2\pi\nu_w}}$, but the coefficients wouldn't max out at α_i but at $\alpha_i e^{\frac{\Omega_w^2}{2}}$.

It can also be observed with the hyperbolic functions, for $\Omega_w > 5$: $sinh(\Omega_w^2 \frac{2\pi\nu_c}{2\pi\nu_w}) \approx cosh(\Omega_w^2 \frac{2\pi\nu_c}{2\pi\nu_w})$ for any practical $\frac{2\pi\nu_c}{2\pi\nu_w}$.

The study of the coefficients weighting $\sin(2\pi\nu_i u + \phi_i)$ at the numerator and $cos(2\pi\nu_i u + \phi_i)$ at the denominator in equation 3.7 provides insightful information on what the MWT can achieve, and when it fails to provide meaningful results.

Notably, phase shift (ϕ_i) is not involved in the coefficients and the frequency of a component does not play any role in the weighting of another (a trivial albeit essential property due to the linearity of the transform).

The contribution of a frequency component to the phase is balanced between its amplitude and the distance of its frequency to the wavelet frequency. The more distant the frequency of the signal to the frequency of the wavelet, the closer the Gaussian window ($e^{-\frac{\Omega_w^2(\nu_i-\nu_w)^2}{2\nu_w^2}}$) gets to zero and so does the weight. But for close frequency components, the sums at the numerator and denominator mix up, and no proper phase (in the sense of a pure oscillator) can be retrieved. In that sense, it tallies with the idea that there is a trade-off between time and frequency accuracy: by increasing the width of the Morlet wavelet in the time domain, it reduces the width of the wavelet in the frequency domain (the role of Ω_w being reversed).

Equation 3.7 gives a possible definition for the "phase" of a combination of sine waves. This phase is defined locally (within the Gaussian window) and applies especially well in the context of signals with local stationarity.

Regarding the analysis of EEG signals, the *arctan* is non-linear and equation 3.7 is a good representation to observe that the influence of the reference in a bipolar channel cannot be removed once the phase is computed. For instance, computing phase differences is not an option to make the reference's influence vanish.

3.3.1 Different combinations of sinusoids produce the same phase

One concern that can be unveiled under this framework is that different combinations of sinusoids at various frequencies can return the same phase. It is illustrated in equation 3.8 with the phase angle difference between two signals, each one composed of a pair of sinusoids (s_0 and s_1, s_2 and s_3) with amplitude α_i and frequency ν_i.

$$\begin{aligned}
&\phi_{s_0+s_1} - \phi_{s_2+s_3} = \\
&\arctan\left(\frac{\alpha_0 e^{-\frac{(\nu_0-\nu_w)^2\Omega_w^2}{2\nu_w{}^2}}\sin(2\pi\nu_0 u) + \alpha_1 e^{-\frac{(\nu_1-\nu_w)^2\Omega_w^2}{2\nu_w{}^2}}\sin(2\pi\nu_1 u)}{\alpha_0 e^{-\frac{(\nu_0-\nu_w)^2\Omega_w^2}{2\nu_w{}^2}}\cos(2\pi\nu_0 u) + \alpha_1 e^{-\frac{(\nu_1-\nu_w)^2\Omega_w^2}{2\nu_w{}^2}}\cos(2\pi\nu_1 u)}\right) \\
-\arctan&\left(\frac{\alpha_2 e^{-\frac{(\nu_2-\nu_w)^2\Omega_w^2}{2\nu_w{}^2}}\sin(2\pi\nu_2 u) + \alpha_3 e^{-\frac{(\nu_3-\nu_w)^2\Omega_w^2}{2\nu_w{}^2}}\sin(2\pi\nu_3 u)}{\alpha_2 e^{-\frac{(\nu_2-\nu_w)^2\Omega_w^2}{2\nu_w{}^2}}\cos(2\pi\nu_2 u) + \alpha_3 e^{-\frac{(\nu_3-\nu_w)^2\Omega_w^2}{2\nu_w{}^2}}\cos(2\pi\nu_3 u)}\right) = 0
\end{aligned} \tag{3.8}$$

This phase difference can be null when the frequencies of sinusoids composing each signals are different, but symmetrically chosen around the wavelet frequency, and the amplitudes are equals. It translates into four hypotheses :

1) $\nu_0 - \nu_w = -(\nu_1 - \nu_w)$

2) $\nu_2 - \nu_w = -(\nu_3 - \nu_w)$

3) $\alpha_0 = \alpha_1$

4) $\alpha_2 = \alpha_3$

With 1) and 2) :

$$\arctan\left(\frac{\alpha_0\sin(2\pi\nu_0 u)+\alpha_1\sin(2\pi\nu_1 u)}{\alpha_0\cos(2\pi\nu_0 u)+\alpha_1\cos(2\pi\nu_1 u)}\right)-\arctan\left(\frac{\alpha_2\sin(2\pi\nu_2 u)+\alpha_3\sin(2\pi\nu_3 u)}{\alpha_2\cos(2\pi\nu_2 u)+\alpha_3\cos(2\pi\nu_3 u)}\right)=0 \tag{3.9}$$

With 3) and 4) :

$$\begin{aligned}
\arctan\left(\frac{\sin(2\pi\nu_0 u)+\sin(2\pi\nu_1 u)}{\cos(2\pi\nu_0 u)+\cos(2\pi\nu_1 u)}\right)-\arctan\left(\frac{\sin(2\pi\nu_2 u)+\sin(2\pi\nu_3 u)}{\cos(2\pi\nu_2 u)+\cos(2\pi\nu_3 u)}\right)&=0\\
\arctan\left(\frac{2\sin\left(\frac{2\pi\nu_0 u+2\pi\nu_1 u}{2}\right)\cos\left(\frac{2\pi\nu_0 u-2\pi\nu_1 u}{2}\right)}{2\cos\left(\frac{2\pi\nu_0 u+2\pi\nu_1 u}{2}\right)\cos\left(\frac{2\pi\nu_0 u-2\pi\nu_1 u}{2}\right)}\right)-\arctan\left(\frac{2\sin\left(\frac{2\pi\nu_2 u+2\pi\nu_3 u}{2}\right)\cos\left(\frac{2\pi\nu_2 u-2\pi\nu_3 u}{2}\right)}{2\cos\left(\frac{2\pi\nu_2 u+2\pi\nu_3 u}{2}\right)\cos\left(\frac{2\pi\nu_2 u-2\pi\nu_3 u}{2}\right)}\right)&=0\\
2\pi(\nu_0+\nu_1-\nu_2-\nu_3)u&=0\\
\nu_0+\nu_1&=\nu_2+\nu_3
\end{aligned}$$

which is true because of 1) and 2): $\nu_0-\nu_w=-(\nu_1-\nu_w)$ and $\nu_2-\nu_w=-(\nu_3-\nu_w)$ are equivalent to $\nu_0+\nu_1=2\nu_w$ and $\nu_2+\nu_3=2\nu_w$.

Relaxing 3) and 4), α_3 in 3.8 can be expressed as a function of the other parameters 3.10.

$$\alpha_3=-\frac{e^{-\frac{(\nu_2-\nu_w)^2\Omega_w^2}{2\nu_w{}^2}}\alpha_2\left(e^{-\frac{(\nu_1-\nu_w)^2\Omega_w^2}{2\nu_w{}^2}}\alpha_1\sin(2\pi\nu_1 u-2\pi\nu_2 u)+e^{-\frac{(\nu_0-\nu_w)^2\Omega_w^2}{2\nu_w{}^2}}\alpha_0\sin(2\pi\nu_0 u-2\pi\nu_2 u)\right)}{e^{-\frac{(\nu_3-\nu_w)^2\Omega_w^2}{2\nu_w{}^2}}\left(e^{-\frac{(\nu_1-\nu_w)^2\Omega_w^2}{2\nu_w{}^2}}\alpha_1\sin(2\pi\nu_1 u-2\pi\nu_3 u)+e^{-\frac{(\nu_0-\nu_w)^2\Omega_w^2}{2\nu_w{}^2}}\alpha_0\sin(2\pi\nu_0 u-2\pi\nu_3 u)\right)} \tag{3.10}$$

In any case, this means that observing a phase difference of 0 over time, does not imply that the components of two signals oscillate at the same frequencies.

3.4 Phase angle for an oscillating burst

Electrical brain activity measured at the scalp is in part rhythmic, and arrives mostly in bursts. A phenomenon which is especially visible in the α, μ, β, θ rhythms. This rhytmicity is at best locally stationary. To study the pertinence of the Morlet Wavelet approach in extracting properties of the underlying activity, one burst of rhythmical brain activity at the scalp is modeled as a Gaussian modulated sinusoid. It mimics the projection of the excitation / inhibition of a given cortical area by a varying (increasing then decreasing) number of neurons from the same or different cortical area.

Following a similar derivation to the one applied to the sine wave, the phase extraction of a Gaussian modulated sinusoid :

$$f(t)=e^{\frac{-2(t-t_0)^2\pi^2\nu_s^2}{\Omega_s^2}}cos\left(2\pi\nu_s(t-t_0)+\phi_s\right) \tag{3.11}$$

where:

t_0 Center of the burst
Ω_s Width of the burst (in number of oscillations)
ν_s Frequency of the burst
ϕ_s Phase of the burst at $t=t_0$

by convolution with a Morlet wavelet gives :

$$\phi(u) = arctan\Bigg(\frac{ e^{\frac{-\Omega_w^2(\nu_s+\nu_w)^2\Omega_s^2-4\pi^2\nu_s^2\nu_w^2(u-t_0)^2}{2\nu_s^2\Omega_w^2+2\nu_w^2\Omega_s^2}} \sin\left(\frac{2\left(\pi(u-t_0)\nu_w-\frac{\phi_s}{2}\right)\Omega_w^2\nu_s^2-2\pi\nu_w^2\Omega_s^2(u-t_0)\nu_s-\Omega_s^2\phi_s\nu_w^2}{\nu_s^2\Omega_w^2+\nu_w^2\Omega_s^2}\right) + e^{\frac{-\Omega_s^2\Omega_w^2(\nu_s-\nu_w)^2-4\pi^2\nu_s^2\nu_w^2(u-t_0)^2}{2\nu_s^2\Omega_w^2+2\nu_w^2\Omega_s^2}} \sin\left(\frac{2\left(\pi(u-t_0)\nu_w+\frac{\phi_s}{2}\right)\Omega_w^2\nu_s^2+2\pi\nu_w^2\Omega_s^2(u-t_0)\nu_s+\Omega_s^2\phi_s\nu_w^2}{\nu_s^2\Omega_w^2+\nu_w^2\Omega_s^2}\right) }{ e^{\frac{-\Omega_w^2(\nu_s+\nu_w)^2\Omega_s^2-4\pi^2\nu_s^2\nu_w^2(u-t_0)^2}{2\nu_s^2\Omega_w^2+2\nu_w^2\Omega_s^2}} \cos\left(\frac{2\left(\pi(u-t_0)\nu_w-\frac{\phi_s}{2}\right)\Omega_w^2\nu_s^2-2\pi\nu_w^2\Omega_s^2(u-t_0)\nu_s-\Omega_s^2\phi_s\nu_w^2}{\nu_s^2\Omega_w^2+\nu_w^2\Omega_s^2}\right) + e^{\frac{-\Omega_s^2\Omega_w^2(\nu_s-\nu_w)^2-4\pi^2\nu_s^2\nu_w^2(u-t_0)^2}{2\nu_s^2\Omega_w^2+2\nu_w^2\Omega_s^2}} \cos\left(\frac{2\left(\pi(u-t_0)\nu_w+\frac{\phi_s}{2}\right)\Omega_w^2\nu_s^2+2\pi\nu_w^2\Omega_s^2(u-t_0)\nu_s+\Omega_s^2\phi_s\nu_w^2}{\nu_s^2\Omega_w^2+\nu_w^2\Omega_s^2}\right) } \Bigg)$$

With similar considerations as those used to obtain equation 3.7, namely whenever $2\Omega_w^2\Omega_s^2\nu_s\nu_w >> \nu_s^2\Omega_w^2+\nu_w^2\Omega_s^2$, a simplification leads to :

$$\phi(u) \approx 2\pi\frac{\nu_w\Omega_w^2\nu_s^2+\nu_s\Omega_s^2\nu_w^2}{\nu_s^2\Omega_w^2+\nu_w^2\Omega_s^2}(u-t_0)+\phi_s$$

For $\nu_w = \nu_s$, the convolution of a synthetic burst with a Morlet Wavelet gives the expected phase: $2\pi\nu_s(u-t_0)+\phi_s$ i.e. the phase and phase shift of the bursts sine wave.

It paves the way for possible bursts properties identification by means of a Morlet wavelet transform, the topic of the research of chapter 5.

3.5 Phase angle for close oscillating bursts

While the Morlet wavelet transform permits the retrieval of the phase and phase shift of a single burst, it may seem unpractical for real EEG applications. Indeed, while a cortical region is likely to generate a single burst at once, because of volume conduction, an electrode might measure several overlapping bursts coming from different regions at about the same time.

The case of two overlapping bursts is generally defined as follows, with similar considerations as in the previous section :

$$f(t,t_{s0},t_{s1}) = \mathrm{e}^{-\frac{2(t-t_{s0})^2\pi^2\nu_{s0}^2}{\Omega_{s0}^2}}\cos(2\pi\nu_{s0}(t-t_{s0})+\phi_{s0}) + \mathrm{e}^{-\frac{2(t-t_{s1})^2\pi^2\nu_{s1}^2}{\Omega_{s1}^2}}\cos(2\pi\nu_{s1}(t-t_{s1})+\phi_{s1}) \qquad (3.12)$$

Three cases are considered to study the evolution of the phase with varying distance between bursts are depicted in figure 3.5. The two bursts share a same frequency and duration, but differ in their center and in their phase shift at the center. In all cases $t_{s1} = 4.$, so that by progressively increasing t_{s0} the two bursts overlap more and more. In the first case where $t_{s0} = 3.$ the two burst centers are distant of 1 second and do not overlap. In the second case where $t_{s0} = 3.5$ the two burst centers are distant of 0.5 second and clearly overlap, yet the two bursts

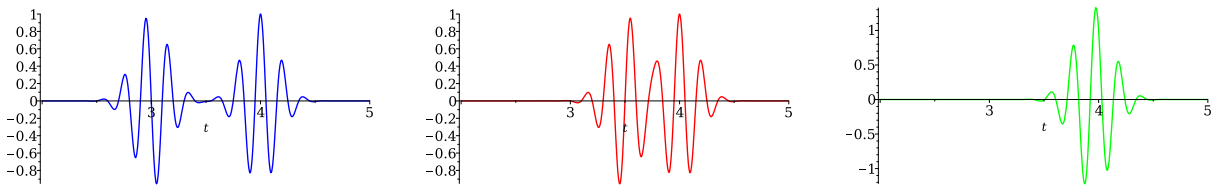

Figure 3.5: I: $t_{s0} = 3$.s, II: $t_{s0} = 3.5$s, III: $t_{s0} = 3.9$s.
$t_{s1} = 4$.s. $\nu_{s0} = \nu_{s1} = 5$. $\Omega_{s0} = \Omega_{s1} = 5$. $\phi_{s0} = \pi/2$. $\phi_{s1} = 0\pi$.

are still distinguishable. In the third and last case where $t_{s0} = 3.9$ the two burst centers are distant of 0.1 second. Of the two bursts only remains the shape asymmetry.

Again, the derivation of the Morlet wavelet transform of f conducts to :

$$
\begin{aligned}
WT_f(u) \approx arctan\Bigg(& \\
& \Omega_{s1}\sqrt{\nu_{s0}^2\Omega_w^2 + \nu_w^2\Omega_{s0}^2}\, \mathrm{e}^{\frac{-\Omega_w^2(\nu_w-\nu_{s1})^2\Omega_{s1}^2 - 4\pi^2\nu_w^2\nu_{s1}^2(u-t_{s1})^2}{2\nu_{s1}^2\Omega_w^2 + 2\Omega_{s1}^2\nu_w^2}} \\
& \cos\left(\frac{2\pi\nu_{s1}^3 t_{s1}\Omega_w^2 + 2\Omega_w^2\left(\pi\left(u-t_{s1}\right)\nu_w + \frac{\phi_{s1}}{2}\right)\nu_{s1}^2 + 2\pi u\nu_{s1}\nu_w^2\Omega_{s1}^2 + \Omega_{s1}^2\phi_{s1}\nu_w^2}{\nu_{s1}^2\Omega_w^2 + \Omega_{s1}^2\nu_w^2}\right) \\
& + \Omega_{s0}\sqrt{\nu_{s1}^2\Omega_w^2 + \Omega_{s1}^2\nu_w^2}\, \mathrm{e}^{\frac{-\Omega_w^2(\nu_w-\nu_{s0})^2\Omega_{s0}^2 - 4\pi^2\nu_w^2\nu_{s0}^2(u-t_{s0})^2}{2\nu_{s0}^2\Omega_w^2 + 2\nu_w^2\Omega_{s0}^2}} \\
& \cos\left(\frac{2\pi\nu_{s0}^3 t_{s0}\Omega_w^2 + 2\Omega_w^2\left(\pi\left(u-t_{s0}\right)\nu_w + \frac{\phi_{s0}}{2}\right)\nu_{s0}^2 + 2\pi u\nu_{s0}\nu_w^2\Omega_{s0}^2 + \phi_{s0}\nu_w^2\Omega_{s0}^2}{\nu_{s0}^2\Omega_w^2 + \nu_w^2\Omega_{s0}^2}\right) \\
& \Bigg/ \\
& \Omega_{s1}\sqrt{\nu_{s0}^2\Omega_w^2 + \nu_w^2\Omega_{s0}^2}\, \mathrm{e}^{\frac{-\Omega_w^2(\nu_w-\nu_{s1})^2\Omega_{s1}^2 - 4\pi^2\nu_w^2\nu_{s1}^2(u-t_{s1})^2}{2\nu_{s1}^2\Omega_w^2 + 2\Omega_{s1}^2\nu_w^2}} \\
& \sin\left(\frac{2\pi\nu_{s1}^3 t_{s1}\Omega_w^2 + 2\Omega_w^2\left(\pi\left(u-t_{s1}\right)\nu_w + \frac{\phi_{s1}}{2}\right)\nu_{s1}^2 + 2\pi u\nu_{s1}\nu_w^2\Omega_{s1}^2 + \Omega_{s1}^2\phi_{s1}\nu_w^2}{\nu_{s1}^2\Omega_w^2 + \Omega_{s1}^2\nu_w^2}\right) \\
& + \Omega_{s0}\sqrt{\nu_{s1}^2\Omega_w^2 + \Omega_{s1}^2\nu_w^2}\, \mathrm{e}^{\frac{-\Omega_w^2(\nu_w-\nu_{s0})^2\Omega_{s0}^2 - 4\pi^2\nu_w^2\nu_{s0}^2(u-t_{s0})^2}{2\nu_{s0}^2\Omega_w^2 + 2\nu_w^2\Omega_{s0}^2}} \\
& \sin\left(\frac{2\pi\nu_{s0}^3 t_{s0}\Omega_w^2 + 2\Omega_w^2\left(\pi\left(u-t_{s0}\right)\nu_w + \frac{\phi_{s0}}{2}\right)\nu_{s0}^2 + 2\pi u\nu_{s0}\nu_w^2\Omega_{s0}^2 + \phi_{s0}\nu_w^2\Omega_{s0}^2}{\nu_{s0}^2\Omega_w^2 + \nu_w^2\Omega_{s0}^2}\right) \\
& \Bigg)
\end{aligned}
\tag{3.13}
$$

To compare the behaviors with respect to phase retrieval, the unwrapped phase is computed with equation 3.13.

Figure 3.6 shows that for case I of figure 3.5, the phase is correctly estimated at $t = 3.$ and $t = 4.$ (respectively equal to 0π and $\pi/2$), for case II an error in the estimation of the bursts starts to appear, and becomes striking for case III. Therefore, the phase and phase shift, even at the center of the bursts cannot be accurately recovered by means of the Morlet wavelet transform where the bursts are too close.

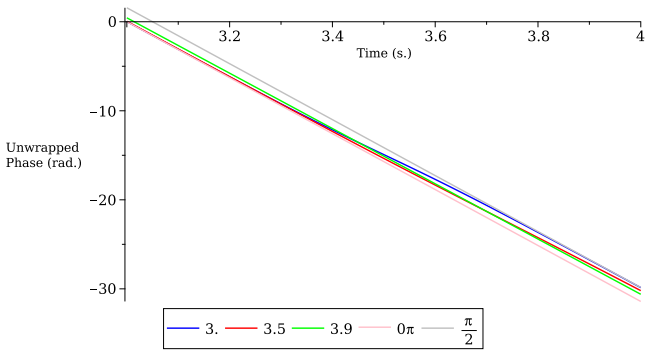

Figure 3.6: Unwrapped phase of the function composed of two bursts whose centers vary in distance to one another. The pink and grey lines corresponds to a linear phase at ν_{s0} frequency ($2\pi\nu_{s0}$) plus their respective phase shift (0π and $\pi/2$).

3.6 Conclusion

Part if not most of the exploitable EEG signal is oscillatory in nature. This justifies considering the EEG signal as a weighted sum of sinusoids, locally stationary. The Morlet wavelet is oscillatory by construction, it is therefore adapted to detect the oscillatory components in the EEG signal. This consideration induces the simplification that allows the derivation of interesting properties on the Morlet Wavelet transform. It notably sets up a first lower bound on the width of the wavelet, below which the course of the phase becomes unrealistic. It sets up a second lower bound on the width of the wavelet to obtain a more tractable expression of the extracted phase. This expression recalls that the reference electrode impairs the computation of the phase if and only if it oscillates in the vicinity of the frequency of the wavelet, and because of the non-linear properties of the arc-tangent, the phase cannot be corrected afterwards. Synchrony measures devised through the difference between phases can be misguiding since different combination of sinusoids produce the same phase. Lastly, such assumption on the EEG signal and the following derivations allow to show that the phase and phase shift of EEG bursts could be retrieved, although it was shown that for close bursts the Morlet wavelet as such is not up to the task.

Chapter 4

Correlation between close wavelet coefficients

Standard inferential statistic tests, such as the parametric Student t-test or the non parametric Mann-Whitney U test, assume that the two compared sets are made of independent samples. If two random variables are linearly correlated, they cannot be independent, and two samples drawn from these dependent random variables are not independent.

In the following derivation, the linear correlation coefficient is calculated for δ distant complex coefficients obtained by an analytic wavelet on an arbitrary signal for which the autocorrelation function is supposed null. In the case of a Morlet wavelet, it is shown that the autocorrelation function of the wavelet coefficients is a Gaussian function centered at 0.

4.1 Wavelet based measures are not independent

Synchrony measures based on the phase or amplitude envelope of real valued signals usually rely on the calculus of their complex analytic counterparts. The three most common options to obtain the complex analytic signal are either: delimitation of overlapping tapering windows on the signal and computation of a Fourier Transform for a specific frequency on these tapering windows, narrow band pass filtering and convolution with the Cauchy Kernel (Hilbert Transform), or convolution of the signal with an analytic wavelet (see chapter 3).

Because the complex coefficients are computed on overlapping windows (Fourier), or by convolution (Hilbert / Wavelets), they are correlated and the level of correlation depends on how spaced (in time) two coefficients are.

Although intuitive, this correlation can be shown under the hypothesis of the EEG signal behaving as a random variable. EEG signals can be modeled by random variables [86] and equivalently a 1D, n samples EEG signal can be modeled by a sequence of draws from n independent random variables X_t with the same mean $\mathbb{E}_X$ and variance $\mathbb{V}_X$:

$$x(t) = X_t, \forall t \; X_t \sim \Gamma(\mathbb{E}_X, \mathbb{V}_X) \tag{4.1}$$

The wavelet coefficient at time step k is obtained by convolution of a wavelet function W, oscillating at a given frequency (unspecified) with the signal x :

$$WT_x(k) = \sum_{t=k-\Gamma}^{k+\Gamma} W(t-k)X_t \tag{4.2}$$

$WT_x(k)$ (written WT(k) further on) is also a random variable. To not limit the development to infinitely wide wavelets, each wavelet has the window $[-\Gamma;\Gamma]$ as support.

The correlation coefficient between two δ_k distant wavelet coefficients is given by:

$$\rho(\,WT(k),\overline{WT(k+\delta_k)}) = \frac{\mathbb{C}[\,WT(k),\overline{WT(k+\delta_k)}]}{\sqrt{\mathbb{V}[\,WT(k)]}\sqrt{\mathbb{V}[\,WT(K+\delta_k)]}}$$

Where the variance equals:

$$\begin{aligned}\mathbb{V}[\,WT(k)] &= \mathbb{V}_X \sum_{t=k-\Gamma}^{k+\Gamma} W(t-k)^2 \\ &= \mathbb{V}_X \sum_{t=-\Gamma}^{\Gamma} W(t)^2\end{aligned}$$

And the covariance equals:

$$\mathbb{C}[\,WT(k),\overline{WT(k+\delta_k)}] = \mathbb{C}[\sum_{t_a=k-\Gamma}^{k+\Gamma} W(t_a-k)X_{t_a}, \sum_{t_b=k+\delta_k-\Gamma}^{k+\delta_k+\Gamma} \overline{W(t_b-(k+\delta_k))}X_{t_b}]$$

With the covariance bilinearity:

$$= \sum_{t_a=k-\Gamma}^{k+\Gamma} \sum_{t_b=k+\delta_k-\Gamma}^{k+\delta_k+\Gamma} W(t_a-k)\overline{W(t_b-(k+\delta_k))}\mathbb{C}[X_{t_a},X_{t_b}]$$

after the two changes of variables $t'_a = t_a - k$ and $t'_b = t_b - (k+\delta_k)$, the expression becomes:

$$= \sum_{t'_a=-\Gamma}^{\Gamma} \sum_{t'_b=-\Gamma}^{\Gamma} W(t'_a)\overline{W(t'_b)}\mathbb{C}[X_{t'_a+k},X_{t'_b+k+\delta_k}]$$

under the formulated hypothesis that the X_t are independent, $\mathbb{C}[X_{t'_a+k},X_{t'_b+k+\delta_k}] \neq 0$ for $t'_a + k = t'_b + k + \delta_k$:

$$= \mathbb{V}_X \sum_{t=-\Gamma}^{\Gamma} W(t)\overline{W(t-\delta_k)}$$

$$\rho(\,WT(k),\overline{WT(k+\delta_k)}) = \frac{\mathbb{V}_X \sum_{t=\Gamma}^{\Gamma} W(t)\overline{W(t-\delta_k)}}{\sqrt{\mathbb{V}_X \sum_{t=-\Gamma}^{\Gamma} W(t)^2 * \mathbb{V}_X \sum_{t=-\Gamma}^{\Gamma} W(t)^2}} \qquad = \frac{\sum_{t=-\Gamma}^{\Gamma} W(t)\overline{W(t-\delta_k)}}{\sum_{t=-\Gamma}^{\Gamma} W(t)^2}$$

The autocorrelation of the Morlet wavelet as a function of the lag ($\pm\delta_t$) is :

$$\int_{-\infty}^{\infty} W(t) * \overline{W(t+\delta_t)}dt = e^{-i2\pi\nu_w\delta_t}e^{-\frac{\pi^2\nu_w^2\delta_t^2}{\Omega_w^2}}$$

and plotted in figure 4.1.

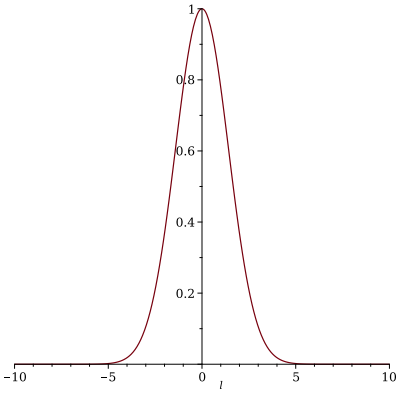

Figure 4.1: Modulus of the autocorrelation of the Morlet Wavelet (oscillating at 3 Hz, with a width (Ω_w) of 10 oscillations), as a function of δ_t.

Its modulus equals :

$$e^{-\frac{\pi^2 \nu_w^2 \delta_t^2}{\Omega_w^2}}$$

It validates a result presented by Ge [89] regarding the absolute value of the correlation coefficient of temporally adjacent wavelet coefficients: $\rho(\Delta b) = e^{-(\Delta b)^2/4a^2}$, where Δb matches δ_t and a matches $\Omega_w/(2\pi\nu_w)$, developed under the hypothesis that the signal follows a Gaussian white noise distribution which is slightly more restrictive than in the current case.

Because the Morlet wavelet function is tapered in time with a Gaussian window (not restricted to $[-\Gamma;\Gamma]$), any two coefficients, regardless of their proximity, will be correlated. This suggests that alternative tapering windows of finite length are to be considered in cases where correlation of samples is an issue, as it provides a guarantee of decorrelation between spaced enough samples (Hanning window).

For infinitely long wavelets Ge [89] proposes to decide of a correlation value (ρ_{ind}) below which two coefficients are deemed independent. From this correlation value, a minimal distance δ_t can be obtained to ensure that the coefficients aren't more correlated than ρ_{ind} :

$$\delta_t \geq 2\sqrt{ln(\rho_{ind})}\Omega_w/(2\pi\nu_w)$$

What if the signal is autocorrelated ? Assuming that an EEG signal is not autocorrelated is convenient, but not realistic. In the following derivation an arbitrary autocorrelation function for the signal is proposed.

$$\begin{aligned}\mathbb{C}[WT(k), \overline{WT(k+\delta_k)}] &= \sum_{t_a=k-\Gamma}^{k+\Gamma} \sum_{t_b=k+\delta_k-\Gamma}^{k+\delta_k+\Gamma} W(t_a-k)\overline{W(t_b-(k+\delta_k))}\mathbb{C}[X_{t_a}, X_{t_b}] \\ &= \sum_{t_a=k-\Gamma}^{k+\Gamma} \sum_{t_b=k+\delta_k-\Gamma}^{k+\delta_k+\Gamma} W(t_a-k)\overline{W(t_b-(k+\delta_k))}\rho(X_{t_a}, X_{t_b})\sqrt{\mathbb{V}[X_{t_a}]}\sqrt{\mathbb{V}[X_{t_b}]}\end{aligned}$$

Because $\mathbb{V}[X_{t_a}] = \mathbb{V}[X_{t_b}] = \mathbb{V}_X$ and $\rho(X_{t_a}, X_{t_b}) = \rho(t_b - t_a)$, i.e. the autocorrelation function:

$$= \mathbb{V}_X \sum_{t_a=k-\Gamma}^{k+\Gamma} \sum_{t_b=k+\delta_k-\Gamma}^{k+\delta_k+\Gamma} W(t_a-k)\overline{W(t_b-(k+\delta_k))}\rho(t_b-t_a)$$

with $t = t_a - k$:

$$= \mathbb{V}_X \sum_{t=-\Gamma}^{\Gamma} \sum_{t_b=k+\delta_k-\Gamma}^{k+\delta_k+\Gamma} W(t)\overline{W(t_b-(k+\delta_k))}\rho(t_b-(t+k))$$

with $t' = t_b - k$:

$$= \mathbb{V}_X \sum_{t=-\Gamma}^{\Gamma} \sum_{t'=\delta_k-\Gamma}^{\delta_k+\Gamma} W(t)\overline{W(t'+k-(k+\delta_k))}\rho(t'+k-(t+k))$$
$$= \mathbb{V}_X \sum_{t=-\Gamma}^{\Gamma} \sum_{t'=\delta_k-\Gamma}^{\delta_k+\Gamma} W(t)\overline{W(t'-\delta_k)}\rho(t'-t)$$

with $t'' = t' - \delta_k$:

$$= \mathbb{V}_X \sum_{t=-\Gamma}^{\Gamma} \sum_{t''=-\Gamma}^{\Gamma} W(t)\overline{W(t'')}\rho(t''-t+\delta_k)$$
$$= \mathbb{V}_X \sum_{t=-\Gamma}^{\Gamma} W(t) \sum_{t''=-\Gamma}^{\Gamma} \overline{W(t'')}\rho(t''-t+\delta_k)$$

because the autocorrelation function is symmetric $\rho(t''-t+\delta_k) = \rho(t-\delta_k-t'')$:

$$= \mathbb{V}_X \sum_{t=-\Gamma}^{\Gamma} W(t) \underbrace{\sum_{t''=-\Gamma}^{\Gamma} \overline{W(t'')}\rho(t-\delta_k-t'')}_{\overline{WT_\rho(t-\delta_k)}}$$
$$= \mathbb{V}_X \underbrace{\sum_{t=-\Gamma}^{\Gamma} W(t)WT_\rho(t-\delta_k)}_{WT(\overline{WT_\rho(\delta_k)})}$$
$$= \mathbb{V}_X g(\delta_k)$$

The correlation between close wavelet coefficients only depends on the interplay between the parameters of the wavelet and the autocorrelation function of the signal. The correlation between two δ_k distant wavelet coefficients can be empirically estimated on real data by convolving the autocorrelation function of the signal twice, once with the conjugate of the wavelet and once with the wavelet itself.

This generalization leads to the previous more specific result when the autocorrelation of the signal was assumed null, i.e. when $\rho(k=0) = 1$ and $\rho(k \neq 0) = 0$.

This result taking into account the autocorrelation of the signal can help guide more accurately the spacing required between two coefficients to minimize their dependence in statistical testing, and does not depend on a specific wavelet choice. Whereas the correlation between close wavelet coefficients introduced by the wavelet transform is artifactual, the autocorrelation of the EEG signal may be the manifestation of features of interest. In other words, it may not be interesting to compensate for.

Chapter 5

Extraction of alpha bursts parameters based on Morlet Wavelet Transforms

The motivation of this chapter is the identification of the temporal properties of oscillating events (namely bursts). They could provide new ways of assessing functional relationships between the cortical regions generating these bursts, and be integrated in functional connectivity based neurofeedback protocols. The description of such bursts can be achieved accurately with a restricted number of parameters and therefore present the advantage of condensing remarkably the signal information. It is proposed to use the Morlet wavelet transform to recover the parameters of these bursts on some selected real data, and describe the outcome.

5.1 Introduction

Electrical brain activity observed on the scalp can be rhythmic. In the α band, these rhythmic events mostly occur in bursts.

Chandran KS et al. [47] provides a review of the existing strategies employed for burst extraction, namely: continuous Gabor transform [42, 337], power estimation [76], wavelet transform [249], Hilbert transform [168], matching pursuit [147, 60, 172]. The strategy described here falls into the wavelet transform category, but differs substantially from the method exposed in [249].

5.2 Data

The toy sample presented in figure 5.1 is taken from the experiment of chapter 7. It consists in 20 seconds of Eyes Closed Relaxation (ECR) EEG recording at electrode O1 of a subject selected for presenting large α waves. The recording sampling rate is of 512 samples per second, and is kept as such during the processing.

5.3 Model

The model is based on the assumption that sources of electric activity in the neocortex have a bursty behavior in the α frequency band. Namely, at the scalp, is recorded a weighted sum of these bursts, according to an unknown

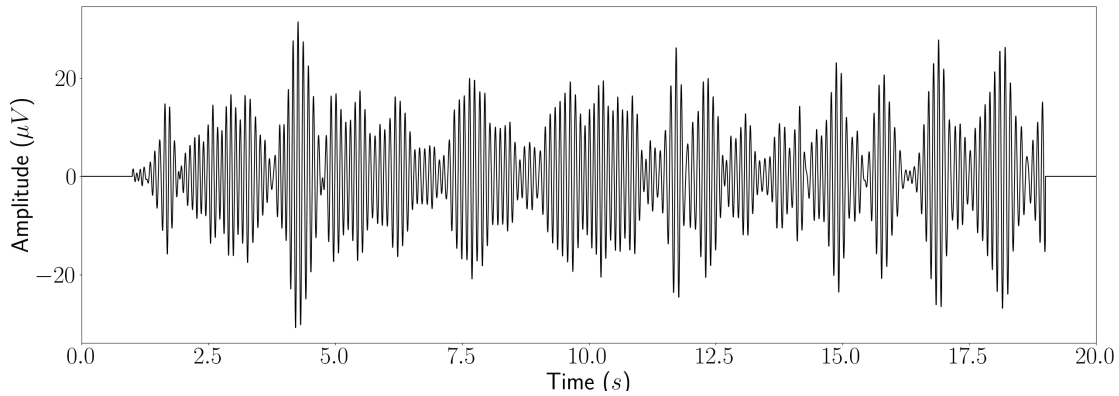

Figure 5.1: 20s sample of Eyes Closed Relaxation (ECR) of a subject selected for presenting large α waves. The sample is high-pass filtered below 8Hz, and low-pass filtered above 12Hz for display. The first and last seconds are ignored because of the filtering effects.

gain matrix[1]:

$$S(t) = \sum_{i}^{N} w_i B_i(t) \tag{5.1}$$

where:

w_i is a projection weight (gain matrix coefficient) of the source activity onto the sensor

and B_i is a burst modeled as a sinusoidal wave modulated by a Gaussian window.:

$$B_i(t) = \alpha_i e^{-\frac{(t-t_i)^2}{2\sigma_i^2}} cos(2\pi f_i(t-t_i) + \phi_i) \tag{5.2}$$

where:

α_i is the amplitude of the source
f_i is the frequency of oscillation of the burst
σ_i is the standard deviation of the Gaussian window
t_i is the time at which the Gaussian is maximized
ϕ_i is the phase shift at t_i

Hence, at the level of the scalp :

$$S(t) = \sum_{i}^{N} w_i \alpha_i e^{-\frac{(t-t_i)^2}{2\sigma_i^2}} cos(2\pi f_i(t-t_i) + \phi_i) \tag{5.3}$$

In the upcoming content, $w_i\alpha_i = A_i$.

[1]This model is also used in [338], where a completely different task is undertaken, notably finding a reference point at infinity in EEG settings.

5.4 Method

The method aims at recovering the amplitude, the time of peak, the frequency and the phase shift of bursts while assuming their duration, based on the Morlet wavelet transform.

The duration parameter ∂_i is fixed to 0.5 seconds for all bursts according to the duration of α bursts found in the literature (which is in accordance with observations in the current toy sample). ∂_i, the width of the Gaussian window at half maximum is linked to its standard deviation σ_i by the formula:

$$\partial_i = 2\sqrt{2\log 2}\sigma_i \tag{5.4}$$

The amplitude A_i, the time t_i at which the maximum of the Gaussian is reached, the frequency f_i and the phase shift ϕ_i are estimated from the coefficients of the continuous complex Morlet wavelet transform.

The Morlet wavelet transform complex coefficients are obtained with a wavelet width of 7 oscillations. The amplitudes map 5.2 and phases map 5.3 are obtained by respectively taking the magnitude and the angle of the complex coefficients. The time t_i and frequency f_i points at which the energy is locally maximal are estimated. At these locations, the amplitude A_i and the phase ϕ_i are retrieved.

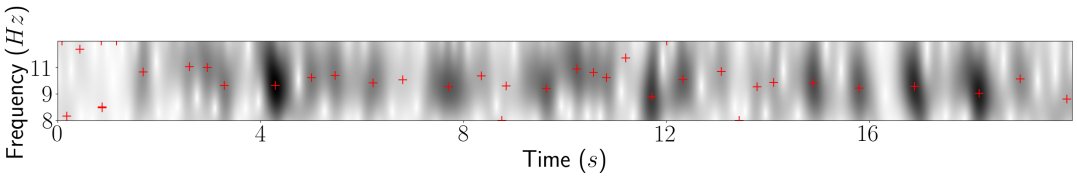

Figure 5.2: Amplitudes map of the signal, obtained as the magnitude of the continuous Morlet wavelet transform coefficients. Local maxima are represented by red crosses, obtained with the Python library scipy, algorithm: maximum_filter.

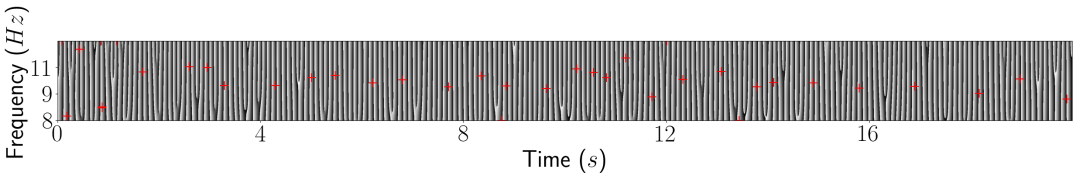

Figure 5.3: Phase map of the signal, obtained as the angle of the continuous Morlet wavelet transform coefficients. Red crosses show the local maxima locations estimated on the amplitude map.

The signal is then reconstructed according to Equation 5.3, and compared to the original signal.

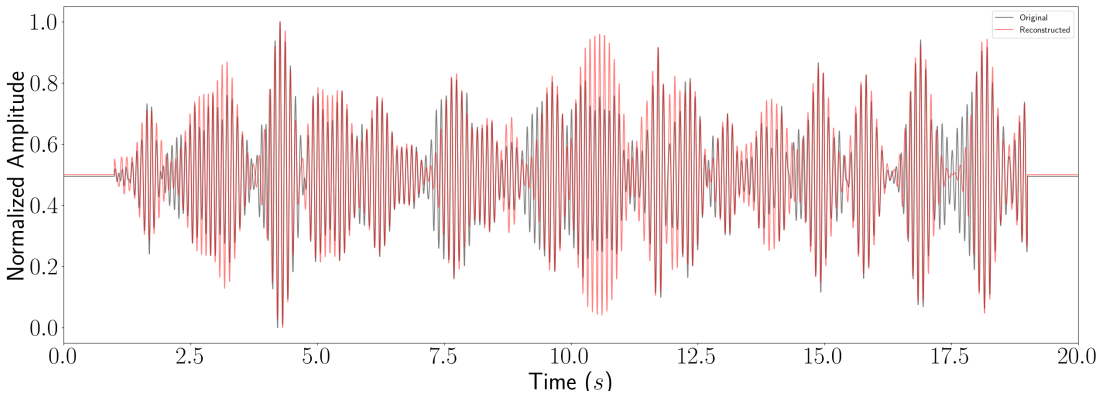

Figure 5.4: In black: Original signal presented in figure 5.1. In red: Reconstructed signal based on the parameters extracted from the Morlet wavelet transform, and assumptions. Edges are removed due to filtering effects. Both signals are normalized w.r. to the original signal.

The amplitudes recovered at (f_i, t_i) in the amplitude map are not accurate when two or more bursts are overlapping, it is actually the sum of all overlapping bursts at (f_i, t_i) 5.5. This effect is especially visible at 10.5s in figure 5.4. Therefore, a correction must be designed, so that the amplitude at a maximum equals the sum of the amplitudes of the bursts at that location :

$$A(f_i, t_i) = \sum_{j}^{N} A_j e^{-\frac{(t'_j - t'_i)^2}{2\sigma^2}} \tag{5.5}$$

where:

t'_i equals $t_i - \frac{\phi_i}{2\pi f_i}$
t'_j equals $t_j - \frac{\phi_j}{2\pi f_j}$
σ equals $\frac{\partial}{2\sqrt{2\log 2}}$

Solving for all maxima at the same time amounts to solving a linear system, with unknown A_j, the actual amplitudes of the bursts. The resolution of the system provides new amplitudes. The correction induces overall a better fit of the bursts to the data presented in figure 5.5. For some bursts, the goodness of fit decreases (at 9s.). Several reasons can lead to the reduction of the goodness of fit, the first one being a wrong estimation of the location in time or frequency or the phase shift. This occurs when bursts oscillating at a similar frequency have their centers too close to one another. In such cases, different optimizations should be considered, among which an optimization involving the procedural removal of the bursts could be interesting (such as matching pursuit [172]).

5.5 Wavelet width estimation

The goodness of fit of the reconstructed signal with the original signal can be used to estimate a good wavelet width. In line with the discussions of chapter 3 regarding the estimation of the width of the wavelet, the number of bursts and the average error between the reconstructed signal and the original signal is computed for varying wavelet widths. The results are presented in figure 5.6. The best result is obtained for the smallest reconstruction error and smallest number of burst. In this example, it occurs for wavelets of 5 to 9 cycles.

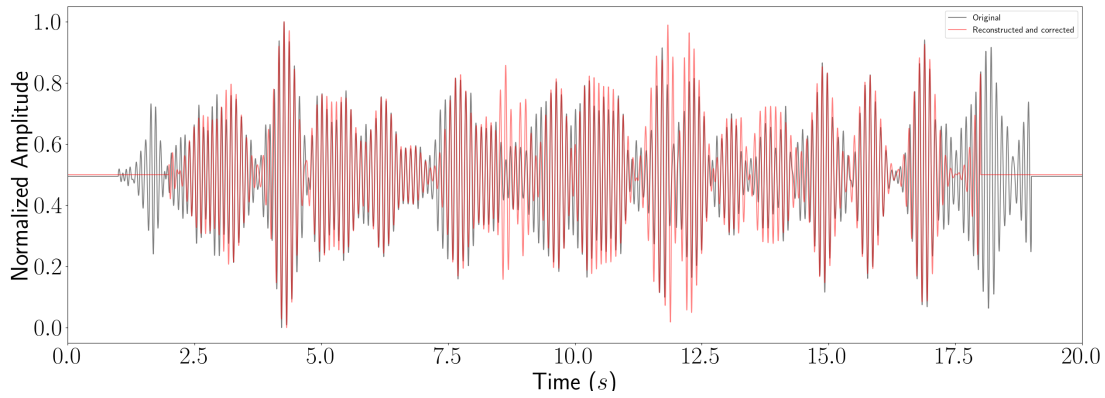

Figure 5.5: The first and last 2 seconds are ignored in the corrected reconstruction.

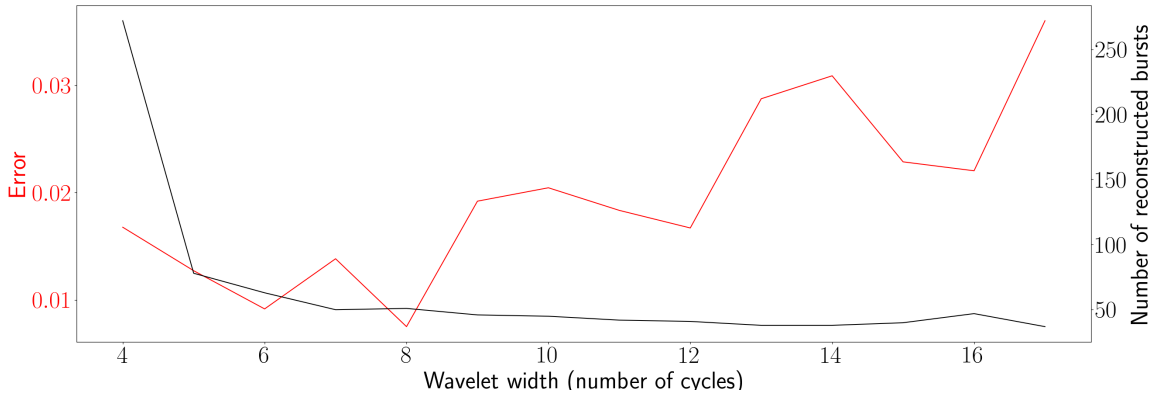

Figure 5.6: Reconstruction error and number of reconstructed bursts with respect to wavelet width, results obtained on an arbitrary 20s segment of EEG during an Eye Closed Relaxation condition (Fp1 electrode referenced at M2).

5.6 Conclusion

In this contribution, the Morlet wavelet transform was used to extract the locations, phase shifts and amplitudes of bursts in a real EEG signal. The main interest of this approach is its simplicity, and the goodness of fit that can be achieved without optimization. A linear optimization based on the amplitudes increases further the goodness of fit.

The Morlet wavelet transform is especially well designed for the purpose of detecting oscillatory bursts. Nonetheless, the wavelet width is paramount in figuring the most adapted time to frequency accuracy. Studying the error of reconstruction of the signal with the presented method along varying wavelet width is a practical data-driven estimation of this parameter.

Moreover, it confirms that the phase extracted at the maximum of amplitude is indeed practically accurate, despite the caveats formulated in chapter 3. While the duration was fixed in this experiment, it could also be extracted from the data. Estimating the duration parameter ∂_i is another step that can be taken to further improve the goodness of fit.

Chapter 6

Phase synchrony in epileptic patients ElectroEncephaloGraphic recordings

This chapter is a joint effort conducted with Jeanne Benoît, neurologist at the university hospital Pasteur in Nice, that emerged during the search for a neuromarker differentiating epileptic patients from healthy subject during interictal period. Indeed, a neuromarker of this kind should be of first choice for neurofeedback protocols. Among the few scalp EEG studies demonstrating such difference stands Bhattacharya [24]. This work reproduces and extends the experimental protocol of the study [24] on a new group of epileptic patients and healthy controls.

Glossary

	MPC: Mean Phase Coherence
EEG: ElectroEncephaloGraphy	*PLI*: Phase Lag Index
EC: Eyes Closed	*FC*: Functional Connectivity
C: Control participants (Healthy)	*NH*: Null Hypothesis
E: Epileptic patients	*WRST*: Wilcoxon Rank Sum Test
TLE: Temporal Lobe Epilepsy	*ROC*: Receiving Operator Characteristic
RTLE: Right TLE	
LTLE: Left TLE	*AUC*: Area Under Curve
MTLE: Mesial TLE	*CHUN*: University Hospital of Nice

6.1 Introduction

Epilepsy is defined by an enduring predisposition of the brain to generate epileptic seizures [81]. Electroencephalography, together with patients' clinical and radiological features, are the key elements to the diagnosis of epilepsy. 8.93 per 1000 (roughly 1%) of the world population suffers from epilepsy [205]. While 70-80% of epilepsy cases can be controlled through adapted and personalized medication, the remaining cases are drug resistant [1]. Moreover, anti-epileptic drugs have a wide range of adverse effects [217], and may be detrimental to daily life. Alternative treatment options must then be considered. Surgically isolating or removing the identified epileptogenic focus is often considered as the alternative in focal epilepsies. While lesional epilepsies are successfully surgically treated in about 70% of the cases, only 50% are successful when the cause is not lesional [299]. Although deemed

[1] Drug resistant epilepsy is defined by Kwan et al. [150] as failure of adequate trials of two tolerated, appropriately chosen and used anti-epileptic drug schedules (whether as monotherapies or in combination) to achieve sustained seizure freedom.

safe, epilepsy surgery is associated with cognitive changes [272], mostly because pre-surgical screening of brain functions can only be partial. In a meta-analysis on surgical outcomes, Sherman et al. [272] note an increased risk of verbal memory and naming impairment with left-sided temporal surgery. It leaves out, considering all epilepsies could be treated surgically, 70% of 30% of 1% of the world population untreated, i.e. 15 million individuals. These 15 million individuals live with disabling seizures justifying an extensive research into additional means of treatment.

Over the past half century, electroencephalographic protocols of operant conditioning have provided an alternative to medication and invasive procedures. By learning to modulate and reinforce specific brain activity patterns, EEG-neurofeedback has shown positive outcomes in reducing the frequency and severity of seizures in epileptic patients (see [296] for a review). These protocols were either based on the control of sensorimotor rhythms: 12-16 Hz oscillations present over the motor area [293][291][166][79][267], or slow cortical potentials: several hundred of millisecond shifts reflecting at the scalp the level of excitability of the underlying cortex [320][144]. While these studies offer a promising alternative, and mechanisms explaining their success have been suggested (inhibitory role of the sensorimotor rhythms: [304], in link with the thalamus [115]), they were not designed based on the current knowledge regarding the differences in brain connectivity associated with epilepsy (for the initial study on sensorimotor and epilepsy see Sterman et al. [292]).

Epilepsy is now recognized as malfunction in a network of brain structures rather than a single epileptogenic region [223][300][326][152]. Indeed Warren et al. [326] and Lagarde et al. [152] show a clear disconnection of the epileptic zone from the rest of the brain network with intracortical measurements. Additionally, magnetoencephalography studies [69][68] revealed global decreases in connectivity of mesiotemporal lobe epilepsy patients based on imaginary coherence. Schevon et al. [262] electrocorticography study revealed an increased local synchrony.

The measure of interictal correlates of epileptic activity in EEG signals could give a more adapted lever to control epileptogenic processes and their unfolding before and during seizure. Finding a measure differentiating epileptic from healthy brains with EEG in the absence of epileptic spikes is challenging but rewarding, as it could be used as marker / feature for a rehabilitating neurofeedback protocol. Characterizing this deviance is at the heart of Z-Score neurofeedback protocols [302].

While many approaches accurately differentiate seizure signals from healthy signals, not many to date differentiate interictal signals from healthy signals with scalp EEG recordings. Lahmiri [153] claim that the Hurst exponents of interictal and healthy recordings are statistically different, despite comparing healthy scalp EEG and interictal intra EEG recordings.

Phase synchrony is a natural way to represent possible functional relationships through the oscillatory nature of the periodic brain events. In a study that claims differentiating epileptic (during interictal stage carefully chosen not to exhibit epileptic spikes) from healthy subjects (both under closed eyes condition), Bhattacharya [24] used the Mean Phase Coherence (MPC), a phase informed synchrony measure. It was calculated on all possible pairs of scalp EEG electrodes within several frequency bands. For each pair of electrode and each frequency band, a Wilcoxon rank sum test was conducted to check if the MPC values of epileptic patients were statistically higher than in controls, and reversely. The positive tests were aggregated in bins. The results are reproduced in figure 6.1. They allow a twofold conclusion: (1) Short-distance pairs showing statistically greater MPC values (in one group than in another) are evenly shared between the epileptic patient group and the control group. (2) Long-distance pairs showing statistically greater MPC values are mostly attributable to the control group, indicating a reduced long range synchrony in epileptic patients. This stand is partially in line with an intracortical study of Lagarde et al. [152].

This work reproduces scrupulously Bhattacharya [24]'s study to ensure whether or not it applies to another group verifying a stricter inclusion criteria (TLE patients, TLE being the most common drug-resistant epilepsy [22]). It extends the latter study by attempting to correct some analysis biases, bringing some natural add-ons such as considering other synchrony measures and the location of the epileptic focus.

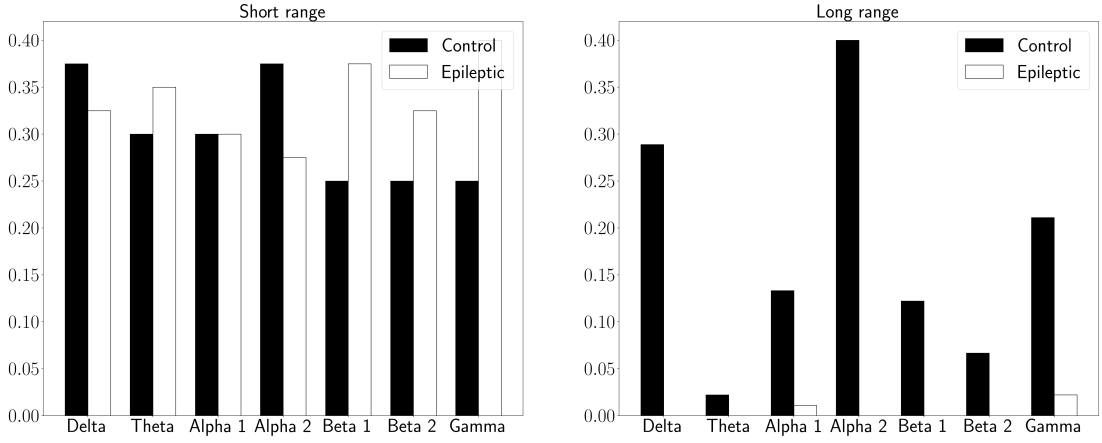

Figure 6.1: Results of Bhattacharya's experiments, EC condition, window length: 8s, window overlapping: 7s, measure: Mean Phase Coherence. Each bin counts the number of pairs that show statistically higher "synchrony" measures according to the Wilcoxon rank-sum test. Left side for "short range" pairs, right side for "long range" pairs. For an easier comparison between short and long range, the bins are normalized respectively by the number of short and long range pairs. Reproduced from Bhattacharya [24].

6.2 Material

The model of EEG recording device is a SD plus (Micromed), and the recording software a PLUS EVOLUTION (Micromed SpA, 01/10/2015 update). The conducting paste is a PATE REEGAPONCE (M.E.I.). The recording sampling rate is fixed at 256Hz and not re-sampled later on. The electrodes are placed following the 10/20 system: Fp1, Fpz, Fp2, F7, F3, Fz, F4, F8, T3, C3, Cz, C4, T4, T5, P3, Pz, P4, T6, O1, Oz, O2. Two additional electrodes are placed on the thorax. All electrodes are referenced to the mean of the earlobes 6.2. The raw signals are recorded.

The experimental protocol was not designed for the purpose of this analysis, but for routine EEG recordings. The protocol follow this pattern:

- 2 blocks of 30s eyes closed / 30s eyes open,
- 1 block of 180s hyperventilation / 180s hyperventilation recovery,
- 1 block of intermittent photic stimulation,
- 1 block of 180s hyperventilation / 180s hyperventilation recovery,
- 1 block of 30s eyes closed / 30s eyes open

Of these eyes closed condition blocks, a neurologist recovered those free of any artifacts (periodic lateralized epileptiform discharges, eye movements, muscle contractions...). This protocol was realized with 23 E (12 LTLE, 11 RTLE), and 12 C. All recording sessions took place at the CHUN Pasteur, Alpes-Maritimes, France. Epileptic patients present focal epilepsies without MRI anomalies. They were under various medical treatments during the period within which the recordings took place (such as in [24]). Each subject has a total of 10 recordings lasting 30 seconds. While the EEG recordings of epileptic patients were recovered from the hospital database, consenting healthy subjects took part to new acquisitions on the same device. These controls declared not having any neurological disorder, nor taking any medication.

Figure 6.2: Routine EEG recordings at CHUN.

6.3 Reproduction

In this first analysis, the methodology proposed in Bhattacharya [24] is reproduced.

6.3.1 Methodology

The methodology of Bhattacharya [24] is reproduced. Electrodes of interest are selected to match that of Bhattacharya [24]: P3, C3, F3, O1, T5, T3, F7, Fp1, P4, C4, F4, O2, T6, T4, F8, Fp2. The EEG signals are notch filtered at 50Hz and then filtered between 1Hz and 70Hz. The signals are filtered in parallel on several frequency bands: delta (1-4 Hz), theta (4-7 Hz), alpha-1 (7-10 Hz), alpha-2 (10-13 Hz), beta-1 (13-18 Hz), beta-2 (18-30 Hz) and gamma (30-70 Hz). Filtering is achieved with a 6th-order Butterworth filter (Infinite Input Response) applied with the "filtfilt" technique performing a zero-phase digital filtering, of importance in broad band phase based measures (although not specified in [24]). The 30s epochs are chopped, into windows of 8s, overlapping by 7s. All possible pairs of scalp electrodes ($\frac{16^2-16}{2}$), are categorized either as long-range, or short range. Short-range pairs are neighboring electrodes within the same hemisphere and amount to 30 pairs. Long-range pairs are either located in opposite hemispheres or are not immediate spatial neighbors and amount to 90 pairs.

The MPC [185] values are computed for each group, each subject, each pair and on each window. For each pair, and each frequency band, the measures obtained for each group (E and C) are compared statistically with two non-parametric one-sided Wilcoxon rank-sum tests, with p-value = 0.05. Once testing if MPC values for E are statistically greater than MPC values for C, and then reversely. The number of pairs for which MPC values of E are statistically greater than MPC values of C are summed up, the same is realized for C > E.

6.3.2 Results

Bhattacharya [24] observed a "reduced long range synchrony" in epileptic patients (patients experiencing seizures), through the MPC computed as in this experiment. From the results of this experiment, presented in figure 6.3, this effect is absent. On the contrary, almost every pair (regardless of the range) in epileptic patients reveal a higher synchrony. Given the discrepancy between the results, caution seem advised, and justifies investigating the methodology. While the variability between Bhattacharya [24] and this reproduction may indicate that the variability in the MPC of epileptic patients is higher than any of the two datasets could capture, the difference in results observed with Bhattacharya [24]'s study could also come from statistical analysis bias. These biases are considered in 6.4.1. Alternatively, this difference could be explained by the generally strong variability of the MPC in epileptic patients. The variability is already high in the dataset of this study, with strict inclusion criteria (a fact unveiled in figure 6.8, I.), one may suppose it is also the case with looser inclusion criteria. In such cases, a restricted number of subjects does not allow to capture the variability of the studied population, and can lead to different analysis results.

Alternatively, the subjects in Bhattacharya [24] study are random epileptic patients; their inclusion criteria is less specific than for this study. Although this effect could not be tested due to the absence of Bhattacharya [24]'s data. Inclusion criteria and statistical analysis biases are considered in 6.4.1.

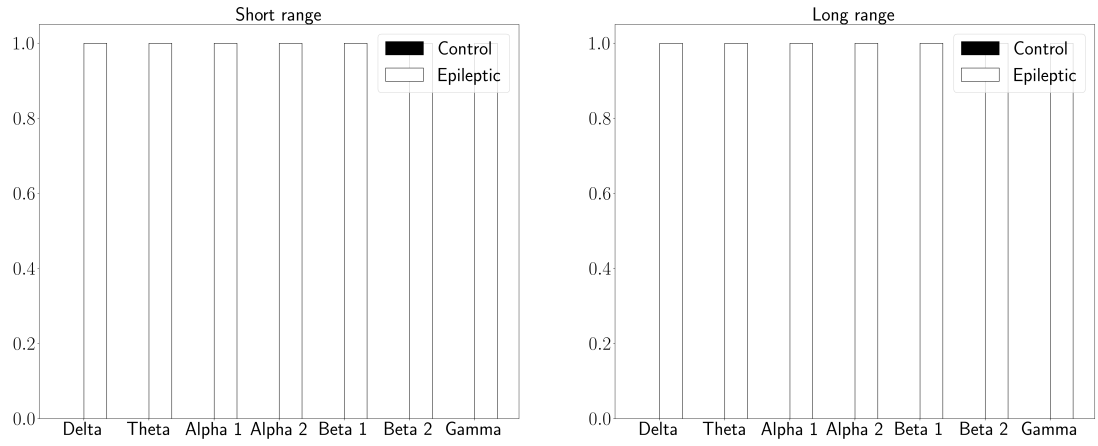

Figure 6.3: Reproduction of Bhattacharya experiments, EC condition, window length: 8s, window overlapping: 7s, measure: Mean Phase Coherence. Each bin counts the number of pairs that show statistically higher "synchrony" measures according to the Wilcoxon rank-sum test. Left side for "short range" pairs, right side pour "long range" pairs. For an easier comparison between short and long range, the bins are normalized respectively by the number of short and long range pairs. Black bins are absent because there is not a single pair of electrodes for which C MPC values are statistically higher than those of E.

6.4 Adaptation

The inclusion criteria are more specific in this study as they only involve TLE patients. In Bhattacharya [24], the independence between draws within groups is not validated to a high degree, the draws are correlated spatially and temporally. First, the MPC values are computed on pairs of sequences of complex coefficients obtained by a convolution operator [89] (see chapter 3) and hence correlated temporally by construction. Second, the MPC values are computed on highly overlapping windows, hence are even more correlated temporally. Third, the MPC measures are recovered on a restricted number of subjects which adds another level of correlation within each subject. Fourth, the different pairs share electrodes, which is not an issue regarding the groups (E and C) comparison at the level of one pair, but impairs the statistical analysis regarding the comparison between accumulated WRSTs in bins. Fifth, MPC values are spatially correlated by volume conduction of brain activity sources; again the issue does not stem at the level of the pair comparison but at the level of bins comparisons.

6.4.1 Methodology

Before diving into the problem of dependent data, shorter epoch length and the absence of overlapping are investigated to match more closely the bursty behavior of brain rhythms (rather short in general), and better capture the synchrony, while still keeping an eye on minimizing the correlation in the data (removing overlap and using PLI).

The dependence within the data is then considered in the light of the Wilcoxon rank-sum test (Mann-Whitney U test). One of the hypotheses of the Wilcoxon rank-sum test is the independence of the draws within groups and mutual independence of the draws between groups [189]. In case of dependence between the draws, the distribution of the test statistic changes: the variance is (potentially strongly) increased [220], and the commonly applied p-value check is not appropriate. In other words, correlated values within each group increase fallaciously the significativity of the test (see the next section) and may bias the conclusions. To partially reduce this correlation the WRST statistic is adapted to take some degree of dependence into account.

The present reproduction eventually adds an additional statistical test to Bhattacharya [24]'s methodology to

not arbitrary decide whether for a given frequency band the epileptic patients have generally more synchronous values that controls. The multinomial distribution of the Wilcoxon Rank Sum Test outcomes is used to gauge the likelihood of observing such results.

Considering shorter epoch length

Epoch length may have a strong influence on synchrony measures. Indeed, too large epochs tend to mix different synchrony states and average low and high synchrony measures of these states. Also, overlapping epochs strongly correlates them, making these less appropriate for statistical testing.

Given the duration of oscillatory components of brain activity of the order of the second (see chapter 5), it is therefore appropriate to consider windows of this duration (2 seconds is chosen), and minimize the overlapping to avoid considering complex statistical corrections.

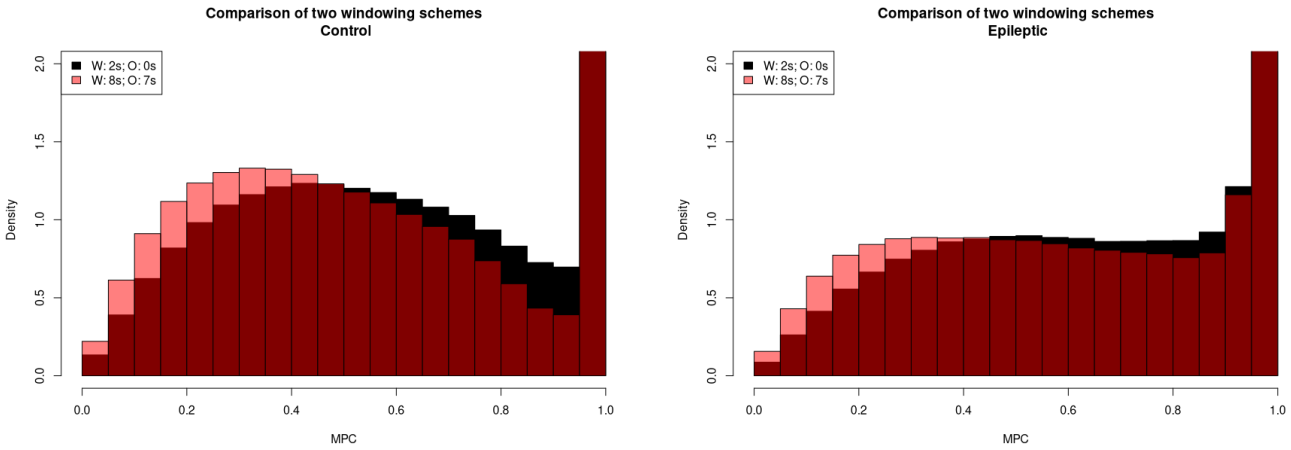

I II

Figure 6.4: In I windowing schemes are compared for healthy subjects, while in II they are compared for epileptic patients. MPC values are obtained on windows of phase differences between all possible pairs of the channels mentioned in the material section, regardless of the notion of range. W: window duration. O: overlapping duration. The bin heights weighted by their widths sum to one.

In figure 6.4, two windowing schemes are compared. Longer windows lead to a decrease in MPC. Also, the distribution is slightly more skewed. These effects are observed in C and E.

Considering the autocorrelation of the synchrony measures

Hereafter synchrony measures are conveniently considered as random processes, and the synchrony measure values as “draws”. Synchrony measures computed on sliding windows (consecutive ”draws”), even when not overlapping, might be strongly correlated in time. To investigate if this is a general property, the autocorrelation function is averaged over all periods of 20 seconds, for all possible pairs, and for the low alpha frequency band in Controls. Two windowing schemes are considered: 8 seconds windows, overlapping by 7 seconds (W: 8s, O: 7s) as in [24], or 2 seconds windows, overlapping by 0 seconds (W: 2s, O: 0s).

Following 6.5, in the case (W: 2s, O: 0s), on average, two consecutive “draws” are not correlated. This is opposed to the case (W: 8s, O: 7s), where correlation remains up to the 4 seconds lag (corresponding to 4 consecutive “draws”).

It encourages to use shorter and non overlapping windows, which is what will be done in the following sections.

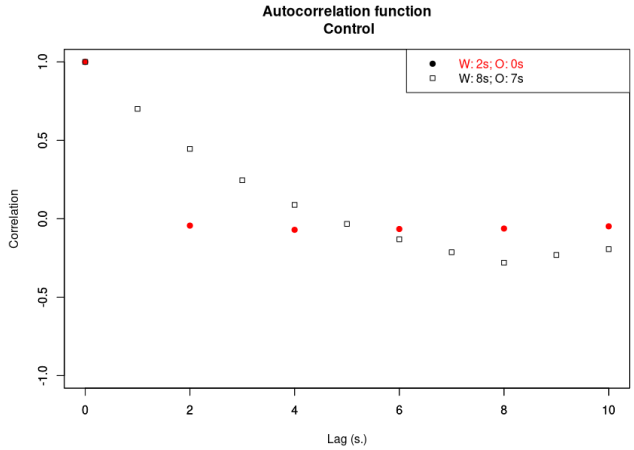

Figure 6.5: Autocorrelation function of MPC measures, according to two windowing schemes. Obtained on 154 recordings from all Controls and 120 pairs of electrodes. W stands for Window duration, O stands for Overlapping duration.

Considering the Phase Lag Index

To mitigate against the spatial correlation due to volume conduction (or gel-bridged electrodes) the PLI is computed [284] for comparison and/or correction. According to the literature, the PLI is not sensible to volume conduction since it disregards phase differences oscillating around 0 or π. A controversial stance was nonetheless presented in chapter 7.

Mann Whitney U test with independence

Two samples $S_\alpha : (s_\alpha^1, ..., s_\alpha^{N_\alpha})$ and $S_\beta : (s_\beta^1, ..., s_\beta^{N_\beta})$ are considered, of respective sample size N_α and N_β. The Mann Whitney U test statistics attributes a rank to each of the realizations of $S_\alpha \cup S_\beta$ from the lowest to the highest value, as an example : $s_\alpha^1 < s_\beta^1 < ... < s_\alpha^{N_\alpha} < s_\beta^k < ... < s_\beta^{N_\beta} < s_\alpha^k$ gives the ranks $(r(s_\alpha^1) = 1, r(s_\beta^1) = 2, ..., r(s_\alpha^{N_\alpha}) = l, r(s_\beta^k) = l + 1, ..., s_\beta^{N_\beta} = (N_\alpha + N_\beta) - 1, s_\alpha^k = (N_\alpha + N_\beta))$. Then the sum of the ranks of each sample is calculated in the general case: $T_\alpha = \sum_{i=1}^{N_\alpha} r(s_\alpha^i)$ and $T_\beta = \sum_{i=1}^{N_\beta} r(s_\beta^i)$, and the test statistic is taken as the smaller T of the two (the larger is noted $\tilde{T}$, by association the number of samples are respectively N and $\tilde{N}$). For sufficiently large N and $\tilde{N}$, the test statistic under the null hypothesis is approximately normally distributed.

$$T \sim \mathcal{N}(\mu, \sigma^2) \tag{6.1}$$

where:

$\mu(T)$ equals $\frac{N(N+\tilde{N}+1)}{2}$
$\sigma^2(T)$ equals $\frac{N\tilde{N}(N+\tilde{N}+1)}{12}$

Mann Whitney U test with dependence

To understand the impact of correlated samples on the power of the test, one may imagine the extreme case were each realization (s_α^i and s_β^i) is duplicated f times (or respectively chosen as close as possible but different to avoid ties). This gives the test statistic T' which is realistic for close overlapping windows. Then compare it to

the usual test statistic $\overline{T}$ constructed with fN_α and fN_β randomly attributed ranks. In both cases the number of samples is the same, namely fN_α and fN_β. In the duplicate case, under the null hypothesis :

$$T' = \sum_{i=1}^{N}\sum_{k=0}^{f-1} f(r(s^i)-1)+1+k = f^2T - \frac{f(f-1)}{2}N \tag{6.2}$$

Since T' and T are both random variables:

$$\mu(T') = f^2\mu(T) - \frac{f(f-1))}{2}N = f^2\frac{N(N+\tilde{N}+1)}{2} - \frac{f(f-1))}{2}N = \frac{fN(fN+f\tilde{N}+1)}{2} = \mu(\overline{T}) \tag{6.3}$$

$$\sigma^2(T') = f^4\sigma^2(T) = f^4\frac{N\tilde{N}(N+\tilde{N})}{12} + f^4\frac{N\tilde{N}}{12} = f\sigma^2(\overline{T}) + (f^4-f^3)\frac{N\tilde{N}}{12} \tag{6.4}$$

Duplication of the ranks is thereby demonstrated to increase in the variance of T''s distribution, as a polynomial function of the duplication, strictly increasing for $f > 1$ (see equation 6.4). The effect is increased for large samples. The variance increase will lead to a more frequent rejection of the null hypothesis for a given significance threshold than for $\overline{T}$. It is typically in line with other works such as [220].

Once the factor f is estimated, the test statistic T' can be standardized to be used in pvalue tables.

$$Z' = \frac{T' - \mu(T')}{\sigma^2(T')} \tag{6.5}$$

In the following, the f values are estimated in different scenarios, with the data of the experiment presented in section 6.2. The estimation of f is achieved by solving the 4th order polynomial of equation 6.4 after introducing the theoretical variance ($\sigma^2(\overline{T})$ given N and $\tilde{N}$), and the variance estimated from the NH with the *a priori* correlated data ($\sigma^2(T')$). The subtlety with the estimation of the Wilcoxon rank sum test statistic distribution under the NH, is that it requires N and $\tilde{N}$ to be constant. This distribution under the NH is built upon the 12 Controls, on all possible combinations of these controls in two groups of size 6 subjects. Leading to $N = \tilde{N}$, and varying from scenario to scenario.

Measure	W. S.	N	Theoretical μ	Theoretical σ	Actual μ	Actual σ	f
MPC (right hemisphere)	W: 8s O: 7s	246960	30494620800	50103116	30494585928	2388109980	180
MPC (right hemisphere)	W: 2s O: 0s	152880	11686147200	24403442	11686197538	797373608	130
PLI (right hemisphere)	W: 2s O: 0s	152880	11686147200	24403442	11686022485	272171620	65
PLI (O1-P3)	W: 2s O: 0s	5460	14905800	164715	14905998.8	803515	17
PLI (O1-P3, α band)	W: 2s O: 0s	780	304200	8896	304231.50	21632	5
PLI (F7-P3, α band)	W: 2s O: 0s	780	304200	8896	304251.33	17423	4

Table 6.1: W. S.: Windowing Scheme, N.H.: Null hypothesis distribution of WRST, μ: mean, σ: standard deviation

Different scenarios of WRST statistics on correlated samples are studied and presented in table 6.1. These scenarios cover more elements of correlation than those described in 6.4.1. More precisely, these scenarios encompass a within hemisphere correlation, as well as a within band correlation that is not present in Bhattacharya [24]. They mainly serve the purpose of presenting the soundness of the f value across incrementally decreasing levels

of synchrony. Two windowing schemes are compared, two phase synchrony measures are compared, two different restrictions on sub-samples are considered (pair and frequency band), and lastly different pairs are compared.

Shortening the windows and removing the overlap between consecutive windows considerably lowers the f value, as it reduces the intuitive redundancy created by overlapping. It goes along the autocorrelation of the MPC measures for varying window lengths and overlaps presented in 6.4.1, that goes to 0 in the short windows / no overlap case and justifies why considering shorter and non overlapping windows in 6.1 lead to a reduction of the f value accounting for dependence. The f value obtained for the PLI measure is again greatly lowered, supposedly because the correlation due to volume conduction is (partly, see conclusion of chapter 7) ignored. Considering only one pair also lowers f, since it avoids the correlation between pairs containing the shared electrodes, and the same activity recorded by two pairs of electrodes. Considering only one pair and one frequency band again lowers f because it removes the correlation between frequency bands (by construction or due to physiological constraints (cross frequency coupling)). f value still unveils some correlation for a single pair of electrodes within a single frequency band (F7-P3 or O1-P3, α band). This is not what is observed with the autocorrelation of the signal as suggested in section 6.4.1, since the autocorrelation is close to 0 for non zero lags. It could capture the within subject dependence that is not accounted for in this framework.

The f values could ultimately be used to correct the WRST employed in the reproduction of Bhattacharya [24] results (see section 6.4.3).

6.4.2 Multiple comparisons correction

Whether working with corrected WRS tests or not, before making any deduction on a pair of bins (such as "MPC values of E are generally higher than of C for long / short range electrode pairs at a given frequency band"), one must ensure that this is not due to chance. Indeed, given the number of comparisons (90 for Long Range and 30 for Short Range), rejections of the null hypothesis at $2 * \alpha$ occur even if the MPC samples come from the same"population". The multinomial experiment is a probabilistic framework to model and explain the construction of these bins.

For each pair of electrodes, WRST statistic is computed over the E and C samples. Under the null hypothesis that both samples belong to the same "population", and the rejection of the null hypothesis at α% on the left (Epileptic are more likely to have lower values than Controls) and α% on the right (Epileptic are less likely to have lower values than Controls), there is a α% chance that the WRST statistic of the Epileptic sample is deemed statistically very low, 100-2α% that it is deemed statistically not extreme and α% that is deemed statistically very high. Each time a WRST statistic is drawn for the Epileptic sample, it can lead to 3 different outcomes: statistically very low, statistically very high, or statistically not extreme. Equation 6.6 gives the probability that a given pair of bins for 90 (for long range pairs) tests occurs.

$$P(K = k, L = l) = \frac{n!}{k!l!(n-k-l)!}\alpha^k(1-2*\alpha)^{(n-k-l)}\alpha^l, n = 90, \alpha = 0.05 \tag{6.6}$$

where:

K is the random variable counting the number of tests that return E significantly more synchronous than C.
L is the random variable counting the number of tests that return C significantly more synchronous than E.
k is the realization of the K random variable.
l is the realization of the L random variable.
n is the number of tests (90 for long range pairs).

What must then be tested is how likely such an extreme scenario is likely to occur under the null hypothesis. The couples (k,l) that are not likely to occur (under 5% off all draws) are determined by summing all probabilities of the less likely couples (according to equation 6.6) until reaching a probability of $\beta = 0.05$. In figure 6.6 the 5% of (k,l) less likely to be drawn are plotted in blue, and the remaining in red. Picking a couple (k, l) in the blue area occurs by chance less than 5% of the time.

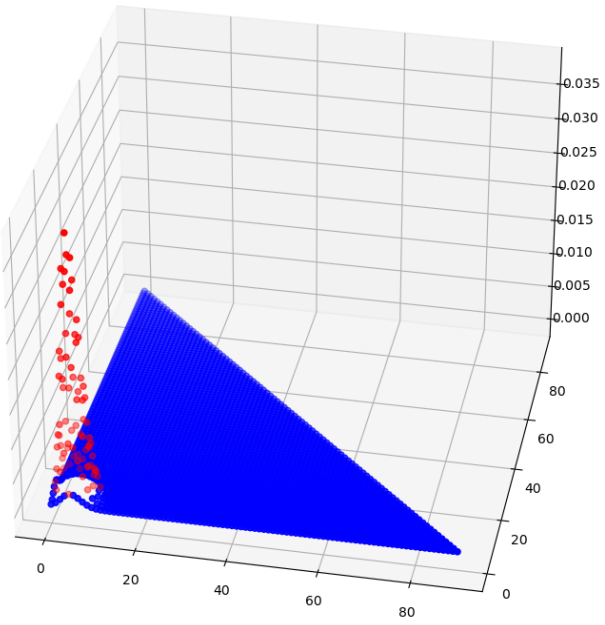

Figure 6.6: z-axis: 6.6. x-axis: k, y-axis: l. In red: couples that are likely to be drawn, in blue: couples unlikely to be drawn. n = 90. *beta* is p-value of this statistical test, and set to 0.05.

Applying these tests to the results of the original study would suggest that some of the differences observed between control and epileptic patients could have happened by chance, or at least would have suggested to be cautious regarding the conclusions. The ultimate problem lies in the correlation between these WRST statistics computed on pairs that share electrodes, the draws of the WRSTs are likely not independent.

Adapt the statistical tools

Despite the adjustments provided in section 6.4.1, alternative statistical tools can be used to approach more closely the levels of dependence in the dataset at hand. As a complement, the synchrony measure can be viewed as a classifier threshold, and a ROC statistic can be inferred [186]. An additional statistical analysis is realized thanks to the AUC of the ROC, providing an alternative mean of differentiating between epileptic patients and controls.

6.4.3 Results

Adapted Wilcoxon-Rank Sum Test

The f values can be used to correct the WRST employed in the reproduction of Bhattacharya [24] results. They are evaluated for each pair of electrodes and each frequency band, on MPC values computed on 8 s. windows with a 7 s. overlap. On average they equal 21.8 with a standard deviation of 3.6 and are sensibly higher for the highest frequency bands. They are used to adapt the standard deviation of the (normal) distributions of the WRST statistics under the null hypothesis, and provide adapted results, displayed in figure 6.7.

While the results in figure 6.7 do not overturn the conclusions made in the reproduction section, they clearly show the impact of mis-considering the correlation in the data. The multiple comparison check presented in section 6.4.2 does not invalidate, that for this dataset, regardless of the frequency band, and for most pairs of electrodes, the epileptic patients have, in general, higher MPC values than controls.

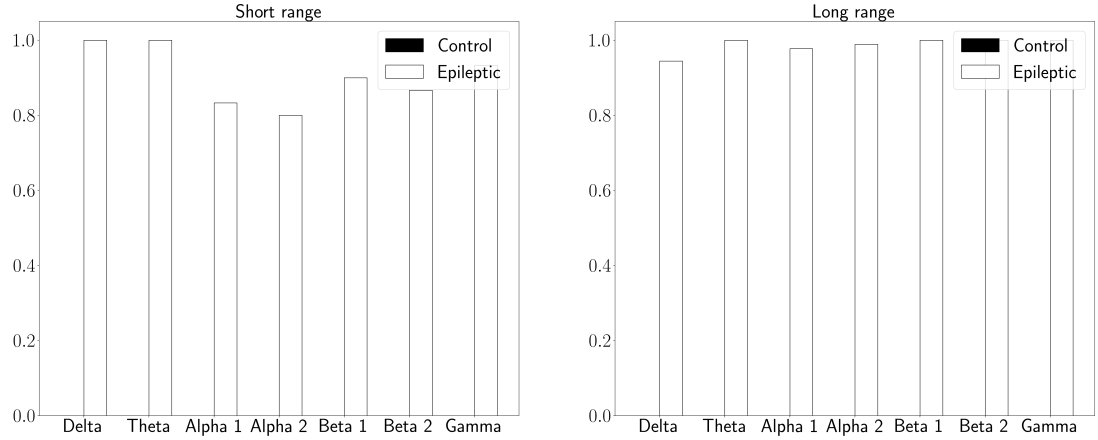

Figure 6.7: Reproduction of Bhattacharya experiments, EC condition, window length: 8s, window overlapping: 7s, measure: Mean Phase Coherence. Each bin counts the number of pairs that show statistically higher "synchrony" measures according to the adapted Wilcoxon rank-sum test. Left side for "short range" pairs, right side pour "long range" pairs. For an easier comparison between short and long range, the bins are normalized respectively by the number of short and long range pairs. Black bins are still absent because there is not a single pair of electrodes for which C MPC values are statistically higher than those of E.

The influence of the localization of the epileptogenic zone with ROC AUC

There is much to believe that the epileptic focus, in TLE, impairs differently the FC of the ipsilateral hemisphere than the FC of the contralateral one. Therefore, the influence of the epileptogenic locus on the MPC is assessed. Because hemispheres differ strongly in the cognitive functions they underlie, the functional connectivity should be different. One hemisphere in epileptic patients is only compared to itself in controls (Right vs Right, Left vs Left).

The ROC statistic is employed to quantify how well a synchrony measure helps in differentiating between the epileptic patients and controls, notably the AUC of the ROC (as in [186]). The more similar the epileptic patients are to controls, the harder it is to differentiate between both, and the AUC of the ROC is close to 0.5. Interestingly, ROC curves are insensitive to class imbalance. To ensure the ROC statistic did not occur by chance when classifying C and E with the synchrony measure, the distribution of the AUC under the null hypothesis must be estimated.

Null hypothesis Because it does not seem feasible to infer theoretically a threshold of the ROC statistic above which it would be guaranteed significant (95% certainty), the AUC distribution of the ROC statistics is drawn from the sample of controls. An underlying hypothesis is that most parameters inducing dependence in the data are the same in C and E. The controls are randomly assigned into two groups of equal number of subjects (6 controls in each), since 12 controls are available, there exist only $\binom{12}{6}$ possible combinations. The AUC is extracted from the ROC statistic computed for each pair of groups. The AUC distributions are roughly normal (slightly skewed to the right), the distribution mean μ and standard deviation σ are obtained by fitting theoretical normal distributions. When comparing E to C, the p-value of the test is estimated with regard to the fitted mean and variance.

Comparisons The data analyzed is the MPC values measured on all pairs (Short range and Long range) of electrodes for which both located on the Right or Left hemisphere, for the Eyes Closed condition. The duration of windows is 2 seconds long and windows do not overlap. The null hypothesis distribution of the test described in 6.4.3 is drawn, σ and μ are estimated by fitting. The comparison results are compiled in 6.2. Ipsi Right

corresponds to the hemisphere of right temporal lobe epilepsy patients and Contra Left to their left hemisphere. A p-value smaller than 0.05 indicates the likelihood that the measure could not differentiate between the two groups (E and C) is less than 5%.

Mean Phase Coherence				
Case	N.H. μ	N.H. σ	AUC	p-value
Ipsi Right	0.53	0.02	0.71	0.0
Contra Left	0.53	0.02	0.71	0.0
Ipsi Left	0.53	0.02	0.52	0.34
Contra Right	0.53	0.02	0.52	0.28

Table 6.2: N.H.: Null hypothesis distribution of AUC, μ: mean, σ: standard deviation. All numbers are rounded after all computations for display.

The results in table 6.2 show that the MPC classification performance can be used to differentiate the group of RTLE patients from the group of controls. Indeed, regardless of the hemisphere of RTLE patients the p-value is close to 0. It is not the case for the group of LTLE patients: the measure does not help to discriminate with controls (p-value close to 0.3). This can be explained by the MPC box-plots presented in the appendix (see figure 6.8). Namely, all sides (Left and Right) confounded, the number of right epileptic patients presenting only high MPC values is higher than the number of left epileptic patients presenting only high MPC values. The causes of these subjects presenting high MPC values were investigated in appendix (see section 6.6.1). Because these individuals could not be removed from the analysis, a selection bias should be hypothesized. This bias could be circumvented by increasing substantially the number of subjects in each group.

Overall, the analysis of the classification performance by MPC does not reveal any difference with respect to the laterality of the epileptic focus within this group of subjects at the level of this experiment.

6.5 Conclusions

This chapter demonstrates through the practical reproduction of a prior statistical study in epileptic patients that phase synchrony measures on scalp EEG recordings are strongly impaired by correlation. While the Wilcoxon rank sum test is appropriate for comparing sets of not normally distributed synchrony measures, the commonly used p-value to assess for statistically significant differences (5%) has to be revised in accordance with the correlation within the data. Although the methodological points developed here address a specific problem, they cover a broad range of possible cases. A mean of computing an approximation of this correlation factor was proposed and tested over several scenarios with varying degrees and form of correlation in real data. While the correction of the Wilcoxon rank sum tests by this correlation factor does not overturn the biased initial tests, some differences become statistically insignificant after correction.

Phase synchrony laterality in mono-lateral (left or right) temporal lobe epilepsies was investigated with an alternative test to the Wilcoxon rank sum test, namely the area under the curve of the receiver operating characteristic. No statistically significant evidence of the epileptic focus laterality in phase synchrony can be unveiled in the dataset at hand.

One major concern in statistical analysis remains the number of independent samples, and all correlation within a given subject accounted for, in the limited number of subjects. And therefore the main limitation of the current study remains in the restricted number of subjects which has to be substantially improved to allow for a definite answer. The availability of data is constrained by two main factors: the cost of expertly examining the EEG records to identify artifacts (eyes, muscles, epileptic spikes...), and differentiate between conditions(EO/EC); as well as the recording of controls. A second limitation stems from the medication that epileptic patients are taking despite still having seizures.

Finding a measure differentiating epileptic from healthy brain at the level of the individual with EEG in the absence of epileptic spikes remains challenging but rewarding, as it could be used as marker / feature for a rehabilitating

neurofeedback protocol, in the form of a Z-Score neurofeedback [302]. These results indicate nonetheless that the mean phase coherence on specific pairs of EEG channels constitutes a neuromarker that should be tested in neurofeedback protocols.

6.6 Appendix

6.6.1 Outliers

Subjects with elevated and localized (reduced spread) MPC distributions were identified unilaterally in the epileptic group (see figure 6.8, I). These possible "outliers" are: 7f4499ef3 (RTLE), 8766fe2ebd (RTLE), f560d1b20e (LTLE), f8766225fd (RTLE).

Figure 6.8: Distribution of the synchrony values for each subject taking part to the experiment, over all recordings, all pairs of either Short Range / Long Range, all frequencies. I) MPC, window length: 2s, window overlapping: 0.s. II) PLI, window length: 2s, window overlapping: 0.s.

They were not removed from the analysis for three reasons: there are other subjects that reach such high values of MPC, they do not behave differently with the PLI (figure 6.8, II), but mostly because a careful supplementary analysis of these EEG recordings did not unveil any peculiarity. An analysis of the medical records of these epileptic patients did not unveil any common specificity.

Reduced interhemispheric synchrony in controls ?

The involvement of hemisphere side in phase synchrony measures was evaluated regardless of the epileptic syndrome. The denomination of the hemisphere side is as follows: Left corresponds to both of the electrodes of a pair are on the left hemisphere, Right corresponds to both of the electrodes of a pair are on the right hemisphere, Both is for pairs that have electrodes on both hemispheres.

Histograms drawn from the MPC values confounding all frequency bands in figure 6.9 I show decreased MPC values for interhemispheric pairs.

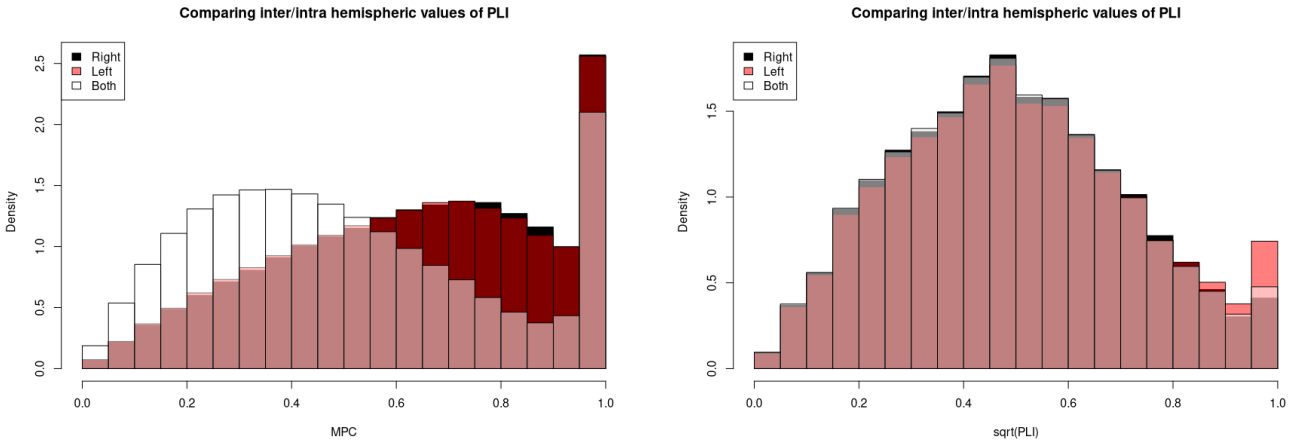

I II

Figure 6.9: I) Superposed histogram densities of MPC values (all frequency bands) of intra (right and left) hemispheres and inter hemispheres pairs of electrodes for C only. II) Superposed histogram densities of the square root of PLI values (all frequency bands) of intra (right and left) hemispheres and inter hemispheres pairs of electrodes for C only. The bin heights weighted by their widths sum to one.

To statistically test the significance of this difference, a simple mixed linear model is devised, with Subject as random factors (Value $\sim$ Side+(1 | Subject)), on C and E separately. In C, the random effect Subject accounts poorly for the variance of the MPC residuals (0.001446 Subject σ^2 for 0.064077 Residuals σ^2). In E, the random effect Subject accounts greatly (by a third) for the variance of the MPC residuals (0.02071 Subject σ^2 for 0.06048 Residuals σ^2). Both results are in line with the box-plots presented in figure 6.8, I, where a lower variance and better consistency are observed in C, and higher variance and variability in E. Therefore, the previous linear mixed model is used for E and a simpler linear model is used for C: Value $\sim$ Side. The linear model confidently shows that interhemispheric MPC values are lower than intrahemispheric MPC values in C by over 0.13. The mixed linear model also shows that interhemispheric MPC values are lower than intrahemispheric MPC values in E by about 0.08 (with respect to 0.66 for Left and Right) whereas Left and Right hemisphere are overall the same.

While a strong reduction of MPC is observed in C as well as in E for crossing pairs (interhemispheric), the PLI in figure 6.9 II does not reveal any difference between interhemispheric and intrahemispheric pairs. The strong reduction of MPC observed in controls (as well as in epileptic patients despite not being presented here) for crossing pairs (interhemispheric) and the absence of this effect in PLI could be explained by volume conduction, since the PLI is not directly sensible to it.

6.6.2 Non significative pairs

For the sake of providing information that could be useful to further analysis, the pairs that do not significatively show that the epileptic group is more synchronous that the control group in figure 6.7 are:

Delta	Theta	Alpha 1	Alpha 2	Beta 1	Beta 2	Gamma
Short range						
		C3-P3 T3-P3 T4-P4 F4-C4 T4-C4	C3-P3 T3-P3 O2-P4 T4-P4 T4-C4 T6-O2	F7-F3 T4-P4 T4-C4	F7-F3 T4-P4 T4-C4 T4-F4	T4-C4 T4-F4
Long range						
T4-C3 F4-F3 T4-F3 C4-F7 F4-F7		C4-F3 C4-F7	T4-O2			

Table 6.3: For each frequency sub-bands: the pairs that did not unveil a statistical significance between the healthy and epileptic group.

Chapter 7

Investigating the origin of phase delays in the alpha band

Traveling waves in the brain are spatial patterns of oscillatory activity which underpin functional relationships. This work investigates traveling waves in scalp EEG recordings, in an eyes-open / eyes-closed paradigm through the prism of neurofeedback. Different electrode montages and different frequency bands are considered to show the specificity of the anteroposterior axis in exhibiting phase differences in the alpha rhythm triggered by the eyes closed condition. It reveals that the variability between subjects is higher than exposed in the literature. Compellingly, it unveils that for a given subject, the phase difference patterns are stable across recordings. A simplistic model of solely two electrical dipolar activities is proposed to account for these traveling waves on the scalp. Finally, the focus on the anteroposterior axis shows that instantaneous estimates of phase differences are not reliable but yet suitable for neurofeedback training.

7.1 Introduction

Traveling (or propagating) waves in the brain are oscillating electrical voltages of identical frequency observed sequentially or simultaneously at different locations, relating them functionally. They are observed at various scales, all over the brain [344], in various frequency bands and following varied stimuli (or in their absence), making them an ubiquitous phenomenon [336].

How are the propagating waves measured? The variety of occurrence of traveling waves requires multiple acquisition approaches. They can be measured with optical imaging method (voltage-sensitive dyes), MEG, EEG, iEEG, ECOG or fMRI. Nonetheless, ensuring their functional relationship is non-trivial. The characterization of consistent phase delays between the oscillations of neuronal populations may serve to unveil existing relationships.

Small scale At the scales of cortical columns or cortical area such as those of sensory systems, the traveling waves propagate within the gray matter. These waves are recorded in the visual [72, 191, 225, 260], olfactory [62, 83, 204, 154, 345], somatosensory [57, 55, 218], auditory[234], and motor [251] systems of multiple species. The propagation occurs with respect to specific directions dictated by the structure of the network [57, 15] and its synaptic weights. Sato et al. [260]'s review suggests that traveling waves in the visual cortex rely on horizontal connections to "long-range" (by opposition to immediate neighboring) cells and permit the integration of information over larger area. The possible interactions between waves patterns add to their complexity. The result of these interactions is sometimes interpreted as having a computing role in the brain [159].

Large scale Other traveling wave patterns can be observed at the largest scale of the whole cortex, notably sleep related waves and alpha waves. Nunez [196] was among the first studies to document traveling waves at the level of the scalp. It described a wavelike shape of the alpha component along midline scalp EEG electrodes. More recently, Zhang et al. [344] observed traveling waves all over the cortex with intra-cranial EEG analysis of the θ and α band in epileptic patients. Their medium of propagation is debatable: Petsche and Šterc [219] show that spreading may be a purely cortical surface event while Nunez [197] seem to favor a cortico-cortical spreading involving white matter fibers over another medium involving thalamocortical fibers [312]. In multimodal (iEEG, scalp EEG, unit firing) recordings, Nir et al. [192] show that these slow waves propagate along major anatomical pathways, usually from medial prefrontal to medial temporal lobe and hippocampus. In any case, the interactions between distant cortical areas are not only the result of anatomical connectivity, because they can be modulated by brain states [274]. The spatiotemporal patterns of slow cortical waves (<4Hz [192], 0.1-5Hz [192]) are the hallmark of non-REM sleep and anesthesia [274]. The sweeping wave of membrane potentials during sleep (<1Hz, 1.2-7.0 m/sec) from prefrontal-orbitofrontal to occipital regions is probably the most reproducible (across nights and subjects) traveling wave [175]. According to [159], the structure of these cortex wide waves is mostly described (in mice) through five patterns: a plane wave (1-directional), a standing wave, a source, a sink or a saddle. Studies focusing on traveling waves of α activity during resting state remain relatively rare [123], and their conclusions regarding the direction of the propagation dividing. While it is a consensus that these waves propagate along the anteroposterior axis, results about the direction of propagation vary: anterior to posterior [122, 121], posterior to anterior [196, 219, 344], or with reversals. Alamia and VanRullen [10] attribute the propagation direction to the paradigm: forward (during visual stimulation) and backward (during rest). In Shaw and McLachlan [271]'s study, stronger arousal level are positively correlated with slower longer time delays (slower propagation). The closest study [123] to the present one unveils traveling waves in the α band, along the anteroposterior axis during periods of high synchronization. It shows, involving 4 healthy subjects, that "during phase synchronization, the pattern of phase difference between sites takes two forms", which appear irregularly over time. One is a pattern with a gradual phase shift, and the other is a pattern with a sudden phase shift of about π radians in the central region.

While the causality between scales remains unclear [181], some studies have advanced that slow rhythms operate as coordinators between brain regions [319, 344], more precisely that the phase of α traveling waves could coordinate the neocortical γ bursts [14].

Roles The roles attributed to the traveling waves are diverse. They occur during the development of the retina in mammals, even before vision is available [133] and could be involved in synaptic remodeling in central visual structures [133]. In the fully formed visual system, they encode position [191] and it has been suggested by Ermentrout and Kleinfeld [72] that the continuum of phase shifts provides means to scan incoming sensory input. This idea of predictive coding was taken up by Alamia and VanRullen [10] for α waves. In the olfactory system, Zochowski and Cohen [345] indicate that propagating waves may carry information about previous olfactory experience. The sleep slow oscillations set up a spatio-temporal framework for increased excitability in neuronal populations [175], and are linked to memory consolidation [329, 187] known to occur during sleep.

More generally, traveling waves occur in sensory processing, sensorimotor transformations and executive control [321]. In addition, they are thought to be behaviorally relevant and necessary to the spatial and temporal segmentation of neural representations [344].

What mechanisms permit the propagation of electrical waves? The ease of propagation of traveling waves can be supported by a sustained mildly depolarized state [336]. The mechanisms for this propagation have been theorized, notably by Ermentrout and Kleinfeld [72], who proposed three possible mechanisms: 1) A unique oscillator activating cortical areas with different time delays (resulting in a spurious wave), 2) A chain of successively activated oscillators, 3) Coupled local oscillators generating wave propagation due to phase delay between individual oscillators and a fourth mechanism is proposed by Huang et al. [117], in which two non-oscillatory pulse generate an oscillation in the form of a spiral wave singularity. According to Wu et al. [336] the strength of the coupling between these oscillators reduce phase gaps, increase velocity, or simply allows for waves in the first place. A failure in GABAergic inhibitory circuits can trigger a"local excitatory activity [that] can become regenerative and propagate to a large area" [336].

Training the speed of the alpha waves Under Shaw and McLachlan [271]'s hypothesis that low alpha traveling waves correlate with high level of arousal, and Nagai et al. [190]'s review that the up-regulation of arousal (increase in sympathetic activity) can reduce epileptic seizures, plus the likelihood that speed of propagation can be trained [109], it is tempting to envision the training of alpha wave speed as a mean to reduce epileptic seizures frequency and/or severity.

This study This study focuses on the α inhibition rhythm propagation, as its voluntary control could prove beneficial to the regulation of seizure propagation. The phase difference distributions between pairs of electrodes on the scalp are analyzed and compared for two different conditions: Eyes Open Fixation (EOF) and Eyes Closed Relaxation (ECR) (or a control condition: Mental Calculus). This study shows that phase differences emerge in the α band along the anteroposterior axis during the ECR condition whereas not in the coronal plane, nor during calculus condition. While these phase differences differ from subject to subject, they appear stable across recordings taken days and years apart. These results suggest a subject to subject variability that is not exhibited in the literature, especially in Ito et al. [123]. A model of two dipolar activities is proposed, and is enough to simulate phase differences similar to those observed experimentally.

7.2 Data

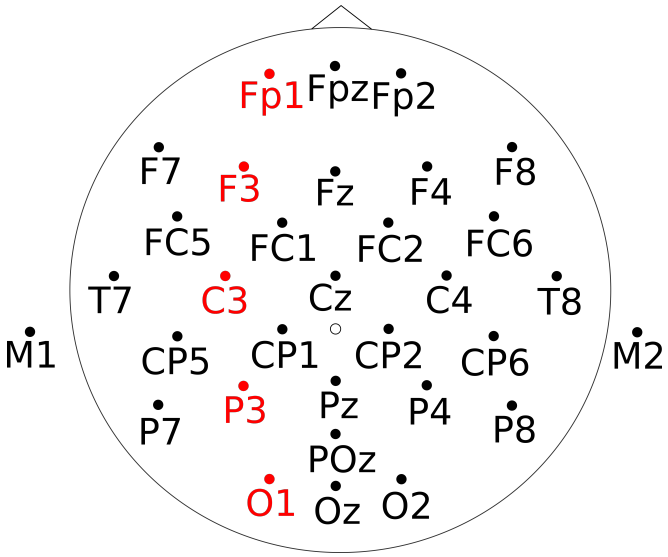

Figure 7.1: Electrode layout of 32 channels ANT Neuro headcap. Black and red disks are the available electrodes (thirty two). It is an extension to the 10/20 system. Red disks are an example of an anteroposterior midline. Black circle (one at the vertex) is the reference electrodes.

EEG recordings of 9 healthy subjects were acquired on a ANT Neuro EEGO32 acquisition device, with a EEGO32 wet electrodes channels headset, referenced at the vertex (CPz), as illustrated figure 7.1. The electrode impedances were kept under 20 $k\Omega$, which is below the recommended maximum of 50 $k\Omega$ for high-impedance eego amplifiers [18].

Each recording alternates between a baseline period (EOF) and a task (either ECR or calculus) period, each lasting 20 s. These periods are interleaved with 5 s-periods that are not analyzed. The recordings were obtained for each subject over a variable number of sessions, occurring over several weeks / years. Each recording lasts 275 seconds as depicted figure 7.2). For each subject the number of recordings is variable, and depends on the number of sessions to which he/she participated (1 to 8), and the number of recordings per session (2 to 4).

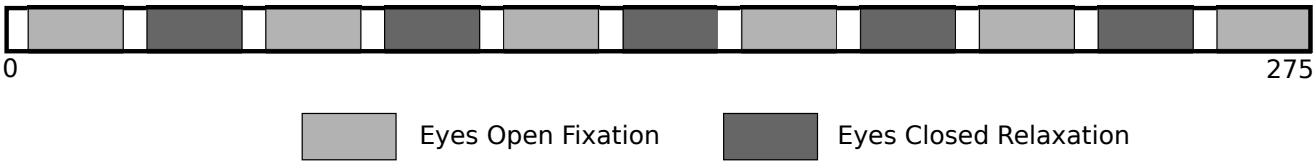

Figure 7.2: Each recording lasts 275 seconds, it alternates between 20 seconds of Eyes Open Fixation (EOF) (6 times), and 20 seconds of Eyes Closed Relaxation (ECR)(5 times) or 20 seconds of Mental Calculus, interleaved with 5 seconds of rest. ECR condition ends with a sound, to inform the participant that he/she has to open his/her eyes.

7.3 Method

Phase differences between channels along the anteroposterior midline ([O1, P3, C3, F3, Fp1]) and medio-lateral midlines ([T7, C3, Cz, C4, T8]) are computed and their probability distributions are compared between EOF, ECR or calculus conditions.

While each subject is analyzed separately, all the recordings obtained on a given subject are considered simultaneously.

The Morlet Wavelet (MWT) computed on several small frequency bands compared to the Hilbert Transform on a single large band of analysis (as in Ito et al. [123]) could provide a more accurate description of the possible phase delays at different frequencies inside the band. It would also limit to which extent the phase information is mixed between two close frequency components (within a larger band), and thus wrong (see chapter 3). The MWT (number of cycles: 12) was therefore applied to each channel, for frequencies (ν) varying from 8 to 12 Hz (sampling step of 0.1 Hz), to deduce complex wavelet coefficients $A(t,\nu)e^{i}\Phi(t,\nu)$ representing the channel in the time-frequency (t,ν) plane. The phase $\Phi(t,\nu)$ and amplitude $A(t,\nu)$ are then extracted from these wavelet coefficients. Both are split according to the EOF and ECR (or calculus) condition periods.

Phase information is used to compute at each time step and frequency step ($\forall(t,\nu)$) the phase differences $\Delta\Phi(t,\nu)$ between channels. Postulating that direct communication between neurons (from one Excitatory Post Synaptic Potential to another) are fast (do no exceed 50ms, which at 10Hz amounts to half a cycle (π)), then $\Delta\Phi(t,\nu) \in [-\pi : \pi]$. In which case, any computed difference greater than π is turned into a difference greater than $-\pi$, and reversely:

$$\Delta\Phi'(t,\nu) = \begin{cases} \Delta\Phi(t,\nu) -= 2\pi & \Delta\Phi(t,\nu) > \pi \\ \Delta\Phi(t,\nu) += 2\pi & \Delta\Phi(t,\nu) < \pi. \end{cases} \tag{7.1}$$

The phase differences $\Delta\Phi'(t,\nu)$ of a given 20 s period are then integrated in a histogram weighted by their associated amplitude products $\prod A(t,\nu)$ in 100 bins over the $[-\pi : \pi]$ interval, providing a dense and smooth coverage of the $[-\pi : \pi]$ lag range. While using the MWT can be beneficial or even necessary, one must be wary that, by opposition to the Hilbert transform on large frequency bands, phase information is more likely to be meaningless because there may be no energy in the signal at that frequency of interest. The option considered herein consists in weighting each phase difference $\Delta\Phi'(t,\nu)$ by its associated amplitude product $\prod A(t,\nu)$ when integrating it to the phase difference probability distribution. Consequently, the contribution of the phase differences computed from phases associated to low amplitudes can be considerably reduced. The effect of such processing is briefly illustrated in the appendix (subsection 7.7.2).

The resulting probability distribution is concatenated to all the distributions of all the periods of all the recordings of a given condition. [1]. An illustration summarizing the pipeline is provided in figure 7.3 and the specificity of integrating the amplitudes is described in figure 7.11. These steps are repeated for all 9 subjects.

In another analysis aiming at showing the stability of the distributions across recordings, the parameters of the

[1] Proceeding this way circumvent the memory storage of all the phase differences at all time and all frequencies, but just those of a given period.

fitted von Mises distributions are extracted, and the locations are plotted on a circular histogram.

Finally, to investigate the possible usage of such information in online protocols, the time course of the phase information is analyzed.

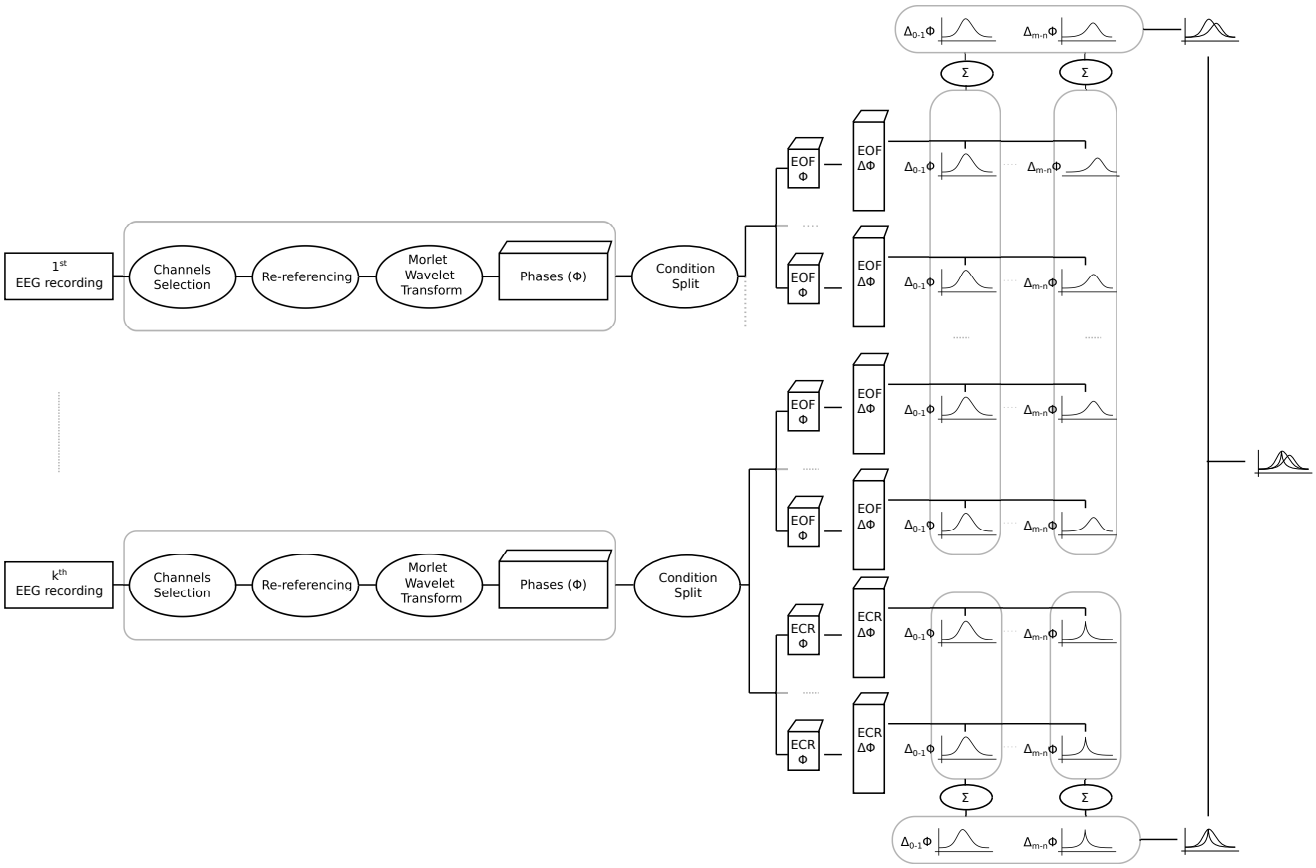

Figure 7.3: The pipeline is presented for a given subject with k recordings. The phase differences are computed on each EEG recording separately and the phase difference histograms are merged in the final steps. For each recording, the channels of interest are selected (O1-P3-C3-F3-Fp1 for instance), these channels are re-referenced (to M1 or M2 for instance), their Morlet wavelet transform is computed with a number of cycles equal to 12 to retrieve the instantaneous phase as a function of time. The phases are split according to whether they occur during the EOF or ECR condition. The phase differences are computed for each pair of channels of the selection with the first one (O1-P3, O1-C3, O1-P3, O1-F3, O1-Fp1), and their histograms are evaluated. All the histograms of a given condition and given pair of electrode are merged together to aggregate all the information. Finally, the EOF and ECR condition are compared.

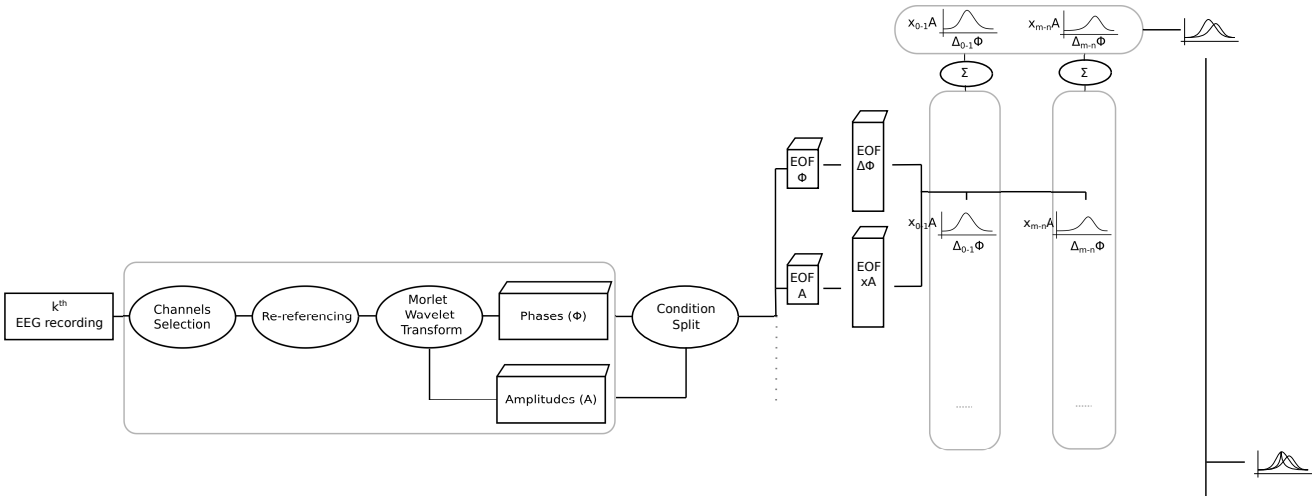

Figure 7.4: To take into account the amplitudes in the phase distribution estimations, the pipeline is modified, and for convenience truncated to the k^{th} recording of a given subject. The amplitude is also extracted from the wavelet coefficients, then the amplitude maps are split according to the condition. For each pair of channels of interest, the product of amplitudes is computed. For each phase difference falling into a bin of the histogram, the product of the amplitudes is added, instead of 1.

7.4 Results

7.4.1 Phase difference distributions

The results presented in figure 7.5 are strikingly similar to the results presented in Ito et al. [123], where phase shift are mostly constrained between 0 and π. However, these results are much more variable between subjects. While the EOF condition leads invariably to two possible outcomes: either a distribution centered on 0 phase lag or a π phase reversal for all channels in the anteroposterior axis, the ECR condition leads to much more diverse results.

Before discussing this diversity, one may take heed of the consistency in the order of the phase differences at which the peaks occur in the ECR condition (O1-P3-C3-F3-Fp1). In most cases, the phase difference are positive and reveal a phase advance of frontal channels with respect to occipital channels. The distance from Fp1 peak to F3 peak is systematically shorter than the distance from C3 peak to F3 peak, despite the similar distance on the scalp. There is a non linear relationship between the distances of the anterior electrodes to O1 and their phase difference peaks. In other words, despite the similar distance between each electrode on the scalp, the phase difference does not evolve linearly from the back to the front of the scalp.

The Fp1 distribution peaks from $\pi/4$ to almost π in most recordings where delays are manifest, except for subject VIII. In subject VIII there seem to be a reversal of the phase distributions, which is not the result of delays exceeding π, as presented in 7.7.1 with simulations in which the order would be maintained. It could be that not only the delays are subject specific, but also the main direction of propagation. This claim is to moderate with respect to the number of periods of 20s. available for this subject (10).

Interestingly, if one compares the histograms obtained over all available recordings to those obtained on a single random recording (presented in the Appendix as figure 7.16), the same global features can be retrieved. One may wonder how stable these patterns are across recordings.

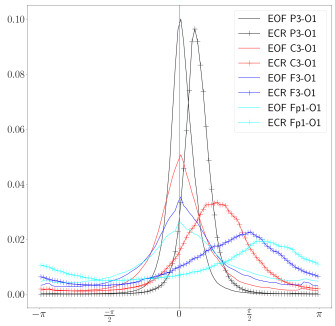

I ECR: 115, EOF: 138

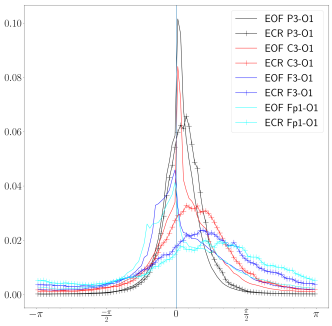

II ECR: 15, EOF: 18

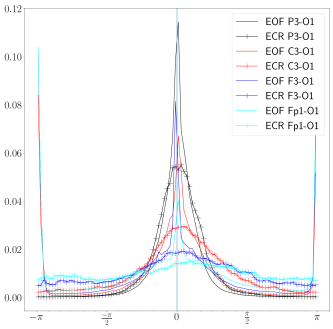

III ECR: 20, EOF: 24

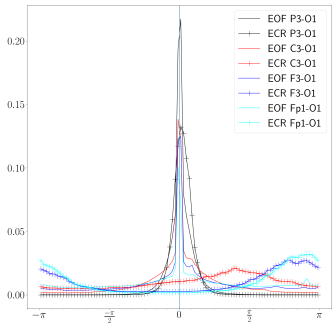

IV ECR: 45, EOF: 54

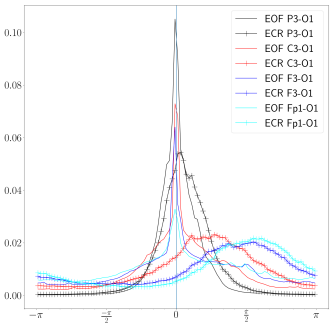

V ECR: 35, EOF: 42

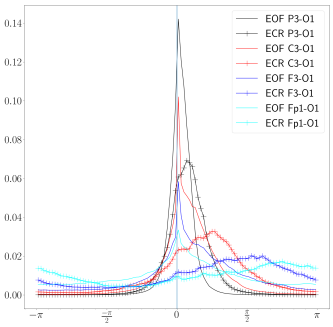

VI ECR: 40, EOF: 48

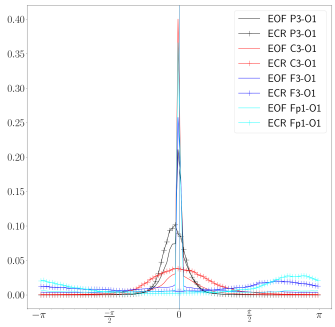

VII ECR: 25, EOF: 30

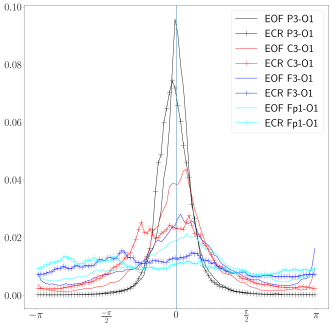

VIII ECR: 10, EOF: 12

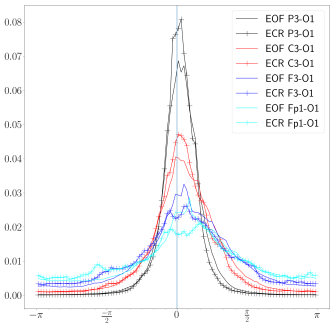

IX ECR: 10, EOF: 12

Figure 7.5: Left anteroposterior axis (O1-P3-C3-F3-Fp1). Referenced at M2. Over the α frequency band: 8-12Hz. Phase difference distributions retrieved from 9 subjects with various number of recordings. Each histogram is computed on a variable number of recordings (4 to 23) 6 * 20 seconds of EOF, 5*20 seconds of ECR. The number of periods of 20s per subject is provided under each histogram.

7.4.2 Stability of traveling waves across recordings

To standardize the process of assessing the stability across recordings of the phase difference peaks, von Mises distribution are fitted to each histogram of phase difference (for each pair of electrodes, and each EOF or ECR periods). The location is extracted from each histogram, and the values plotted in a polar histogram. The results are presented for the subject with most recordings in figure 7.6. To assess the soundness of the results, three controls are devised. One reproduces the pipeline on recordings based on the same protocol, replacing ECR with calculus. A second reproduces the pipeline in a different frequency band (part of the β band: 20-24Hz). A last control reproduces the pipeline on coronal selection of electrodes.

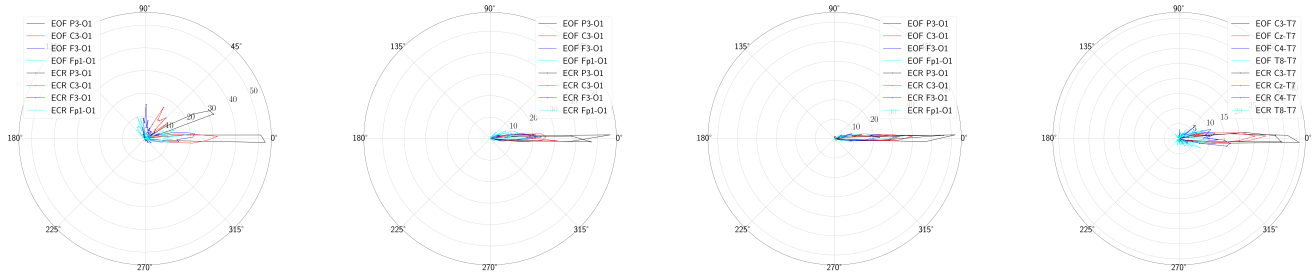

1 2 3 4

Figure 7.6: Polar histogram of the estimated locations of von Mises phase difference distributions. (EOF, ECR) or (EOF, Calculus). For this subject: (23 * 6 * 20 s. of EOF and 23 * 5 * 20 s. of ECR) or (20 * 6 * 20 s. of EOF and 20 * 5 * 20 s. of Calculus) are analyzed. These were recorded over the course of 2 years. Referenced at M2. 1) EOF and ECR, [P3, C3, F3, Fp1] - O1, in the 8-12 Hz frequency band. 2) EOF and Calculus, [P3, C3, F3, Fp1] - O1, in the 8-12 Hz frequency band. 3) EOF and ECR, [P3, C3, F3, Fp1] - O1, in the 20-24 Hz frequency band. 4) EOF and ECR, [C3, Cz, C4, T8] - T7, in the 8-12 Hz frequency band.

First, the controls show that these phase differences do not occur by chance, nor because of data processing. Second, the phase difference distributions are always located at approximately the same angles across recordings. The further from O1 the more variation can be observed.

Interestingly, in the calculus paradigm, a likely non-zero phase difference appear for frontal (Fp1) electrodes. While no synchrony is measured in the 20-24 Hz frequency band for ECR paradigm.

7.4.3 Explaining phase delays

The phase delays measured reliably can be turned into transmission delays and therefore propagation speed. The distances are estimated as the geodesic distances between electrodes on the scalp. The time required to cover theses distances is estimated with cross multiplication from the phase delays knowing that at about 10 Hz, a cycle (2π) lasts 100 ms.

Phase delays ($\Delta\Phi$) to time delays ($\Delta\tau$) (ms)				
	$\Delta\Phi$	$\Delta\tau$	Scalp Distance (cm)	Speed (m.s-1)
O1-P3	$\frac{\pi}{8}$	6.25	5.5	8.8
O1-C3	$\frac{\pi}{4}$	12.5	11.5	9.4
O1-F3	$\frac{\pi}{2}$	25	17	6.8
O1-Fp1	$\frac{5\pi}{8}$	30.625	25	8.2

Table 7.1: $\Delta\tau = \frac{\Delta\Phi}{2\pi} \times 100$ ms, where 100 ms corresponds to the duration of 1 cycle (2π) at 10 Hz. The phase delays were obtained from the approximated locations of the peaks in 7.5 I.

Several hypotheses can explain phase delays at electrodes located along the anteroposterior axis. An interesting hypothesis consider as many sources as there are phase delays. If the sources are located directly beneath the electrodes, the average propagation speed on the scalp would be of 8.3 m.s-1, which seems too high to be compatible with propagation speed in the cortex or white matter, despite these speed values being still discussed.

A second hypothesis involves bidirectionally coupled oscillators (as many as phase delays) that would allow for small phase differences (and therefore high velocity). One easily observes a consistency in the sign of phase delays between electrodes, regardless of the subject. It seems unlikely that the phase differences are the consequence of bidirectionally coupled oscillators for which the phase difference could be of an arbitrary sign.

A third, more simple and more likely hypothesis requires only two sources with oscillating activities and their possible mixing at the different electrode sites. In such model, one source is located in the occipital region, and the other in the frontal region. Both oscillate at a similar frequency, but are phased shifted with arbitrary phase values. Considering these two sources as $\sin(\omega t + \phi_0)$ and $\sin(\omega t + \phi_1)$

At the i^{th} electrode:

$$\begin{aligned}
&\alpha_i \sin(\omega t + \phi_0) + \beta_i \sin(\omega t + \phi_1) \\
&= \sin(\omega t) \underbrace{\alpha_i \cos(\phi_0) + \beta_i \cos(\phi_1)}_{A_i} + \cos(\omega_t) \underbrace{\alpha_i \sin(\phi_0) + \beta_i \sin(\phi_1)}_{B_i} \\
&= R_i \sin(\omega t + \phi_i)
\end{aligned}$$

where:

ϕ_0 is the phase shift of the first source (0)
ϕ_1 is the phase shift of the second source (1)
α_i is the volume conduction weight of the i^{th} electrode associated to the first source (0)
β_i is the volume conduction weight of the i^{th} electrode associated to the second source (1)
R_i equals $\sqrt{A_i^2 + B_i^2}$
ϕ_i equals $atan(\frac{B_i}{A_i})$

The mixing of these sources gives rise to sinusoids oscillating at the same frequencies to the frontal and occipital ones, for which the phase shift only depends on the geometrical configuration given by the α_i and β_i. The α_i and β_i are typically functions of source to electrode distance and source orientation with respect to source to electrode orientation. Phase differences computed between electrodes will therefore be differences between the ϕ_i. In this model, the major requirement is that the two sources have a constant relative phase shift in time.

To test the soundness of this model, it was simulated on two nested spheres (for the cortex and the scalp), using equations for electromagnetic waves propagation [259], and a constant conductivity value. Gaussian noise was added to the signal by a signal to noise ratio of 1 to 1.5. Geometric configuration and results are presented in figure 7.7.

The simulation unveils that two sources are sufficient to produce phase delays similar to those observed on real data (figure 7.5). More details are provided in the appendix for alternative geometries.

Since the geometry is paramount in explaining the phase differences, the position of the head-cap electrodes with respect to the generators is crucial. And the different scalp morphologies could partly explain the discrepancy between the results observed between subjects in figure 7.5.

Other arguments against the fact that these phase differences are attributable to anatomical wiring only is that they can strongly vary from one subject to the other, that the relationship between phase delays and distance is non linear and that they can be trained [109].

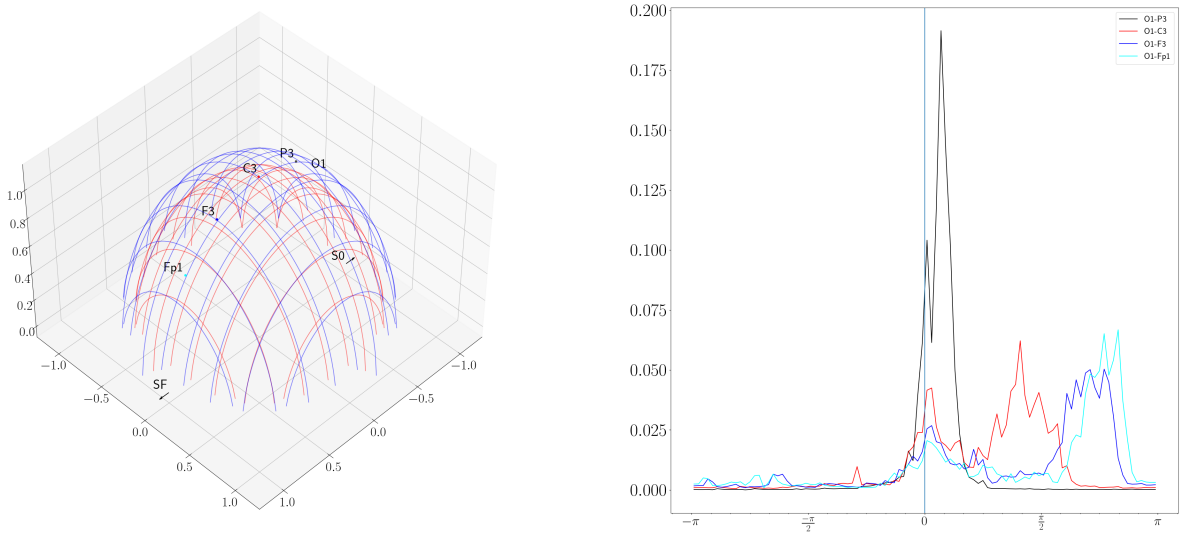

1 2

Figure 7.7: Geometry of the traveling wave simulation (1), and associated phase distributions (2). Sources are represented as arrows (SF: Source Frontal, SO: Source Occipital), on the inner red hemisphere. The sources are two sinusoidal waves oscillating at 10 Hz, with added gaussian noise. They are phase shifted from one another by 0.93π. Electrodes are represented as spheres of different colors (O1, P3, C3, F3, Fp1), on the outer blue hemisphere. Electrodes are placed along the anteroposterior axis. The histograms are obtained exactly as in 7.5, where the electrodes are referenced to O1.

7.4.4 Course of phase difference

The temporal fluctuation of phase difference along the anteroposterior axis unveils a cyclic pattern that corresponds to the EOF / ECR periods (figure 7.8, 1). Despite this overall trend, the local temporal variations are strong. Averaging (figure 7.8, 2), or finding the mode over larger windows provide a way to find respectively more stable or physically more meaningful patterns. Averaging can be an option for neurofeedback protocols based on traveling waves, were the subject exert control on up or down regulating the "speed of traveling waves", regardless of its value.

Averaging (figure 7.8, 2) shows in a (among other) specific recording some episodic phase reversal events (underlined in black), which could correspond to backward "propagation", or a switch of the drive between the neural sources. These events are not occurring sufficiently to appear in global phase differences distributions. They could add to the complexity of the neurofeedback training, but should definitely be taken into consideration in the possible levers to control the visual / auditory clue.

7.5 Discussion

Despite the so-called lack of spatial resolution, scalp EEG setups can provide insightful perspectives on synchronous activity in the form a phase synchrony.

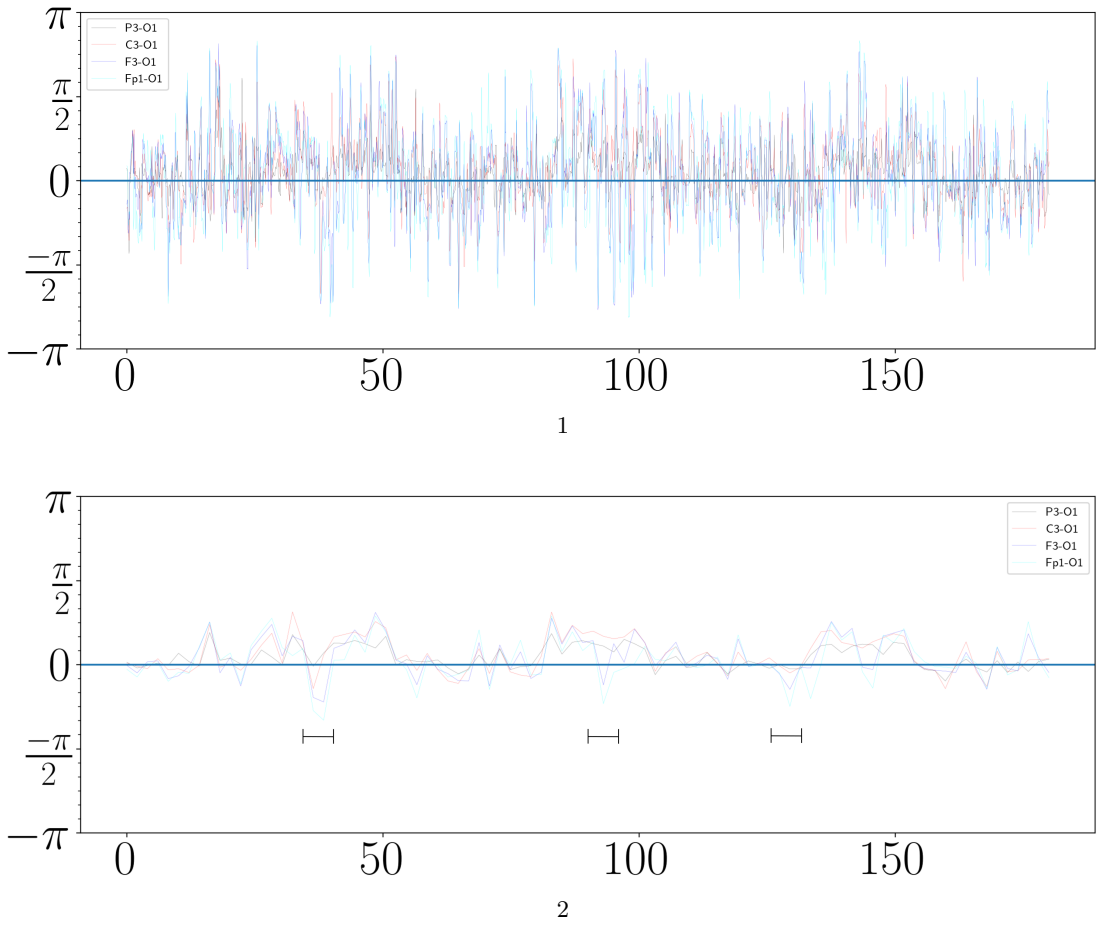

Figure 7.8: Temporal fluctuation of phase difference with O1, alternating 20s EOF / 20s ECR / 20s EOF / 20s ECR, during a single recording. Reference electrode: M2. In 1), each point is local average of 25 time points (1./sampling rate * 25 seconds) * 40 frequency scales = 700 phase differences. Sampling rate: 512 Hz. In 2), each point is a 2 seconds average.

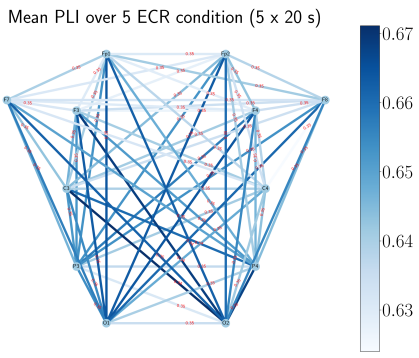

Figure 7.9: Phase Lag Index computed within the α (8-12 Hz) band on windows of 0.5 s overlapping by 0.4 s during the ECR condition on one recording (amounting to 5 x 20 s of ECR condition) of subject I.

7.5.1 Phase synchrony

A number of measures are devised with respect to phase differences, such as the Phase Locking Value [151], the Phase Lag Index (PLI) [194] or the weighted PLI. The PLI gives an estimate of the stability of phase difference within a given time window. If the idea behind the model presented in 7.4.3 is at least partly true, the synchrony measures based on the phase could be biased. The PLI was computed within the α band on windows of 0.5 s overlapping by 0.4 s during the ECR condition on one recording (amounting to 5 x 20 s of ECR condition) of an arbitrary subject. The result is illustrated in figure 7.9, where strong PLI connectivity is visible between electrodes along the anteroposterior axis, and even between left and right hemispheres.

It can be deduced that an index of mean synchrony (*i.e.* an average of PLI values) over all pairs could lead to an overestimation of actual synchrony, in such a case where two sources synchronize many electrodes at once. It is to emphasizes on the need for careful interpretation of phase informed synchrony measures in EEG, which is already subject to a number of pitfalls, or the necessity of using high resolution headset for source current density estimation and / or MRI acquisitions for sources reconstruction.

7.5.2 Online usage of phase difference

Phase synchrony occurs over short periods and is not better captured by measures such as the commonly used PLI and PLV, than by coherence [40]. The frequency at which phase differences vary over time hinders the retrieval of averaged phase differences (see figure 7.8), which would pull the phase difference to lower values, not representative of the actual phase difference during synchrony periods. While the average of phase differences over time windows would not provide a meaningful phase difference, it still can be put to use in the construction of a marker. Indeed, averaging over windows of 2 seconds allows to classify with great accuracy periods of EOF and ECR, but also gives a confident guess of the direction of propagation of the "traveling wave".

To add to the complexity of providing an online protocol, any phase informed measure also suffer an incompressible delay because of the inherent delay introduced by phase extraction, which in some applications (especially those focused on learning) is a shortcoming.

7.5.3 Perspectives

Histograms weighting The choice of weighting the histograms by the amplitudes have the adverse effect of hiding low amplitude synchronies. Indeed, synchrony patterns involve different cortical units whose activations of likely different size lead to favor the appearance of the synchrony patterns involving the largest activated cortical units. Other histogram constructs could be devised instead of weighting by the product of the amplitudes, such as counting the number of phase difference falling into a bin only if the product of the amplitudes is above an estimated threshold below which the phase difference is assumed spurious.

Source reconstruction The model of two dipolar activities oscillating at the same frequency with an arbitrary phase shift can be used as a constraint to localize these dipoles using the phase gradient. For such operation, a realistic model of the head would have to be employed, as well as an accurate registration of the electrodes on this realistic model of the head.

Training the propagating waves Following the simplistic model proposed in this work, it would seem that controlling the speed of propagation of this α wave would consist in enhancing / reducing the coupling between the two generators responsible for the wave. This appears considerably simpler than learning to control the activity of several coupled oscillators.

7.6 Conclusion

The phase difference distributions between pairs of electrodes on the scalp were analyzed and compared for two different conditions (and control): Eyes Open Fixation (EOF), Eyes Closed Relaxation (ECR) (, Mental Calculus). This study clearly showed von Mises phase difference distributions whose locations are clearly identifiable along the anteroposterior axis. While the locations are mostly organized close to a 0π phase lag in the EOF condition (and other control conditions), in the ECR condition and within the α band they show shifts between channels mostly restricted to the $[-\pi;\pi]$ interval. A simplistic model of two sources is enough to let appear such phase difference, and actually explains more simply the small phase difference that would lead to inconsistent transmission delays if hypothesized as such. In addition this model also explains the results observed for the control conditions. These results unveil a subject to subject variability that is not exhibited in the literature Ito et al. [123], which could be the effect of variable placement of the electrodes with respect to the α oscillations generators, an effect well illustrated with the model. Nonetheless, repeating the automatic evaluation of anteroposterior phase differences over more than a 100 periods of 20s showed that they are stable across recordings taken days and years apart. While the instantaneous phase differences are not stable on very short time scale, averaging over windows of 1 to 2 seconds display much more stable patterns. Despite their lack of physical significance, they could be used in BCI applications.

7.7 Appendix

7.7.1 Frequency specificity of traveling waves

In Inouye et al. [122] the direction of propagation depends on the frequency of the alpha peak, and in Zhang et al. [344] there is a correlation between frequency and speed of the traveling waves. The analysis of phase differences is therefore split with respect to frequency, the results are presented in figure 7.10. Instead of considering the whole 8-12Hz range, subbands of 1Hz are considered (8-9 Hz, 9-10 Hz, 10-11 Hz, 11-12 Hz).

While the phase differences appearing during ECR do not depend on the frequency subband at the level of all the recordings of a given subject, some interesting patterns appear in the EOF condition of dedicated recordings. In the EOF condition of one recording appears a reversal of phase difference distribution locations from 8-9 to 11-12Hz. The location of the peak differs in the different frequency bands. To ensure that this effect was not an effect of the processing on increasing phase differences, synthetic sin waves at 10Hz (ν) with a constant phase shift for all waves (ϕ_c) plus a varying phase shift for each wave (ϕ_k) were constructed ($sin(2\pi\nu t + \phi_c + k * \phi_k)$), with $k \in \{0., 0.1, 0.2, 0.3, 0.4\}$. The phase differences between these sin waves on the different sub-bands were identical, suggesting that the effect is not an artifact of data processing. Then, the constant phase shift was increased from $\pi/2$ to $3\pi/4$ to π. Leading to three possible cases: all phase differences are located between $\pi/2$ and π, half phase difference are located between $\pi/2$ and π and the other half between π and $3\pi/2$. Regardless of the constant phase shift, the order of the peaks is maintained, by opposition to what is observed in the real data. In this example, this is in opposition to the idea that propagation speed depends on the frequency of oscillation or reversely. This is mostly in support of Inouye et al. [122]'s work, in which α traveling waves direction is supposed to depend on the frequency of oscillation of the wave.

7.7.2 Phase difference weighting by amplitude product in histogram estimation

While considering the amplitude products does not shift the histogram peaks, it does remove a seemingly uniform distribution to the phase difference histograms of distant pairs (figure 7.11, 1 and 7.11, 2). Since a uniform distribution would be observed for unrelated phases, or random phase differences, it could be guessed that the transformation considering the amplitudes has the effect of removing a type of noise introduced by the MWT.

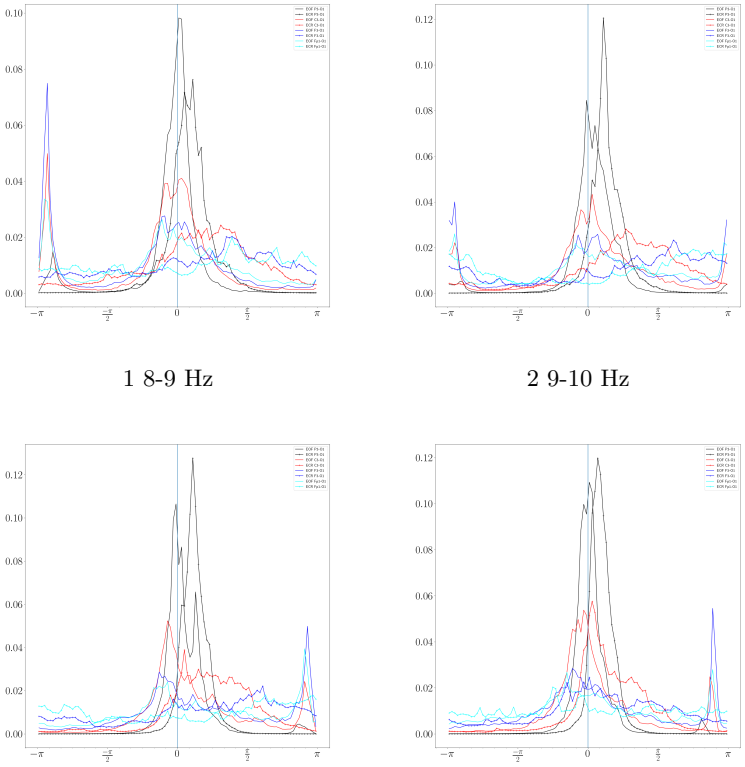

1 8-9 Hz

2 9-10 Hz

3 10-11 Hz

4 11-12 Hz

Figure 7.10: Right anteroposterior axis (O1-P3-C3-F3-Fp1), referenced at M2. Phase difference distributions retrieved from 1 recording of subject I, on various frequency subbands. Each histogram is computed either a variable number of recordings 6 * 20 seconds of EOF, 5*20 seconds of ECR.

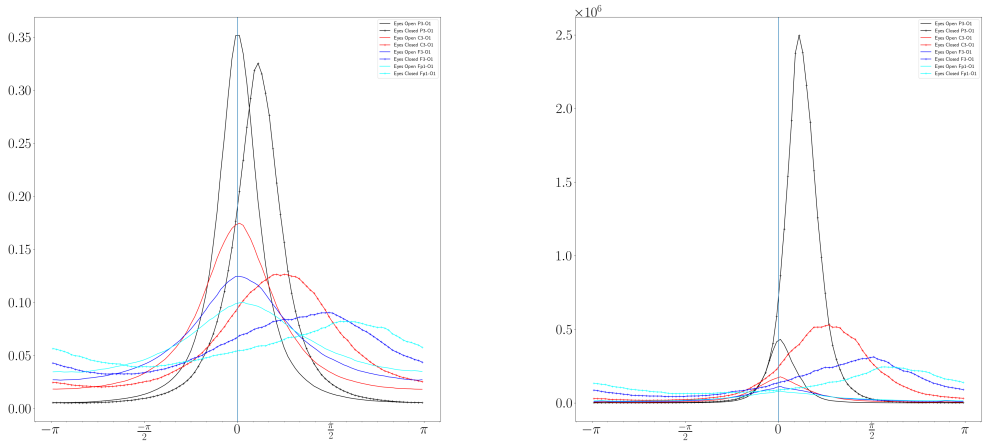

1 2

Figure 7.11: 1) Phase difference distributions based on phase difference occurrence only. 2) Phase difference distributions weighted by the amplitude product.

7.7.3 Statistical testing of dependent realizations of the circle

Specific statistical tests exist on angular measurements [285] [286], as well as on angular measurement distributions [163]. In this study only distributions are available, and the cited distribution tests require the estimation of the concentration parameter, through tables. Both tests suppose independence between the realizations. Unfortunately, phase difference estimation through any strategy introduce artifactual dependence between close phase difference (in time and frequency) and because of volume conduction in EEG recordings. The formal derivation of close wavelet coefficients dependence is presented in chapter 4. Then, the dependence between phase differences is not straightforward (notably because of the nonlinear definition of the phase) to evaluate. To avoid misjudging the location of the von Mises distributions based on the pvalue of a statistical test, the null hypothesis along which the location of the von Mises distribution is zero is refuted by looking directly at the probability distributions.

7.7.4 Von Mises distribution parameters estimation

Due to the massive amount of realizations for each pair of channels, the theoretical von Mises distributions are not directly fit to the empirical distributions of phase differences. To fit a von Mises distribution of parameters κ and μ, a large (but reasonable N=1000 realizations) artificial sample is drawn from the empirical distribution, and a von Mises distribution is fitted to this large sample. Figure 7.12 shows that the sample distributions match the empirical distribution. While this approach allows to identify the parameters of the empirical distribution, the goodness of fit of the artificial sample distribution with the von Mises distribution of estimated parameters κ and μ is to link to the arbitrary artificial sample size.

7.7.5 Effect of the common reference on the phase difference

Choosing M1 or M2 as reference electrode does not change the baseline (EOF), except for M1 that removes the phase difference peak at -π/2 present for M2. The locations of the F4-02 electrode peaks differ slightly from M1 to M2, but the order is maintained. This could partly be explained by the varying distance of M1 and M2 to these electrodes.

Choosing CPz as reference electrode, located at the vertex (white disk in Figure 7.1), introduce phase differences

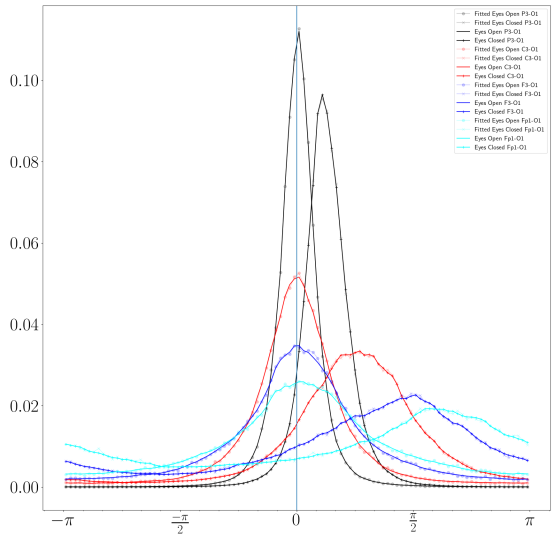

Figure 7.12: Flattened polar empirical probability distribution of phase difference distributions for all periods of either EOF or ECR, accompanied by draws (N=1000) from these empirical probability distributions. The draws are in turn used to obtain the κ and μ parameters of the von Mises distribution by fitting.

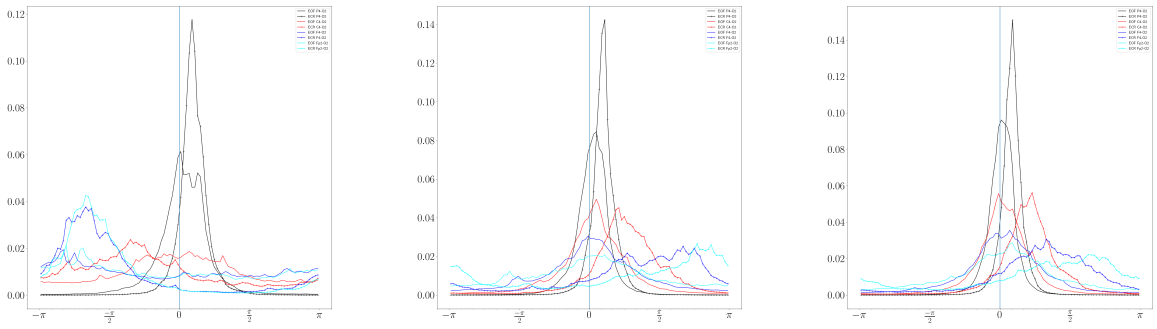

1 CPz reference 2 M2 reference 3 M1 reference

Figure 7.13: Histograms of phase differences along the anteroposterior axis (between P3, C4, F4, Fp2 and O2), with different common references (Cpz, M2, M1).

far from 0 during EOF that could be due to the sensorimotor rhythms especially close to the vertex. It also shows a reversal of phase difference during ECR that cannot be observed with M1 or M2 as reference.

The similarity between two distinct electrodes M1 / M2 (although rather symmetrically distributed) and the distinction with CPz causing a phase difference reversal tend to give arguments into favoring either the M1 / M2 or their mean as the new reference in this specific problem.

7.7.6 Simulations

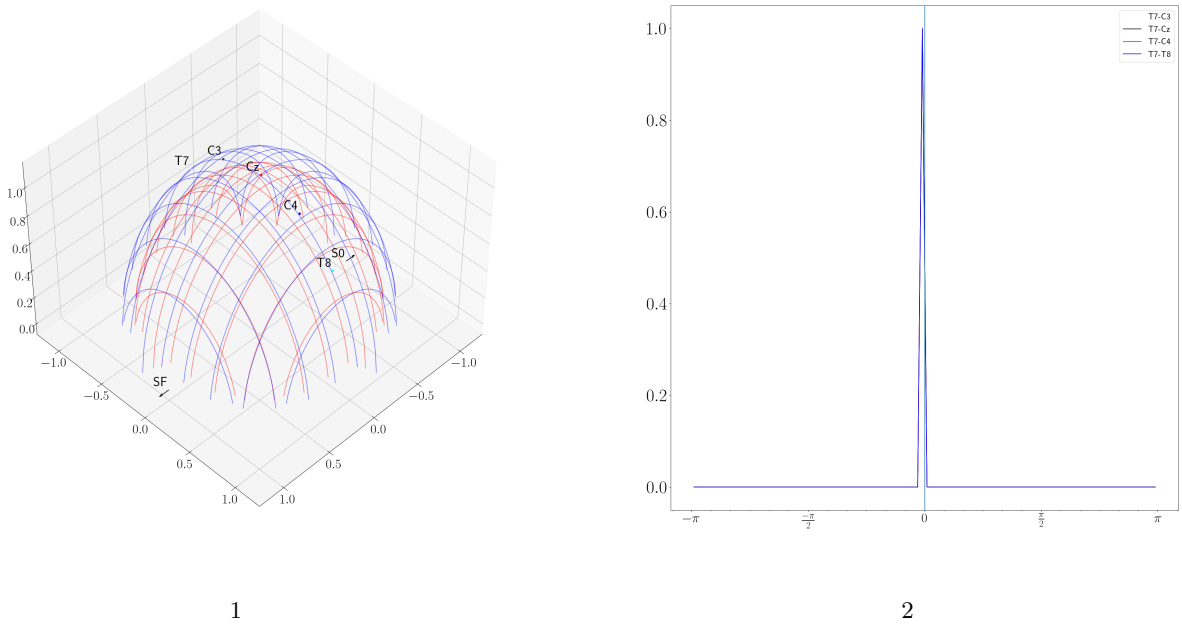

1 2

Figure 7.14: Geometry of the traveling wave simulation (1), and associated phase difference distributions (2) for a coronal axis. Sources are represented as arrows (SF: Source Frontal, SO: Source Occipital), on the inner red hemisphere. The sources are two sinusoidal waves oscillating at 10 Hz, with added gaussian noise. They are phase shifted from one another by 0.93π. Electrodes are represented as spheres of different colors (T7, C3, Cz, C4, T8), on the outer blue hemisphere. Electrodes are placed along the coronal plane. The histograms are obtained exactly as in 7.5.

Coronal plane electrodes The simulation of two sources located in the occipital and frontal areas and their projection onto sensors located on the coronal plane (figure 7.14, 1) unveils no phase difference (figure 7.14, 2). It reproduces what could be observed on real data (as suggested in figure 7.6, 4). It adds to the likelihood of the third hypothesis presented in 7.4.3.

Electrodes shift The same simulation allows us to test the influence of the placement of the head-cap on the scalp with respect to these traveling waves (see figure 7.15, 1 and 2). The electrodes are shifted of $\pi/12$ toward the nose. The effect on phase difference distributions of such manipulation is high. It demonstrates the importance of placing the head-cap with the greatest care when attempting to measure phase delays in EEG. While care was brought to the placement of the EEG head-cap (proved by the reproducibility over sessions), the relative position of the electrode with respect to the generators cannot be guaranteed. As mentioned in the perspectives, this "traveling wave" could be a supplementary information to be of use for source localization.

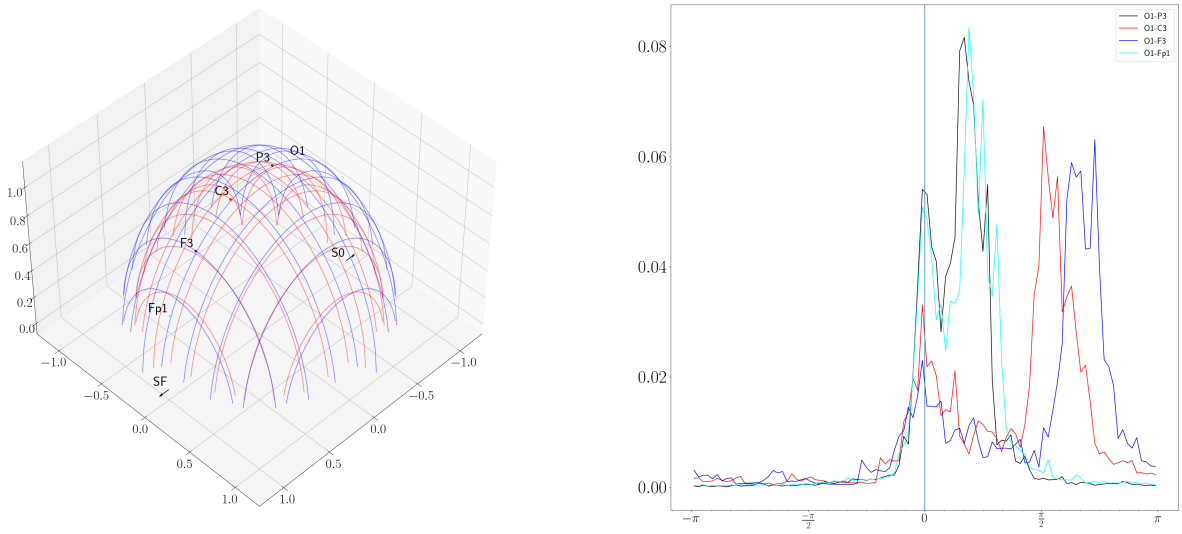

1 2

Figure 7.15: Geometry of the traveling wave simulation (1), and associated phase distributions (2). Sources are represented as arrows (SF: Source Frontal, SO: Source Occipital), on the inner red hemisphere. The sources are two sinusoidal waves oscillating at 10 Hz, with added gaussian noise. They are phase shifted from one another by π. Electrodes are represented as spheres of different colors (O1, P3, C3, F3, Fp1), on the outer blue hemisphere. Electrodes are placed along the anteroposterior axis, and shifted by $\pi/12$ with respect to 7.7 toward the nose. The histograms are obtained exactly as in 7.5.

7.7.7 Distributions on one recording

Figure 7.16, obtained on typical single recordings is interesting with regard to its similarity to figure 7.5, obtained on many recordings. Not only does it suggests that the phase differences distributions are consistent across recordings, but that a restricted number of blocks are necessary to assess the phase difference peaks.

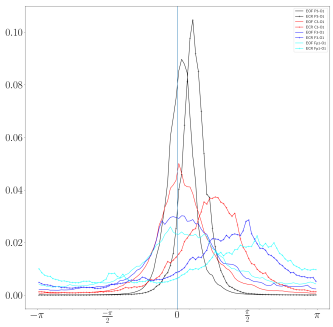

I ECR: 5, EOF: 6

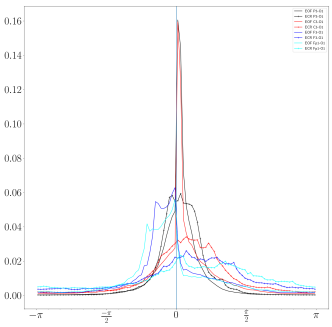

II ECR: 5, EOF: 6

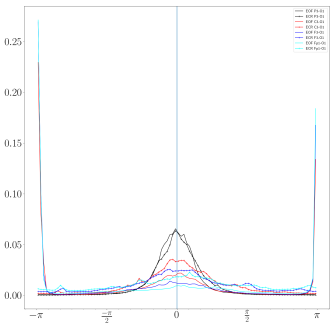

III ECR: 5, EOF: 6

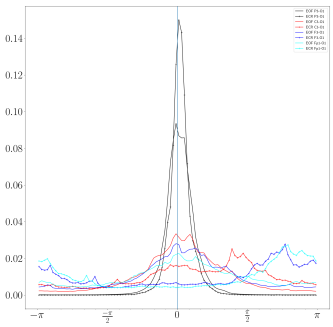

IV ECR: 5, EOF: 6

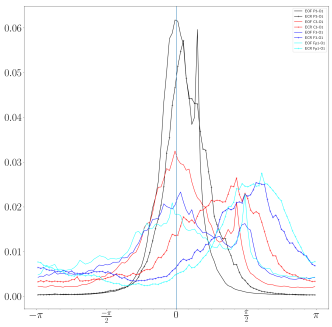

V ECR: 5, EOF: 6

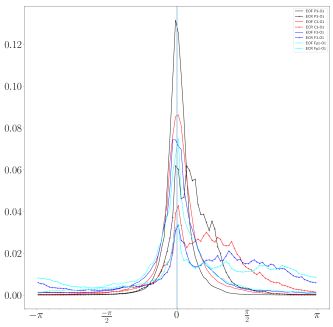

VI ECR: 5, EOF: 6

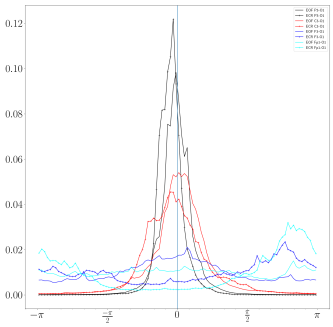

VII ECR: 5, EOF: 6

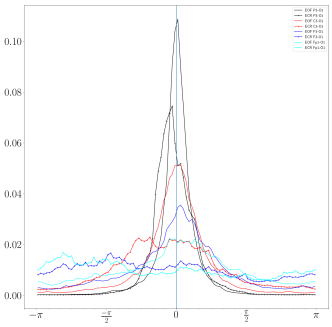

VIII ECR: 5, EOF: 6

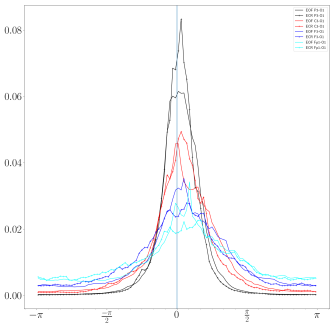

IX ECR: 5, EOF: 6

Figure 7.16: Left anteroposterior axis (O1-P3-C3-F3-Fp1). Phase difference distributions retrieved from 9 subjects. Each histogram is computed either over 6 * 20 seconds of EOF, 5*20 seconds of ECR. The channels are referenced at M2.

General conclusion

Summary of the contributions

This manuscript covers the tentative conception of a neurofeedback protocol to treat epilepsy on the basis of neural synchrony. Neural synchrony is approached through the study of phase synchrony between distant brain area activity oscillations, a paradigm available to high frequency recording media such as EEG or MEG. Despite the causal link between an excess of neural synchrony and epilpsy, studies linking phase synchrony to epilepsy are not legion. Bhattacharya [24] study unveiled a difference in phase synchrony between epileptic patients and healthy subjects, paving the way for a promising neuromarker. Given the experimental cost of testing a neurofeedback protocol based on a chosen neuromarker, it foundations must be solid. Building solid foundations meant reproducing the aforementioned study on a novel dataset. This brought us to the investigation of how phase information is extracted from EEG signals, how statistical tests can be employed to ensure the statistical significance of tests involving such phase information and derived phase synchrony measures. Additionally, the exploration of bare phase differences across the scalp led to observe a phenomenon called traveling waves (which could be a potential alternative neuromarker).

Extraction of instantaneous phase information, although commonly employed in the literature, is not as trustworthy as assumed. It was demonstrated with the Morlet wavelet transform of a generic sum of sinusoids that close frequency components have an intricate effect on phase estimation, and that the choice of a reference electrode minimizing its effect in the frequency band of analysis is paramount. The same derivation was achieved on overlapping bursts and showed the limits of the Morlet wavelet transform regarding phase extraction at the level of the scalp. Nonetheless, in practice, it was shown on real data not only that the alpha component in the eyes closed condition is well modeled by a sum of Gaussian bursts, but that some of the parameters (phase shift, amplitude) can be extracted in the time frequency planes of the Morlet wavelet transform.

The statistical testing making use of instantaneous phase information, or derived measures was studied from two perspectives. As a theoretical approach, it was shown that the very construction of the instantaneous phase with the Morlet wavelet transform already correlates close values: for non autocorrelated signals the correlation between close complex coefficients is equal to the autocorrelation function of the Morlet wavelet, and for autocorrelated signals it still can be expressed and calculated practically. The data-driven approach consists in devising an original measure of the correlation between synchrony measures computed on pairs of redundant EEG channels in the framework of the Mann Whitney U test. These statistical considerations and a freshly acquired dataset lead to discuss the original study. Essentially, the original study could not be reproduced on the new dataset, with or without the statistical corrections for correlation. What emerged is that epileptic patients tend to show higher synchrony levels, as measured with the mean phase coherence. While the statistical corrections did not affect the conclusion, it however affected the statistical significance of some pairs of electrodes.

The exploration of phase differences across the scalp, on a second original dataset, to better understand phase synchrony led to observe specific patterns on the scalp. Notably, an anteroposterior phase difference relationship was revealed in the α frequency band during the eyes closed condition. While several bio-physiological models of the literature could account for this finding, a simple model of two phase related sources was enough to explain for these many phase differences on the basis of the spherical geometry of the head. It would have influential consequences on phase synchrony measures, even those claimed insensitive to volume conduction, since they

predict strong functional connectivity between regions that are not necessarily functionally related during the task.

A complete neurofeedback software solution is provided alongside this manuscript. It is at the root of an ongoing collaboration with the university hospital La Timone. Due to the uncertainties regarding phase synchrony measures, the neuromarker of the upcoming protocol is based upon the lagged correlation between channels, that is thought to expose cortical excitability.

While it may seem unsatisfactory that this thesis does not unveil an efficient neuromarker for epilepsy reduction (among the few), solid tools have been designed to ease future endeavors on the matter.

Limitations and prospects

Neurofeedback protocols

Cross-correlation neurofeedback A neurofeedback protocol proposal submitted in the frame of our collaboration with hopital La Timone has received the funding required for its practical application. It aims at training a patient to desynchronize brain areas by reducing their functional connectivity. This functional connectivity is calculated as the smoothed averaged cross-correlation between chosen pairs of scalp EEG electrodes. The primary goal of this neurofeedback protocol is to show that reducing the synchrony between brain areas translates into reducing the frequency of epileptic seizures after neurofeedback.

Alpha "traveling waves' auditory neurofeedback Chapter 7 showed that there were some predominant phase differences between electrodes along the anteroposterior axis in the α band during the eyes closed condition for most of the subjects involved in the study. While phase differences were variable from subject to subject, they were highly stable across recordings. These phase differences can be measured on relatively short windows, making them suitable for neurofeedback protocols. Learning to accelerate or slow down the communication between the brain areas involved in these specific patterns could train general capacities of self-regulation beneficial to the control of seizure propagation. Because these patterns require the subjects to have their eyes shut, an auditory feedback seems appropriate. Incidently, it was implemented in the course of this research: the sound level of the audio track is modulated with regard to the performance of the subject. An interesting and barely approached observation is the phase reversals occurring in short windows. Learning to increase these phase reversals, and correlating the success to the strategies employed, could shed light on the underlying principles guiding the observed phase differences and their reversal.

Statistical methodology

Phase correlation Correlation between temporally close wavelet coefficients was calculated under mean and variance stationarity hypothesis on the EEG signal. The following step consists in obtaining the correlation between close phase values, relying on the fact that the phase can be extracted as the ratio between the imaginary and the real part of the wavelet coefficients. The correlation between phase difference can be obtained and hopefully lead to an estimation of the correlation within and across different phase synchrony measures. While correlation was studied through the prism of temporality, the analytic wavelet coefficients are also correlated frequentially. For statistical analysis of constructs incorporating different frequency steps (such as histograms of phase differences within a given frequency sub-band) frequency correlation should be addressed similarly as to time correlation. Lastly, spatial correlation, one of EEG's major caveat, must be considered: in statistical analyses incorporating several pairs of channels, redundancy is present and should be accounted for. A generalization of the work proposed in chapter 4 to pairs of random processes with different mean and variance should be investigated in the hope of finding an expression of the correlation between wavelet coefficients depending not only on the autocorrelation within the signals but also their cross correlation.

Models for correlation simulation Despite providing consistent and convincing insights into the correlation between related phase synchrony measures, the f values presented in chapter 6 were only estimated on real data. These f values should be matched to controlled correlation within the data. A framework for this is auto-regressive modeling as these models are defined on the basis of autocorrelation coefficients.

Bursts delays

On one hand, chapter 7 illustrated that phase differences are notably noisy. On the other hand, chapter 5 showed that most of the parameters of the α bursts could be retrieved by means of the Morlet wavelet transform when bursts were not too overlapped. Instead of retrieving the phase difference from the signal itself, it could be computed on the basis of the parameters of the bursts. The location and the phase shift can be used to infer relationships between bursts at the different electrodes, and therefore grant an original synchrony marker.

Sources synchrony

Another approach consists in estimating the activity of cortical sources, limiting the conduction effects affecting the scalp EEG synchrony measures. Nonetheless, to estimate such activity, the volume conduction must still be addressed. These activities can be approximately recovered by solving a blind sources separation problem such as an independent component analysis, by calculating the source current density, or by attempting to solve the inverse problem of projecting the sensors activity onto cortical sources. The main caveat of such methods is that they require a sensor density much higher than that usually available for home usage.

Appendices

A.1 Zither, a new open-source neurofeedback software product / platform

Neurofeedback involves at its core the computation of a neuromarker of the ongoing brain activity that serves as feedback.

Existing open-source software such as OpenVibe [236], provide an efficient, versatile, although aging, computationally expensive and hardly improvable mean to design such protocols.

Zither is a new neuro-recording experimental and neuro-feedback platform. It embeds the most common and simple tools required for processing EEG signal. Most parameters of the processing pipeline can be modified on the fly, which can considerably ease the prototyping phase of experiments. Not only does it work online, offline analysis of EEG signal is also a possibility, using the Python prototyping language.

Although at heart to be of use to many in the field, this software platform was developed mainly to accommodate the needs of this PhD research. For this reason, some features are not implemented in the most abstract way, and could in their current state, not be usable by all.

Pipeline

The four building objects of the platform are the **Configuration**, the **Chunk**, the **Event** and the **Node**. The pipelines are designed as linear chains of operations on chunks of data. A chain is composed solely of connected **Node** objects, between which pass **Configuration** and **Chunk** objects, or **Event** objects. A complete example is provided in figure 8.17.

Together, the **Chunk** and the **Configuration** are the two objects representing the EEG data. A **Chunk** holds a matrix storing a contiguous piece of data, and a vector associating the timestamp of each sample. The **Configuration** holds common information such as the sampling rate, the names of the channels, their units and additional data such as the physical and numerical limits of the signal. Basically, the **Configuration** is the information of the stream that does not change with each **Chunk**. If a property of the signal changes (a dynamic change of the sampling rate for instance), a new **Configuration** can be passed, and the **Node** must adapt to the modified **Configuration**. The rule is that before the first **Chunk** is passed to a given **Node**, the **Configuration** must be passed.

The **Node** is an abstraction for an operation on the data. The **Node** is fed with a **Configuration**, then computes a **Configuration** (associated to the new **Chunk**s the **Node** will generate) and sends it to the next **Node**, then, it is fed **Chunk** after **Chunk**. The **Node** will send a new **Chunk** to the next **Node** when appropriate.

The **Event** is a time-stamped information running through the pipeline, which can be a trigger for displaying some text on the screen, turning on the music, switching the state of a Node...

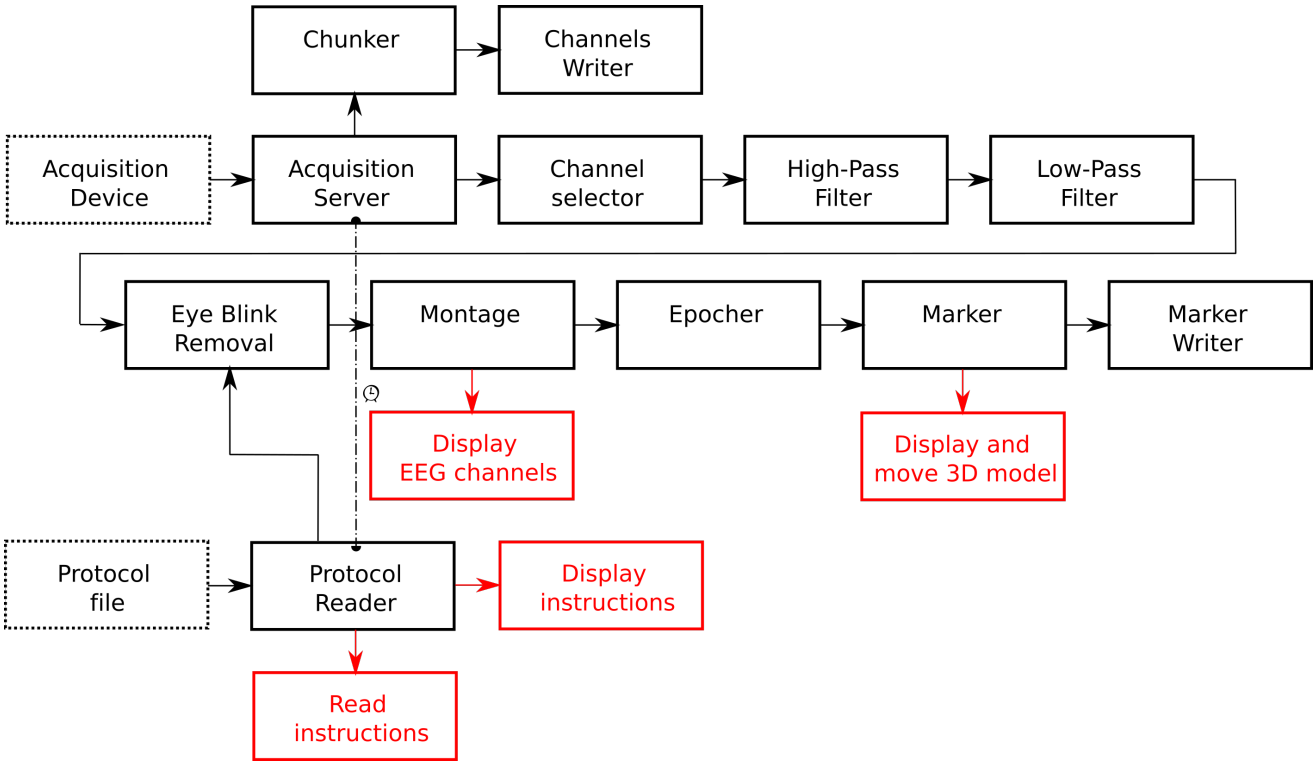

Figure 8.17: Example of a pipeline set for a neurofeedback protocol. Each black box is the implementation of a **Node**. **Configuration** and **Chunk** pass from box to box (**Node** to **Node**). The *Acquisition Server* and the *Event Reader* are synchronized to start at the same time. The EEG data is acquired from an EEG acquisition device, and the events are read from a file (see subsection 7.7.7). The EEG channels are displayed on the experimenter screen, the 3D model is animated on the participant screen, so are displayed and read the instructions. The raw signal is saved in a file, as well as the marker with which the participant is trained.

Example

This example illustrates the backbone of a pipeline designed for a neurofeedback experiment. It presents the role of each component to the workings of the machinery. It is based on figure 8.17.

Configuration The first **Node** of the pipeline is the *Acquisition Server*, whose purpose is to feed **Chunk**s to the pipeline. Based on the *Acquisition Server* properties (sampling rate=512, number of channels=32...), a **Configuration** object is created. This **Configuration** object is passed to the *Channel Selector*, that compares the selection with which it is parametrized with the channels of the **Configuration**, creates a new **Configuration** object, with the restricted channels list, and pass it further down the pipeline. The same step is reproduced by all **Node**s, each with its own specificities, until it reaches either a *Writer*, or a Display **Node**, that will simply read the **Configuration**. Figure 8.18 illustrates the processing of the configuration through three abstract **Node**s.

Chunks The *Acquisition Server* can either record data on the fly, or read prerecorded data (of use in Sham experiments). The data is saved raw through a *Chunker* that ensures the duration of each block is constant when saved, in order to match the *Writer* requirements (EDF file format). The **Chunk**s generated by the *Acquisition Server* are filtered in the *Channel Selector* to match a selection provided as parameter (as an external file). Then they pass through a *High Pass Filter* and a *Low Pass Filter*, whose parameters can be changed on the fly (without stopping the experiment). The filtered signal goes through the *Eye Blink Removal*, that initially learns to detect blinks (when it receives a specific **Event**, paragraph 7.7.7). Once blinking is learned and a spatial filter calculated, the mode is switched to filtering (thanks to a second **Event**). The EEG channels are combined in

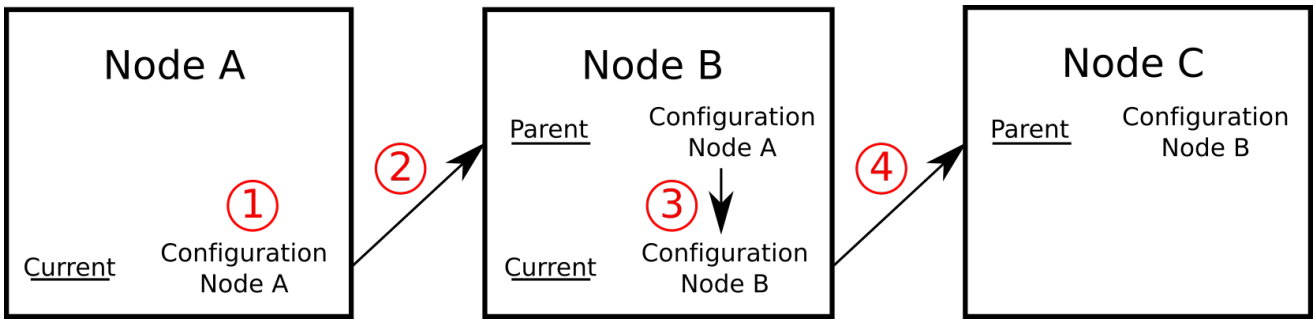

Figure 8.18: A **Node** keeps track of its current **Configuration** as well as its parent's **Configuration**. 1, in **Node** A, the initial **Configuration** is created. 2, the configuration of **Node** A is sent to **Node** B, which stores the **Configuration** of **Node** A. 3, **Node** B creates a new **Configuration** adapted to the **Chunk**s it is about to send. 4, the **Configuration** of **Node** B is sent to **Node** C.

the *Montage* into a bipolar montage (various bipolar montages can be tested and switched on the fly by simply selecting another montage file). The data is then epoched by the *Epocher* to overlapping windows (of 1 second, overlapping by 0.95 second). One epoch of 1 second is sent every 0.05 seconds the *Marker*. The *Marker* role is to compute a neuromarker from the epoched data. The neuromarker is then saved in the *Marker Writer* for later analysis.

Events The *Protocol Reader* start-up is synchronized with the *Acquisition server*'s. It reads the participants instructions from a *Protocol file*, and displays instructions on the screen. At the same time, it plays the recorded instructions on speakers. The *Protocol Reader* also controls the *Eye Blink Removal*, by switching its mode from learning (the correction to apply) to filtering. Ultimately, the *Protocol Reader* sends the termination signal, to stop the pipeline when the experiment ends.

Designing experimental protocols

The platform allows to design experimental protocols. Such a protocol where the subject is asked to open / close his eyes when requested (see code 7.7.7) is designed in a text file and can be loaded in the app:

```
5000 baseline {"control":"start", "text":"Keep␣your␣eyes␣open.", "description":"Request␣the␣
    ↪ subject␣to␣keep␣his␣eyes␣open."}
25000 baseline {"control":"stop", "text":"End␣of␣task.␣Relax.", "description":"Request␣to␣
    ↪ relax."}
30000 alpha {"control":"start", "text":"Close␣your␣eyes␣and␣relax.", "description":"Request␣
    ↪ to␣close␣his␣eyes␣and␣relax."}
50000 alpha {"control":"stop", "sound" : "bells", "text":"Open␣your␣eyes␣and␣stop␣relaxing.",
    ↪  "description":"Request␣the␣subject␣to␣open␣his␣eyes␣and␣stop␣relaxing."}
55000 baseline {"control":"start", "text":"Keep␣your␣eyes␣open.", "description":"Request␣the␣
    ↪ subject␣to␣keep␣his␣eyes␣open."}
75000 baseline {"control":"stop", "text":"End␣of␣task.␣Relax.", "description":"Request␣to␣
    ↪ relax."}
80000 alpha {"control":"start", "text":"Close␣your␣eyes␣and␣relax.", "description":"Request␣
    ↪ to␣close␣his␣eyes␣and␣relax."}
100000 alpha {"control":"stop", "sound" : "bells", "text":"Open␣your␣eyes␣and␣stop␣relaxing."
    ↪ , "description":"Request␣the␣subject␣to␣open␣his␣eyes␣and␣stop␣relaxing."}
105000 baseline {"control":"start", "text":"Keep␣your␣eyes␣open.", "description":"Request␣the
    ↪ ␣subject␣to␣keep␣his␣eyes␣open."}
...
```

Because the recording and the protocol files are launched and read simultaneously, the timestamps of the protocol file match the recording. For this reason, inserting triggers in the EDF file is optional (and not provided as of the last release).

The format of this file follows the rule that each line is an event. Each line comprises three elements: the timestamp in milliseconds, the label (which does not have to be unique, and may be used to match "stop" to "start" control), and a dictionary (in the JSON format).

Texts *text* keyword followed by the text to display. Text can be displayed to the participants, and the size is optimized to fill the available space.

Sounds *sound* keyword followed by one of the available sounds ("bells", "bip-06". "bip-07"). Sounds can be played once to the participants (for instance to inform he/she must open his/her eyes).

Sound tracks *track* keyword followed by the location of the track on the disk. Instructions can be read if provided as audio files, music tracks can also be played (mp3 format).

Random calculation *calculus* keyword followed by an empty string. Random calculations verifying pre-implemented rules (the sum of two products of two digits numbers) can be submitted to the participant.

Description May be used to display errors regarding the processing of the events, or simply to track in the file what a given line does.

Specific Events Events can also be used to trigger specific behaviors (turning on/off certain **Node**s, activating certain modes, stopping the experiment...). For instance the *Eye blink Removal* reacts to the keyword *exp_status* followed by either "training_eye_removal" or "evaluation_eye_removal".

Feedback

Visual The software provides a simplistic 3D environment of a hot air balloon going up and down with a neuromarker. Neuromarkers can be directly controlled by looking at the curve, since any **Chunk** passing between **Node**s can be plotted.

Audio The software also provides a **Node** to control the sound volume of the application. A music track can be chosen, it starts to play as the experiment is launched. As the neuromarker goes up and down, so does the volume of the music.

Python wrapping

Prototyping is arguably easier and faster on higher level language such as Python (or Javascript, Java, C#...). Since offline analyses are mostly prototyping, it seems reasonable that they are solved in Python. For the sake of reproducibility between online C++ routines and offline Python operations, (and for efficiency motives) the C++ routines have to be available and used in Python. The SWIG wrapping tool has been extensively used, and wrapper routines specifically developed for this purpose. C++ objects can be created from Python :

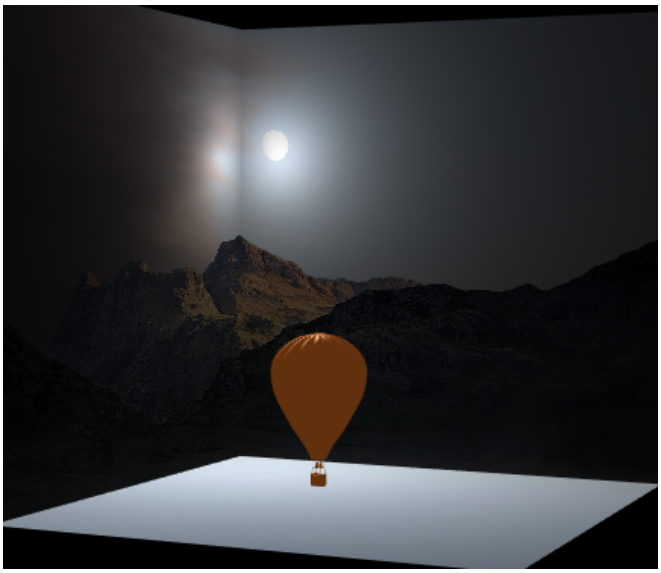

Figure 8.19: A neuromarker controls the altitude of the hot air balloon. The model (balloon) can be replaced with any other model stored on the computer. The images displayed on the panels can also be changed at will.

Listing 8.1: This snippet provides a complete set of instructions to read a modified EDF file (with less constraints than the original library 7.7.7) in Python. data is a numpy array, channels is a Python array, sampling_rate is a float

```
import numpy as np
import ztrcore

ztrcore.setVerboseLoading(True)
ztrcore.setAutoLoading(True)
ztrcore.initialize() # For plugin handling

reader_edf_file = ztrcore.processReader_pluginFactory().create("
    ↪ ztrProcessReaderEdfFile")
reader_edf_file.setFilePath(str(f))
reader_edf_file.run()
data = reader_edf_file.output()
channels = reader_edf_file.channels() # Channels x Time (real values)
sampling_rate = reader_edf_file.samplingRate()
```

Technical points

Latency According to Belinskaia et al. [19], the faster the feedback the longer lasting the neurofeedbacks effect. They show, with feedback of P4 electrode alpha envelope power, that the magnitude of sustained changes is negatively correlated with feedback latency. To minimize the latency the computation must occur as the signal is recovered, and as quickly as possible. Obtaining the necessary flexibility and performance, requires the usage of low level programming language. Low programming languages, and complete leverage on the manipulation of the memory ensures that it can be optimized to minimize the latency.

The reality directing the choices regarding delay is that the visual feedback cannot be provided faster than the refreshing speed of the computer screen. The data is pulled from the acquisition device every 1000 ms / 24. Then the pipeline must process the data and display the neuromarker before the next data chunk is pulled (duration

of the pipeline must be lower than 1000 ms / 24). The threshold is large enough for the computations at hand here, even when marker are computed 50 times a second.

Event-loop and jitter Built upon Qt, it relies on its event loop. In an object oriented language, an event loop is a design pattern that dispatch messages from all sender objects to all receiver objects. While it does not guarantee the absence of jitter, it offers flexibility, and clarity of code. It is used by thousands of applications.

Shared pointers **Chunk** and **Configuration** are encapsulated in a shared pointer : whenever the **Chunk** or **Configuration** is not used, it is deleted.

Dependencies

Although fully developed in C++, it relies on C / C++ / fortran librairies. To permit L-GPL licensing, all the proprietary / GPL optional dependencies are built as plugins, a process facilitated by the Qt plugin layer.

Qt Qt is the library upon which the software is based. It provides the Event-Loop 7.7.7, the connections between objects, the windowing, the drawing of the widgets. It allows the 2D plotting of the electroencephalogram, 2D plotting of electrodes during the impedance setup, it plays the various sounds and sound tracks.

dtk-... dtk is a modular toolkit for the efficient design of scientific applications. dtk-core is used extensively for creating the parameters of the **Node**s. dtk-widgets is used to handle the menu-bar aggregating all the parameters of the various **Node**s, as well as the splitting between views. dtk-fonts is used to have access to font-awesome fonts within a Qt application. dtk-themes is used for an easy switch between color themes / styles of the application.

xtensor xtensor is a fast, robust, and still maintained matrices manipulation library. It attempts to reach the simplicity of usage of numpy (in Python), while in the C++ language. Notably, it offers wrappers for linear algebra operations, which are required for some spatial filters. xtensor-fftw is especially used to compute Fourier transform related calculations.

edflib One of the most common extension for EEG data is EDF (European Data Format), such as in Obeid and Picone [201], or exports from Nice CHU. The exported files from Nice CHU did not match strictly the specifications, and could not be read as such by the library. The library was modified so that these files could be processed: the checks triggering abort of the program were turned off.

DSP Filters The DSP Filters library provides solid digital filtering tools [73], of the many objects that are offered by the library, only a handful are used. This handful comprises the SmoothedFilterDesign orchestrating either one of Bessel, Butterworth or Legendre filters, as either band-pass, band-stop, low-pass or high-pass filter.

VTK Visualisation ToolKit is a C++ library that provides a 3D scientific visualization engine.

Conda recipes and packaging

The dependencies can be installed with a simple one-liner on linux and MacOS.

```
conda create -n zither -f path/to/recipe.yml
```

The software can then be installed with CMake.

Pseudonymisation

Statistical analyses can be biased if the statistician has a view on the origin of the data (for instance from which subject it was acquired). Moreover, discussing subject specific results without compromising the identity of the subject requires some kind of anonymization. Lastly, it is part of General Data Protection Regulation (GDPR) which defines pseudonymization at the EU level in Article 4(5). Pseudonymisation is a middle groung accomodation that removes any identification of the subject in EEG records, while keeping track, in a dedicated table of the pairing between subject information and EEG records. The access to the table of pairing is restricted. In the frame of this thesis work, only the neurologist had access to the table.

A Python script was developed to pseudonymize the EEG records acquired in the EDF (European Data Format). It removes subject identification and replace it by a unique identifier. This unique identifier is filled in the table alongside the name of the subject.

A.2 Mental workload classification

The present work is a joint effort conducted with Sara Sedlar (Inria) and Johann Benerradi (University of Nottingham). It was presented at the Neuroergonomics conference 2021, to compete in the "Grand Challenge: Passive BCI Hackathon". This challenge aimed at facing the large within-subject variability affecting brain signals leading to often poorly performing passive brain computer interfaces. Several pre-processing strategies (including computing the Morlet wavelet coefficients) and neural networks (classical CNNs) have been implemented. The methodology stemming for the research work of Sara Sedlar stood out and was deemed to be presented in this chapter.

Abstract

Assessing mental workload could prove invaluable in many safety-critical situations, notably situations where fatigue impairs cognitive and behavioral functions. Passive Brain Computer Interfaces (PBCI) can be a solution of choice for the purpose of assessing the mental workload of users performing various tasks with different levels of mental demand. One main problem is the variability across sessions of the EEG of different mental workloads. The "Grand Challenge: Passive BCI Hackathon" organized for the Neuroergonomics 2021 conference enabled to challenge researchers with a real-life scenario of a mental workload PBCI: classifying mental workload of an unlabeled session after training on only 2 labeled sessions. The proposed strategy is based on a convolutional neural network with rank-1 constraint fed with EEG signals projected on a basis of spherical harmonics. It performed modestly: 48.20% on an unlabeled session, with a chance level at 33%. Despite this modest performance, it ranked second out of eleven participants. This clearly unveiled the difficulty of classifying correctly mental workload with EEG on unseen sessions.

Introduction

Assessing the mental workload of individuals in risky situations is critical: it could for instance be used to reduce plane crashes relating to the inattention of pilots. It could also be employed to design interfaces that are not overwhelming to users, and therefore ease the usage of the interface.

A number of approaches have been put forward to classify mental workload, and involve one or several recording modalities. The most influential [193] psychophysiological features in classifying mental workload level are brain electrical activity or blood oxygenation, heart rate [110], breath rate, eye blink measures and pupillometry [11]. Some studies involve several features at the same time such as this of Liu et al. [161] (EEG, fNIRS, physiological).

The classification algorithms making use of these signals are as diverse as the pre-processing the signals undergo. Pre-processing may involve time-frequency decomposition of the signals, or independent source decomposition [228] among other approaches.

Classification procedures are of at least three families: RandomForest, Riemannian geometry or deep-learning. Deep-learning approaches have become mainstream in challenging these problems: adaptive stacked denoising

autoencoder [339], CNN [254] are such approaches that have hailed promising results.

In the current approach, the pre-processing of the EEG signal involves the projection of the raw signal onto a spherical harmonics basis. These coefficients feed a CNN deep-learning framework model (with reduced number of parameters). While the time-frequency decomposition is not performed in the pre-processing, it is partially achieved in the first layer (rank-1 constrained) of the CNN.

Data

The dataset provided for this challenge [113] was composed of the EEG recordings of 15 participants (6 female; average 25 y.o.). These participants were asked to perform the Multi-Attribute Task Battery-II (MATB-II developed by NASA) in 3 one-week-apart sessions. Each session is composed of 3 5-minutes blocks of different difficulties: easy, medium and difficult, and accompanied by a 1-minute resting state baseline with eyes open. The order of presentation of the different difficulty block was randomized, meaning that participants did not necessarily start with the easy task first. The easy blocks (label 0) involved a TRACK (manual control of a target within a window) and a SYSTEM MONITORING (monitoring 4 gauges and 2 warning lights) tasks. The medium blocks (label 1) involved an additional and third task: RESOURCE MANAGEMENT in which a set of pumps had to be activated / deactivated to control for the allocation of fuel to several reservoirs. The difficult blocks (label 2) incorporated a fourth task: COMMUNICATION in which exchanges had to be made through radio messages by changing the frequencies of different radios.

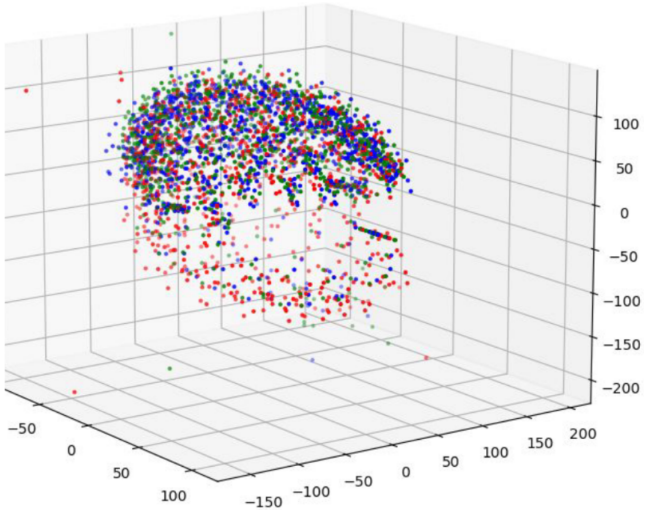

Figure 8.20: Electrodes of all subjects on the same 3D plot. Electrode orientations are not consistent, and some are either misplaced on the scalp or mislocated.

The original signals were acquired on a 64 EEG electrodes headcap placed along the 10-20 system and sampled at 500Hz. The exact location of the electrodes was obtained by means of a 3D camera. The data made available by the organizers of the contest was already pre-processed. It involved a selection of 62 electrodes (whose positions for all participants are drawn are figure 8.20) referenced to the right mastoid. These channels were down-sampled to 250Hz. The signals were high-pass filtered above 1Hz (FIR), and low-pass filtered below 40Hz (FIR). An independent component analysis was used to identify the artifacts and reject them. The data was ultimately split into epochs of 2 seconds for a total 447 epochs for each session and each participant.

While three sessions were recorded, the difficulty labels were provided only for the 2 first sessions. The third and remaining session is used by the organizers to evaluate the classification performances of all the submitted classifiers.

Method

In order to perform the classification of 3-level mental workload tasks, this approach proposed a deep-learning model based on a convolutional neural network (CNN) with rank-1 constraint [59, 138] fed with spherical representations of EEG spatio-temporal patterns.

A spatio-temporal EEG pattern can also be represented as a linear combination of spherical harmonics $\hat{S}$, which has the advantage of being invariant to rotations.

$$\hat{S} = \hat{Y}^{-1}X \tag{8.2}$$

where:

X is the matrix of raw EEG signals
$\hat{Y}^{-1}$ is the inverted spherical harmonics basis
$\hat{S}$ is the matrix of EEG signals in the spherical harmonic basis

The projection matrix $\hat{Y}^{-1}$ (equation 8.2) is obtained by the pseudo inversion of real basis of spherical harmonic with least mean square optimization regularized with Laplace-Beltrami regularization term ($\lambda = 0.001$) [56]:

$$\hat{Y}^{-1} = (Y^T Y + \lambda R_{LB})^{-1} Y^T \tag{8.3}$$

where:

Y is the spherical harmonic basis computed for each subject with the electrodes locations expressed as angles

The complex form of the elements of Y are obtained as:

$$y_n^m(\theta, \phi) = \sqrt{\frac{2+1}{4\pi}\frac{(n-m)!}{(n+m)!}} e^{im\theta} P_n^m(cos(\phi)) \tag{8.4}$$

where:

m is the order of the harmonic
n is the degree of the harmonic
P_n^m is the associated Legendre polynomial
θ is the azimuthal coordinate
ϕ is the polar coordinate

Their real form is then extracted with:

$$y_n^m = \begin{cases} \sqrt{2}\,(-1)^m\,\Im\left(y_n^{|m|}\right) & \text{if } m < 0 \\ y_n^0 & \text{if } m = 0 \\ \sqrt{2}\,(-1)^m\,\Re\left(y_n^m\right) & \text{if } m > 0. \end{cases} \tag{8.5}$$

The angles ϕ and θ are obtained after the electrodes were fit onto a sphere whose center and radius were optimized for each subject separately.

The projection of spatio-temporal EEG patterns on a spherical harmonics basis has several advantages. It mitigates the subject to subject and session to sessions variability in sensors position, which is strong in the dataset at hand (see figure 8.20) and allows to reduce the dimensionality of the problem by reducing the number of spatial

components. To evaluate the order to use, learning and validation have been conducted several times, with a maximal degree of spherical harmonics varying from 2 to 4. The learning curve was optimal for a degree of 3 corresponding to 16 basis elements. This had the effect of reducing the spatial dimension from 62 to 16. One drawback is that it approximates the head to a sphere, and therefore introduces some distortions. The signals expressed in the SH basis ($\hat{S}$) are down-sampled at 42 samples per second ($\hat{S}_{ds}$) to only consider oscillatory components below 20Hz.

The classifier, illustrated in figure 8.21, takes $\hat{S}_{ds}$ as input. It is solely composed of 3 convolutional layers and 3 dense layers. The first convolutional layer has 5 kernels, each verifying a rank-1 constraint. These kernels are outer-products of spatial ($\hat{w}_s$) and temporal weights ($\hat{w}_t$), and represent spatio-temporal atoms. This is especially convenient for capturing short lived neural events (described at length in chapter 3 and chapter 5). The second and third convolutional layers are standard and shorter convolutional filters, 3 kernels of size 5×3 and 3 kernels of size 3×3 respectively. These convolutional layers are followed by ReLU activation functions. The 3 dense layers are of respectively 15, 4 and 3 nodes. These dense layers are respectively followed by ReLU, ReLU and Softmax activation functions. It gives rise to a total of of 342 parameters.

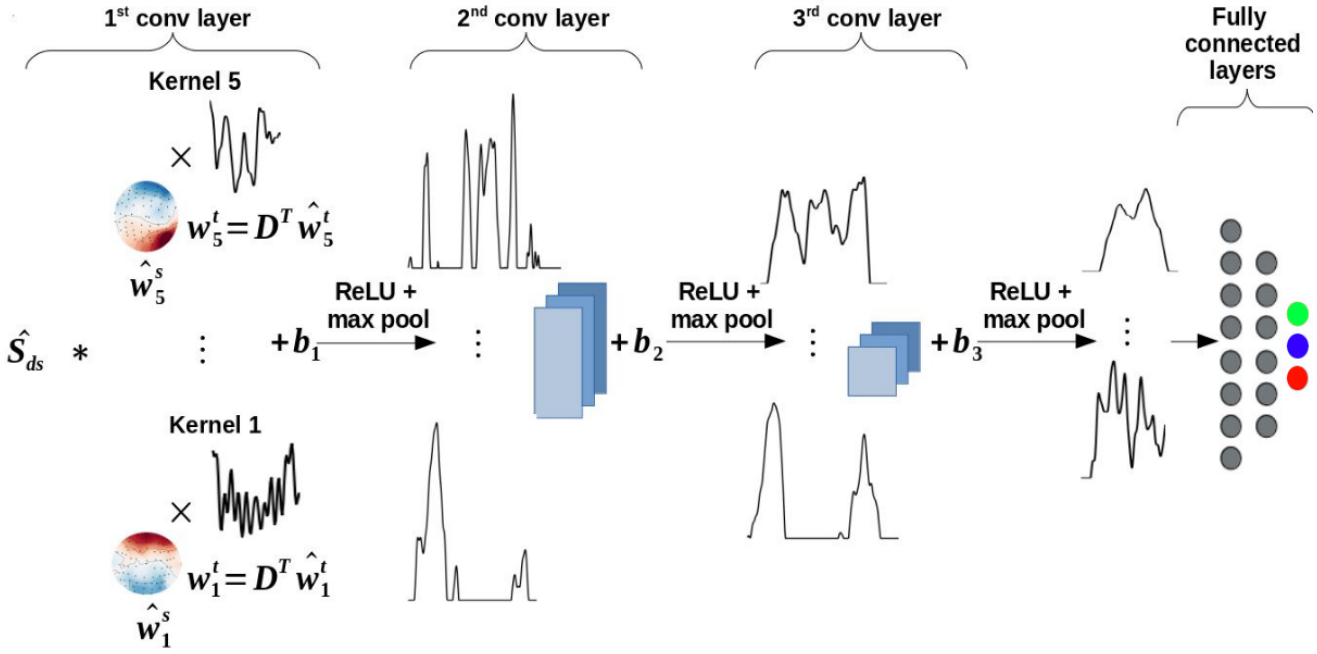

Figure 8.21: Rank 1 convolutional neural network architecture for mental workload classification of EEG signals. The last layer (green, blue and red disks) gives the probabilities of belonging to either one of the three (easy, medium, difficult) classes.

The model is trained over 100 epochs with batch size 64 and an initial learning rate of 0.0005. For two following triplets of epochs with validation classification accuracy difference greater than 10^{-4}, the learning rate is slowed by a factor 0.9. The loss function is categorical cross entropy and the models are trained with the Adam optimizer.

Results

The model is trained on 9 subjects, 3 are used for validation and the remaining 3 for testing. 3 repetitions of this procedure with random assignation of subjects are realized to obtain confidence intervals. The validation set accuracy after training on the first session is of about 46.6% (figure 8.22, II). The performance is consistently higher than the chance level of 33.33% (or an upper-bound of about 38% after considering the number of trials per class) as seen in figure 8.22, II with the confidence interval showing that the training is relatively robust over repeated training.

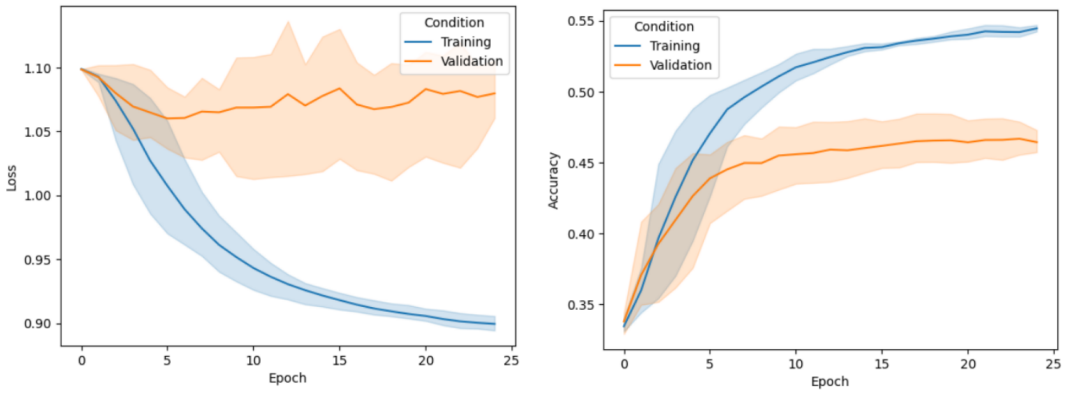

I II

Figure 8.22: Training graphs of the CNN rank-1 model (loss on the left, accuracy on the right), using one labeled session for the train set and the other labeled session for the validation set (assigned randomly for each participant). The bands represent the 95% confidence intervals on 3 repetitions of the procedure with random training/validation splits.

The model was re-trained on all the subjects of the 1st and 2nd labeled sessions in order to produce the final network sent to the competition. The results obtained by the BCI challenge organizers on the 3rd unlabeled session (48.20%) match the order of magnitude of the validation tests (46.6%). The slightly improved results may be due to the increase in the size of the training data.

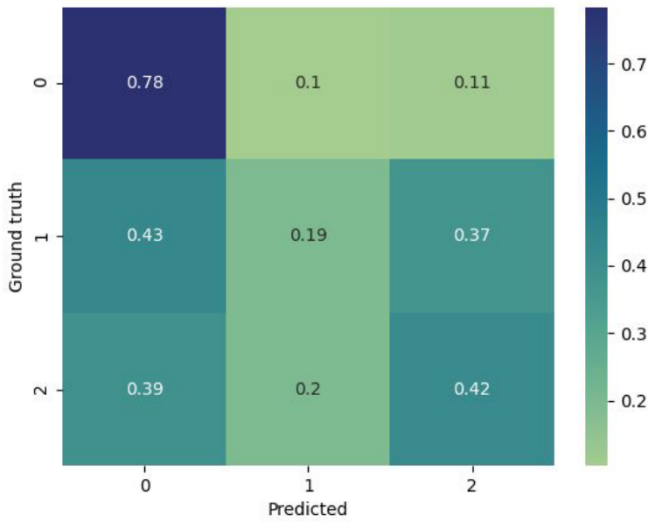

Figure 8.23: Overall confusion matrix of the CNN rank-1 model on 3 repetitions of the procedure with random training/validation splits.

As displayed in figure 8.23, the model is biased towards the easy task in the sense that is predicts the label 0 way more often than it occurs. An interesting result is that the label 0 is rarely confused for another label. A surprising effect is that the label 1 is either predicted as label 0 or label 2, which suggests that the features (if any) in the EEG signal of the label 1 were not captured by the classifier.

Discussion

By comparison to the other deep-learning strategies employed in the competition [250], the network was shallow. The design helped to capture EEG signal by learning atoms matching the events manifested during the different tasks. It was better tailored to the amount of available data and low signal to noise ratio which avoided over-fitting, a point raised by Roy et al. [250].

Several leads should be considered in improving the network. The 3rd session baseline was not used to further constrain the final network, and transfer learning approaches could benefit from this additional information. The model was trained on all subjects at once (with randomized epochs) because of the restricted amount of epochs, nonetheless, was more data available, personalized training or personalized fine-tuning should be considered.

Conclusion

This rank-1 constraint CNN model, despite a moderate performance at classifying unlabeled 3-class mental workload tasks, reached the 2nd place out of 11 at the "Grand Challenge: Passive BCI Hackathon" that took place during the online 2021 Neuroergonomics conference.

It was outperformed by a Riemannian geometry classifier [212] but outperformed another [52] and several deep learning algorithms. This shows that deep-learning do not always outperform more "classical" approaches, but that the careful design of the network is at the heart of its performance. This inter-session exercise is difficult because it involves a longitudinal (there is variability from session to session) component that is hard to learn on such a restricted number of sessions.

While the literature usually brings out attractive classification results, it appears that in competitions where evaluation data is unknown and hard tweaking to this data impossible, the results are more modest.

A.3 Cortical Synchrony Neurofeedback

This additional content describes an ongoing collaboration with hospital La Timone in Marseille on a neurofeedback (NFB) protocol design for epileptic patients.

Introduction

The PhD thesis at Inria gave the opportunity to build up a platform for EEG signal processing and feedback delivery. The potential of EEG channels cross-correlation control learning will be evaluated. The effects of attempting to down-regulate general levels of cross-correlation will be studied. These general levels of cross-correlation of the EEG channels are thought to possibly reveal excited states favoring seizures.

Methods

Various neuromarkers have been implemented over the course of this doctoral research. Given the moderate confidence in using MPC / PLI / Coherence or Imaginary Coherence developed in the study of phase synchrony in epileptic patients (see chapter 7 and chapter 6), an alternative measure was selected: the smoothed average lagged cross correlation between selected pairs of scalp EEG electrodes.

To avoid considering correlations due to volume conduction, the 0 and π lag correlations should be discarded.

EEG-NFB procedures

The procedure involves the neurofeedback platform Zither (stemming from the collaboration between Nice CHU, Marseille CHU and Inria Sophia) for impedance checks, recording, processing and feedback delivery. It is illustrated in figure 8.24, and described hereafter.

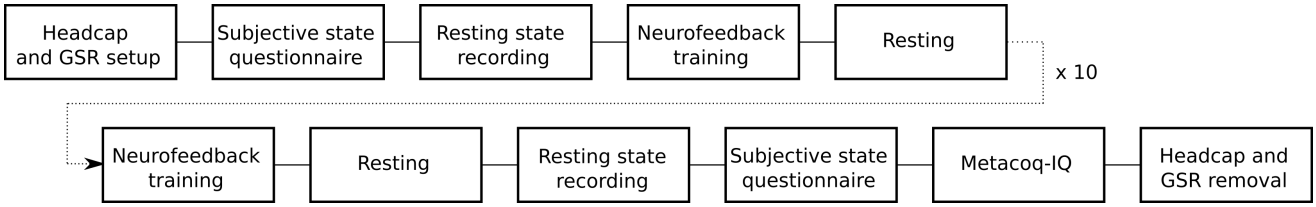

Figure 8.24: Procedure summary of the neurofeedback experiment.

At the beginning of each session, the subject will be invited to sit in front of a computer screen. A head-cap of 32 gel electrodes (10-20 system) will be set up on his/her scalp. Electrode-impedance will be lowered below 10kOhm, and stored for further inspection. Two additional electrodes will be placed on the 2nd phalange of the

middle and index fingers to record the galvanic skin response (GSR). The raw EEG and GSR signal will be stored for further inspection.

At this time, the subject will be invited to ask any question and will proceed to the completion of a questionnaire about his/her subjective state. This questionnaire has been developed with the Association française de psychiatrie biologique et Neuropsychopharmacologie (AFPBN), in order to evaluate cognitive states during NFB training sessions [référence appropriée].

Then, the investigator will explain to the patient that EEG will be recorded in a resting state condition for 30 seconds before the NFB procedure starts. For this recording, the subject will be asked to stay in a relaxed and wakeful state, without any particular task to perform and with his/her eyes closed, which provides better data quality and presents less muscular artifacts than with open eyes.

After recording resting-state EEG, the tasks of the EEG-NFB procedure will start. The task will be performed by the subject in an environment with as few distractions as possible and in the presence of the investigator who will remain purely passive and neutral. The subject will be informed to look at a computer screen displaying a hot air balloon which can be commanded to either go up or down, in a simplified 3D environment. If the level of EEG inter-channel synchrony goes down, the balloon goes up, if the level goes up, the balloon goes down (uplifting the balloon is rewarding). The subject will never receive negative feedback in order to avoid loss of motivation. Overall, the NFB procedure will consist of 10 blocks of training lasting 75 seconds separated by resting intervals of 15 seconds to avoid fatigue and decreased attention (lasting a total of 15 minutes). The test procedure will aim at decreasing the mean EEG inter-channel instantaneous correlation in the 1-40 Hz band. The GSR is recorded to be used for further analyses such as tests of correlation between cortical desynchronization and high sudation, and comparison with previous studies of GSR biofeedback in the context of epilepsy.

BCI skills are unevenly shared among subjects. Instructions provided outside of the tasks can help some subjects getting started. The first instruction given to the subject will be to carefully perform mental calculation tasks. The second instruction will be to carefully perform motor imagination tasks. The subject will have the opportunity to adapt their strategy based on feedback reward to improve their NFB performance. At the end of each session, 30 seconds of resting-state EEG will be recorded in the same conditions as before the NFB procedure.

Finally, the subject will complete the post-intervention version of the NExT-Q questionnaire about their subjective state at the end of the session. He / She will be asked by the investigator about his/her experience during the session, and the strategy (or strategies) he/she used to "succeed at the game" (Metacog-IQ). This semi-structured standardized questionnaire is based on a metacognitive interview during which the investigator accompanies the subject to identify and understand the strategies used during EEG-NFB learning, to foster introspection, and to facilitate the process of empowerment. The Metacog-IQ should allow a better transfer of NFB learning in everyday life. Overall each EEG-NFB session will last about 20 minutes, explanations and discussion with the subject: 15 minutes, setting up the headcap and fingers electrodes: 20 minutes, removing and washing the headcap 10 minutes.

To enable a double blind experiment, the software will randomly feed the EEG of the subject, or of a different subject recorded only for this purpose of substitution (placebo). The algorithm ensures that half the sessions / subjects are placebo.

The 16 patients definitely enrolled in each group will undergo 12 EEG-NFB sessions over 4 weeks.

Bibliography

[1] Eugenio Abela, Adam D Pawley, Chayanin Tangwiriyasakul, Siti N Yaakub, Fahmida A Chowdhury, Robert DC Elwes, Franz Brunnhuber, and Mark P Richardson. Slower alpha rhythm associates with poorer seizure control in epilepsy. *Annals of clinical and translational neurology*, 6(2):333–343, 2019.

[2] M Abeles, Y Prut, H Bergman, and E Vaadia. Synchronization in neuronal transmission and its importance for information processing. In *Progress in brain research*, volume 102, pages 395–404. Elsevier, 1994.

[3] Paul S Addison. Introduction to redundancy rules: the continuous wavelet transform comes of age, 2018.

[4] Edgar D Adrian. Olfactory reactions in the brain of the hedgehog. *The Journal of physiology*, 100(4):459, 1942.

[5] Edgar D Adrian and Bryan HC Matthews. The interpretation of potential waves in the cortex. *The Journal of physiology*, 81(4):440–471, 1934.

[6] Ehud Ahissar and David Kleinfeld. Closed-loop neuronal computations: focus on vibrissa somatosensation in rat. *Cerebral Cortex*, 13(1):53–62, 2003.

[7] Seppo P Ahlfors, Jooman Han, John W Belliveau, and Matti S Hämäläinen. Sensitivity of meg and eeg to source orientation. *Brain topography*, 23(3):227–232, 2010.

[8] Omar J Ahmed. Mechanisms of subiculum hyperexcitability in temporal lobe epilepsy. *Epilepsy Currents*, 21(6):441–443, 2021.

[9] Omar J Ahmed and Sydney S Cash. Finding synchrony in the desynchronized eeg: the history and interpretation of gamma rhythms. *Frontiers in integrative neuroscience*, 7:58, 2013.

[10] Andrea Alamia and Rufin VanRullen. Alpha oscillations and traveling waves: Signatures of predictive coding? *PLoS Biology*, 17(10):e3000487, 2019.

[11] Tobias Appel, Christian Scharinger, Peter Gerjets, and Enkelejda Kasneci. Cross-subject workload classification using pupil-related measures. In *Proceedings of the 2018 ACM Symposium on Eye Tracking Research & Applications*, pages 1–8, 2018.

[12] Sergul Aydore, Dimitrios Pantazis, and Richard M Leahy. A note on the phase locking value and its properties. *Neuroimage*, 74:231–244, 2013.

[13] Yasaman Bagherzadeh, Daniel Baldauf, Dimitrios Pantazis, and Robert Desimone. Alpha synchrony and the neurofeedback control of spatial attention. *Neuron*, 105(3):577–587, 2020.

[14] Ali Bahramisharif, Marcel AJ van Gerven, Erik J Aarnoutse, Manuel R Mercier, Theodore H Schwartz, John J Foxe, Nick F Ramsey, and Ole Jensen. Propagating neocortical gamma bursts are coordinated by traveling alpha waves. *Journal of Neuroscience*, 33(48):18849–18854, 2013.

[15] Weili Bao and Jian-young Wu. Propagating wave and irregular dynamics: spatiotemporal patterns of cholinergic theta oscillations in neocortex in vitro. *Journal of neurophysiology*, 90(1):333–341, 2003.

[16] Bryan S Barker, Aradhya Nigam, Matteo Ottolini, Ronald P Gaykema, Nicholas J Hargus, and Manoj K Patel. Pro-excitatory alterations in sodium channel activity facilitate subiculum neuron hyperexcitability in temporal lobe epilepsy. *Neurobiology of disease*, 108:183–194, 2017.

[17] EA Bartnik, Katarzyna J Blinowska, and Piotr J Durka. Single evoked potential reconstruction by means of wavelet transform. *Biological Cybernetics*, 67(2):175–181, 1992.

[18] Elham Barzegaran, Vladimir Y Vildavski, and Maria G Knyazeva. Fine structure of posterior alpha rhythm in human eeg: Frequency components, their cortical sources, and temporal behavior. *Scientific reports*, 7 (1):1–12, 2017.

[19] Anastasiia Belinskaia, Nikolai Smetanin, Mikhail Lebedev, and Alexei Ossadtchi. Short-delay neurofeedback facilitates training of the parietal alpha rhythm. *Journal of Neural Engineering*, 17(6):066012, 2020.

[20] Larry S Benardo and Robert E Foster. Oscillatory behavior in inferior olive neurons: mechanism, modulation, cell aggregates. *Brain research bulletin*, 17(6):773–784, 1986.

[21] Hans Berger. Über das elektroenkephalogramm des menschen. *Archiv für psychiatrie und nervenkrankheiten*, 87(1):527–570, 1929.

[22] Boris C Bernhardt, Leonardo Bonilha, and Donald W Gross. Network analysis for a network disorder: the emerging role of graph theory in the study of epilepsy. *Epilepsy & Behavior*, 50:162–170, 2015.

[23] Olivier Bertrand, François Perrin, and Jacques Pernier. A theoretical justification of the average reference in topographic evoked potential studies. *Electroencephalography and Clinical Neurophysiology/Evoked Potentials Section*, 62(6):462–464, 1985.

[24] Joydeep Bhattacharya. Reduced degree of long-range phase synchrony in pathological human brain. *Acta neurobiologiae experimentalis*, 61(4):309–318, 2001.

[25] Joydeep Bhattacharya and Hellmuth Petsche. Phase synchrony analysis of eeg during music perception reveals changes in functional connectivity due to musical expertise. *Signal processing*, 85(11):2161–2177, 2005.

[26] Joydeep Bhattacharya, Hellmuth Petsche, Ute Feldmann, and Brigitte Rescher. Eeg gamma-band phase synchronization between posterior and frontal cortex during mental rotation in humans. *Neuroscience Letters*, 311(1):29–32, 2001.

[27] Joydeep Bhattacharya, Hellmuth Petsche, and Ernesto Pereda. Long-range synchrony in the γ band: role in music perception. *Journal of Neuroscience*, 21(16):6329–6337, 2001.

[28] Sayak Bhattacharya, Matthieu BL Cauchois, Pablo A Iglesias, and Zhe Sage Chen. The impact of a closed-loop thalamocortical model on the spatiotemporal dynamics of cortical and thalamic traveling waves. *Scientific reports*, 11(1):1–19, 2021.

[29] Yuanhong Bi, Quansheng Liu, Jingyi Zhao, and Wuritu Yang. Dynamical analyses on beta oscillations in a stn-gpe-gpi model of parkinson's disease. *Complexity*, 2020, 2020.

[30] Marc D Binder, Nobutaka Hirokawa, and Uwe Windhorst. *Encyclopedia of neuroscience*, volume 3166. Springer Berlin, 2009.

[31] Ingmar Blumcke, Roberto Spreafico, Gerrit Haaker, Roland Coras, Katja Kobow, Christian G Bien, Margarete Pfäfflin, Christian Elger, Guido Widman, Johannes Schramm, et al. Histopathological findings in brain tissue obtained during epilepsy surgery. *New England Journal of Medicine*, 377(17):1648–1656, 2017.

[32] Boualem Boashash. Estimating and interpreting the instantaneous frequency of a signal. i. fundamentals. *Proceedings of the IEEE*, 80(4):520–538, 1992.

[33] Gerd Boehmer, Wolfgang Greffrath, Erich Martin, and Sven Hermann. Subthreshold oscillation of the membrane potential in magnocellular neurones of the rat supraoptic nucleus. *The Journal of physiology*, 526(Pt 1):115, 2000.

[34] Leo H Bonati, Yvonne Naegelin, Heinz-Gregor Wieser, Peter Fuhr, and Stephan Ruegg. Beta activity in status epilepticus. *Epilepsia*, 47(1):207–210, 2006.

[35] CB Boulay, WA Sarnacki, JR Wolpaw, and DJ McFarland. Trained modulation of sensorimotor rhythms can affect reaction time. *Clinical Neurophysiology*, 122(9):1820–1826, 2011.

[36] Michael Breakspear, Leanne M Williams, and Cornelis J Stam. A novel method for the topographic analysis of neural activity reveals formation and dissolution of 'dynamic cell assemblies'. *Journal of computational neuroscience*, 16(1):49–68, 2004.

[37] Reggie Brown and Ljupčo Kocarev. A unifying definition of synchronization for dynamical systems. *Chaos: An Interdisciplinary Journal of Nonlinear Science*, 10(2):344–349, 2000.

[38] Peter C Bruce. *Introductory statistics and analytics: a resampling perspective*. John Wiley & Sons, 2014.

[39] Andreas Bruns. Fourier-, hilbert-and wavelet-based signal analysis: are they really different approaches? *Journal of neuroscience methods*, 137(2):321–332, 2004.

[40] TH Bullock, MC McClune, JZ Achimowicz, VJ Iragui-Madoz, RB Duckrow, and SS Spencer. Temporal fluctuations in coherence of brain waves. *Proceedings of the National Academy of Sciences*, 92(25):11568–11572, 1995.

[41] Richard J Burman and R Ryley Parrish. The widespread network effects of focal epilepsy. *Journal of Neuroscience*, 38(38):8107–8109, 2018.

[42] Samuel P Burns, Dajun Xing, Michael J Shelley, and Robert M Shapley. Searching for autocoherence in the cortical network with a time-frequency analysis of the local field potential. *Journal of Neuroscience*, 30 (11):4033–4047, 2010.

[43] Timothy J Bussey, Janice L Muir, and John P Aggleton. Functionally dissociating aspects of event memory: the effects of combined perirhinal and postrhinal cortex lesions on object and place memory in the rat. *Journal of Neuroscience*, 19(1):495–502, 1999.

[44] Cristiano Capone, Beatriz Rebollo, Alberto Muñoz, Xavi Illa, Paolo Del Giudice, Maria V Sanchez-Vives, and Maurizio Mattia. Slow waves in cortical slices: how spontaneous activity is shaped by laminar structure. *Cerebral cortex*, 29(1):319–335, 2019.

[45] Roberta Carabalona. Attitude of the subject towards feedback and its implications for bci use in neurorehabilitation. In *2010 3rd International Symposium on Applied Sciences in Biomedical and Communication Technologies (ISABEL 2010)*, pages 1–4. IEEE, 2010.

[46] James F Cavanagh, Michael X Cohen, and John JB Allen. Prelude to and resolution of an error: Eeg phase synchrony reveals cognitive control dynamics during action monitoring. *Journal of Neuroscience*, 29(1): 98–105, 2009.

[47] Subhash Chandran KS, Chandra Sekhar Seelamantula, and Supratim Ray. Duration analysis using matching pursuit algorithm reveals longer bouts of gamma rhythm. *Journal of neurophysiology*, 119(3):808–821, 2018.

[48] MH Chase and RM Harper. Somatomotor and visceromotor correlates of operantly conditioned 12–14 c/sec sensorimotor cortical activity. *Electroencephalography and clinical Neurophysiology*, 31(1):85–92, 1971.

[49] Anastasios Chatzikonstantinou. Epilepsy and the hippocampus. *The Hippocampus in Clinical Neuroscience*, 34:121–142, 2014.

[50] Ming-Yang Cheng, Chung-Ju Huang, Yu-Kai Chang, Dirk Koester, Thomas Schack, and Tsung-Min Hung. Sensorimotor rhythm neurofeedback enhances golf putting performance. *Journal of Sport and Exercise Psychology*, 37(6):626–636, 2015.

[51] Luis V Colom. Septal networks: relevance to theta rhythm, epilepsy and alzheimer's disease. *Journal of neurochemistry*, 96(3):609–623, 2006.

[52] Marie-Constance Corsi, Sylvain Chevallier, Quentin Barthélemy, Isabelle Hoxha, and Florian Yger. Ensemble learning based on functional connectivity and riemannian geometry for robust workload estimation. In *Neuroergonomics conference 2021*, 2021.

[53] FH Lopes Da Silva, JE Vos, J Mooibroek, and A Van Rotterdam. Relative contributions of intracortical and thalamo-cortical processes in the generation of alpha rhythms, revealed by partial coherence analysis. *Electroencephalography and clinical neurophysiology*, 50(5-6):449–456, 1980.

[54] Nathalie Delprat, Bernard Escudié, Philippe Guillemain, Richard Kronland-Martinet, Philippe Tchamitchian, and Bruno Torresani. Asymptotic wavelet and gabor analysis: Extraction of instantaneous frequencies. *IEEE transactions on Information Theory*, 38(2):644–664, 1992.

[55] Dori Derdikman, Rina Hildesheim, Ehud Ahissar, Amos Arieli, and Amiram Grinvald. Imaging spatiotemporal dynamics of surround inhibition in the barrels somatosensory cortex. *Journal of Neuroscience*, 23(8): 3100–3105, 2003.

[56] Maxime Descoteaux, Elaine Angelino, Shaun Fitzgibbons, and Rachid Deriche. Regularized, fast, and robust analytical q-ball imaging. *Magnetic Resonance in Medicine: An Official Journal of the International Society for Magnetic Resonance in Medicine*, 58(3):497–510, 2007.

[57] M Di Volo and I Férézou. Nonlinear collision between propagating waves in mouse somatosensory cortex. *Scientific Reports*, 11(1):1–15, 2021.

[58] John P Donoghue, Jerome N Sanes, Nicholas G Hatsopoulos, and Gyongyi Gaal. Neural discharge and local field potential oscillations in primate motor cortex during voluntary movements. *Journal of neurophysiology*, 79(1):159–173, 1998.

[59] Tom Dupré la Tour, Thomas Moreau, Mainak Jas, and Alexandre Gramfort. Multivariate convolutional sparse coding for electromagnetic brain signals. *Advances in Neural Information Processing Systems*, 31, 2018.

[60] Piotr J Durka, Dobieslaw Ircha, and Katarzyna J Blinowska. Stochastic time-frequency dictionaries for matching pursuit. *IEEE Transactions on Signal Processing*, 49(3):507–510, 2001.

[61] JC Eccles. Interpretation of action potentials evoked in the cerebral cortex. *Electroencephalography and clinical neurophysiology*, 3(4):449–464, 1951.

[62] Frank H Eeckman and Walter J Freeman. Correlations between unit firing and eeg in the rat olfactory system. *Brain research*, 528(2):238–244, 1990.

[63] Tobias Egner and M Barry Sterman. Neurofeedback treatment of epilepsy: from basic rationale to practical application. *Expert Review of Neurotherapeutics*, 6(2):247–257, 2006.

[64] Thomas Elbert. Slow cortical potentials reflect the regulation of cortical excitability. In *Slow potential changes in the human brain*, pages 235–251. Springer, 1993.

[65] Rafael Elul. The genesis of the eeg. *International review of neurobiology*, 15:227–272, 1972.

[66] Andreas K Engel, Pascal Fries, and Wolf Singer. Dynamic predictions: oscillations and synchrony in top–down processing. *Nature Reviews Neuroscience*, 2(10):704–716, 2001.

[67] Jerome Engel Jr. Introduction to temporal lobe epilepsy. *Epilepsy research*, 26(1):141–150, 1996.

[68] Dario J Englot, Leighton B Hinkley, Naomi S Kort, Brandon S Imber, Danielle Mizuiri, Susanne M Honma, Anne M Findlay, Coleman Garrett, Paige L Cheung, Mary Mantle, et al. Global and regional functional connectivity maps of neural oscillations in focal epilepsy. *Brain*, 138(8):2249–2262, 2015.

[69] Dario J Englot, Peter E Konrad, and Victoria L Morgan. Regional and global connectivity disturbances in focal epilepsy, related neurocognitive sequelae, and potential mechanistic underpinnings. *Epilepsia*, 57(10): 1546–1557, 2016.

[70] Stefanie Enriquez-Geppert, Diede Smit, Miguel Garcia Pimenta, and Martijn Arns. Neurofeedback as a treatment intervention in adhd: Current evidence and practice. *Current psychiatry reports*, 21(6):1–7, 2019.

[71] G Bard Ermentrout and Carson C Chow. Modeling neural oscillations. *Physiology & behavior*, 77(4-5): 629–633, 2002.

[72] G Bard Ermentrout and David Kleinfeld. Traveling electrical waves in cortex: insights from phase dynamics and speculation on a computational role. *Neuron*, 29(1):33–44, 2001.

[73] Vinnie Falco. Dspfilters, 2021. URL `https://github.com/vinniefalco/DSPFilters`.

[74] SF Farmer. Rhythmicity, synchronization and binding in human and primate motor systems. *The Journal of physiology*, 509(1):3–14, 1998.

[75] George Fein, Jonathan Raz, Fiona F Brown, and Edward L Merrin. Common reference coherence data are confounded by power and phase effects. *Electroencephalography and clinical neurophysiology*, 69(6):581–584, 1988.

[76] Joseph Feingold, Daniel J Gibson, Brian DePasquale, and Ann M Graybiel. Bursts of beta oscillation differentiate postperformance activity in the striatum and motor cortex of monkeys performing movement tasks. *Proceedings of the National Academy of Sciences*, 112(44):13687–13692, 2015.

[77] Antonio Fernández-Ruiz, Sagrario Munoz, Miguel Sancho, Julia Makarova, Valeri A Makarov, and Oscar Herreras. Cytoarchitectonic and dynamic origins of giant positive local field potentials in the dentate gyrus. *Journal of Neuroscience*, 33(39):15518–15532, 2013.

[78] Eberhard E Fetz. Operant conditioning of cortical unit activity. *Science*, 163(3870):955–958, 1969.

[79] William W Finley, Hoyt A Smith, and Murray D Etherton. Reduction of seizures and normalization of the eeg in a severe epileptic following sensorimotor biofeedback training: Preliminary study. *Biological psychology*, 2(3):189–203, 1975.

[80] Robert S Fisher. Redefining epilepsy. *Current opinion in neurology*, 28(2):130–135, 2015.

[81] Robert S Fisher, Carlos Acevedo, Alexis Arzimanoglou, Alicia Bogacz, J Helen Cross, Christian E Elger, Jerome Engel Jr, Lars Forsgren, Jacqueline A French, Mike Glynn, et al. Ilae official report: a practical clinical definition of epilepsy. *Epilepsia*, 55(4):475–482, 2014.

[82] Zsuzsanna Fodor, Enikő Sirály, András Horváth, Pál Salacz, Zoltán Hidasi, Éva Csibri, Ádám Szabó, and Gábor Csukly. Decreased event-related beta synchronization during memory maintenance marks early cognitive decline in mild cognitive impairment. *Journal of Alzheimer's Disease*, 63(2):489–502, 2018.

[83] Walter J Freeman. Spatial properties of an eeg event in the olfactory bulb and cortex. *Electroencephalography and clinical neurophysiology*, 44(5):586–605, 1978.

[84] Mark G Frei, Hitten P Zaveri, Susan Arthurs, Gregory K Bergey, Christophe C Jouny, Klaus Lehnertz, Jean Gotman, Ivan Osorio, Theoden I Netoff, Walter J Freeman, et al. Controversies in epilepsy: debates held during the fourth international workshop on seizure prediction. *Epilepsy & Behavior*, 19(1):4–16, 2010.

[85] Xiaoxuan Fu, Youhua Wang, Manling Ge, Danhong Wang, Rongguang Gao, Long Wang, Jundan Guo, and Hesheng Liu. Negative effects of interictal spikes on theta rhythm in human temporal lobe epilepsy. *Epilepsy & Behavior*, 87:207–212, 2018.

[86] Akira Furui, Ryota Onishi, Akihito Takeuchi, Tomoyuki Akiyama, and Toshio Tsuji. Non-gaussianity detection of eeg signals based on a multivariate scale mixture model for diagnosis of epileptic seizures. *IEEE Transactions on Biomedical Engineering*, 68(2):515–525, 2020.

[87] Line Garnero. Les bases physiques et physiologiques de la magnétoencéphalographie et de l'electroencéphalographie, 1998.

[88] Manling Ge, Danhong Wang, Guoya Dong, Baoqiang Guo, Rongguang Gao, Wei Sun, Jijun Zhang, and Hesheng Liu. Transient impact of spike on theta rhythm in temporal lobe epilepsy. *Experimental neurology*, 250:136–142, 2013.

[89] Zhongfu Ge. Significance tests for the wavelet cross spectrum and wavelet linear coherence. In *Annales Geophysicae*, volume 26, pages 3819–3829. Copernicus GmbH, 2008.

[90] C Gemma, L Imeri, and M Mancia. Hippocampal type 1 (movement-related) theta rhythm positively correlates with serotonergic activity. *Archives italiennes de biologie*, 137(2):151–160, 1999.

[91] NG Gencer, SJ Williamson, A Gueziec, and R Hummel. Optimal reference electrode selection for electric source imaging. *Electroencephalography and clinical neurophysiology*, 99(2):163–173, 1996.

[92] Laurent George and Anatole Lécuyer. An overview of research on" passive" brain-computer interfaces for implicit human-computer interaction. In *International Conference on Applied Bionics and Biomechanics ICABB 2010-Workshop W1" Brain-Computer Interfacing and Virtual Reality"*, 2010.

[93] Audrey Girouard, Erin Treacy Solovey, and Robert JK Jacob. Designing a passive brain computer interface using real time classification of functional near-infrared spectroscopy. *International Journal of Autonomous and Adaptive Communications Systems*, 6(1):26–44, 2013.

[94] Graham V Goddard, Dan C McIntyre, and Curtis K Leech. A permanent change in brain function resulting from daily electrical stimulation. *Experimental neurology*, 25(3):295–330, 1969.

[95] Charles M Gray and David A McCormick. Chattering cells: superficial pyramidal neurons contributing to the generation of synchronous oscillations in the visual cortex. *Science*, 274(5284):109–113, 1996.

[96] Charles M Gray, Peter König, Andreas K Engel, and Wolf Singer. Oscillatory responses in cat visual cortex exhibit inter-columnar synchronization which reflects global stimulus properties. *Nature*, 338(6213):334–337, 1989.

[97] Thomas Gruber and Matthias M Müller. Effects of picture repetition on induced gamma band responses, evoked potentials, and phase synchrony in the human eeg. *Cognitive Brain Research*, 13(3):377–392, 2002.

[98] John H Gruzelier. Eeg-neurofeedback for optimising performance. i: a review of cognitive and affective outcome in healthy participants. *Neuroscience & Biobehavioral Reviews*, 44:124–141, 2014.

[99] Ramón Guevara, José Luis Pérez Velazquez, Vera Nenadovic, Richard Wennberg, Goran Senjanović, and Luís Garcia Dominguez. Phase synchronization measurements using electroencephalographic recordings. *Neuroinformatics*, 3(4):301–313, 2005.

[100] B Gustafsson. Afterpotentials and transduction properties in different types of central neurones. *Archives italiennes de biologie*, 122(1):17–30, 1984.

[101] Yoram Gutfreund, Yosef Yarom, and Idan Segev. Subthreshold oscillations and resonant frequency in guinea-pig cortical neurons: physiology and modelling. *The Journal of physiology*, 483(3):621–640, 1995.

[102] Elly Gysels and Patrick Celka. Phase synchronization for the recognition of mental tasks in a brain-computer interface. *IEEE Transactions on neural systems and rehabilitation engineering*, 12(4):406–415, 2004.

[103] Saskia Haegens, Verónica Nácher, Rogelio Luna, Ranulfo Romo, and Ole Jensen. α-oscillations in the monkey sensorimotor network influence discrimination performance by rhythmical inhibition of neuronal spiking. *Proceedings of the National Academy of Sciences*, 108(48):19377–19382, 2011.

[104] Milan Halgren, István Ulbert, Hélène Bastuji, Dániel Fabó, Lorand Erőss, Marc Rey, Orrin Devinsky, Werner K Doyle, Rachel Mak-McCully, Eric Halgren, et al. The generation and propagation of the human alpha rhythm. *Proceedings of the National Academy of Sciences*, 116(47):23772–23782, 2019.

[105] Toshiaki Hamano, Hans O Lüders, Akio Ikeda, Thomas F Collura, Youssef G Comair, and Hiroshi Shibasaki. The cortical generators of the contingent negative variation in humans: a study with subdural electrodes. *Electroencephalography and Clinical Neurophysiology/Evoked Potentials Section*, 104(3):257–268, 1997.

[106] Chuanliang Han, Robert Shapley, and Dajun Xing. Gamma rhythms in the visual cortex: functions and mechanisms. *Cognitive Neurodynamics*, pages 1–12, 2021.

[107] Zulfi Haneef, Sharon Chiang, Hsiang J Yeh, Jerome Engel Jr, and John M Stern. Functional connectivity homogeneity correlates with duration of temporal lobe epilepsy. *Epilepsy & Behavior*, 46:227–233, 2015.

[108] Simon Hanslmayr, Paul Sauseng, Michael Doppelmayr, Manuel Schabus, and Wolfgang Klimesch. Increasing individual upper alpha power by neurofeedback improves cognitive performance in human subjects. *Applied psychophysiology and biofeedback*, 30(1):1–10, 2005.

[109] Russell Hebert, Dietrich Lehmann, Gabriel Tan, Fred Travis, and Alarik Arenander. Enhanced eeg alpha time-domain phase synchrony during transcendental meditation: Implications for cortical integration theory. *Signal Processing*, 85(11):2213–2232, 2005.

[110] Andreas Henelius, Kati Hirvonen, Anu Holm, Jussi Korpela, and Kiti Muller. Mental workload classification using heart rate metrics. In *2009 annual international conference of the ieee engineering in medicine and biology society*, pages 1836–1839. IEEE, 2009.

[111] Oscar Herreras. Local field potentials: myths and misunderstandings. *Frontiers in neural circuits*, 10:101, 2016.

[112] Nicole A Himmelstoss, Christina P Brötzner, Andrea Zauner, Hubert H Kerschbaum, Walter Gruber, Julia Lechinger, and Wolfgang Klimesch. Prestimulus amplitudes modulate p1 latencies and evoked traveling alpha waves. *Frontiers in human neuroscience*, 9:302, 2015.

[113] Marcel F Hinss, Bertille Somon, Frédéric Dehais, and Raphaëlle N Roy. Open eeg datasets for passive brain-computer interface applications: Lacks and perspectives. In *2021 10th International IEEE/EMBS Conference on Neural Engineering (NER)*, pages 686–689. IEEE, 2021.

[114] Gregory L Holmes, Chengju Tian, Amanda E Hernan, Sean Flynn, Devon Camp, and Jeremy Barry. Alterations in sociability and functional brain connectivity caused by early-life seizures are prevented by bumetanide. *Neurobiology of disease*, 77:204–219, 2015.

[115] RC Howe and MB Sterman. Somatosensory system evoked potentials during waking behavior and sleep in the cat. *Electroencephalography and clinical neurophysiology*, 34(6):605–618, 1973.

[116] Jen-Jui Hsueh, Tzu-Shan Chen, Jia-Jin Chen, and Fu-Zen Shaw. Neurofeedback training of eeg alpha rhythm enhances episodic and working memory. *Human brain mapping*, 37(7):2662–2675, 2016.

[117] Xiaoying Huang, William C Troy, Qian Yang, Hongtao Ma, Carlo R Laing, Steven J Schiff, and Jian-Young Wu. Spiral waves in disinhibited mammalian neocortex. *Journal of Neuroscience*, 24(44):9897–9902, 2004.

[118] J Hughlings-Jackson. On right or left-sided spasm at the onset of epileptic paroxysms, and on crude sensation warnings, and elaborate mental states. *Brain*, 3(2):192–206, 1880.

[119] Bruce Hutcheon and Yosef Yarom. Resonance, oscillation and the intrinsic frequency preferences of neurons. *Trends in neurosciences*, 23(5):216–222, 2000.

[120] Tetsuya Iidaka. Fluctuations in arousal correlate with neural activity in the human thalamus. *Cerebral cortex communications*, 2(3):tgab055, 2021.

[121] Tsuyoshi Inouye, Kazuhiro Shinosaki, and Akemi Yagasaki. The direction of spread of alpha activity over the scalp. *Electroencephalography and Clinical Neurophysiology*, 55(3):290–300, 1983.

[122] Tsuyoshi Inouye, Kazuhiro Shinosaki, Seigo Toi, Yuko Matsumoto, and Naoaki Hosaka. Potential flow of a activity in the human electroencephalogram. *Neuroscience letters*, 187(1):29–32, 1995.

[123] Junji Ito, Andrey R Nikolaev, and Cees Van Leeuwen. Spatial and temporal structure of phase synchronization of spontaneous alpha eeg activity. *Biological cybernetics*, 92(1):54–60, 2005.

[124] Alice F Jackson and Donald J Bolger. The neurophysiological bases of eeg and eeg measurement: A review for the rest of us. *Psychophysiology*, 51(11):1061–1071, 2014.

[125] Andrew Jackson, Jaideep Mavoori, and Eberhard E Fetz. Long-term motor cortex plasticity induced by an electronic neural implant. *Nature*, 444(7115):56–60, 2006.

[126] S Rao Jammalamadaka and Ambar Sengupta. *Topics in circular statistics*, volume 5. world scientific, 2001.

[127] Premysl Jiruska, Marco De Curtis, John GR Jefferys, Catherine A Schevon, Steven J Schiff, and Kaspar Schindler. Synchronization and desynchronization in epilepsy: controversies and hypotheses. *The Journal of physiology*, 591(4):787–797, 2013.

[128] Daniel Johnston and David G Amaral. Hippocampus. 2004.

[129] Matthew W Jones and Matthew A Wilson. Theta rhythms coordinate hippocampal–prefrontal interactions in a spatial memory task. *PLoS biology*, 3(12):e402, 2005.

[130] Stephanie R Jones, Dominique L Pritchett, Michael A Sikora, Steven M Stufflebeam, Matti Hämäläinen, and Christopher I Moore. Quantitative analysis and biophysically realistic neural modeling of the meg mu rhythm: rhythmogenesis and modulation of sensory-evoked responses. *Journal of neurophysiology*, 102(6): 3554–3572, 2009.

[131] Tulga Kalayci, Ozcan Ozdamar, and Nurgun Erdol. The use of wavelet transform as a preprocessor for the neural network detection of eeg spikes. In *Proceedings of SOUTHEASTCON'94*, pages 1–3. IEEE, 1994.

[132] Fumi Katsuki and Christos Constantinidis. Bottom-up and top-down attention: different processes and overlapping neural systems. *The Neuroscientist*, 20(5):509–521, 2014.

[133] Larry C Katz and Carla J Shatz. Synaptic activity and the construction of cortical circuits. *Science*, 274 (5290):1133–1138, 1996.

[134] Teiji Kawano, Noriaki Hattori, Yutaka Uno, Keiichi Kitajo, Megumi Hatakenaka, Hajime Yagura, Hiroaki Fujimoto, Tomomi Yoshioka, Michiko Nagasako, Hironori Otomune, et al. Large-scale phase synchrony reflects clinical status after stroke: An eeg study. *Neurorehabilitation and Neural Repair*, 31(6):561–570, 2017.

[135] Teiji Kawano, Noriaki Hattori, Yutaka Uno, Megumi Hatakenaka, Hajime Yagura, Hiroaki Fujimoto, Michiko Nagasako, Hideki Mochizuki, Keiichi Kitajo, and Ichiro Miyai. Association between aphasia severity and brain network alterations after stroke assessed using the electroencephalographic phase synchrony index. *Scientific reports*, 11(1):1–14, 2021.

[136] Houman Khosravani, C Robert Pinnegar, J Ross Mitchell, Berj L Bardakjian, Paolo Federico, and Peter L Carlen. Increased high-frequency oscillations precede in vitro low-mg2+ seizures. *Epilepsia*, 46(8):1188–1197, 2005.

[137] Bjørg Elisabeth Kilavik, Manuel Zaepffel, Andrea Brovelli, William A MacKay, and Alexa Riehle. The ups and downs of beta oscillations in sensorimotor cortex. *Experimental neurology*, 245:15–26, 2013.

[138] Hyein Kim, Jungho Yoon, Byeongseon Jeong, and Sukho Lee. Rank-1 convolutional neural network. *arXiv preprint arXiv:1808.04303*, 2018.

[139] Wolfgang Klimesch, Paul Sauseng, and Simon Hanslmayr. Eeg alpha oscillations: the inhibition–timing hypothesis. *Brain research reviews*, 53(1):63–88, 2007.

[140] Gennady G Knyazev. Eeg delta oscillations as a correlate of basic homeostatic and motivational processes. *Neuroscience & Biobehavioral Reviews*, 36(1):677–695, 2012.

[141] Silvia Erika Kober, Matthias Witte, Christa Neuper, and Guilherme Wood. Specific or nonspecific? evaluation of band, baseline, and cognitive specificity of sensorimotor rhythm-and gamma-based neurofeedback. *International Journal of Psychophysiology*, 120:1–13, 2017.

[142] N Kopell, GB Ermentrout, MA Whittington, and RD Traub. Gamma rhythms and beta rhythms have different synchronization properties. *Proceedings of the National Academy of Sciences*, 97(4):1867–1872, 2000.

[143] Aaron C Koralek, Rui M Costa, and Jose M Carmena. Temporally precise cell-specific coherence develops in corticostriatal networks during learning. *Neuron*, 79(5):865–872, 2013.

[144] Boris Kotchoubey, Ute Strehl, C Uhlmann, Susanne Holzapfel, M König, W Fröscher, V Blankenhorn, and Niels Birbaumer. Modification of slow cortical potentials in patients with refractory epilepsy: a controlled outcome study. *Epilepsia*, 42(3):406–416, 2001.

[145] Michael Koutroumanidis, Carmen Martin-Miguel, Michael J Hennessy, Nozomi Akanuma, Antonio Valentin, Gonzalo Alarcón, Jozef M Jarosz, and Charles E Polkey. Interictal temporal delta activity in temporal lobe epilepsy: correlations with pathology and outcome. *Epilepsia*, 45(11):1351–1367, 2004.

[146] Zbigniew J Kowalik, Andrzej Wróbel, and Andrzej Rydz. Why does the human brain need to be a nonlinear system? *Behavioral and Brain Sciences*, 19(2):302–303, 1996.

[147] Subhash Chandran KS, Ashutosh Mishra, Vinay Shirhatti, and Supratim Ray. Comparison of matching pursuit algorithm with other signal processing techniques for computation of the time-frequency power spectrum of brain signals. *Journal of Neuroscience*, 36(12):3399–3408, 2016.

[148] William N Kuhlman. Functional topography of the human mu rhythm. *Electroencephalography and clinical neurophysiology*, 44(1):83–93, 1978.

[149] AP Kulaichev. The informativeness of coherence analysis in eeg studies. *Neuroscience and behavioral physiology*, 41(3):321, 2011.

[150] Patrick Kwan, Alexis Arzimanoglou, Anne T Berg, Martin J Brodie, W Allen Hauser, Gary Mathern, Solomon L Moshé, Emilio Perucca, Samuel Wiebe, and Jacqueline French. Definition of drug resistant epilepsy: consensus proposal by the ad hoc task force of the ilae commission on therapeutic strategies, 2010.

[151] Jean-Philippe Lachaux, Eugenio Rodriguez, Jacques Martinerie, and Francisco J Varela. Measuring phase synchrony in brain signals. *Human brain mapping*, 8(4):194–208, 1999.

[152] Stanislas Lagarde, Nicolas Roehri, Isabelle Lambert, Agnès Trebuchon, Aileen McGonigal, Romain Carron, Didier Scavarda, Mathieu Milh, Francesca Pizzo, Bruno Colombet, et al. Interictal stereotactic-eeg functional connectivity in refractory focal epilepsies. *Brain*, 141(10):2966–2980, 2018.

[153] Salim Lahmiri. Generalized hurst exponent estimates differentiate eeg signals of healthy and epileptic patients. *Physica A: Statistical Mechanics and its Applications*, 490:378–385, 2018.

[154] Ying-Wan Lam, Lawrence B Cohen, Matt Wachowiak, and Michal R Zochowski. Odors elicit three different oscillations in the turtle olfactory bulb. *Journal of Neuroscience*, 20(2):749–762, 2000.

[155] ILAN Lampl and YOSEF Yarom. Subthreshold oscillations of the membrane potential: a functional synchronizing and timing device. *Journal of neurophysiology*, 70(5):2181–2186, 1993.

[156] MATTHEW E Larkum, MARC G Rioult, and HANS-R Luscher. Propagation of action potentials in the dendrites of neurons from rat spinal cord slice cultures. *Journal of neurophysiology*, 75(1):154–170, 1996.

[157] Michel Le Van Quyen, Jack Foucher, Jean-Philippe Lachaux, Eugenio Rodriguez, Antoine Lutz, Jacques Martinerie, and Francisco J Varela. Comparison of hilbert transform and wavelet methods for the analysis of neuronal synchrony. *Journal of neuroscience methods*, 111(2):83–98, 2001.

[158] Maxime Lévesque and Massimo Avoli. The kainic acid model of temporal lobe epilepsy. *Neuroscience & Biobehavioral Reviews*, 37(10):2887–2899, 2013.

[159] Yuqi Liang, Chenchen Song, Mianxin Liu, Pulin Gong, Changsong Zhou, and Thomas Knöpfel. Cortex-wide dynamics of intrinsic electrical activities: propagating waves and their interactions. *Journal of Neuroscience*, 41(16):3665–3678, 2021.

[160] Shuang Liu, Xinyu Hao, Xiaoya Liu, Yuchen He, Ludan Zhang, Xingwei An, Xizi Song, and Dong Ming. Sensorimotor rhythm neurofeedback training relieves anxiety in healthy people. *Cognitive Neurodynamics*, pages 1–14, 2021.

[161] Yichuan Liu, Hasan Ayaz, and Patricia A Shewokis. Multisubject "learning" for mental workload classification using concurrent eeg, fnirs, and physiological measures. *Frontiers in human neuroscience*, 11:389, 2017.

[162] Rodolfo Llinas and Urs Ribary. Coherent 40-hz oscillation characterizes dream state in humans. *Proceedings of the National Academy of Sciences*, 90(5):2078–2081, 1993.

[163] RA Lockhart and MA Stephens. Tests of fit for the von mises distribution. *Biometrika*, 72(3):647–652, 1985.

[164] Eric Lowet, Mark J Roberts, Pietro Bonizzi, Joël Karel, and Peter De Weerd. Quantifying neural oscillatory synchronization: a comparison between spectral coherence and phase-locking value approaches. *PloS one*, 11(1), 2016.

[165] Joel F Lubar. Neocortical dynamics: Implications for understanding the role of neurofeedback and related techniques for the enhancement of attention. *Applied psychophysiology and biofeedback*, 22(2):111–126, 1997.

[166] Joel F Lubar and WW Bahler. Behavioral management of epileptic seizures following eeg biofeedback training of the sensorimotor rhythm. *Biofeedback and Self-regulation*, 1(1):77–104, 1976.

[167] Evgueniy V Lubenov and Athanassios G Siapas. Hippocampal theta oscillations are travelling waves. *Nature*, 459(7246):534–539, 2009.

[168] Mikael Lundqvist, Jonas Rose, Pawel Herman, Scott L Brincat, Timothy J Buschman, and Earl K Miller. Gamma and beta bursts underlie working memory. *Neuron*, 90(1):152–164, 2016.

[169] Cheng Luo, Dongmei An, Dezhong , and Jean Gotman. Patient-specific connectivity pattern of epileptic network in frontal lobe epilepsy. *NeuroImage: Clinical*, 4:668–675, 2014.

[170] Zsófia Maglóczky. Sprouting in human temporal lobe epilepsy: excitatory pathways and axons of interneurons. *Epilepsy research*, 89(1):52–59, 2010.

[171] Andrzej Majkowski, Łukasz Oskwarek, Marcin Kołodziej, and Remigiusz J Rak. An attempt to localize brain electrical activity sources using eeg with limited number of electrodes. *Biocybernetics and Biomedical Engineering*, 36(4):686–696, 2016.

[172] Stéphane G Mallat and Zhifeng Zhang. Matching pursuits with time-frequency dictionaries. *IEEE Transactions on signal processing*, 41(12):3397–3415, 1993.

[173] Michael G Mariscal, Elizabeth Berry-Kravis, Joseph D Buxbaum, Lauren E Ethridge, Rajna Filip-Dhima, Jennifer H Foss-Feig, Alexander Kolevzon, Meera E Modi, Matthew W Mosconi, Charles A Nelson, et al. Shifted phase of eeg cross-frequency coupling in individuals with phelan-mcdermid syndrome. *Molecular autism*, 12(1):1–12, 2021.

[174] Fabienne Marlats, Guillaume Bao, Sylvain Chevallier, Marouane Boubaya, Leila Djabelkhir-Jemmi, Ya-Huei Wu, Hermine Lenoir, Anne-Sophie Rigaud, and Eric Azabou. Smr/theta neurofeedback training improves cognitive performance and eeg activity in elderly with mild cognitive impairment: a pilot study. *Frontiers in Aging Neuroscience*, 12:147, 2020.

[175] Marcello Massimini, Reto Huber, Fabio Ferrarelli, Sean Hill, and Giulio Tononi. The sleep slow oscillation as a traveling wave. *Journal of Neuroscience*, 24(31):6862–6870, 2004.

[176] Kyle E Mathewson, Tyler JL Harrison, and Sayeed AD Kizuk. High and dry? comparing active dry eeg electrodes to active and passive wet electrodes. *Psychophysiology*, 54(1):74–82, 2017.

[177] Nobuyoshi Matsumoto, Takuma Kitanishi, and Kenji Mizuseki. The subiculum: Unique hippocampal hub and more. *Neuroscience Research*, 143:1–12, 2019.

[178] Robert L Maulsby. An illustration of emotionally evoked theta rhythm in infancy: Hedonic hypersynchrony. *Electroencephalography and Clinical Neurophysiology*, 31(2):157–165, 1971.

[179] Alberto Mazzoni, Henrik Linden, Hermann Cuntz, Anders Lansner, Stefano Panzeri, and Gaute T Einevoll. Computing the local field potential (lfp) from integrate-and-fire network models. *PLoS computational biology*, 11(12):e1004584, 2015.

[180] Alexander C MettingVanRijn, Anthony P Kuiper, Taco E Dankers, and Cees A Grimbergen. Low-cost active electrode improves the resolution in biopotential recordings. In *Proceedings of 18th Annual International Conference of the IEEE Engineering in Medicine and Biology Society*, volume 1, pages 101–102. IEEE, 1996.

[181] Lisa Meyer-Baese, Harrison Watters, and Shella Keilholz. Spatiotemporal patterns of spontaneous brain activity: a mini-review. *Neurophotonics*, 9(3):032209, 2022.

[182] Eri Miyauchi, Keiichi Kitajo, and Masahiro Kawasaki. Tms-induced theta phase synchrony reveals a bottom-up network in working memory. *Neuroscience Letters*, 622:10–14, 2016.

[183] Victoria L Morgan, Benjamin N Conrad, Bassel Abou-Khalil, Baxter P Rogers, and Hakmook Kang. Increasing structural atrophy and functional isolation of the temporal lobe with duration of disease in temporal lobe epilepsy. *Epilepsy research*, 110:171–178, 2015.

[184] RS Morison and DL Bassett. Electrical activity of the thalamus and basal ganglia in decorticate cats. *Journal of Neurophysiology*, 8(5):309–314, 1945.

[185] Florian Mormann, Klaus Lehnertz, Peter David, and Christian E Elger. Mean phase coherence as a measure for phase synchronization and its application to the eeg of epilepsy patients. *Physica D: Nonlinear Phenomena*, 144(3-4):358–369, 2000.

[186] Florian Mormann, Thomas Kreuz, Christoph Rieke, Ralph G Andrzejak, Alexander Kraskov, Peter David, Christian E Elger, and Klaus Lehnertz. On the predictability of epileptic seizures. *Clinical neurophysiology*, 116(3):569–587, 2005.

[187] Lyle Muller, Frédéric Chavane, John Reynolds, and Terrence J Sejnowski. Cortical travelling waves: mechanisms and computational principles. *Nature Reviews Neuroscience*, 19(5):255–268, 2018.

[188] Suresh D Muthukumaraswamy, Blake W Johnson, and Nicolas A McNair. Mu rhythm modulation during observation of an object-directed grasp. *Cognitive brain research*, 19(2):195–201, 2004.

[189] Nadim Nachar et al. The mann-whitney u: A test for assessing whether two independent samples come from the same distribution. *Tutorials in quantitative Methods for Psychology*, 4(1):13–20, 2008.

[190] Yoko Nagai, Christopher Iain Jones, and Arjune Sen. Galvanic skin response (gsr)/electrodermal/skin conductance biofeedback on epilepsy: a systematic review and meta-analysis. *Frontiers in neurology*, 10: 377, 2019.

[191] Zoran Nenadic, Bijoy K Ghosh, and Philip Ulinski. Propagating waves in visual cortex: A large-scale model of turtle visual cortex. *Journal of computational neuroscience*, 14(2):161–184, 2003.

[192] Yuval Nir, RichardáJ Staba, Thomas Andrillon, VladyslaváV Vyazovskiy, Chiara Cirelli, Itzhak Fried, and Giulio Tononi. Regional slow waves and spindles in human sleep. *Neuron*, 70(1):153–169, 2011.

[193] Jeremy B Noel, Kenneth W Bauer Jr, and Jeffrey W Lanning. Improving pilot mental workload classification through feature exploitation and combination: a feasibility study. *Computers & operations research*, 32(10): 2713–2730, 2005.

[194] Guido Nolte, Ou Bai, Lewis Wheaton, Zoltan Mari, Sherry Vorbach, and Mark Hallett. Identifying true brain interaction from eeg data using the imaginary part of coherency. *Clinical neurophysiology*, 115(10): 2292–2307, 2004.

[195] Marlene M Normand, Zbigniew K Wszolek, and Donald W Klass. Temporal intermittent rhythmic delta activity in electroencephalograms. *Journal of clinical neurophysiology: official publication of the American Electroencephalographic Society*, 12(3):280–284, 1995.

[196] Paul L Nunez. Wavelike properties of the alpha rhythm. *IEEE Transactions on Biomedical Engineering*, pages 473–482, 1974.

[197] Paul L Nunez. Implications of white matter correlates of eeg standing and traveling waves. *Neuroimage*, 57 (4):1293–1299, 2011.

[198] Paul L Nunez, Larry Reid, and Reginald G Bickford. The relationship of head size to alpha frequency with implications to a brain wave model. *Electroencephalography and clinical Neurophysiology*, 44(3):344–352, 1978.

[199] Paul L Nunez, Ramesh Srinivasan, Andrew F Westdorp, Ranjith S Wijesinghe, Don M Tucker, Richard B Silberstein, and Peter J Cadusch. Eeg coherency: I: statistics, reference electrode, volume conduction, laplacians, cortical imaging, and interpretation at multiple scales. *Electroencephalography and clinical neurophysiology*, 103(5):499–515, 1997.

[200] Rafael Angel Gutierrez Nuno and Koushik Maharatna. A phase lag index hardware calculation for real-time electroencephalography studies. In *2019 41st Annual International Conference of the IEEE Engineering in Medicine and Biology Society (EMBC)*, pages 644–647. IEEE, 2019.

[201] Iyad Obeid and Joseph Picone. The temple university hospital eeg data corpus. *Frontiers in neuroscience*, 10:196, 2016.

[202] Francisco E Olucha-Bordonau, Lluis Fortes-Marco, Marcos Otero-García, Enrique Lanuza, and Fernando Martínez-García. Amygdala: structure and function. In *The rat nervous system*, pages 441–490. Elsevier, 2015.

[203] Thom F Oostendorp, Jean Delbeke, and Dick F Stegeman. The conductivity of the human skull: results of in vivo and in vitro measurements. *IEEE transactions on biomedical engineering*, 47(11):1487–1492, 2000.

[204] Harry S Orbach and Lawrence B Cohen. Optical monitoring of activity from many areas of the in vitro and in vivo salamander olfactory bulb: a new method for studying functional organization in the vertebrate central nervous system. *Journal of Neuroscience*, 3(11):2251–2262, 1983.

[205] World Health Organization, Global Campaign against Epilepsy, Programme for Neurological Diseases, Neuroscience (World Health Organization), International Bureau for Epilepsy, World Health Organization. Department of Mental Health, Substance Abuse, International Bureau of Epilepsy, and International League against Epilepsy. *Atlas: epilepsy care in the world*. World Health Organization, 2005.

[206] Alexei Ossadtchi, Tatiana Shamaeva, Elizaveta Okorokova, Victoria Moiseeva, and Mikhail A Lebedev. Neurofeedback learning modifies the incidence rate of alpha spindles, but not their duration and amplitude. *Scientific reports*, 7(1):1–12, 2017.

[207] Hannes Osterhage, Florian Mormann, Matthäus Staniek, and Klaus Lehnertz. Measuring synchronization in the epileptic brain: a comparison of different approaches. *International Journal of Bifurcation and Chaos*, 17(10):3539–3544, 2007.

[208] Ismael Palacios-García, Jaime Silva, Mario Villena-González, Germán Campos-Arteaga, Claudio Artigas-Vergara, Nicolas Luarte, Eugenio Rodríguez, and Conrado A Bosman. Increase in beta power reflects attentional top-down modulation after psychosocial stress induction. *Frontiers in human neuroscience*, 2021.

[209] E Palma, M Amici, F Sobrero, G Spinelli, S Di Angelantonio, D Ragozzino, A Mascia, C Scoppetta, V Esposito, R Miledi, et al. Anomalous levels of cl- transporters in the hippocampal subiculum from temporal lobe epilepsy patients make gaba excitatory. *Proceedings of the National Academy of Sciences*, 103(22):8465–8468, 2006.

[210] J Matias Palva, Satu Palva, and Kai Kaila. Phase synchrony among neuronal oscillations in the human cortex. *Journal of Neuroscience*, 25(15):3962–3972, 2005.

[211] J Matias Palva, Simo Monto, Shrikanth Kulashekhar, and Satu Palva. Neuronal synchrony reveals working memory networks and predicts individual memory capacity. *Proceedings of the National Academy of Sciences*, 107(16):7580–7585, 2010.

[212] Liping Pang, Liang Guo, Jie Zhang, Xiaoru Wanyan, Hongquan Qu, and Xin Wang. Subject-specific mental workload classification using eeg and stochastic configuration network (scn). *Biomedical Signal Processing and Control*, 68:102711, 2021.

[213] Roberto Domingo Pascual-Marqui et al. Standardized low-resolution brain electromagnetic tomography (sloreta): technical details. *Methods Find Exp Clin Pharmacol*, 24(Suppl D):5–12, 2002.

[214] Paula R Patel and Orlando De Jesus. Partial epilepsy. *StatPearls*, 2020.

[215] Timothy M Patten, Christopher J Rennie, Peter A Robinson, and Pulin Gong. Human cortical traveling waves: dynamical properties and correlations with responses. *PLoS One*, 7(6):e38392, 2012.

[216] Lorraine Perronnet. *Combining EEG and FMRI for Neurofeedback*. PhD thesis, University of Rennes I, 2017.

[217] Piero Perucca and Frank G Gilliam. Adverse effects of antiepileptic drugs. *The Lancet Neurology*, 11(9): 792–802, 2012.

[218] Carl CH Petersen, Amiram Grinvald, and Bert Sakmann. Spatiotemporal dynamics of sensory responses in layer 2/3 of rat barrel cortex measured in vivo by voltage-sensitive dye imaging combined with whole-cell voltage recordings and neuron reconstructions. *Journal of neuroscience*, 23(4):1298–1309, 2003.

[219] H Petsche and J Šterc. The significance of the cortex for the travelling phenomenon of brain waves. *Electroencephalography and clinical neurophysiology*, 25(1):11–22, 1968.

[220] AN Pettitt and V Siskind. Effect of within-sample dependence on the mann–whitney–wilcoxon statistic. *Biometrika*, 68(2):437–441, 1981.

[221] Ingrid HCHM Philippens, Jacqueline A Wubben, Raymond AP Vanwersch, Dave L Estevao, and Peter A Tass. Sensorimotor rhythm neurofeedback as adjunct therapy for parkinson's disease. *Annals of clinical and translational neurology*, 4(8):585–590, 2017.

[222] Paul F Pinsky and John Rinzel. Intrinsic and network rhythmogenesis in a reduced traub model for ca3 neurons. *Journal of computational neuroscience*, 1(1):39–60, 1994.

[223] Francesca Pittau, Pierre Mégevand, Laurent Sheybani, Eugenio Abela, Frédéric Grouiller, Laurent Spinelli, Christoph M Michel, Margitta Seeck, and Serge Vulliemoz. Mapping epileptic activity: sources or networks for the clinicians? *Frontiers in neurology*, 5:218, 2014.

[224] Susan Pockett, Gary EJ Bold, and Walter J Freeman. Eeg synchrony during a perceptual-cognitive task: Widespread phase synchrony at all frequencies. *Clinical Neurophysiology*, 120(4):695–708, 2009.

[225] JC Prechtl, LB Cohen, B Pesaran, PP Mitra, and D Kleinfeld. Visual stimuli induce waves of electrical activity in turtle cortex. *Proceedings of the National Academy of Sciences*, 94(14):7621–7626, 1997.

[226] Friedemann Pulvermüller, Andreas Keil, and Thomas Elbert. High-frequency brain activity: perception or active memory? *Trends in cognitive sciences*, 3(7):250–252, 1999.

[227] SM Purcell, DS Manoach, C Demanuele, BE Cade, S Mariani, R Cox, G Panagiotaropoulou, R Saxena, JQ Pan, JW Smoller, et al. Characterizing sleep spindles in 11,630 individuals from the national sleep research resource. *Nature communications*, 8(1):1–16, 2017.

[228] Hongquan Qu, Yiping Shan, Yuzhe Liu, Liping Pang, Zhanli Fan, Jie Zhang, and Xiaoru Wanyan. Mental workload classification method based on eeg independent component features. *Applied Sciences*, 10(9):3036, 2020.

[229] R Quian Quiroga, A Kraskov, T Kreuz, and Peter Grassberger. Performance of different synchronization measures in real data: a case study on electroencephalographic signals. *Physical Review E*, 65(4):041903, 2002.

[230] Rajasimhan Rajagovindan and Mingzhou Ding. From prestimulus alpha oscillation to visual-evoked response: an inverted-u function and its attentional modulation. *Journal of cognitive neuroscience*, 23(6): 1379–1394, 2011.

[231] Jan-Marino Ramirez, Andrew K Tryba, and Fernando Peña. Pacemaker neurons and neuronal networks: an integrative view. *Current opinion in neurobiology*, 14(6):665–674, 2004.

[232] Malte J Rasch, Arthur Gretton, Yusuke Murayama, Wolfgang Maass, and Nikos K Logothetis. Inferring spike trains from local field potentials. *Journal of neurophysiology*, 99(3):1461–1476, 2008.

[233] Chrystal M Reed, Sandra Dewar, Itzhak Fried, Jerome Engel Jr, and Dawn Eliashiv. Failed epilepsy surgery deserves a second chance. *Clinical neurology and neurosurgery*, 163:110–115, 2017.

[234] Antonia Reimer, Peter Hubka, Andreas K Engel, and Andrej Kral. Fast propagating waves within the rodent auditory cortex. *Cerebral Cortex*, 21(1):166–177, 2011.

[235] Susanne Maria Reiterer, Ernesto Pereda, and Joydeep Bhattacharya. On a possible relationship between linguistic expertise and eeg gamma band phase synchrony. *Frontiers in psychology*, 2:334, 2011.

[236] Yann Renard, Fabien Lotte, Guillaume Gibert, Marco Congedo, Emmanuel Maby, Vincent Delannoy, Olivier Bertrand, and Anatole Lécuyer. Openvibe: An open-source software platform to design, test, and use brain–computer interfaces in real and virtual environments. *Presence*, 19(1):35–53, 2010.

[237] Tian Renton, Alana Tibbles, and Jane Topolovec-Vranic. Neurofeedback as a form of cognitive rehabilitation therapy following stroke: A systematic review. *PloS one*, 12(5):e0177290, 2017.

[238] U Ribary, AA Ioannides, Krish Devi Singh, R Hasson, JP Bolton, F Lado, A Mogilner, and R Llinas. Magnetic field tomography of coherent thalamocortical 40-hz oscillations in humans. *Proceedings of the National Academy of Sciences*, 88(24):11037–11041, 1991.

[239] Justin Riddle, Kai Hwang, Dillan Cellier, Sofia Dhanani, and Mark D'Esposito. Causal evidence for the role of neuronal oscillations in top–down and bottom–up attention. *Journal of Cognitive Neuroscience*, 31 (5):768–779, 2019.

[240] Jorge J Riera, Takeshi Ogawa, Takakuni Goto, Akira Sumiyoshi, Hiroi Nonaka, Alan Evans, Hiroyoshi Miyakawa, and Ryuta Kawashima. Pitfalls in the dipolar model for the neocortical eeg sources. *Journal of neurophysiology*, 108(4):956–975, 2012.

[241] Bertrand Rivet, Antoine Souloumiac, Virginie Attina, and Guillaume Gibert. xdawn algorithm to enhance evoked potentials: application to brain–computer interface. *IEEE Transactions on Biomedical Engineering*, 56(8):2035–2043, 2009.

[242] Aline Roc, Léa Pillette, Jelena Mladenovic, Camille Benaroch, Bernard N'Kaoua, Camille Jeunet, and Fabien Lotte. A review of user training methods in brain computer interfaces based on mental tasks. *Journal of Neural Engineering*, 18(1):011002, 2021.

[243] Eugenio Rodriguez, Nathalie George, Jean-Philippe Lachaux, Jacques Martinerie, Bernard Renault, and Francisco J Varela. Perception's shadow: long-distance synchronization of human brain activity. *Nature*, 397(6718):430–433, 1999.

[244] Pieter R Roelfsema, Andreas K Engel, Peter König, and Wolf Singer. Visuomotor integration is associated with zero time-lag synchronization among cortical areas. *Nature*, 385(6612):157–161, 1997.

[245] Michael Rosenblum, Arkady Pikovsky, and Jürgen Kurths. Phase synchronization in noisy and chaotic oscillators. In *Stochastic Dynamics*, pages 232–244. Springer, 1997.

[246] MICHAEL ROSENBLUM, PETER TASS, Jürgen Kurths, JENS VOLKMANN, ALFONS SCHNITZLER, and HANS-JOACHIM FREUND. Detection of phase locking from noisy data: application to magnetoencephalography. In *Chaos In Brain?*, pages 34–51. World Scientific, 2000.

[247] Giuseppina Rota, Giacomo Handjaras, Ranganatha Sitaram, Niels Birbaumer, and Grzegorz Dogil. Reorganization of functional and effective connectivity during real-time fmri-bci modulation of prosody processing. *Brain and language*, 117(3):123–132, 2011.

[248] SR Roth, MB Sterman, and CD Clemente. Comparison of eeg correlates of reinforcement, internal inhibition and sleep. *Electroencephalography and clinical Neurophysiology*, 23(6):509–520, 1967.

[249] Stéphane G Roux, Tristan Cenier, Samuel Garcia, Philippe Litaudon, and Nathalie Buonviso. A wavelet-based method for local phase extraction from a multi-frequency oscillatory signal. *Journal of neuroscience methods*, 160(1):135–143, 2007.

[250] Raphaëlle N Roy, Marcel F Hinss, Ludovic Darmet, Simon Ladouce, Emilie S Jahanpour, Bertille Somon, Xiaoqi Xu, Nicolas Drougard, Frédéric Dehais, and Fabien Lotte. Retrospective on the first passive brain-computer interface competition on cross-session workload estimation. *Frontiers in Neuroergonomics*, page 4, 2022.

[251] Doug Rubino, Kay A Robbins, and Nicholas G Hatsopoulos. Propagating waves mediate information transfer in the motor cortex. *Nature neuroscience*, 9(12):1549–1557, 2006.

[252] Sergio Ruiz, Sangkyun Lee, Surjo R Soekadar, Andrea Caria, Ralf Veit, Tilo Kircher, Niels Birbaumer, and Ranganatha Sitaram. Acquired self-control of insula cortex modulates emotion recognition and brain network connectivity in schizophrenia. *Human brain mapping*, 34(1):200–212, 2013.

[253] Nikolai F Rulkov, Mikhail M Sushchik, Lev S Tsimring, and Henry DI Abarbanel. Generalized synchronization of chaos in directionally coupled chaotic systems. *Physical Review E*, 51(2):980, 1995.

[254] Marjan Saadati, Jill Nelson, and Hasan Ayaz. Convolutional neural network for hybrid fnirs-eeg mental workload classification. In *International Conference on Applied Human Factors and Ergonomics*, pages 221–232. Springer, 2019.

[255] Sepideh Sadaghiani, René Scheeringa, Katia Lehongre, Benjamin Morillon, Anne-Lise Giraud, Mark d'Esposito, and Andreas Kleinschmidt. Alpha-band phase synchrony is related to activity in the fronto-parietal adaptive control network. *Journal of Neuroscience*, 32(41):14305–14310, 2012.

[256] Ram Sankaraneni and Deepak Lachhwani. Antiepileptic drugs—a review. *Pediatric annals*, 44(2):e36–e42, 2015.

[257] MP Saradzhishvili, Geladze TSh, and Toidze OSh. Various features of the mu-rhythm in epileptics. *Zhurnal Nevropatologii i Psikhiatrii Imeni SS Korsakova (Moscow, Russia: 1952)*, 84(6):801–806, 1984.

[258] J Sarnthein, Hellmuth Petsche, P Rappelsberger, GL Shaw, and A Von Stein. Synchronization between prefrontal and posterior association cortex during human working memory. *Proceedings of the National Academy of Sciences*, 95(12):7092–7096, 1998.

[259] Jukka Sarvas. Basic mathematical and electromagnetic concepts of the biomagnetic inverse problem. *Physics in Medicine & Biology*, 32(1):11, 1987.

[260] Tatsuo K Sato, Ian Nauhaus, and Matteo Carandini. Traveling waves in visual cortex. *Neuron*, 75(2): 218–229, 2012.

[261] Nicola Scafetta. The complex planetary synchronization structure of the solar system. *arXiv preprint arXiv:1405.0193*, 2014.

[262] Catherine A Schevon, J Cappell, Ronald Emerson, J Isler, P Grieve, R Goodman, Guy Mckhann Jr, H Weiner, W Doyle, Ruben Kuzniecky, et al. Cortical abnormalities in epilepsy revealed by local eeg synchrony. *Neuroimage*, 35(1):140–148, 2007.

[263] Steven J Schiff. Dangerous phase. *Neuroinformatics*, 3(4):315, 2005.

[264] Robert Schmidt, Maria Herrojo Ruiz, Bjørg E Kilavik, Mikael Lundqvist, Philip A Starr, and Adam R Aron. Beta oscillations in working memory, executive control of movement and thought, and sensorimotor function. *Journal of Neuroscience*, 39(42):8231–8238, 2019.

[265] Joscha T Schmiedt, Alexander Maier, Pascal Fries, Richard C Saunders, David A Leopold, and Michael C Schmid. Beta oscillation dynamics in extrastriate cortex after removal of primary visual cortex. *Journal of Neuroscience*, 34(35):11857–11864, 2014.

[266] D Schmitz, T Gloveli, J Behr, T Dugladze, and U Heinemann. Subthreshold membrane potential oscillations in neurons of deep layers of the entorhinal cortex. *Neuroscience*, 85(4):999–1004, 1998.

[267] AR Seifert and JFl Lubar. Reduction of epileptic seizures through eeg biofeedback training. *Biological Psychology*, 3(3):157–184, 1975.

[268] Rivi Selaa and Meirav Shaked-Toledanob. Neurofeedback treatments enable the eeg-normalization and total seizure control of epilepsy–a case study. In *APPLIED PSYCHOPHYSIOLOGY AND BIOFEEDBACK*, volume 39, pages 142–143. SPRINGER/PLENUM PUBLISHERS 233 SPRING ST, NEW YORK, NY 10013 USA, 2014.

[269] L Senhadji, G Carrault, and JJ Bellanger. Interictal eeg spike detection: a new framework based on wavelet transform. In *Proceedings of IEEE-SP International Symposium on Time-Frequency and Time-Scale Analysis*, pages 548–551. IEEE, 1994.

[270] Lotfi Senhadji, Jean-Louis Dillenseger, Fabrice Wendling, Cristina Rocha, and Abel Kinie. Wavelet analysis of eeg for three-dimensional mapping of epileptic events. *Annals of biomedical engineering*, 23(5):543–552, 1995.

[271] JC Shaw and KR McLachlan. The association between alpha rhythm propagation time and level oe arousal. *Psychophysiology*, 4(3):307–310, 1968.

[272] Elisabeth MS Sherman, Samuel Wiebe, Taryn B Fay-McClymont, Jose Tellez-Zenteno, Amy Metcalfe, Lisbeth Hernandez-Ronquillo, Walter J Hader, and Nathalie Jetté. Neuropsychological outcomes after epilepsy surgery: systematic review and pooled estimates. *Epilepsia*, 52(5):857–869, 2011.

[273] Laurent Sheybani, Gwenaël Birot, Alessandro Contestabile, Margitta Seeck, Jozsef Zoltan Kiss, Karl Schaller, Christoph M Michel, and Charles Quairiaux. Electrophysiological evidence for the development of a self-sustained large-scale epileptic network in the kainate mouse model of temporal lobe epilepsy. *Journal of Neuroscience*, 38(15):3776–3791, 2018.

[274] Daisuke Shimaoka, Chenchen Song, and Thomas Knöpfel. State-dependent modulation of slow wave motifs towards awakening. *Frontiers in cellular neuroscience*, 11:108, 2017.

[275] Margaret N Shouse. Thalamocortical mechanisms of state-dependent seizures during amygdala kindling and systemic penicillin epilepsy in cats. *Brain research*, 425(1):198–203, 1987.

[276] Amanpreet Sidhu and Andrew Cooke. Electroencephalographic neurofeedback training can decrease conscious motor control and increase single and dual-task psychomotor performance. *Experimental brain research*, 239(1):301–313, 2021.

[277] Wolf Singer. Synchronization of cortical activity and its putative role in information processing and learning. *Annual review of physiology*, 55(1):349–374, 1993.

[278] Wolf Singer and Charles M Gray. Visual feature integration and the temporal correlation hypothesis. *Annual review of neuroscience*, 18(1):555–586, 1995.

[279] Ranganatha Sitaram, Tomas Ros, Luke Stoeckel, Sven Haller, Frank Scharnowski, Jarrod Lewis-Peacock, Nikolaus Weiskopf, Maria Laura Blefari, Mohit Rana, Ethan Oblak, et al. Closed-loop brain training: the science of neurofeedback. *Nature Reviews Neuroscience*, 18(2):86–100, 2017.

[280] Bernhard Spitzer and Saskia Haegens. Beyond the status quo: a role for beta oscillations in endogenous content (re) activation. *eneuro*, 4(4), 2017.

[281] Ramesh Srinivasan, William R Winter, Jian Ding, and Paul L Nunez. Eeg and meg coherence: measures of functional connectivity at distinct spatial scales of neocortical dynamics. *Journal of neuroscience methods*, 166(1):41–52, 2007.

[282] Carl E Stafstrom. The role of the subiculum in epilepsy and epileptogenesis. *Epilepsy Currents*, 5(4): 121–129, 2005.

[283] Cornelis J Stam and BW Van Dijk. Synchronization likelihood: an unbiased measure of generalized synchronization in multivariate data sets. *Physica D: Nonlinear Phenomena*, 163(3-4):236–251, 2002.

[284] Cornelis J Stam, Guido Nolte, and Andreas Daffertshofer. Phase lag index: assessment of functional connectivity from multi channel eeg and meg with diminished bias from common sources. *Human brain mapping*, 28(11):1178–1193, 2007.

[285] MA Stephens. Exact and approximate tests for directions. i. *Biometrika*, 49(3/4):463–477, 1962.

[286] MA Stephens. Tests for the von mises distribution. *Biometrika*, 56(1):149–160, 1969.

[287] M Steriade. Thalamic origin of sleep spindles: Morison and bassett (1945). *Journal of neurophysiology*, 73 (3):921–922, 1995.

[288] M Steriade. Grouping of brain rhythms in corticothalamic systems. *Neuroscience*, 137(4):1087–1106, 2006.

[289] Mircea Steriade, David A McCormick, and Terrence J Sejnowski. Thalamocortical oscillations in the sleeping and aroused brain. *Science*, 262(5134):679–685, 1993.

[290] Mircea Steriade, Florin Amzica, and Diego Contreras. Synchronization of fast (30-40 hz) spontaneous cortical rhythms during brain activation. *Journal of Neuroscience*, 16(1):392–417, 1996.

[291] MB Sterman and L Friar. Suppression of seizures in an epileptic following sensorimotor eeg feedback training. *Electroencephalography and clinical neurophysiology*, 33(1):89–95, 1972.

[292] MB Sterman, RW LoPresti, and MD Fairchild. Electroencephalographic and behavioral studies of monomethylhydrazine toxicity in the cat. Technical report, CALIFORNIA UNIV LOS ANGELES BRAIN RESEARCH INST, 1969.

[293] MB Sterman, W Wyrwicka, and S Roth. Electrophysiological correlates and neural substrates of alimentary behavior in the cat. *Annals of the New York Academy of Sciences*, 157(2):723–739, 1969.

[294] Catherine Tallon-Baudry and Olivier Bertrand. High-frequency brain activity: perception or active memory? reply. *Trends in Cognitive Sciences*, 3(7), 1999.

[295] Catherine Tallon-Baudry and Olivier Bertrand. Oscillatory gamma activity in humans and its role in object representation. *Trends in cognitive sciences*, 3(4):151–162, 1999.

[296] Gabriel Tan, John Thornby, D Corydon Hammond, Ute Strehl, Brittany Canady, Kelly Arnemann, and David A Kaiser. Meta-analysis of eeg biofeedback in treating epilepsy. *Clinical EEG and neuroscience*, 40 (3):173–179, 2009.

[297] Kenji Tanaka, Yuji Mizuno, Toshihisa Tanaka, and Keiichi Kitajo. Detection of phase synchronization in eeg with bivariate empirical mode decomposition. In *2013 35th Annual International Conference of the IEEE Engineering in Medicine and Biology Society (EMBC)*, pages 973–976. IEEE, 2013.

[298] William O Tatum IV. Mesial temporal lobe epilepsy. *Journal of Clinical Neurophysiology*, 29(5):356–365, 2012.

[299] José F Téllez-Zenteno, Lizbeth Hernández Ronquillo, Farzad Moien-Afshari, and Samuel Wiebe. Surgical outcomes in lesional and non-lesional epilepsy: a systematic review and meta-analysis. *Epilepsy research*, 89(2-3):310–318, 2010.

[300] John R Terry, Oscar Benjamin, and Mark P Richardson. Seizure generation: the role of nodes and networks. *Epilepsia*, 53(9):e166–e169, 2012.

[301] F Irsel Tezer, Jan Rémi, Nurhan Erbil, Soheyl Noachtar, and Serap Saygi. A reduction of sleep spindles heralds seizures in focal epilepsy. *Clinical Neurophysiology*, 125(11):2207–2211, 2014.

[302] Robert W Thatcher and Joel F Lubar. *Z score neurofeedback: Clinical applications*. Academic Press, 2014.

[303] Maria Thom. Hippocampal sclerosis in epilepsy: a neuropathology review. *Neuropathology and applied neurobiology*, 40(5):520–543, 2014.

[304] Aiko K Thompson, Hannah Carruth, Rachel Haywood, N Jeremy Hill, William A Sarnacki, Lynn M McCane, Jonathan R Wolpaw, and Dennis J McFarland. Effects of sensorimotor rhythm modulation on the human flexor carpi radialis h-reflex. *Frontiers in neuroscience*, 12:505, 2018.

[305] David J Thurman, Dale C Hesdorffer, and Jacqueline A French. Sudden unexpected death in epilepsy: assessing the public health burden. *Epilepsia*, 55(10):1479–1485, 2014.

[306] Zoran Tiganj, Sylvain Chevallier, and Eric Monacelli. Influence of extracellular oscillations on neural communication: a computational perspective. *Frontiers in computational neuroscience*, 8:9, 2014.

[307] Anton Tokariev, Kirsi Palmu, Aulikki Lano, Marjo Metsä, and Sampsa Vanhatalo. Phase synchrony in the early preterm eeg: development of methods for estimating synchrony in both oscillations and events. *Neuroimage*, 60(2):1562–1573, 2012.

[308] Roger D Traub, Miles A Whittington, Ian M Stanford, and John GR Jefferys. A mechanism for generation of long-range synchronous fast oscillations in the cortex. *Nature*, 383(6601):621–624, 1996.

[309] Antonio Ivano Triggiani, Anna Valenzano, Claudio Del Percio, Nicola Marzano, Andrea Soricelli, Annamaria Petito, Antonello Bellomo, Erol Başar, Ciro Mundi, Giuseppe Cibelli, et al. Resting state rolandic mu rhythms are related to activity of sympathetic component of autonomic nervous system in healthy humans. *International journal of psychophysiology*, 103:79–87, 2016.

[310] Logan T Trujillo, Mary A Peterson, Alfred W Kaszniak, and John JB Allen. Eeg phase synchrony differences across visual perception conditions may depend on recording and analysis methods. *Clinical Neurophysiology*, 116(1):172–189, 2005.

[311] BABAK V-GHAFFARI, M Kouhnavard, and T Kitajima. Biophysical properties of subthreshold resonance oscillations and subthreshold membrane oscillations in neurons. *Journal of biological systems*, 24(04):561–575, 2016.

[312] Pedro A Valdés-Hernández, Alejandro Ojeda-González, Eduardo Martínez-Montes, Agustín Lage-Castellanos, Trinidad Virués-Alba, Lourdes Valdés-Urrutia, and Pedro A Valdes-Sosa. White matter architecture rather than cortical surface area correlates with the eeg alpha rhythm. *Neuroimage*, 49(3):2328–2339, 2010.

[313] Timo Van Kerkoerle, Matthew W Self, Bruno Dagnino, Marie-Alice Gariel-Mathis, Jasper Poort, Chris Van Der Togt, and Pieter R Roelfsema. Alpha and gamma oscillations characterize feedback and feedforward processing in monkey visual cortex. *Proceedings of the National Academy of Sciences*, 111(40):14332–14341, 2014.

[314] Remko van Lutterveld, Edwin van Dellen, Prasanta Pal, Hua Yang, Cornelis Jan Stam, and Judson Brewer. Meditation is associated with increased brain network integration. *Neuroimage*, 158:18–25, 2017.

[315] Bernadette van Wijk, Peter J Beek, and Andreas Daffertshofer. Neural synchrony within the motor system: what have we learned so far? *Frontiers in human neuroscience*, 6:252, 2012.

[316] Martin Vinck, Marijn van Wingerden, Thilo Womelsdorf, Pascal Fries, and Cyriel MA Pennartz. The pairwise phase consistency: a bias-free measure of rhythmic neuronal synchronization. *Neuroimage*, 51(1): 112–122, 2010.

[317] Martin Vinck, Robert Oostenveld, Marijn Van Wingerden, Franscesco Battaglia, and Cyriel MA Pennartz. An improved index of phase-synchronization for electrophysiological data in the presence of volume-conduction, noise and sample-size bias. *Neuroimage*, 55(4):1548–1565, 2011.

[318] Sid Visser, Rachel Nicks, Olivier Faugeras, and Stephen Coombes. Standing and travelling waves in a spherical brain model: the nunez model revisited. *Physica D: Nonlinear Phenomena*, 349:27–45, 2017.

[319] Astrid Von Stein and Johannes Sarnthein. Different frequencies for different scales of cortical integration: from local gamma to long range alpha/theta synchronization. *International journal of psychophysiology*, 38 (3):301–313, 2000.

[320] W Grey Walter, R Cooper, VJ Aldridge, WC McCallum, and AL Winter. Contingent negative variation: an electric sign of sensori-motor association and expectancy in the human brain. *Nature*, 203(4943):380–384, 1964.

[321] Peng Wang, Florian Göschl, Uwe Friese, Peter König, and Andreas K Engel. Long-range functional coupling predicts performance: Oscillatory eeg networks in multisensory processing. *Neuroimage*, 196:114–125, 2019.

[322] X-J Wang and J Rinzel. Spindle rhythmicity in the reticularis thalami nucleus: synchronization among mutually inhibitory neurons. *Neuroscience*, 53(4):899–904, 1993.

[323] Yi Wang, Cenglin Xu, Zhenghao Xu, Caihong Ji, Jiao Liang, Ying Wang, Bin Chen, Xiaohua Wu, Feng Gao, Shuang Wang, et al. Depolarized gabaergic signaling in subicular microcircuits mediates generalized seizure in temporal lobe epilepsy. *Neuron*, 95(1):92–105, 2017.

[324] Yijun Wang, Bo Hong, Xiaorong Gao, and Shangkai Gao. Phase synchrony measurement in motor cortex for classifying single-trial eeg during motor imagery. In *2006 international conference of the IEEE engineering in medicine and biology society*, pages 75–78. IEEE, 2006.

[325] Yun Wang, Amey Barakat, and Hongwei Zhou. Electrotonic coupling between pyramidal neurons in the neocortex. *PloS one*, 5(4):e10253, 2010.

[326] Christopher P Warren, Sanqing Hu, Matt Stead, Benjamin H Brinkmann, Mark R Bower, and Gregory A Worrell. Synchrony in normal and focal epileptic brain: the seizure onset zone is functionally disconnected. *Journal of neurophysiology*, 104(6):3530–3539, 2010.

[327] Duncan J Watts and Steven H Strogatz. Collective dynamics of 'small-world'networks. *nature*, 393(6684): 440–442, 1998.

[328] Nikolaus Weiskopf, Klaus Mathiak, Simon W Bock, Frank Scharnowski, Ralf Veit, Wolfgang Grodd, Rainer Goebel, and Niels Birbaumer. Principles of a brain-computer interface (bci) based on real-time functional magnetic resonance imaging (fmri). *IEEE transactions on biomedical engineering*, 51(6):966–970, 2004.

[329] Jason C Wester and Diego Contreras. Generating waves in corticothalamocortical networks. *Neuron*, 77(6): 995–997, 2013.

[330] Britta U Westner, Sarang S Dalal, Alexandre Gramfort, Vladimir Litvak, John C Mosher, Robert Oostenveld, and Jan-Mathijs Schoffelen. A unified view on beamformers for m/eeg source reconstruction. *NeuroImage*, 246:118789, 2022.

[331] Miles A Whittington, Roger D Traub, Howard J Faulkner, Ian M Stanford, and John GR Jefferys. Recurrent excitatory postsynaptic potentials induced by synchronized fast cortical oscillations. *Proceedings of the National Academy of Sciences*, 94(22):12198–12203, 1997.

[332] Miles A Whittington, Roger D Traub, N Kopell, Bard Ermentrout, and Eberhard H Buhl. Inhibition-based rhythms: experimental and mathematical observations on network dynamics. *International journal of psychophysiology*, 38(3):315–336, 2000.

[333] JO Willoughby, SP Fitzgibbon, KJ Pope, Lorraine Mackenzie, AV Medvedev, CR Clark, MP Davey, and RA Wilcox. Persistent abnormality detected in the non-ictal electroencephalogram in primary generalised epilepsy. *Journal of Neurology, Neurosurgery & Psychiatry*, 74(1):51–55, 2003.

[334] Mary D Womack and Kamran Khodakhah. Somatic and dendritic small-conductance calcium-activated potassium channels regulate the output of cerebellar purkinje neurons. *Journal of Neuroscience*, 23(7): 2600–2607, 2003.

[335] Charles C Wood and Truett Allison. Interpretation of evoked potentials: A neurophysiological perspective. *Canadian Journal of Psychology/Revue canadienne de psychologie*, 35(2):113, 1981.

[336] Jian-Young Wu, Xiaoying Huang, and Chuan Zhang. Propagating waves of activity in the neocortex: what they are, what they do. *The Neuroscientist*, 14(5):487–502, 2008.

[337] Dajun Xing, Yutai Shen, Samuel Burns, Chun-I Yeh, Robert Shapley, and Wu Li. Stochastic generation of gamma-band activity in primary visual cortex of awake and anesthetized monkeys. *Journal of Neuroscience*, 32(40):13873–13880a, 2012.

[338] Dezhong Yao. A method to standardize a reference of scalp eeg recordings to a point at infinity. *Physiological measurement*, 22(4):693, 2001.

[339] Zhong Yin and Jianhua Zhang. Cross-session classification of mental workload levels using eeg and an adaptive deep learning model. *Biomedical Signal Processing and Control*, 33:30–47, 2017.

[340] Thorsten Zander, C. Kothe, S. Welke, and Matthias Roetting. Enhancing human-machine systems with secondary input from passive brain-computer interfaces. *Proceedings of the 4th International BCI Workshop & Training Course*, pages 144–149, 01 2008.

[341] Thorsten O Zander, Christian Kothe, Sebastian Welke, and Matthias Rötting. Utilizing secondary input from passive brain-computer interfaces for enhancing human-machine interaction. In *International Conference on Foundations of Augmented Cognition*, pages 759–771. Springer, 2009.

[342] Thorsten O Zander, Christian Kothe, Sabine Jatzev, and Matti Gaertner. Enhancing human-computer interaction with input from active and passive brain-computer interfaces. In *Brain-computer interfaces*, pages 181–199. Springer, 2010.

[343] Hitten P Zaveri, Björn Schelter, Catherine A Schevon, Premysl Jiruska, John GR Jefferys, Gregory Worrell, Andreas Schulze-Bonhage, Rasesh B Joshi, Viktor Jirsa, Marc Goodfellow, et al. Controversies on the network theory of epilepsy: Debates held during the ictals 2019 conference. *Seizure*, 2020.

[344] Honghui Zhang, Andrew J Watrous, Ansh Patel, and Joshua Jacobs. Theta and alpha oscillations are traveling waves in the human neocortex. *Neuron*, 98(6):1269–1281, 2018.

[345] Michal R Zochowski and Lawrence B Cohen. Oscillations in the olfactory bulb carry information about odorant history. *Journal of neurophysiology*, 94(4):2667–2675, 2005.

Utilisabilité des marqueurs de synchronie de phase dans les protocoles de neurofeedback EEG pour la réduction des crises épileptiques *Court résumé* Le cerveau est un organe complexe et pourtant fiable qui supervise de nombreuses fonctions vitales. Des disfonctionnements peuvent pourtant survenir et avoir des conséquences graves comme dans les troubles épileptiques. Certaines fonctions du cerveau sont permises par les oscillations de populations de neurones. Ces oscillations se produisent à des rythmes et dans des régions corticales différents. La phase d'une oscillation caractérise dans le temps les cycles d'activation d'une population neuronale. Quant à la synchronie de phase, elle capture la stabilité d'une relation de phase entre deux oscillations. Bien que la synchronie entre activités oscillatoires de régions cérébrales soit une coordinatrice nécessaire, son excès est la cause de certaines crises épilepiques. Ce travail se focalise donc sur la modulation en temps réel de la synchronie de phase entre régions corticales dans le but d'offrir de nouvelles opportunités de traitement pour certaines épilepsies.

Usability in EEG neurofeedback protocols of phase synchrony neuromarkers for epileptic seizure reduction *Short summary* Despite the fascinating complexity of the brain associated to an incredible consistency, failures do occur and have severe consequences such as in epilepsies. Major functions in the brain are enabled through the oscillatory activity of neuronal assemblies. These oscillations occur at different rhythms, over different regions, depending on the mental task. The oscillatory pattern of a neuronal assembly is characterized by the phase. Phase synchrony captures the stability of a phase relationship between neuronal assembly activities. While synchrony between the oscillatory activities of brain regions is presented as a necessary coordinator, its excess, such as in epilepsy, causes dramatic outcomes, indicating that a balance is necessary. This work focuses on learning a balance with the real-time modulation of phase synchrony measured by means of electroencephalography (EEG) to offer new treatment opportunities for certain epileptic disorders.